Towards a smartphone-connected point-of-care test for HIV

Valérian Turbé

University College London

Thesis submitted for the degree of Doctor of Philosophy

30th March 2017

Supervised by:
Prof. Rachel McKendry
Dr. Eleni Nastouli

Industry supervisors:
Dr. Dale Athey
Dr. Hiromi Yatsuda

I, Valérian Turbé, confirm that the work presented in this thesis is my own. Where information has been derived from other sources, I confirm that this has been indicated in the thesis.

Abstract

The devastation caused by HIV is driving the development of new point-of-care diagnostics. The work presented in this thesis aims to help develop a new generation of smartphone-connected HIV tests designed to address the very high levels of undiagnosed HIV-infected individuals, by widening access to HIV testing to doctors surgeries, pharmacies and developing countries. The biosensor is based on mass manufacturable surface acoustic wave (SAW) devices, and uses piezoelectricity to transduce the binding of biomarkers on the surface of the device into a measurable electric signal, making the test low cost, easy to use and reliable. In addition, the SAW biosensor presented here has the ability to wirelessly and securely transmit results to healthcare providers to potentially offer follow-up appointments at local clinics, or virtually. This thesis begins with the theory behind SAW biosensors. A more focussed characterisation of the specific device developed is then presented, followed by the details of the work done to optimise the biosensor in order to make it a good candidate for a point-of-care test for HIV. Key results include the proof of concept detection of different biomarkers of HIV infection, as well as a demonstration of the ability of the SAW biosensor to deliver a fast response. Different pilot studies are then presented, demonstrating the performance of the device as a diagnostic test, highlighting 100% sensitivity and 100% specificity. These were conducted with more than 30 confirmed HIV positive patient samples and more than 100 healthy volunteers. The following chapter then examines the fundamental mechanisms underpinning the SAW biosensor output and an empirical method to ultimately design more sensitive devices in future antigen detection. This thesis concludes with a summary of the main results and future work, including the potential for larger clinical studies, and field trials in developing countries.

Acknowledgements

The work presented here is in many ways the result of a collective effort, and I am grateful to many people for helping me put it together.

Rachel, first and foremost, for her constant guidance, help and support, and for being so passionate and inspirational. I would like to express my gratitude both to Dale and Yatsuda-san, for trusting me with this work and sharing their technology and knowledge. I feel fortunate to have worked with such approachable industry supervisors. Thanks also to my additional UCL supervisors, Eleni and Robin.

Eleanor's contribution was invaluable, whether it was for the scientific discipline, infectious enthusiasm for science or the meticulous comments on this manuscript; all that despite having to share my company for long days of testing samples in a very crowded biosafety cabinet (here's some data for you E., we spent nearly 1% of my PhD on these uncomfortable chairs!). It has also been a privilege working alongside Jenny and Claudio, and benefiting from their advice and direction.

None of this work would have materialised without the help of everyone at OJ-Bio and Orla in Newcastle, who provided various bits of prototypes, proteins and chemicals, as well as much appreciated advice all along the way. I would especially like to thank Kondoh-sensei, and everyone at JRC and Shizuoka University, for being so welcoming and helpful during my visit to Japan.

Many people have contributed in one way or another to making the long hours in the lab and writing up much more enjoyable: all former and current members of Rachel's group, especially Kailey and Izzy (thanks for the help with the last edits!), Candice, Tania, Anca, Ben, Natascha and Alice. It was great spending this time in and out of the lab with all of you, along with Sam, Alice, Joe, Rodolfo and many others at the LCN.

So many essential moments of fun with many of you outside of work too. Thank you to Valeria, and to all the cyclists, swimmers and various sports fanatics, here in London and back in Nantes, Los Caricatos and their fans. And, finally, my parents and my two wonderful sisters, to whom I owe so much.

Contents

List of Figures

List of Tables

Abbreviations

AFM	Atomic force microscope
AIDS	Acquired immune deficiency syndrome
ART	Antiretroviral therapy
BLI	Bio-layer interferometry
BSA	Bovine serum albumin
CI	Confidence interval
DNA	Deoxyribonucleic acid
DSP	Dithiobis(succinimidyl propionate)
DTSSP	3,3'-dithiobis(sulfosuccinimidyl propionate)
EIA	Enzyme immunoassay
ELISA	Enzyme-linked immunosorbent assay
FDA	Food and Drug Administration
FN	False negative
FP	False positive
gp120	Human immunodeficiency virus envelope glycoprotein
gp41	Human immunodeficiency virus transmembrane glycoprotein
HIV	Human immunodeficiency virus
HIVST	HIV self-test
HRP	Horseradish peroxidase
HSA	Human serum albumin
IDT	Interdigitated transducer
IgG	Immunoglobulin G
IgM	Immunoglobulin M
JRC	Japan Radio Company
NHS	National Health Service

NHS-EDC	N-hydroxysulfosuccinimide and carbodiimide chemistry
p24	Human immunodeficiency virus capsid protein
PATH	Program for Appropriate Technology in Health
PBS	Phosphate-buffered saline
PCR	Polymerase chain reaction
PoCT	Point-of-care test
PPMCC	Pearson product-moment correlation coefficient
PrEP	Pre-Exposure Prophylaxis
QCM	Quartz crystal microbalance
qPCR	quantitative polymerase chain reaction
RNA	Ribonucleic acid
SAW	Surface acoustic wave
SDS	Sodium dodecyl sulfate
SH-SAW	Shear-horizontal surface acoustic wave
SPR	Surface plasmon resonance
TBS-T	a mixture of Tris-buffered saline and Tween 20
TN	True negative
TP	True positive
VHH	Variable region of a heavy chain of a heavy chain-only antibody
WHO	World Health Organization
XPS	X-ray photoelectron spectroscopy

Symbols

Symbol	Name	Unit
x	distance	m
V	speed	$\mathrm{m.s^{-1}}$
λ	wavelength	m
k_0	wavenumber	$\mathrm{m^{-1}}$
ω	angular frequency	$\mathrm{rad.s^{-1}}$
f	frequency	$\mathrm{s^{-1}}$
ϕ	phase shift	degree
A	acoustic amplitude	m
IL	insertion loss	dB
α	attenuation coefficient	$\mathrm{m^{-1}}$
δ	acoustic penetration depth	m
ρ	density	$\mathrm{kg.m^{-3}}$
η	viscosity	Pa.s
j	imaginary unit	-

Chapter 1

Introduction

Since it was first identified in 1981, one of the most important challenges to public health has been the human immunodeficiency virus (HIV) and acquired immune deficiency syndrome (AIDS) pandemic. In 30 years, more than 60 million people have been infected, causing nearly 30 million deaths.[1] A significant minority of HIV infected persons (about a quarter in the UK[2]) are unaware of their infection. These people are not only at risk for their own health - people diagnosed at a late stage have a tenfold increased risk of dying within a year of diagnosis[2]- but it also represents a risk for society, as a person unaware of their infection is more likely to transmit it.[3] These alarming statistics, and more generally the devastation caused by HIV, are driving the development of new diagnostics, which are an effective path to both treatment and prevention. In addition, the potential for significant savings associated with widening access to HIV testing outside of hospital settings[4] has led to notable policy drivers to support HIV testing in hospital emergency services, doctors surgeries, community outreach centres[5] and most recently, the legalisation of HIV self-testing at home in the UK.[6]

This thesis aims at describing a prototype of a biosensor for HIV infection based on surface acoustic wave (SAW) devices. The prototype is designed to work with a smartphone, providing the test with the connectivity needed to analyse, record and send test data securely to health care providers. The principle is first discussed from a theoretical point of view. A characterisation of the SAW biosensor is then presented, along with a description of proof-of-concept studies to illustrate the biosensor's ability to detect key biomarkers of

HIV infection. The results of a series of clinical pilot studies are then discussed, highlighting the capacity for the test to deliver results under 5 minutes with high sensitivity and specificity. A method used to characterise the biosensor's response and help optimise its design parameters is then presented.

1.1 HIV diagnostic needs

Different methods can be used to diagnose a patient with HIV, the gold standard tests being based on enzyme linked immunosorbent assays (ELISA) and polymerase chain reaction (PCR). Significant advances have been made recently in the field of bacterial and viral nucleic acid sequencing applied to diagnostics. Analysis of the genome leads to an accurate identification of the infection, and provides a crucial tool to prescribe the most effective drugs against a particular strain, as well as revealing a possible resistance to a particular drug. This can be achieved in approximately a week, and avoids lengthy periods of trial and failure in the process of drug prescription. Sequencing is already routinely used to help prescribe the best drugs to HIV patients.[7]

However, these diagnostic techniques are confined to centralised laboratories which require large, sophisticated and costly instrumentation, as well as highly trained staff. Patients have to experience unavoidable delays between sample collection, sample delivery to the diagnostic laboratory and receiving results before follow-up appointments.[8–10] These delays in correct diagnosis of the infection, and the fact patients have to visit their clinic multiple times before receiving treatment, also contribute to increasing the risk that the patient does not return.

Access to testing has recently been improved through policies aimed at widening the usage of point of care tests (PoCT), which are affordable, simple tests designed to reduce testing time down to a few minutes. This followed several cost effectiveness studies related to the implementation of PoCT on a large scale. As an example, the National Institute for Health and Clinical Excellence (NICE) estimate that despite the high costs involved in implementing a program to increase the uptake of HIV testing among black Africans and men who have sex with men in England (around £15.8 million), the balanced savings generated by reducing treatment costs would increase annually.[11,12] In addition, modelling suggests that in the UK, changes in clinical practice towards achieving earlier diagnosis of

HIV would lead to significant savings: a discounted cost per life-year gain of £11,146 and a discounted cost per quality-adjusted life years (QALY) gain of £7,504.[13] In 2014, the WHO started to investigate the legal, ethical, gender, human rights and public health implications of HIV self-testing (HIVST).[14] A recent review mentioned the need for clear policies and regulations to be put in place before the implementation of HIVST, but that pilot studies conducted globally documented a high acceptability towards HIVST.[15] In addition, a study conducted in 2015 in South Africa suggests that the implementation of HIVST in the country would have positive effects on HIV testing uptake, particularly on hard to reach groups such as men.[16]

However, the performance of PoCT sometimes referred to as rapid PoCT and their implementation still remain a challenge.[17] The World Health Organisation (WHO) recommends that newly designed PoCT meet the ASSURED criteria:[18]

- Affordable by those at risk of infection
- Sensitive, with very few false-negatives
- Specific, with very few false-positives
- User-friendly: tests that are simple to perform and require minimal training
- Rapid, to enable treatment at first visit, and Robust, for example not requiring refrigerated storage
- Equipment-free
- Delivered to those who need it

Currently, the most common PoCT are based on lateral flow technology. They are relatively slow, requiring a 10-20 minutes waiting time for results,[19] which exceeds a typical doctors appointment (8-10 mins in the UK[20]). It is also notoriously difficult to interpret a faint lateral flow test line by eye, particularly for non-experts (e.g. self-testers)[8]. These tests are insensitive to recently acquired infections[21] and lack the ability to automatically record the test results electronically. This increases the risk of an incorrect reading and data loss, and leaves missed opportunities to link patients to care efficiently.

Recent advances in smartphone-connected diagnostic tests include nanophotonic-devices which interface with smartphone cameras to read out current commercial lateral flow tests,[22] overcoming the need to visually read tests by eye. Microfluidic technologies such as the mChip and a dongle reported by Sia *et al.* recreate all the functions of an ELISA to diagnose HIV and syphilis within 15 minutes, using nanoparticle signal enhancements.[23] However, this rapid test requires the user to perform 7 steps, making it insufficiently simple to use by untrained staff. A recent study conducted in Kenya, Malawi and South Africa illustrated the importance of simplicity of use of PoCT, as a panel of untrained participants were asked to use several prototypes and commercially available HIV self-tests, and less than 25% performed all the tests steps correctly.[24]

This thesis aims at addressing the need for a better, high performance, simple-to-use, fast and connected PoCT for early HIV infection. A new approach was adopted by investigating the technology of surface acoustic wave (SAW) sensors. The promising potential offered by SAW sensors to rapidly detect biomarkers of early HIV infection, as an element of a simple-to-use and smartphone-connected PoCT, constituted the basis of this thesis.

1.2 Brief introduction to SAW biosensors

SAW sensors rely on piezoelectricity to sense perturbations occurring on their surface. An electromagnetic wave is transformed into an acoustic wave, which propagates along the surface of a piezoelectric crystal, before being transformed back into an electromagnetic wave. The effects of the perturbation on the acoustic wave are monitored *via* the electromagnetic wave. Different types of acoustic waves can be made to propagate through a piezoelectric crystal, depending on the nature and cut of the crystal. Lord Rayleigh first predicted the existence of surface acoustic waves in 1885[25] and since then different modes of acoustic wave propagation have been used and reported, the most recent and most sensitive being the shear-horizontal SAW (SH-SAW)[26] and Love wave modes.[27]

As SAW sensors are commonly used as frequency filters in the telecommunications industry, they can be mass manufactured easily and are inherently low cost. When used in liquid, acoustic wave sensors can be used to detect variations in sample viscosity, pH or temperature. They can also be engineered into biosensors able to detect the binding of proteins to their surface. SAW sensors have been reported to rapidly detect *Salmonella typhimurium*

in food products with a high sensitivity,[28] as well as viral agents such as the Sin Nombre virus (SNV), which causes serious pulmonary disease.[29] Detection of biomarkers of HIV infection have also been reported, but so far the sensitivity has not been improved enough to detect biomarkers at clinically relevant levels.[30]

Unlike lateral flow tests, which are commonly read by eye, the readout provided by SAW sensors is entirely electronic, therefore avoiding the risk of incorrect interpretation of the test result. The absence of need for interpretation of the test result, simplicity of use, low cost and self-explanatory presentation of the test result are key points that form part of the target product profile for HIV self-tests set out by the Program for Appropriate Technology in Health (PATH).[31] With their low cost, small size and ease of use, they meet most of the criteria of the ASSURED criteria for PoCT. The potential of SAW sensors to rapidly detect biomarkers of HIV infection at clinically relevant levels has, however, not been achieved yet, and constitutes the main challenge of the work presented here.

1.3 Aims and objectives of the thesis

The different objectives of this thesis, represented in Figure 1.1, merged towards contributing to the development of a new, higher performance and connected PoCT for HIV. Successfully developing such a test would benefit millions of people in various ways. The patients, first and foremost, by directing them to appropriate care quicker and increasing their life expectancy. Then, society in general, by providing effective tools to monitor the spread of the infection as well as potential outbreaks, and up to date crucial information to inform adequate policies aiming at protecting the general public. Finally, the costs associated with HIV treatment are considerable, and savings made by public health care providers would be significant. In the UK, treatment provided to 100,000 patients costs the NHS about £1 billion annually.[32]

The work presented in this thesis focused on the development, optimization and characterisation of a biosensor with the capacity to diagnose early HIV infection. This key element of the biosensor is a SAW device optimised to sense the presence of biomarkers of HIV infection in a patient sample.

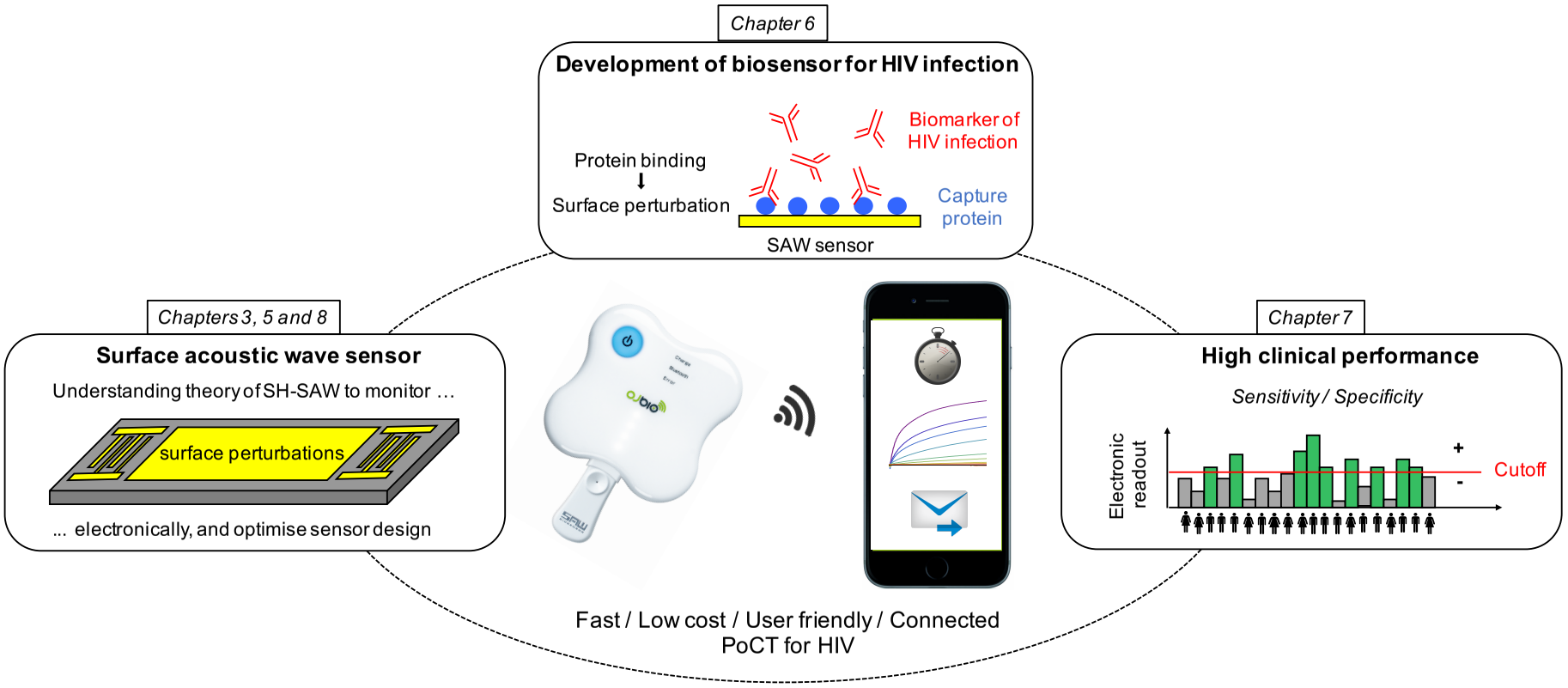

Figure 1.1: Thesis objectives overview. The biosensor for HIV infection presented in this thesis relies on the monitoring of perturbations occurring at the surface of a SAW sensor. The objectives of this thesis are to understand how to optimise and use the SAW sensor to monitor the specific perturbation caused by the presence of key HIV biomarkers, in order to design a fast, low cost, easy to use PoCT operated with a smartphone, and characterised by a high clinical sensitivity and specificity.

The biosensor presented in this thesis is designed to be used with a smartphone, thereby harnessing its mobile computing power. It can also take advantage of other sensors found within smartphones such as Global Positioning System (GPS). The connectivity aspect, which gives the test operator the option to record and send the test data to healthcare providers, is a key objective of this work and distinguishes the new test from currently available lateral flow PoCT. Avoiding the loss of data -and therefore patients- is crucial in the eventuality of home testing, or non-traditional testing locations.[33,34] It brings the benefit of facilitating linkage of the patient into the care cascade, from the point of diagnosis through to care and treatment. A recent study using a mathematical model and focusing on a high risk group of men who have sex with men in Seattle showed that replacing clinic-based tests by home-based tests could indeed increase HIV testing, but at the same time may increase the rate of false-negative tests and therefore decrease linkage to HIV care. This study was performed using the commercially available OraQuick In-Home HIV Test (OraSure Technologies, Inc, Bethlehem, USA), which is not a connected test. An online study in South Africa is currently looking into whether a smartphone app can increase linkage to care amongst newly diagnosed HIV patients in South Africa.[35] In addition, the test connectivity helps healthcare organisations to build a dataset comprising the necessary information to monitor the spread of the infection. Such information is also crucial in the process of designing more efficient public healthcare policies aiming at addressing the fight against the pandemic.

There are now more mobile device subscriptions than people on the planet and their number is estimated to be growing five times faster than the human population.[36] The number of smartphone users in the world is predicted to rise to 6.4 billion by 2021, meaning that roughly 70% of the world population will have access to a smartphone in five years time[36] and consequently there is potential for a long-term sustainable platform for diagnostic testing worldwide. Emerging markets are expected to play a key part in this spectacular growth, with regions like Asia Pacific, the Middle East and Africa predicted to account for 80% of all new subscriptions in the next five years.[36] These billions of phones can be used to improve access to rapid tests and public surveillance efforts everywhere. Aside from the use of the smartphone as a diagnostic tool, it has been shown that the use of specific apps can increase HIV testing uptake among high risk groups such as men who have sex with men.[37]

This thesis focusses on the use of a SAW device as a key element of a biosensor for HIV. The aims of this work were to investigate and improve the performance of the biosensor from different angles. First, the intrinsic sensitivity of the SAW device to a given perturbation, which is dependent on the design of some elements of the device, such as the length of the delay line, the operating frequency, and the strategy used to cancel out the noise in the signal. The objective was to show, using the theoretical definition of the SAW device sensitivity, that the device used had the optimal sensitivity to the range of perturbations it would have to sense.

Second, the biosensors ability to rapidly detect key biomarkers of HIV at clinically relevant concentrations. The optimisation of the surface chemistry used to functionalise the surface of the device with appropriate capture proteins was a central step in the biosensor optimization. The aims here were to (i) investigate the response of different antibodies and specificity testing using a non-specific antibody (negative control), (ii) test the reproducibility of measurements on a single SAW biochip, (iii) demonstrate the detection of clinically relevant concentrations of anti-HIV antibodies; (iv) reduce the time to result for ultra-rapid testing, in order to achieve a time to result of less than 5 minutes, as recommended by PATH in their target product profile for HIV self-tests,[31]; (v) show the proof of concept detection of the HIV p24 antigen, key marker of early infection; and (vi) investigate signal amplification strategies using gold nanoparticles.

Third, the biosensors clinical performance. An essential stage of development of a new biosensor is to test its clinical sensitivity and specificity to biomarkers of HIV using a panel of patient samples. The target product profile set out by PATH for HIV self-tests recommends a clinical sensitivity and specificity both larger than 99% (optimistic requirements, the minimum requirements are: clinical sensitivity >99%, clinical specificity >98%).[31] Conducting pilot studies with a panel of patient samples and achieving these requirements was a key objective of this work.

Finally, a last objective was to characterise the fundamental physical parameters contributing to the signal output measured with the biosensor. Using a method developed by Saha and Gizeli,[38] the aim was to try and disentangle the contributions of different physical parameters contributing to the signal, in the hope that a better understanding of the transduction mechanisms would provide additional tools to improve the device performance.

1.4 Industrial partners and funding

This work was supported by a studentship funded *via* the UCL Impact award in collaboration with industrial partners OJ-Bio Ltd., a Newcastle-based SME. OJ-Bio Ltd. is a leading telecommunications company developing biosensors for real time point-of-care diagnostic tools. It was created in 2009 by Orla Proteins Technologies and Japan Radio Company Ltd. (JRC). JRC is a multinational company with 100 years of electronics and wireless communications expertise based in Saitama, Japan. Orla is a biotechnology company with expertise in protein engineering, manufacture and surface technologies. In addition, grants from the NIHR i4i program (II-LA-1111-20004) and EPSRC i-sense Early Warning Sensing Systems in Infectious Diseases (EP/K031953/1) also supported the work presented here. i-sense is a five year, £11m EPSRC-funded programme that was launched in October 2013. Its vision is to engineer a new generation of early-warning sensing systems to identify disease outbreaks much earlier than before, using self-reported symptoms on the web and mobile phone-connected diagnostic tests.

1.5 Outline of thesis structure

This thesis was articulated into the following 8 Chapters in order to assess the different objectives, introduce the materials and methods used and present the various results obtained:

- Chapter 2 gives an overview of AIDS, from its origin in the 1980s to the status of the pandemic today. A brief presentation of the structure and mechanism of action of HIV is given, leading to the identification of the key biomarkers of infection. A timeline representing the order of appearance and temporal dynamics of different biomarkers over time is then explained. Finally, an overview of the key requirements for the design, characteristics and performance of PoCT for HIV is given, as well as a review of the state of the art in this field.

- Chapter 3 presents the theory of shear-horizontal SAW (SH-SAW) devices, and outlines their potential as a good candidate for developing the biosensor. After presenting the concept of piezoelectricity, a brief history of acoustic wave sensors is given. An

introduction to the perturbation theory applied to SH-SAW follows, and how it can be used to justify the choice of certain parameters to monitor perturbations detected by the sensor.

- Chapter 4 is a detailed description of all materials and methods involved in the process of obtaining the results presented in this thesis. In particular, this includes a presentation of the prototype of the SH-SAW device and associated control box used to obtain the results.

- Chapter 5 presents a characterisation of the SH-SAW device used throughout this thesis. Different aspects are studied, to investigate the intrinsic sensitivity of the device as well as its performance as a disposable, easy to use test.

- Chapter 6 reports a systematic study to demonstrate the ability of the biosensor to detect key biomarkers of HIV at clinically relevant concentrations. Highlights include ultrafast detection within 10 seconds after sample injection, and detection of a key biomarker of early infection. Methods to amplify the SAW signal down to pg/ml sensitivity are reported.

- Chapter 7 demonstrates the very good performance of the biosensor by assessing its clinical sensitivity and specificity using a panel of 30 HIV patient samples and more than 100 healthy volunteers. An investigation is presented to look into the speed at which the result can be delivered without compromising the test performance.

- Chapter 8 presents a method to characterise the SH-SAW device, some of the liquid sample properties, as well as some physical parameters associated with the proteins detected by the biosensor. This work, which relies on a method described by Gizeli *et al.*, opens up new ways of improving the SH-SAW devices performance in the future.

- Chapter 9 aims at summarising the main conclusions presented throughout the thesis. It brings together the different results obtained and their contribution towards the initial objectives, before opening up the exciting opportunities created by this work to advance towards future new objectives.

Chapter 2

HIV Diagnostic Needs

In this chapter, an introduction to the history and the impact caused by the HIV/AIDS pandemic is given. The structure of the HIV-1 virus is presented, along with the key biological markers of infection and their temporal dynamics. The benefits of early detection are discussed, and, in the light of recommendations and guidelines provided by the WHO and PATH, a portrait of the ideal PoCT for HIV infection is given. Finally, an overview of the current HIV diagnostics is given, highlighting the current limitations in the field.

2.1 The HIV/AIDS pandemic

2.1.1 History

Nascent awareness of acquired immunodeficiency syndrome (AIDS) arose in 1981. In Los Angeles and New York, incidences of homosexual men with unusual symptoms such as a rare type of lung infection or rare skin tumours were reported.[39] More importantly, the patients were found to have a severe reduction in CD4 cells, or T cells.[40,41] These cells play an important role in the immune system as they are involved in, amongst other functions, killing virus-infected cells, activating macrophages and driving inflammation.[41]

In the following months, this disease was recognized across the United States, Western Europe, and Africa. In 1983, the etiological agent, the human immunodeficiency virus (HIV), was identified by researchers in France and the United States who classified the virus that causes AIDS as a member of the group of viruses called retroviruses.[42,43] It is

generally accepted that the virus had spread throughout most of the world by the end of the 1980s.[40,41] There are two species of the virus, called HIV-1 and HIV-2. Both evolved from a simian immunodeficiency virus (SIV). The original SIV was found in chimpanzees in the case of HIV-1 while HIV-2 evolved from an SIV in a type of monkey called the sooty mangabey.[40,44–46]

HIV-1, which is responsible for the vast majority of AIDS cases worldwide, is divided into three groups, depending on mutations and the general evolutionary path the virus has followed:[41,47] group M (for Major), group O (for Outlier) and group N (for Non M, Non O). Group M is the dominant group, as it represents 90 percent of all infections worldwide, while groups N and O are rarer. Within the M group there are at least nine strains (or subtypes) of HIV-1. Those different strains undergo continuous mutations, and often end up recombining with each other, resulting, in combination with historical migration and trade routes, in more associated recombinant strains of the virus. HIV-2 is not as virulent and is restricted mainly to West Africa, where it originated.[41,48]

HIV infection causes AIDS, but the definition of AIDS given by the World Health Organization (WHO) is the development of a low CD4 cell count (lower than 350 cells/mm^3[32]). The HIV/AIDS pandemic consists of many separate epidemics. Each epidemic has its own distinct origin, both in terms of geography and specific populations affected, and involve different types of risky behaviours and practices, for example, unprotected sexual intercourse with multiple partners or sharing drug injection equipment.

2.1.2 The situation today (2016)

The HIV/AIDS pandemic has spread over the world and now ranks among the most devastating infectious diseases in human history, infecting more than 78 million people and 39 million deaths[49] with tremendous burden of illness in Sub-Saharan Africa, as illustrated by the latest UNAIDS prevalence map in Figure 2.1.

UNAIDS indicates in its latest report that in 2015, approximately 2.1 million people acquired HIV infection, and approximately 36.7 million people were estimated to be living with HIV globally.[51] Antiretroviral therapy (ART) has been shown to reduce rate of HIV-related mortality[52,53] and to increase life expectancy.[54,55] Some efforts to implement access to ART have been successful. Since 2000, the percentage of HIV patients on ART

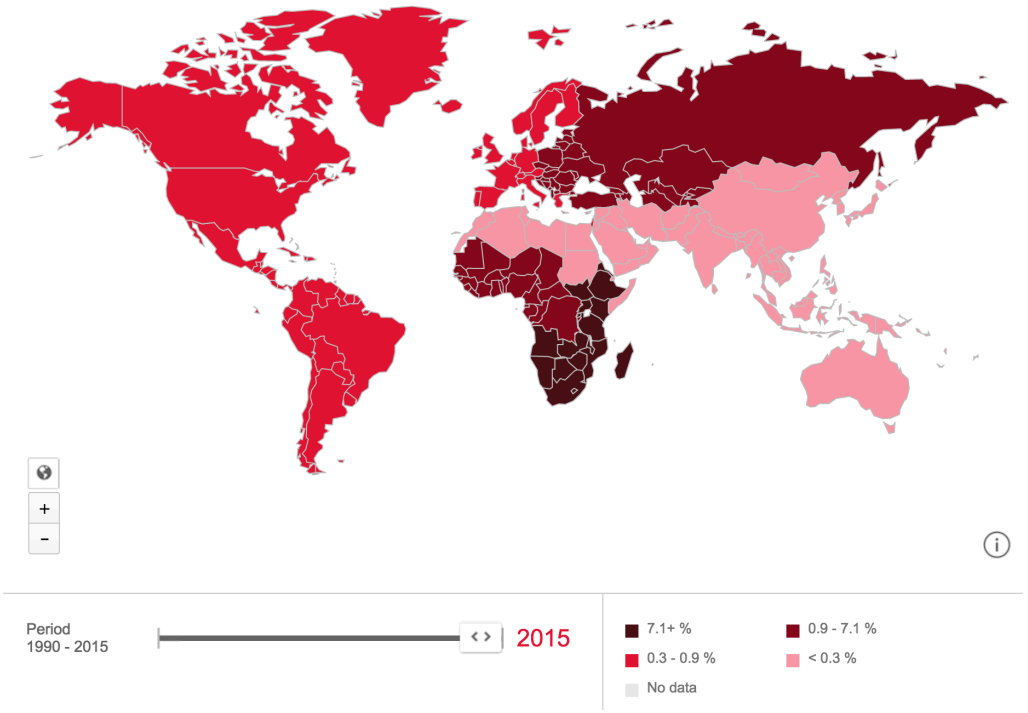

Figure 2.1: HIV prevalence globally, 2015. The HIV/AIDS pandemic has spread over the world since the late 1980s. Sub-saharan Africa is particulary impacted, with prevalence as high as 7% and more in some countries. Adapted from [50]

increased from approximately 3% to more than 45% in 15 years. [51] As a consequence, the number of AIDS-related deaths has been decreasing annually since 2005. [51] This is illustrated in Figure 2.2.

2.1.3 Benefits of early detection

As mentioned in Chapter 1, strategies based on the use of antiretroviral drugs exist to prevent transmission of the infection, and are recommended by the WHO. [56,57] In a press release in 2014, the US Centre for Disease Control and prevention (CDC) recommended the use of PrEP to those at high risk of contracting the infection, as it has been shown to reduce the risk of infection by 92%. [58] The UK public health care system (National Health Service NHS) has recently been made legally responsible to fund and implement PrEP nationally. [59]

In parallel to these recent developments, and in the absence of a vaccine, a major aspect of the fight against the HIV/AIDS pandemic remains the detection of the infection. In 2014, UNAIDS set out the challenging 90-90-90 target: aiming for 90% of people living with HIV

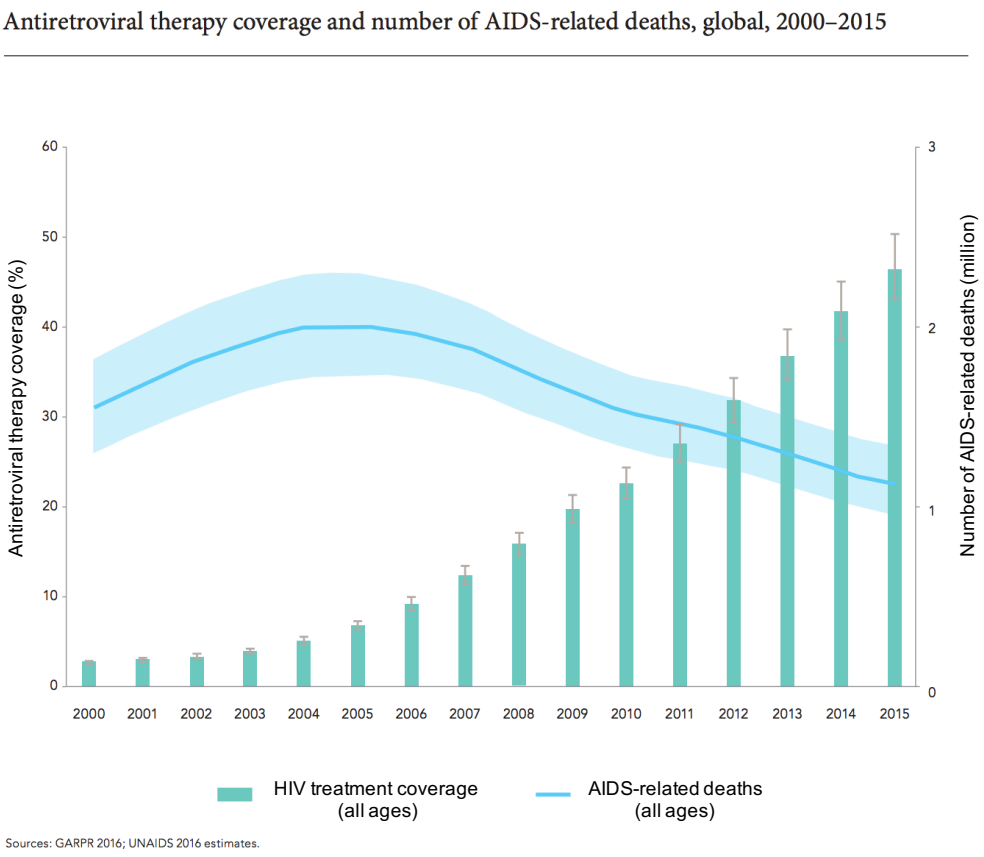

Figure 2.2: Global evolution of antiretroviral therapy coverage, and AIDS-related deaths, since 2000. Adapted from: UNAIDS global AIDS update 2016 [51]

know their HIV status, 90% of people who know their HIV-positive status access ART and 90% of people on treatment have suppressed viral loads. [60] At a recent International AIDS conference in Durban, South Africa, UNAIDS announced significant progress has been made towards this ambitious target. [61] One of the reasons to explain the increase observed in the antiretroviral therapy coverage, as well as the decrease in AIDS-related deaths since 2005 (see Figure 2.2), is the increase in access to testing. [1] However, the need for better diagnostic tools remains, highlighted by the very high number of HIV-infected individuals who are unaware of their infection. In 2015, it was estimated that around 17% of the individuals living with HIV in the UK were unaware of their infection. [62] That proportion is 12.5% in the USA [63], 55% in South Africa [64] and probably more in less developed countries. In 2014, UNAIDS estimated that globally, this figure could be as high as 54%. [64]

Individuals who are unaware of their infection are at risk for their own health, as they are likely to start their treatment too late. It is estimated that people diagnosed late

(CD4 cell count fewer than 350 cell/mm^3) have a tenfold increased risk of dying within a year of diagnosis.[32,62] Early diagnosis and access to antiretroviral treatment increases life-expectancy by 10 years.[65] It also represents a public health problem, as individuals unaware of their infection are likely to transmit it, particularly during the early acute stage of infection.[66] A study has shown that pregnant women reduce the risk of transmitting the virus to their babies to less than 1% when diagnosed early and treated.[67]

In addition to the human benefits associated with early diagnosis, the economic benefits are potentially significant. According to the CDC, every case of HIV that is prevented saves $380,000 in lifetime treatment costs.[67] In the UK, Public Health England (PHE) estimates the annual cost for treatment and care in the UK to be in the region of £858 million, and that if the estimated 4,000 UK-acquired infections diagnosed in 2011 had been prevented, £1.9 billion in lifetime treatment and clinical care costs would have been saved.[32] In 2013, another study in the UK modelled the cost effectiveness of HIV care and concluded that the lifetime costs associated with 3,000 new HIV infections was likely to be in excess of 1 billion.[68]

Early detection of HIV benefits patients by triggering faster access to care with better health outcomes, the public by contributing to stop the spread of the infection, and it generates significant public savings. Early diagnosis relies on the identification and detection of specific biomarkers of infection. The following section gives an insight into the common biomarkers of early HIV infection.

2.2 Biomarkers of HIV infection

2.2.1 HIV-1 structure

HIV-1 is a retrovirus; more specifically a lentivirus. Lentiviruses are characterised by a long latency period between infection and the start of the disease (8 to 12 years), and can infect non-dividing cells.[47] Retroviruses are characterised by a capsid core protecting the genetic information they carry (two single-stranded RNA molecules). The replication cycle begins even before the virus gets in contact with the cell, as reverse transcription (transcribing RNA into double stranded DNA by reverse transcriptase) begins in the virion. Infection

triggers a series of processes that lead to the DNA being integrated into the hosts genome, and a new infectious virion being created.[69]

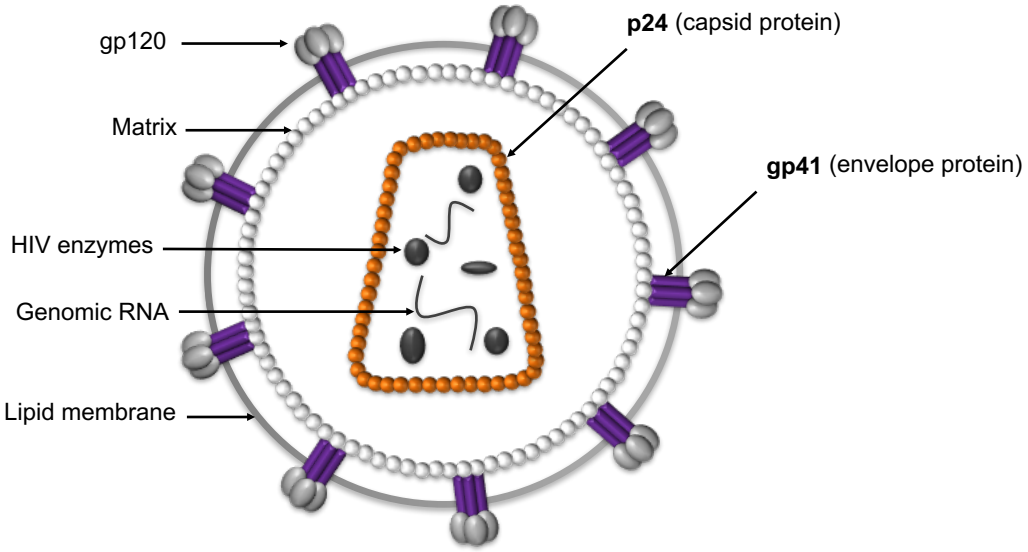

Figure 2.3: HIV-1 structure. Schematic to illustrate the main elements forming the structure of HIV-1. The two proteins that were key to this work are highlighted in orange (p24) and purple (gp41). Adapted from[70]

The general structure of HIV-1 is schematised in Figure 2.3. The genome, which consists of two copies of single-stranded RNA, is protected by a capsid composed of p24 proteins, also known as capsid protein (CA). The capsid is itself surrounded by the virus envelope, which is composed of an inner matrix of proteins and interacts directly with the environment through spikes of trimers of envelope proteins which will be described further.[69]

The viral RNA is about 10 kilobases (9719 nucleotides) long and contains 9 different genes coding for 15 different proteins. Those proteins are classified in three categories: structural proteins, regulatory proteins and accessory proteins.[71] Two of the structural proteins were essential to this work: the capsid protein (CA) p24 and the transmembrane protein (TM) gp41. As will be discussed further on, the antibodies raised against these two proteins (anti-p24 and anti-gp41) as well as p24 itself, are essential biomarkers of HIV infection. The structural, regulatory and accessory proteins as well as the enzymes the virus needs to replicate, are all derived from the cleavage of polyproteins that are encoded by three genes: *env*, *gag* and *pol*.[69,72,73]

The *env* gene codes for a precursor protein, the glycoprotein gp160. This protein is then cleaved by cellular protease into two smaller proteins, gp41 and the external surface protein

(SU) gp120. Those two products of the cleavage of gp160 remain bound together but only by non-covalent bonds: they form a non-covalently bound heterodimer. Those heterodimers are grouped into trimers to form spikes on the surface of the virus. The gp41 protein is embedded into the virus envelope while the gp120 protein in exposed to the external environment and contains the recognition site for the cell surface receptor protein. The gp120 protein is therefore directly involved in the first step of the process where the virus attaches to and enters the cell.[69,72,74]

The *gag* gene also codes for a precursor polyprotein called Pr55. This polyprotein is cleaved by viral proteases. It is cleaved by viral proteases - instead of cellular proteases like in the case of gp160 - because the cleavage happens after the virus has budded out from the cell (or during the budding process), in a step called the maturation process. The products of the cleavage of Pr55 by virus proteases are four smaller proteins: p17, p24, p9 and p6. The p17 protein, also known as matrix protein (MA) forms the inner layer of the virus envelope. As mentioned earlier, p24 constitutes the capsid core protecting the viral RNA. The p9 protein, also called nucleocapsid (NC), is associated with the RNA genome in the capsid core and plays a role in the early stages of reverse transcription. The p6 protein plays a role in the assembly process by helping incorporate accessory proteins into the virion.[73,75]

Finally, the *pol* gene codes for the polyprotein Pr160. The cleavage products of Pr160 are the enzymatic components of the virus: protease, reverse transcriptase and integrase. As mentioned before, the protease is responsible for the cleavage of Pr55, as well as for maturation and hence production of an infectious virion (an immature virion is non-infectious[76]). Reverse transcriptase produces the complementary DNA from the viral RNA template. Integrase is necessary to insert the transcribed double-stranded DNA into the cells genome.[69,75]

The role of regulatory proteins is to help help control the synthesis of other proteins necessary to the replication cycle. Finally, HIV-1 accessory proteins help replicative cycles to be productive. They modify the local environment within infected cells to ensure viral persistence, replication, dissemination, and transmission.[69,72,75]

As mentioned earlier, p24 is a key marker of early HIV infection. As it constitutes the core capsid of the virus, its sequence is highly conserved compared to envelope proteins, making it easier to design capture protein against it. Despite being a core structural protein, p24

gets released continuously in the blood stream following the virus replication cycle, cell lysis or host attack of the virus.[70,73,74,77,78]

2.2.2 Temporal dynamics of key biomarkers of HIV infection

There are several biomarkers of HIV infection in blood or saliva. They can be directly related to the virus itself (viral RNA or actual virus proteins such as p24 or envelope proteins), or antibodies raised against the different HIV proteins.[79] The graph in Figure 2.4, adapted from references,[80–82] shows the temporal dynamics of key HIV markers, in blood, starting from transmission (day 0). The markers of interest here are viral RNA, p24, anti-gp41 IgM, anti-p24 IgG and anti-gp120 IgG (IgM antibodies are produced first and only during a short period of time, until the antibody response matures and the production of IgG antibodies takes over). On this plot, it is important to note that the units on the two y axes are different, and that the levels of RNA in blood are significantly lower than the levels of the different HIV proteins or associated antibodies (for instance, for two copies of viral RNA, approximately 1400 copies of p24 are produced[83]). In addition, as the left axis shows signal over cut-off values, it is important to point at that while a peak of p24 might be lower than 400pg/ml, antibody levels reach values higher than a few micrograms per millilitre.

The virus needs some time to replicate enough and spread from local to systemic infection. As a consequence, the different markers of infection have a distinct order of appearance and for some there is a defined window of detection. While this may differ in individuals, this is true for a population level.

Viral RNA and p24 arise first, as they are part of the virus, before the host mounts a detectable response. RNA can be detected after approximately 7 days, while the window period for the detection of p24 is from approximately 2 to 5 weeks after transmission. The host needs time to produce the antibodies that are raised against different HIV proteins, which explains why there is a delay between the viral markers and the antibody response. What looks like a slight delay between the appearance of viral RNA and p24 in the body is probably an artefact of the difference in detection method used for the two markers. The conventional method to detect RNA is to lyse the virus (by adding detergent to the sample, which bursts open the envelope and the capsid), purify the RNA, use reverse transcriptase

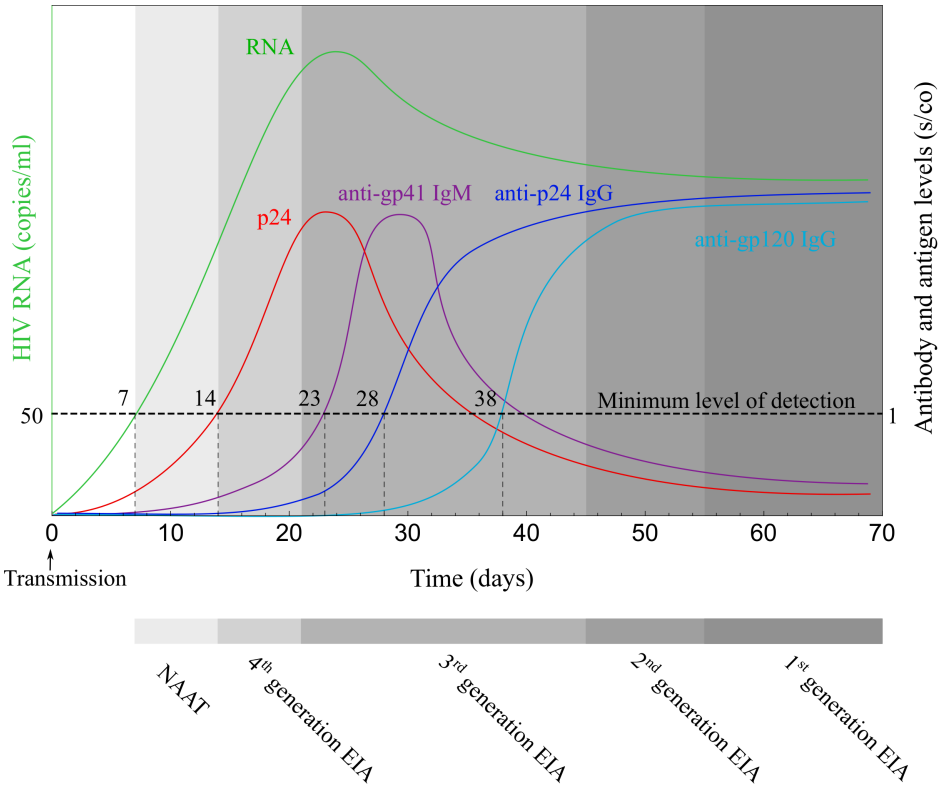

Figure 2.4: Evolution of HIV markers over time. Left axis shows viral RNA levels in copies/ml. Right axis (not to scale) shows protein or antibody level as signal over cut-off (s/co). Minimum level of detection represents a s/co of 1 for the proteins/antibodies and 50 copies of viral RNA per millilitre of blood, using standard current techniques. Adapted from.[80–82] The different windows of detection corresponding to different generations of laboratory tests for HIV are indicated. EIA stands for enzyme Immunoassay. NAAT refers to nucleic acid amplification tests.

enzymes to reverse transcribe the RNA into DNA and run a qPCR (quantitative Polymerase Chain Reaction) to evaluate the amount of DNA, which therefore directly relates to the viral load of the starting sample. Amplification of nucleic acid is easy and signal amplifications of 10^9 are not uncommon for RNA/DNA. The conventional methods to detect the presence of protein markers (antibody or antigen) can not compare with these levels of signal amplification and are therefore less sensitive.

The first HIV antibody to appear is generally anti-gp41 IgM, and unlike IgG, there is only a short window to detect it (approximately 3 to 6 weeks after transmission). This is because it is an IgM, which, by nature, is only produced during a few weeks before the antibody responses matures and IgG antibodies are produced. Then comes anti-p24 antibodies, which can be detected from around 4 weeks after transmission, and anti-gp120 IgG, detectable approximately 5 weeks after transmission.[84]

The differences observed in terms of timing of the different antibodies can be explained by the nature of the protein they are raised against. When a foreign protein is introduced in the organism, it gets complexed by macrophages and various antigen presenting cells who chop it up into peptides (short chains of amino acids, usually no longer than 10 amino acids). The peptides are then presented to T cells. Recognition of the peptide antigen by the T cell receptor leads to activation of the T cell, which in turn will activate B cells which, in turn, produce the antibody against this sequence of amino acids.[69] The more conserved the original foreign protein (i.e. the more its structure does not tend to evolve a lot following mutations), the easier it is for the organism to raise antibodies against it. It is more likely to be difficult for the organism to raise antibodies against a highly mutating protein such as gp120 (envelope protein, interacts directly with the outside environment) than against conserved proteins such as gp41 (which is embedded in the envelope) and p24 (capsid, inside the virus). This explains why anti-p24 comes second, and anti-gp120 comes last. Furthermore, gp120 is a highly glycosylated protein, making it more difficult for the macrophages and antigen presenting cells to present peptides properly.

The windows of detection of the different generations of laboratory-based tests are indicated on the graph in Figure 2.4. Nucleic acid tests can reliably be used to diagnose HIV infection from 7 days after infection, while the most recent generation of ELISA can be used from 14 days after infection (it detects p24). Detecting HIV infection in the acute stage is still challenging in point-of-care settings. Rapid antibody tests are highly accessible but they cannot detect HIV during the very acute stage,[21] and therefore highlight the need for antigen/antibody combination assays.[85] The need for detecting both anti-p24 and anti-gp41 has been discussed, as cases have been observed when a patient could be wrongly diagnosed because one antibody was undetectable.[86]

2.2.3 Clinical range of key biomarkers of HIV infection

The clinical range of the three main proteins biomarkers of HIV infection can be found in Table 2.1.

Biomarker	Clinical range
p24	0.1 - 1000pg/ml 4.2×10^{-3} - 41.7pM
Anti-p24	82 - 1900μg/ml 0.5 - 12.7μM
Anti-gp41	5.4 - 5194μg/ml 0.03-34.7μM

Table 2.1: Clinical range of the three main proteins biomarkers of HIV infection. [82,87–89]

2.3 The ideal PoCT for HIV

2.3.1 Benefits of PoCT implementation

As mentioned in Chapter 1, a range of methods can be used in hospital settings to accurately diagnose HIV infection. These include ELISA and PCR. However, these diagnostic techniques are associated with high costs (staff training, instrumentation) and delays for the patients, who need to return to the clinic or hospital to obtain their results or attend a follow-up appointment. [8–10] These delays increase the risk transmission of the infection. The common procedure to test for HIV in hospitals differs from country to country. The UK guidelines state that a positive HIV antibody test should be confirmed by three independent assays and at least one of them should distinguish between HIV-1 and HIV-2, [90] whereas in the US a positive screening test and one positive confirmatory test should be performed to make a diagnosis. [91] Both the WHO and the BHIVA recommend that all individuals diagnosed with HIV should be offered treatment as soon as possible following diagnosis, in an effort to prevent onward transmission of the infection. [56,92]

In addition, several cost-effectiveness studies were conducted; their conclusions all point towards the potential for significant public savings associated with the implementation of PoCT or HIVST. [11–13] These economic benefits, and the constraints and flows associated with traditional gold standard diagnostic techniques, are driving a push towards the implementation of PoCT outside of hospitals or clinics, [4,5] as well as the legalisation of self-testing in several countries like the UK [6], France [93] or the USA. [94] HIVST is also recommended by the WHO. [14] HIVST has been widely shown to be well accepted by patients, [15] is believed to increase HIV testing uptake in general, [16] and to play an important role in the near future to facilitate both treatment and prevention. [95]

The general trend of the increase in the use of PoCT to diagnose HIV is illustrated by the proportion of PoCT procured by the WHO globally, compared to ELISA or confirmatory tests. Figure **??** shows that PoCT have largely dominated the WHO HIV test kit procurement program since 2003, and the latest data indicate that more than 80% of the HIV tests kit provided by the WHO around the world were PoCT in 2009.[96]

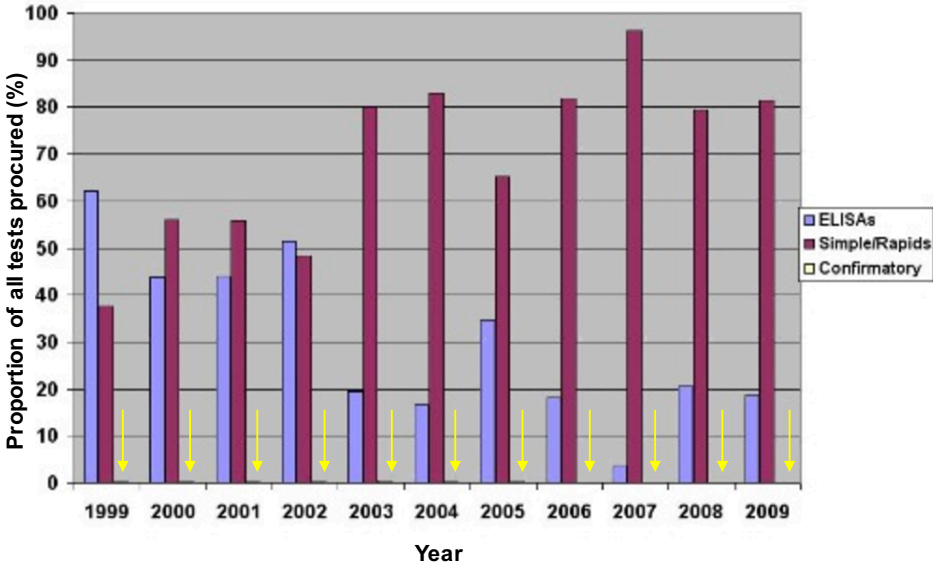

Figure 2.5: Procurement of HIV diagnostics by the WHO. HIV test kits procured by WHO, by assay type, 1999-2009.[96] Simple/Rapid refers to PoCT.

2.4 PoCT design criteria

As mentioned in Chapter 1, the WHO issued some general guidelines about the design of PoCT in general, illustrated by the acronym ASSURED.[18] The recommendation is that every PoCT needs to be low cost, exhibit good performance indicators (sensitivity and specificity), be simple to use, rapid and robust, equipment-free and it should be possible to deliver the test to regions where it is needed, taking into account shipping and changing conditions of temperature and pressure. These guidelines are general and apply to PoCT to any infection. PATH has issued more specific criteria that apply to HIVST.[31] As it is assumed that a self-test could be purchased and performed anywhere in the world, the requirements are stricter and therefore constitute a good set of criteria when developing the ideal PoCT for HIV infection.

PATH identified 51 variables, grouped into 6 requirement categories: Context (use case), Performance requirements, User requirements, Operational requirements, Kit Requirements and Commercialisation requirements. The variables belonging to the last two categories would have to be improved at the scaling up stage of the manufacturing process, as they range from the packaging to the waste management and quality control.

As some of the variables are met by most of the PoCT currently available, Table 2.2 lists the requirements that are not yet fully met, and will be discussed further on. These targets were the motivation of the work presented here.

2.4.1 Overview of current PoCT for HIV infection

There are dozens of HIV PoCT and HIVST on the market, some reliable, some less. As of 2016, the US Food and Drug Administration (FDA) has officially approved no fewer than 41 PoCT for HIV.[97] The two most common types of commercially available PoCT for HIV are lateral flow tests, and flow-through tests. An example of each is show in Figure 2.6.

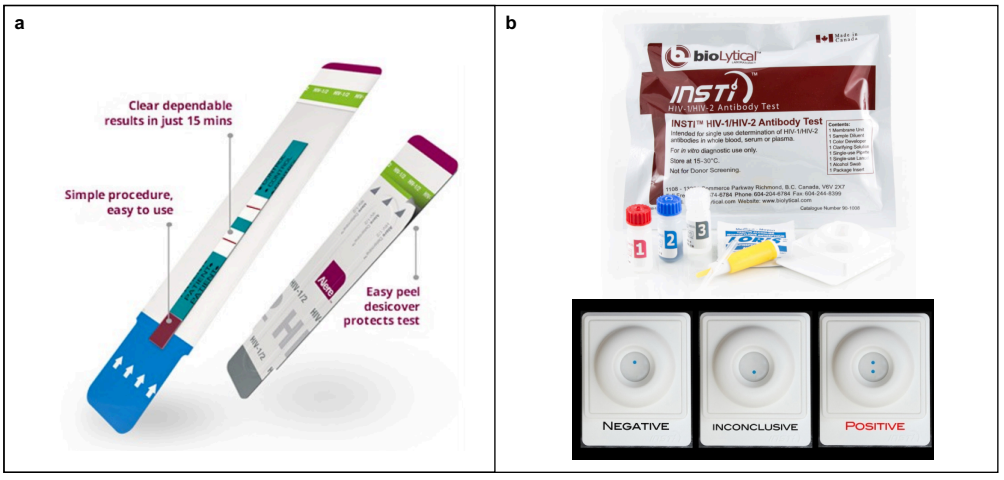

Figure 2.6: Example of commercially available PoCT for HIV infection. a) Lateral flow test Alere Determine HIV-1/2 (Alere, USA)[98] **b)** Flow-through test Insti HIV-1/HIV-2 Antibody test (bioLytical Laboratories, Canada)[99]

Initial field testing has shown promising results. A 2007 study in 11 African countries found that 15 FDA-approved commercially available PoCT for HIV gave accurate and comparable results whether they were used in laboratory settings or in the field. Furthermore, the conclusions of the study were positive about the potential to scale up the implementation of these tests to national level.[100] However, inferior performances have also been reported

Requirement category	Variable	Minimum requirement	Optimistic requirement
Context (use case)	Data handling	Developed communication system that will instruct target users on linking and reporting HIV self-test results with appropriate care (follow-up testing and counseling).	Developed communication system that will instruct target users on linking and reporting HIV self-test results with appropriate care (follow-up testing and counseling. Additional work may be required to define additional optimal requirements.
	Analyte	Qualitative detection of HIV infection, antibody.	Qualitative detection of HIV infection, antibody, biomarker, and nucleic acid.
Performance requirements	Clinical sensitivity and specificity	Sensitivity >99% Specificity >98%	Sensitivity >99% Specificity >99%
	Rate of errors in device interpretation	Correct interpretation rates: 98% for negative, strong positive, and invalid; 95% for low positive.	No interpretation needed.
User Requirements	Result presentation	The result can be read with the naked eye or with an integrated reader. Result wells should be clearly marked and/or not require much instruction or explanation to interpret. Test and control lines are easily distinguishable.	Results are presented in a manner that is self-explanatory and need little or no instructions or explanation to interpret. No weak color lines (and only strong results).
	Level of complexity	Low number of test steps (e.g., three to five) that are easy to conduct.	One easy and intuitive operator step (not timed), excluding waste disposal.
Operational requirements	Sample types	Oral fluid/saliva. Finger-prick whole blood.	Finger-prick capillary blood (maximum 10 L). One swab of gums for oral fluid.
	Sample volume	Finger-prick capillary blood (maximum 50 L). Multiple gum swabs or prolonged oral fluid collection (up to one minute).	One easy and intuitive operator step (not timed), excluding waste disposal.
	Time to result	20 minutes or less.	5 minutes or less.

Table 2.2: PATH requirements for HIVST. Adapted from PATH Target Product Profile HIV Self-Test Version 4.1 [31]

when using commercially available PoCT in the field. A recent study performed in Cape Town, South Africa, highlighted how one commercially available PoCT (brand not specified) was unreliable compared to standards and to another similar commercially available PoCT (also not specified). The levels of sensitivity to HIV infection observed in the clinic increased from 68.7% to 93.5% simply by using a different brand of PoCT for HIV. Both tests claimed a sensitivity of at least 99%.[17]

The most common PoCT for HIV on the market are lateral flow tests. The operating principle is schematised in Figure 2.7. They are cheap, as paper-based, and relatively easy to use. In a similar way to pregnancy tests, a drop of sample is applied at one end of the paper strip and flows through the strip using capillary effect. The presence or absence of a coloured line in the middle of the strip a few minutes after sample addition reveals the presence or absence of the target protein.

The vast majority of the tests on the market meet the requirements of the ideal PoCT in terms of cost, storage conditions and portability. However, some aspects are yet to be fully optimised - or absent, e.g. antigen detection - as is discussed in the following paragraphs.

2.4.2 The interpretation of the test result needs to be easy

One of the main disadvantages of lateral flow tests is the subjectivity involved in interpreting the test. It can be difficult to judge on the presence (or absence) of a line on the test strip if the target protein is present at low concentration, or if the light conditions are not ideal, for example.[8] In 2008, a study in the KwaZulu-Natal province of South Africa investigated the performance of 4 commercially available PoCT for HIV, all lateral flow tests (First Response HIV Card Test 1-2.0 (PMC Medical, India Pvt Ltd), Pareekshak HIV Triline (UCB Pharma), Abbott-Determine HIV-1/2 (Abbott Diagnostics, USA) and Sensa (Seyama Solutions, SA)). Nurses were asked to perform the tests in the field, and the results were compared with the results of the same tests performed in the lab on the same samples by trained technicians. The conclusion of the study was that there was a clear user dependence. If the sensitivity and specificity of the tests proved to be as high as claimed by the manufacturer when performed by trained technicians in the lab, it dropped by a few percent when performed by nurses in the field, arguably because of the subjectivity involved in interpreting the test result.[102]

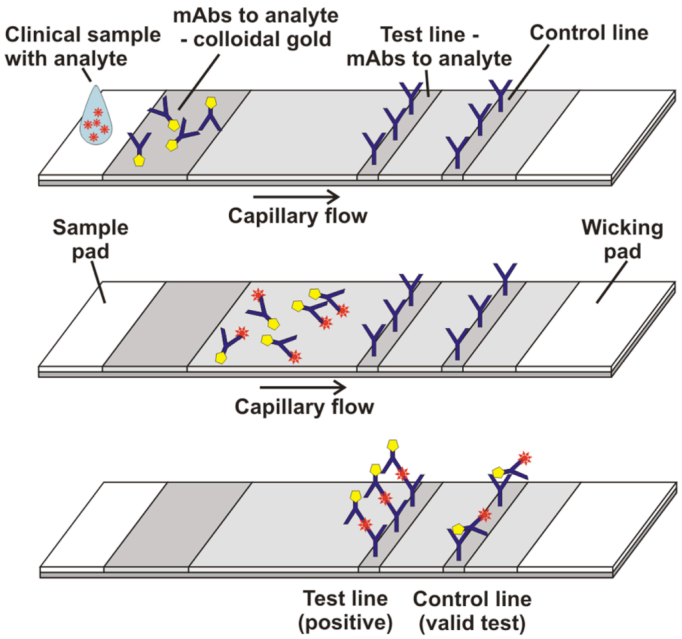

Figure 2.7: Lateral flow test principle. Adapted from [101]. The drop of sample is mixed with gold nanoparticles functionalised with proteins that bind the target protein. Complexes are formed if the target protein is present. The sample then flows through a strip of paper using capillary action. A line in the middle of the paper strip is functionalised with capture proteins engineered or raised against the target protein. If the target protein is present, the complexes they formed with the gold nanoparticles binds to the line, forming an immunosandwich which reveals the line with a red colour: the test is reactive. If the target protein was not present, the gold nanoparticles do not bind the line, no colour appears on the line and the test is negative. An additional line is engineered to bind to anti-human antibodies in a similar way and is used as a control, to ensure the test result is valid.

2.4.3 PoCT would benefit from connectivity

Recently, an optical device has been developed to detect the presence of fluorescently labelled nanoparticles in a sample. The device attaches to a smartphone and uses an inbuilt laser diode to excite fluorescent nanoparticles, and a system of filters and lenses to facilitate a smartphone camera read out of the signal. [22] In general, the smartphone camera and processing power can easily be used, in principle, to perform the readout of simple lateral flow tests. Using a smartphone to interpret the test result has already been applied to the interpretation of drug-of-abuse lateral flow tests. [103] This technique would bring the joint benefit of removing user bias in interpretation of the test result, as well as connectivity. Indeed, lateral flow tests used without an electronic readout cannot record the test results electronically. A recent systematic review of HIV self-tests highlighted the lack of post-test

linkage, counselling and reporting of test result,[104] all of which would be made easier and automatic by using the tests in association with a smartphone.

2.4.4 PoCT need to be simple to use

As mentioned earlier, the simplicity of use is crucial to correct usage. While a number of studies have reported users finding tests easy to use,[105–107] in many studies users did not perform the test correctly. A study conducted in South Africa highlighted the lack of simplicity associated with the use of a commercially available PoCT for HIV (brand not specified), as the sensitivity observed increased from 93.5% to 95.1% when providing additional training to the staff performing the test, instead of relying simply on the instructions provided with the test.[17] In another recent study, a panel of lay participants (i.e. untrained users) were asked to use 5 commercially available HIV self-tests, as well as interpret the results of tests performed using these PoCT. The participants were filmed and the protocol they used was analysed and compared with instructions provided by the test manufacturer. More than three quarters of participants made at least one mistake when performing the test, and test results were correctly interpreted by only 80% of the participants.[24] Similarly, only 15% of participants were found to correctly use a HIVST in a study conducted in Singapore where participants were asked to perform a test using the Abbott Determine HIV-1/2 rapid test (Abbott Laboratories, Abbott Park, IL).[108] The percentage of correct usage of the test can be improved by adapting instructions following feedback from this type of study, as has been shown in Spain using the Determine HIV Combo (Alere, USA)[109] and in Malawi using a commercially available oral HIVST.[110] Aside from lateral flow tests, a recent development using microfluidic has been reported, where an ELISA dongle is used to diagnose HIV and syphilis by performing all the steps of a traditional ELISA on a small chip. The test can easily be connected to a smartphone and has shown promising sensitivity and specificity to biomarkers of HIV infection. Because of the complexity of ELISA, however, this test requires too many steps (currently 7) to be performed by untrained users without prohibitive risk of mistakes and invalid results.[23]

Test	**Manufacturer**	**Time to result (manufacturer's guidelines)**
Determine HIV-1/2 Ag/Ab Combo	Alere, USA	20-40min
Sure Check HIV 1/2 Assay	Chembio Diagnostic Systems, Inc., USA	15-20min
SD Bioline HIV-1/2 3.0	Standard Diagnostics, Inc., UK	10-20min
insti HIV-1/2	bioLytical Laboratories Inc., Canada	5min

Table 2.3: Time to result of some common PoCT used in the UK.

2.4.5 The time to result needs to be reduced to less than 5 minutes

In a study conducted in South Africa, it was found that a majority of participants (nearly 70%) did not wait for long enough and read the test result before the time window recommended by the manufacturers instructions.[17] Lateral flow tests usually require at least 10 minutes between sample injection and result[19], which exceeds both a typical doctors appointment (8-10min in the UK[20]) and the 5 minutes recommended by PATH for HIVST. The time to result of some commonly used PoCT for HIV can be found in Table 2.3. The fastest test on the market at the moment, the insti HIV 1/2 is not fast enough as it requires 5 minutes between sample injection and test result.

2.4.6 The window of detection needs to be reduced

Currently, only one commercially available PoCT is sensitive to recently acquired infections, the Alere Determine HIV-1/2 Ag/Ab Combo (Alere, USA), which detects both antigen (p24) and anti-HIV antibodies. Trials have been conducted and have shown very variable results. When testing samples from sample in acute infection stage, the sensitivity varied from 0% to 82.1% for the antigen, and from 0% to 66.7% for the antibody. The specificity varied from 0% to 100%. When testing samples from patients past the acute infection stage, the results were better: the observed sensitivity ranged from 88.2 to 99.8%, the specificity from 89.5 to 100%.[111–121] These poor field trial results highlight the need for PoCT with the capacity to detect both antibody and antigen.

Chapter 3

SAW Device for Biosensing

The previous chapter gave an insight on the structure of HIV and how it relates to the choice of the best biomarkers of HIV infection. The benefits of developing better PoCT for HIV were presented, as well as an overview of the state of the art in that domain. The limitations of current commercially available tests were pointed out, in the light of recommendations given by the WHO and PATH concerning the design of the ideal PoCT for HIV. This chapter aims at explaining the choice of sensor used as the basis of the smartphone-connected PoCT for HIV presented in this thesis. First, a general introduction to the concept of piezoelectricity and related applications is given. A focus is then made on the use of the piezoelectric effect for sensing perturbations, and the particular case of acoustic wave based sensors is detailed, followed by a brief history of the different types of surface acoustic wave (SAW) sensors. The particular case of the shear-horizontal SAW (SH-SAW) sensor is then explored, with an introduction to the perturbation theory applied to SH-SAW and how it justifies the choice of certain parameters (phase shift ϕ and insertion loss IL) to monitor the perturbation of interest in the context of a biosensor. Finally, the electric circuit used to monitor these parameters is explained.

3.1 Acoustic wave based sensors

3.1.1 Piezoelectricity

Piezoelectricity is a phenomenon observed in some solid materials and is described as the conversion of mechanical stress into a change in electrical polarization, and *vice versa*. The word *piezo* is Greek for "push" or "press", therefore *piezoelectricity* can be interpretated as "electricity resulting from pressure". The phenomenon was discovered by Pierre and Jacques Curie in 1880, and first reported in 1908 after Pierre Curie's death.[122–124] The *direct* piezoelectric effect refers to a change in the electrical polarization of the material when it is subjected to a mechanical stress, whereas the *inverse* piezoelectric effect refers to a deformation of the material when it is subjected to an external electric field. This is illustrated in the schematics in Figure 3.1.

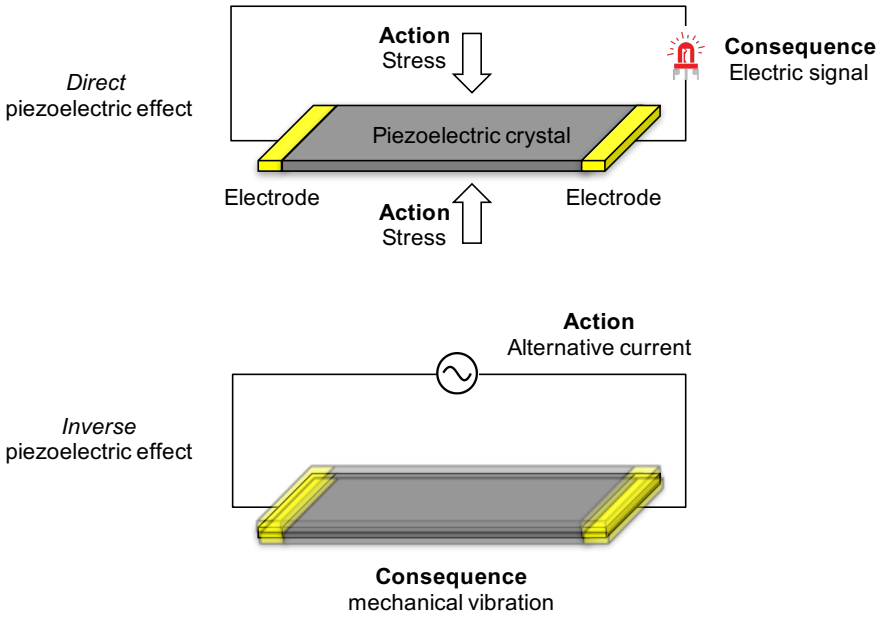

Figure 3.1: Piezoelectric effect. Schematics to illustrate the piezoelectric effect. A piezoelectric crystal is integrated into an electric circuit using two electrodes that are directly attached to the crystal. When stress is applied to the crystal, an electric signal is induced in the circuit, this is the *direct* piezoelectric effect (top). If an alternative current is applied to the circuit, a mechanical vibration of the crystal is observed, this is the *inverse* piezoelectric effect (bottom).

A range of solid materials exhibit the piezoelectric effect. Most of them do so as a result of their anisotropic crystalline structure.[125] However, some materials can be engineered to exhibit piezoelectric behaviour, by using a process called poling, whereby the crystal is

subjected to a very high electric field, which incurs an anisotropy. The piezoelectric effect is exhibited by 20 out of 32 crystal classes,[126] which are associated with noncentrosymmetric crystals, meaning that their unit structure does not possess a centre of symmetry. Some non-crystal piezoelectrics include ceramics and some large proteins have also been found to be piezoelectric, such as DNA.[127]

There are a number of applications of the *inverse* piezoelectric effect, one of the most well known being the use of piezoelectric crystals as actuators. As the movement, or change in dimensions, of a piezoelectic crystal can be controlled down to sub-micrometre accuracy, they are extensively used to position other objects with a high precision. One of the most notable applications is the atomic force microscope (AFM), which uses a number of piezoelectric crystals as actuators to bring the sensing cantilever tip down in contact with the sample, but also to move the sample stage itself in two dimensions in order to scan an area of the sample.

On the other hand, the *direct* piezoelectric effect finds a lot of applications in sensing: a piezoelectric crystal can easily be used to transduce a mechanical vibration into an electric signal. Provided the perturbation of interest results in a mechanical vibration that induces enough stress to generate a vibration of the piezoelectric crystal, the resulting electric signal is a direct indication of the initial perturbation. The most common application of the piezolelectric effect from a sensing perspective is the detection of sound. Indeed, the propagation of a sound wave through a medium corresponds to a variation of pressure (compression and decompression) within this medium. A common example of this application are the piezoelectric microphones found below the strings of an electric guitar. The vibration of the strings generates a sound wave that travels towards the nearby piezoelectric crystal. The sound wave propagates through the crystal and is transduced into an electric signal that can then be amplified and sent to a speaker.

Because the phenomenon is reversible, it is possible to make use of both the *direct* and *inverse* effects to induce the propagation of a mechanical vibration in a piezoelectric crystal using an electric potential, while monitoring the electric signal generated by this mechanical vibration. This allows the monitoring of the mechanical vibration propagating through the crystal and forms the basis of most acoustic wave based biosensors, including the one presented in this thesis. Such biosensors generate and monitor a baseline vibration that

can be affected by very fine pertubations occuring on the surface of the crystal.[128,129] These fine perturbations could not be detected using the *direct* piezoelectric effet only.

The mechanical vibration resulting from the application of an electric potential to the piezoelectric crystal is characterised by its direction of propagation, as well as the particle displacement direction, which indicates the direction of movement of the particles when the wave propagates through the crystal. A piezoelectric crystal can be cut to different angles with regards to its centre of symmetry and unit structure. The choice of the cut of the crystal has important consequences for the use of the *inverse* piezoelectric effect, as it defines the direction of propagation of the wave through the crystal, as well as the particle displacement direction.[130] The following section details the main categories of acoustic wave sensors that have been reported for sensing applications. Depending on the crystal used and the cut chosen, different modes of acoustic wave propagation are observed. In order to simplify the notation and compare between modes of operation of the different sensors presented, all the propagation directions and particle displacement directions mentioned refer to those as shown in Figure 3.3.

3.1.2 Quartz crystal microbalance (QCM)

The first acoustic wave sensor was reported in 1959 by Sauerbrey.[131] He described a gas sensor based on a quartz crystal connected to a plate electrode on top and grounded at the bottom. Applying an electric potential to this system generates an acoustic wave that propagates as a thickness shear mode (TSM). In this mode, the wave propagates in the x_3 direction, and the particles are displaced in a direction contained in the (x_1x_2) plane, as can be seen in Figure 3.3.

Sauerbrey's 1959 paper featured the equation that gives a directly linear relationship between the shift in frequency and the mass added on the surface of the crystal:

$$\Delta f = C\Delta m, \tag{3.1}$$

where Δf is the shift in the acoustic wave frequency before and after perturbation, Δm is the mass added to the surface of the crystal and causing the perturbation, and C is a

material constant that depends on the crystal density, shear modulus and surface area of the crystal used, as well as the resonnant frequency.

Over the years, QCM has been very popular in the field of gas sensing, with many applications reported such as the detection of methane,[132] ammonia[133] or nitric oxyde.[134]

QCM was used as a sensor in liquid medium for the first time in 1980, when Nomura and Minemura reported the application of QCM to detect the presence of cyanide in aqueous solution.[135] This was a major step towards the use of acoustic wave sensors as biosensors, most of which require the sample to be in liquid form. A few years later, Kanazawa and Gordon derived the Sauerbrey equation to relate the frequency shift to viscosity and density of the liquid.[136] QCM has since then been used for numerous applications, such as the monitoring of phase transitions in polymers,[137] the study of protein adsorption[138] or the detection of DNA for diagnosis.[139] However, one of the limitations of QCM is the thickness of the crystal: the frequency shift in equation 3.1, which is key to the sensitivity of the device, is inversely proportional to the thickness of the crystal. Therefore, for each type of crystal, there is a physical limit to how sensitive a QCM can be, which corresponds to the minimum possible thickness of the crystal used. Other types of acoustic wave sensors have been developped since the early 1980s, using different modes of acoustic wave propagation.

3.1.3 Interdigitated transducer (IDT) induced surface acoustic waves

A number of other acoustic wave based sensors have been reported over the years, each of them being associated with a particular type of acoustic wave. Those acoustic waves, referred to as surface acoustic waves (SAW) differ by their mode of propagation, but have in common the fact they are induced by IDTs in contact with the crystal. The concept of IDTs was first introduced by White and Voltmer in 1965.[140] The IDTs play the role of the electrodes that transduce the electric signal into a mechanical vibration (input IDT) and *vice-versa* (output IDT).[141]

An IDT consists of an array of electrodes directly attached to the surface of the piezoelectric crystal.[130] The array of electrodes consists of an alternation of positive and negative electrodes. Applying an electric potential to an electrode generates a distortion of the material around the electrode. Combined with all the electrodes in the array, when applying an alternative current, the individual distortions construct into a mechanical wave that

propagates in the crystal. This is schematised in Figure 3.2. As explained above, the mode of propagation of the acoustic wave generated depends on the crystal type and crystal cut. The design of the IDT defines the acoustic wavelength λ, as two electrodes of opposite polarity are separated from each other by a distance of λ. Similarily, the operating frequency of the device is dictated by the geometry of the IDT.[142] When two IDTs are present (input and ouptut), the distance in between the two IDTs is called the delay line. Its surface corresponds to the area of propagation of the SAW, and is also referred to as the sensing area.

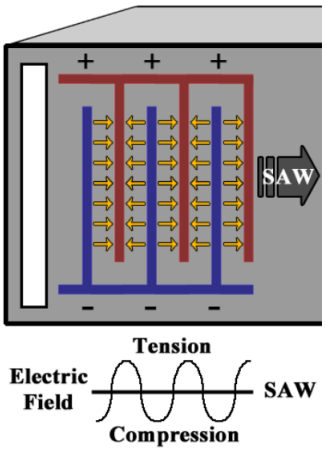

Figure 3.2: Interdigitated transducers. Schematic to illustrate the principle of operation of IDT. Applying an alternating current to the electrodes of opposite polarity (blue and red) results in the electric field represented by the yellow arrows. The deformation of the crystal around each individual electrode creates regions of tension and compression alternating between the electrodes. The resulting mechanical wave then propagates away from the IDT. Adapted from Kirschner *et al.*[143]

Acoustic waves generated by IDT are extensively used in the telecommunications industry. As a radio wave is emited at a fixed frequency, if the IDT on the SAW device is designed to operate at this resonance frequency, it will transduce the vibration of the radiowave into an electric signal. Therefore, such devices are mainly used as frequency filters: out of the many electromagnetic waves emited in its environment, the acoustic wave device will only pick the one associated with its operating frequency and translate it into an electric signal. Some of the different modes of acoustic wave propagation are detailed in Figure 3.3.

A Rayleigh SAW (R-SAW) propagates in the x_1 direction, and the particles are displaced in the x_1 and x_3 directions. Lord Rayleigh predicted the existence of R-SAW in 1885,[25] and the use of a Rayleigh wave based acoustic device as a gas sensor was reported for the

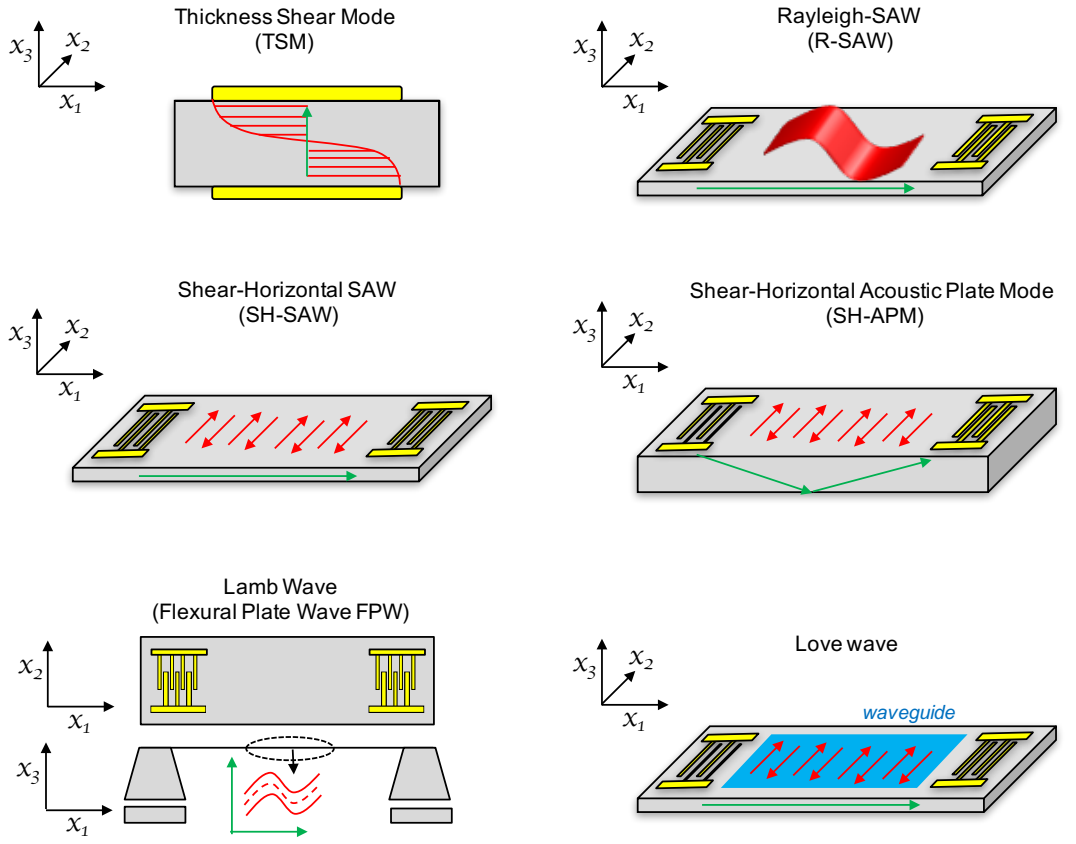

Figure 3.3: Acoustic wave based sensors. Schematics to illustrate the different acoustic wave modes of propagation. On each schematic, the green arrows represents the direction of propagation, the red arrows represent the particle displacement directions.

first time in 1979 by Wohltjen and Dessy.[144] They demonstrated the ability of their sensor to detect thermomechanical perturbations. They published two additional papers the same year, one reporting the use of their Rayleigh wave based device as a way to detect phase transitions in polymers,[145] the other one describing the use of such a device to perform gas chromatography and detect various polar and non-polar molecules.[146] It was only a few years later that the same authors published a proposition of an analytical explanation of their experimental results,[147] based on the perturbation theory applied to SH-SAW described later.

In 1987, Moriizumi *et al.*[26] reported the use of a leaky Shear Horizontal SAW (SH-SAW) based device as a sensor in liquid, and also demonstrated a method to estimate the ideal crystal cut in order to achieve the optimal sensitivity for biosensing applications. A SH-SAW propagates in the x_1 direction, particles are displaced in the x_2 direction. The biosensor presented in this thesis is based on a SH-SAW device. An approach to understanding

the theory behind the sensing mechanism of SH-SAW devices was proposed by Auld [148] and further refined by Kondoh *et al.* [149] A detailled description of the approach is provided in the next section.

The use of Shear Horizontal Acoustic Plate Mode (SH-APM) as a sensor was first reported by Ricco and Martin in 1987, when they described a device capable of measuring the viscosity of liquid samples. [150] Later on that year, SH-APM was reported to be used as a chemical sensor, for the detection of Cu^{2+} ions. [151] In this configuration, the acoustic wave propagates in the x_1 and $-x_3$ directions, while the particles are displaced in the x_2 direction.

In the Flexural Plate Wave (FPW) mode, the acoustic wave, also called a Lamb Wave, propagates in the x_1 and $-x_3$ directions, and the particles are displaced in the x_1 and x_3 directions. In this configuration, the sensing surface is on the opposite side of the IDTs, which adds complexity to the design of the device as it requires the crystal to be mounted on a support, as can be seen in Figure 3.3. Indeed, the particles located in the section formed between the IDTs on the opposite surface of the crystal have to be be able to be displaced without being in contact with anything other than the sample. The use of a Lamb Wave sensor was first reported by White and Wenzel in 1988. [152]

A leaky SH-SAW, which propagates both along the surface (x_1 direction) and inside the crystal ($-x_3$ direction) can be transformed into a pure SH-SAW by adding a thin film of a different material on the surface of the crystal, in between the IDTs. The resulting wave, called a Love Wave, only propagates in the x_1 direction, while the particles are displaced in the x_2 direction, as in the pure SH-SAW mode. To achieve this result, the velocity of the acoustic wave through the guiding layer on the surface has to be significantly smaller than the velocity of sound in the crystal below. The first sensor using a Love Wave was reported in 1992 by Gizeli *et al.* [27] Since then, a number of biosensing applications have been reported, for example the monitoring of adsorption of phospholipids [153] or the detection of nucleid acids. [154]

3.1.4 Clinical applications of acoustic biosensors

Acoustic wave-based sensors have been used to detect the presence of a number of pathogens in clinical samples. A study by Berkenpas *et al.* presented the detection of *Escherichia*

coli O157:H7, present in food and water samples and responsible for severe diarrhea or kidney failure.[155] They obtained their results using a prototype system which is a first step towards a point-of-care test. Detection of the same pathogen was also detected by Deobagkar *et al.* using a SH-SAW sensor.[156] Howe and Harding also reported the use of a Love-wave device to quantitatively detect the presence of *Legionella* and *E. Coli.*[157]

Applications of acoustic wave-based sensors for viral infection diagnosis have also been reported. A number of such applications involve using QCM to detect the presence of avian influenza virus H5N1,[158,159] fish pathogenic virus (VHSV),[139] dengue virus,[160] or more recently, hepatitis B.[161] Wang *et al.* demonstrated the use of a leaky SAW sensor to detect the presence of human papilloma virus and quantify the levels of virus in human samples, and reported a good agreement between their results and a more conventional PCR-based method.[162] Hepatitis B surface antibodies (HBsAb) can also be detected in whole blood samples, according to a study by Lee *et al.*[163]

The detection of presence of a number of biomarkers in human samples, down to clinically relevant concentrations, can be achieved using acoustic wave biosensors. Gizeli *et al.* combined a SAW sensor and microfluidics to build a system able to detect multiple cardiac markers in order to inform cardiovascular risk assessment.[164] Martin *et al.* demonstrated the use of QCM for cholesterol determination in clinical samples,[165] while Yao *et al.* used a SAW resonnator to analyse the amount of urease in whole blood samples, using the relation between frequency shift and the solution conductivity. They showed the results obtained with the biosensor compared favourably to gold standard methods and could therefore be used for diagnostic purposes.[166].

Acoustic wave sensors can also be used to detect genetic mutations in DNA. Gronewold *et al.* disentangled the mass and viscosity contributions of the signal measured using a Love-wave sensor to detect individual point mutations in DNA fragements of genes associated with cancer.[167] Another interesting application that was reported is the estimation of blood pressure. Ye *et al.* reported the modelling and fabrication of a series of SAW devices that can be used to evaluate the pressure of blood, in the hope this can be implemented to a wireless and passive implantable blood pressure device.[168]

The work presented in this thesis explores the use of a SH-SAW device as a biosensor. This was justified by the fact SH-SAW devices meet most of the criteria for the ideal PoCT for HIV presented in Chapter 2. They are already mass-manufacturaed for the

telecommunications industry, therefore their production cost is low enough to consider them disposable. As will be shown in the following chapters, they can be enginereed to detect biomarkers of HIV infection with very high sensisitivty and specificity, in a very simple one step test. Additionally, they offer the potential for extremely fast time to result, as will be described further on. To this date, a number of biosensing applications using SH-SAW devices have been reported. Kondoh *et al.* immobilised different enzymes on the surface of the delay line to detect variations in pH of the solution following enzymatic reaction.[169] The detection of various antibodies[155,170] and bacteria[157] have also been reported, as well as the detection of DNA hybridization.[171] In all of these cases, the general principle is the monitoring of the SH-SAW and how it is affected by the perturbation of interest. The following introduces the concepts and notations necessary to the study of the perturbation of a SH-SAW.

3.2 Perturbation of a Shear Horizontal SAW

3.2.1 Parameters of interest and notations

A sensor measures the variation of one or more parameters. Those parameters vary following the nature and intensity of the perturbations occuring at the sensor proximity or, in the case of this thesis, on the sensor surface. In the following calculations, the indexes 0 and 1 are used to describe a given parameter before and after a perturbation has occured on the surface:

$$\begin{cases} W_0 & \text{describes the parameter } W \textbf{ before} \text{ perturbation} \\ W_1 & \text{describes the parameter } W \textbf{ after} \text{ perturbation.} \end{cases} \tag{3.2}$$

The wave velocity V (m.s^{-1}) can be defined as:

$$V = \frac{\lambda\omega}{2\pi} = \lambda f, \tag{3.3}$$

where λ (m) is the wavelength, ω (radian.s^{-1}) is the angular frequency and f (s^{-1}) is the frequency.

The wave angular frequency ω, expressed in radians or in degrees, is linked to the wave frequency f by the relation:

$$\begin{cases} \omega = 2\pi f \quad \text{(rad)} \\ \omega = 360 f \quad \text{(deg)}. \end{cases} \tag{3.4}$$

In the particular case of the device used here, the frequency is fixed, therefore in the following no indices will be attributed to the notation f or ω ($f_0 = f_1 = f$ and $\omega_0 = \omega_1 = \omega$). This is due to the choice of electric circuit used to drive the crystal and monitor the parameters, and is detailed further on.

The wave number k_0 (m^{-1}) can be described using the wave angular frequency ω, the wavelength λ and the wave velocity in the crystal V:

$$k_0 = \frac{2\pi}{\lambda} = \frac{\omega}{V}. \tag{3.5}$$

The acoustic wave is characterised by its complex propagation factor β, which can be defined as[172]:

$$\beta = \alpha + jk_0, \tag{3.6}$$

where k_0 is the wave number, α is the attenuation coefficient and j is the imaginary unit satisfying the equation $j^2 = -1$.

If we define the difference in complex propagation factor $\Delta\beta$ before and after perturbation as:

$$\Delta\beta = \beta_1 - \beta_0, \tag{3.7}$$

then the following expression of the difference in complex propagation factor $\Delta\beta$ normalised by the wave number k_0, can be derived, assuming that the change in velocity is comparibly negligible with respect to the initial velocity ($\Delta V \ll V_0$):[172]

$$\frac{\Delta\beta}{k_0} = \frac{\Delta\alpha}{k_0} - j\frac{\Delta V}{V_0}. \tag{3.8}$$

The imaginary part $\frac{\Delta V}{V_0}$ and real part $\frac{\Delta\alpha}{k_0}$ will be referred to as *velocity change* and *attenuation change* (respectively). Those two parameters contain useful information for the analysis of the propagation of an acoustic wave submitted to perturbations. They are the key parameters involved in the perturbation theory applied to SH-SAW devices, which is presented below.

3.2.2 Perturbation theory, applied to SH-SAW

In 1973, Auld applied the perturbation theory to the problem of solving the propagation of an acoustic wave launched on the surface of a piezoelectric crystal. He derived a relation between the complex propagation constant defined in equation 3.6 and the acoustic wave equation.[148] In 1993, Kondoh and Shiokawa applied Auld's work to the specific case of a SH-SAW device sensing perturbations in a liquid sample. They derived a relation between some of the wave parameters (*velocity change* and *attenuation change*) and some of the sample characteristics, presented below.[173]

The first set of equations corresponds to a **viscosity** perturbation, which means the SH-SAW is perturbed by a change in viscosity only on the surface of the delay line. The assumptions that lead to the following expression of the *velocity change* and *attenuation change* are that the acoustic wave propagates in a pure SH-SAW mode, and that the sample on the surface of the delay line is a Newtonian fluid. Under these assumptions:

$$\frac{\Delta V}{V_0} = -\frac{V_0 v_2^2}{4\omega P}\left(\sqrt{\frac{\omega\rho_1\eta_1}{2}} - \sqrt{\frac{\omega\rho_0\eta_0}{2}}\right), \tag{3.9}$$

$$\frac{\Delta\alpha}{k_0} = \frac{V_0 v_2^2}{4\omega P}\sqrt{\frac{\omega\rho_1\eta_1}{2}}, \tag{3.10}$$

where V_0 and k_0 are the velocity and wave number (respectively) before perturbation, v_2 is the particle velocity in the displacement direction x_2, ω is the angular frequency, P is the sample power flow, ρ_0 and η_0 are the sample density and viscosity (respectively) before

perturbation. ρ_1 and η_1 are the sample density and viscosity (respectively) after perturbation.

The second set of equations in the perturbation theory appplied to SH-SAW refers to a **mass** perturbation. This means that the propagation of the SH-SAW is attenuated by the formation of a thin film on the surface of the delay line. Once again, the acoustic wave is assumed to propagate in a pure SH-SAW mode. In addition, the thin film formed on the surface of the delay line is assumed to be uniform and isotropic, and the material that it consists of is assumed to be a hard material. Under these assumptions, the *velocity change* and *attenuation change* can be expressed as:

$$\frac{\Delta V}{V_0} = -\frac{V_0 h}{4P}\left(\rho_1 - \frac{\mu_1 \beta^2}{\omega^2}\right) v_2^2, \tag{3.11}$$

$$\frac{\Delta \alpha}{k_0} = 0, \tag{3.12}$$

where h is the thickness of the film deposited on the surface, μ_1 is the Lamé constant of the film formed on the surface and β is the complex wave number.

A third set of equations gives an estimation of the electric perturbation however it is not applicable here as the biosensor features a thin gold layer on top (see Chapter 4) that acts as an electric shield for the crystal. Therefore the SH-SAW cannot be perturbed electrically. Finally, an additional set of equations was derived by Kondoh *et al.*[174] to express the *velocity change* and the *attenuation change* following a perturbation of the viscoelasticity at the proximity of the crystal surface.

The *velocity change* and the *attenuation change* are the key parameters in the perturbation theory applied to SH-SAW. Taking into account the assumptions that led to their expression, they provide information about the perturbation of interest. In the following, the exact approximation of the two parameters presented in equations 3.9 to 3.12 (as well as the set of equations proposed by Kondoh *et al.*) will not be used as such as they require some assumptions that are not matched by the perturbations of interest in the context of

a biosensor. As an example, the binding of proteins to the surface of the delay line is very unlikely to drive the formation of a hard, uniform isotropic thin film.

However, the fact that these equations show that the two parameters are directly linked perturbations occuring on the surface of the delay line is key to justify the results presented in Chapters 5 to 8. Indeed, the perturbation caused by the binding of proteins to the surface of the delay line is likely to consist of a combination of the simple perturbations considered in the perturbation theory described above (viscosity and mass). Because the *velocity change* and the *attenuation change* are not directly measurable, it is essential to relate them to measurable parameters in order to be able to monitor the perturbation, and possibly extract information about the nature of the perturbation. The following demonstrates how to express the *velocity change* and the *attenuation change* as a function of measurable parameters.

3.3 Expressing the key parameters of the perturbation theory applied to SH-SAW as a function of measureable parameters

3.3.1 Relation between Velocity and Phase shift

The phase shift ϕ corresponds to the difference in phase between the initial electric signal applied to the input IDT, and the electric signal measured at the output IDT after conversion of the acoustic wave back into an electromagnetic wave. The phase shift is defined as:

$$\phi = \frac{\omega L}{V}, \tag{3.13}$$

where L is the length of the delay line. Therefore, the output phase shifts ϕ_0 and ϕ_1 before and after perturbation (respectively) can be expressed as:

$$\begin{cases} \phi_0 = \frac{\omega L}{V_0} \\ \phi_1 = \frac{\omega L}{V_1}. \end{cases} \tag{3.14}$$

If we define the difference in output phase shift before and after perturbation as:

$$\Delta\phi = \phi_1 - \phi_0, \tag{3.15}$$

and the difference in wave velocity before and after perturbation as:

$$\Delta V = V_1 - V_0, \tag{3.16}$$

then the following relation can be obtained, assuming that the change in velocity is comparibly neglegible to the initial velocity ($\Delta V \ll V_0$):

$$\frac{\Delta\phi}{\phi_0} = -\frac{\Delta V}{V_0}. \tag{3.17}$$

From equation 3.17 and the definition of ϕ_0 in equation 3.14, the relation between the *phase change* and the *velocity change* can be derived:

$$\frac{\Delta V}{V_0} = -\frac{V_0}{\omega L}\Delta\phi = -\frac{V_0}{2\pi f L}\Delta\phi. \tag{3.18}$$

Note: The value of the initial wave velocity V_0 can be modelled knowing the design of the input IDT.

3.3.2 Relation between Attenuation and Amplitude

The amplitude A of a plane acoustic wave propagating through a crystal decays as a function of the distance x, which is expressed by the equation:

$$A = A_0 e^{-\alpha x}, \tag{3.19}$$

where A_0 is the initial amplitude and α is the attenuation coefficient.

The output amplitude A_{out} of a SH-SAW device characterised by a driving amplitude A_{in} and a delay line of length L can therefore be expressed as (assuming the SH-SAW propagates purely in one direction):

$$A_{out} = A_{in}e^{-\alpha L}. \tag{3.20}$$

If we define α_0 and α_1 as the attenuation coefficients before and after perturbation (respectively), then the output amplitudes A^0_{out} and A^1_{out} before and after perturbation (respectively) can be expressed as:

$$\begin{cases} A^0_{out} = A_{in}e^{-\alpha_0 L} \\ A^1_{out} = A_{in}e^{-\alpha_1 L}. \end{cases} \tag{3.21}$$

If we define the attenuation change $\Delta\alpha$ as:

$$\Delta\alpha = \alpha_1 - \alpha_0, \tag{3.22}$$

then it can be expressed, using equation 3.21 as:

$$\Delta\alpha = -\frac{1}{L}\ln\left(\frac{A^1_{out}}{A^0_{out}}\right), \tag{3.23}$$

which leads to the expression of the attenuation change:

$$\frac{\Delta\alpha}{k_0} = -\frac{1}{k_0 L}\ln\left(\frac{A^1_{out}}{A^0_{out}}\right). \tag{3.24}$$

Conclusion: Both key parameters in the perturbation theory applied to SH-SAW, the *velocity change* and the *attenuation change*, can be expressed as a combination of known quantities and the two measurable parameters that are the phase shift ϕ and the output amplitude A_{out}. The results obtained using the SH-SAW device and presented in Chapters 5 to 8 were obtained by monitoring ϕ and a parameter called the insertion loss (IL). The insertion loss is directly related to A_{out}, as will be shown in the following section.

3.4 Monitoring the phase shift ϕ and insertion loss IL : electric circuit

Depending on the design of the electric circuit used to drive the SAW device, different parameters can be monitored. There are two main types of circuits used: phase fixed circuit, and frequency fixed circuit. In a phase fixed circuit, one of the measured outputs is the frequency shift. This requires a feedback loop that allows the signal generator to adapt the input signal in order to fix the phase shift to 0. In other words, this type of circuit monitors the frequency shift needed to achieve a zero phase shift despite the perturbation occuring on the surface of the delay line. The insertion loss is also an output.

The electric circuit used to obtain the results presented in this thesis is a frequency fixed circuit. The output parameters are the phase shift ϕ and the insertion loss IL. A schematic of the circuit is shown in Figure 3.4, and the following section details the differents components on this schematic.

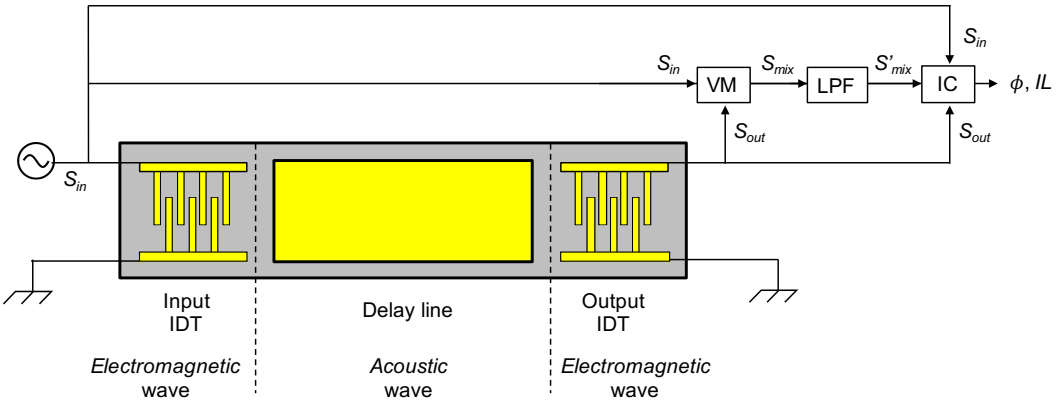

Figure 3.4: SH-SAW electric circuit. Schmatic of the electric circuit used to monitor ϕ and IL. The SH-SAW device receives the input signal S_{in} at the input IDT. The electromagnetic wave is transduced into an acoustic wave which travels along the delay line, before being transduced back into an electromagnetic wave at the output IDT. S_{in} and the output signal S_{out} are multiplied together by the voltage multiplier VM. The resulting signal S_{mix} goes through a Low Pass Filter to eliminate the high frequency term of S_{mix}. The resulting signal S'_{mix} is sent to the integrated circuit IC, which perfoms the operations to output the phase shift ϕ. Both $S_{in}$and S_{out} are also sent directly to the IC, which perfoms the operations to output the insertion loss IL.

3.4.1 Phase shift

Monitoring the phase shift ϕ is the result of a process that involves an integrated circuit to perform operations on electrical signals. The signal sent to the input IDT is an electromagnetic wave that can be described as:

$$S_{in} = A_{in} \cos(\omega t), \tag{3.25}$$

where A_{in} is the amplitude of the input signal, measured at the input IDT.

As explained earlier, after being converted into an acoustic wave, travelling along the delay line between the IDTs and converted back into an electromagnetic wave, the wave has been submitted to a phase shift ϕ and an amplitude change. This is illustrated in Figure 3.5 at the end of this section. The output signal has the form:

$$S_{out} = A_{out} \cos(\omega t + \phi), \tag{3.26}$$

where A_{out} is the amplitude of the output signal, measured at the ouput IDT.

As can be seen in Figure 3.4, the input signal and the output signal are multiplied in a voltage multiplier. The resulting signal, called S_{mix}, can be expressed as:

$$S_{mix} = \gamma S_{in} S_{out}, \tag{3.27}$$

where γ is a constant which depends on the configuration of the voltage multiplier.

S_{mix} can be derived as:

$$\begin{aligned} S_{mix} &= \gamma A_{in} A_{out} \cos(\omega t) \cos(\omega t + \phi) \\ &= \frac{\gamma}{2} A_{in} A_{out} [\cos\phi + \cos(2\omega t + \phi)]. \end{aligned} \tag{3.28}$$

The term $\cos(2\omega t + \phi)$ represents a high frequency signal. It is filtered out using a Low Pass Filter (LPF). Therefore, the remaining signal S'_{mix} after the voltage multiplier and the LPF can be expressed as:

$$S'_{mix} = \frac{\gamma}{2} A_{in} A_{out} \cos(\phi). \tag{3.29}$$

The amplitudes A_{in} and A_{out} are measured directly at the input and ouput IDT (respectively). The phase shift ϕ can therefore be extracted from the signal S_{mix} measured at the output IDT using the integrated circuit to perfom the following operation:

$$\phi = \arccos\left(\frac{2S'_{mix}}{\gamma A_{in} A_{out}}\right). \tag{3.30}$$

3.4.2 Insertion loss

3.4.2.1 Definition of the insertion loss

To introduce the concept of insertion loss, it is important to define the decibel (dB) unit. A decibel is a relative measure of two different power levels. It is used for quantifying the gain G (or loss, if the gain value is negative) of one device in relation to another one. It is not an absolute number, but a ratio. The formula for calculating the gain between two devices of respective electrical powers P_1 and P_2 is given by:

$$G = 10\log_{10}\left(\frac{P_1}{P_2}\right). \tag{3.31}$$

In the particular case of comparing the output power P_{out} to the input power P_{in} of a device, the gain will be defined as:

$$G = 10\log_{10}\left(\frac{P_{out}}{P_{in}}\right). \tag{3.32}$$

If $P_{out} > P_{in}$, it is common to use the term gain, while if $P_{out} < P_{in}$, it is more common to use the term loss. For example, if:

$$\frac{P_{out}}{P_{in}} = 10^{-3}, \tag{3.33}$$

it is common to say the device is characterised by a loss of -30dB.

In the particular case of the SH-SAW device used in this work, the loss of electrical power is caused by the presence of the sensor in the circuit: the amplitude of the electromagnetic wave measured at the ouput IDT is attenuated compared to the one sent to the input IDT. This simply corresponds to an attenuation of the acoustic wave amplitude as a consequence of being exposed to a perturbation. This is illustrated in Figure 3.5 at the end of this section.

In the case of an alternating current (AC), the electric circuit power P (measured in Watt, W, averaged over a period of time proportional to the the wave time period), is defined in relation to the electric current I (Ampere, A), electric voltage E_v (Volt, V) and the circuit resistance R (Ohm, Ω):

$$P = \frac{E_v^2}{R} \quad = IR. \tag{3.34}$$

In the circuit used in this thesis, the input signal is a sinusoidal wave that can be described by the simple wave function:

$$z(t) = A_{in} \cos(\omega t). \tag{3.35}$$

Although the electrical power can not be measured directly, the amplitude is a measurable parameter as it corresponds to the electric voltage. By measuring the output voltage $(E_v)_{out}$, it is therefore possible to calculate the absolute output power P_{out} using equation 3.34 and then the loss due to the presence of the device in the circuit.

Note: In the particular case of the electric circuit used in this thesis, the circuit resistance R is equal to 50Ω and the input power P_{in} is $1mW$. Therefore, using equation 3.34, the input voltage $(E_v)_{in}$, or driving amplitude A_{in} can be calculated:

$$A_{in} = \sqrt{RP_{in}} = 223mV. \tag{3.36}$$

3.4.2.2 Expression of the insertion loss

The insertion loss IL corresponds to the loss of electrical power in the circuit, which according to equation 3.32 can be expressed as:

$$IL = 10 \log_{10} \left(\frac{P_{out}}{P_{in}} \right). \tag{3.37}$$

Combining with equation 3.34, this transforms into:

$$IL = 20 \log_{10} \left(\frac{A_{out}}{A_{in}} \right). \tag{3.38}$$

The insertion loss can therefore be monitored by measuring A_{in} and A_{out}. The change in insertion loss ΔIL following a perturbation can then be defined as:

$$\Delta IL = IL_1 - IL_0. \tag{3.39}$$

Since the input amplitude A_{in} is constant regardless of the perturbation, combining equations 3.38 and 5.2 leads to:

$$\Delta IL = \frac{20}{\ln(10)} \ln \left(\frac{A^1_{out}}{A^0_{out}} \right). \tag{3.40}$$

Finally, combining equations 3.24 and 3.40 leads to the following expression of the insertion loss:

$$\Delta IL = -\frac{20}{\ln(10)} \Delta \alpha L. \tag{3.41}$$

It was therefore shown that monitoring the amplitude at the output IDT A_{out} is directly related to monitoring the insertion loss IL. In addition, monitoring the change in insertion loss ΔIL before and after a perturbation is an easy way to get an indication of the change in attenuation coefficient $\Delta \alpha$ associated with that perturbation.

3.4.3 Illustration of the effect of a perturbation on both the electromechanical and acoustic wave

As explained above, the principle behind using a shear-horizontal surface acoustic wave device to detect and quantify a perturbation occuring on the surface of the delay line relies on the transduction of an electromechanical wave into an acoustic vibration, and *vice versa*. By being exposed to a perturbation when in the form of an acoustic wave, the wave amplitude is attenuated and the wave undergoes a phase shift ϕ. This concepts is illustrated in Figure 3.5.

Under the initial state (perturbation 0), which could correspond to the delay line being in contact with buffer for example, the electromagnetic wave measured at the output IDT (top left plot, blue line) is characterised by an initial phase shift ϕ_0 from the input signal (black line) as well as an amplitude A^0_{out} that differs from the initial amplitude A_{in}. This is because the acoustic wave has been submitted to this first perturbation when travelling along the delay line (blue line, right hand side plot). Under the next perturbation (perturbation 1) - which could correspond to a change in sample viscosity, or to the binding of a protein to the surface of the delay for example - the electromagnetic wave measured at the ouptut IDT (bottom left plot, orange line) is characterised by a different phase shift ϕ_1 as well as a different amplitude A^1_{out}.

Monitoring the change in phase shift $\Delta\phi$ and insertion loss ΔIL (based on the measure of A^0_{out} and A^1_{out}) provides information on what happened at the surface of the delay line, which corresponds to a change in the perturbation the SAW device was submitted to. This change in perturbation can be measured from one sample to another. More interestingly, as ϕ and A_{out} can be measured continuously, the change in perturbation can be monitored continuously within the same sample. In this case, the change in pertubation occurs over time instead of corresponding to a change of sample. This allows, for example, the monitoring of proteins slowly binding to the surface of the sensor. Most of the results presented in Chapters 5 to 8 were obtained using this principle.

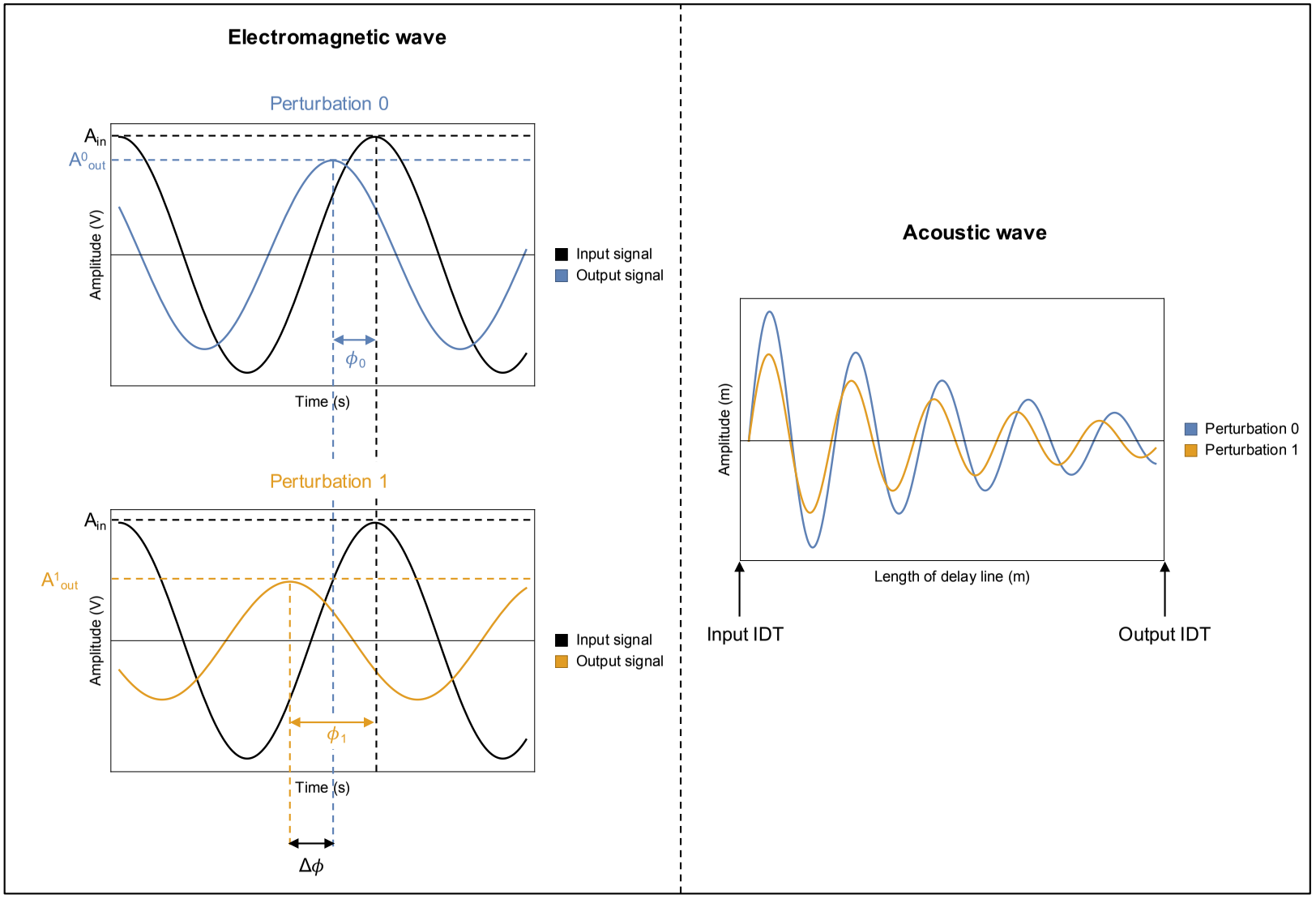

Figure 3.5: Representation of the electromagnetic and acoustic wave. On the left hand side, the electromagnetic wave measured at the input and ouput IDT is represented, for two different perturbations. On the right hand side, the acoustic wave is represented for both perturbations. The coloured line correpsonding to the output signal on each of the left hand side plots represents the transduced acoustic wave at the specific point corresponding to the end of the delay line

Chapter 4

Materials and Methods

4.1 SAW biosensor prototype

The prototypes of SAW biosensor used during this work consists of three components: (i) a disposable SAW device; (ii) a control box sending and receiving the signal to and from the SAW device; (iii) a portable device (smartphone or laptop) with processing power to analyse the data generated by the control box. This device is also used to power the control box.

Two versions of SAW biosensors were developed by industrial partners OJ-Bio Ltd. They are presented in Figure 4.1. The laboratory version, described further on, was used throughout this work to generate the results presented in Chapters 5 to 8. A more advanced development prototype device, containing all the same elements as the laboratory prototype, is shown in Figure 4.1b and 4.1d, where the SAW biochip is mounted on a disposable cassette resembling a USB stick and results sent to a smartphone app either via a cable or via Bluetooth. This prototype was not used for the work presented here.

4.1.1 Laboratory control box

The pocket-sized laboratory control box ($14\times10\times4$ cm^3) sends and receives an analog signal to and from the SAW devices, and converts it to a digital signal. Up to four SAW devices can be connected in parallel to the control box via the four chip holders, allowing for multiplex detection of different biomarkers and control measurements. The analog signal

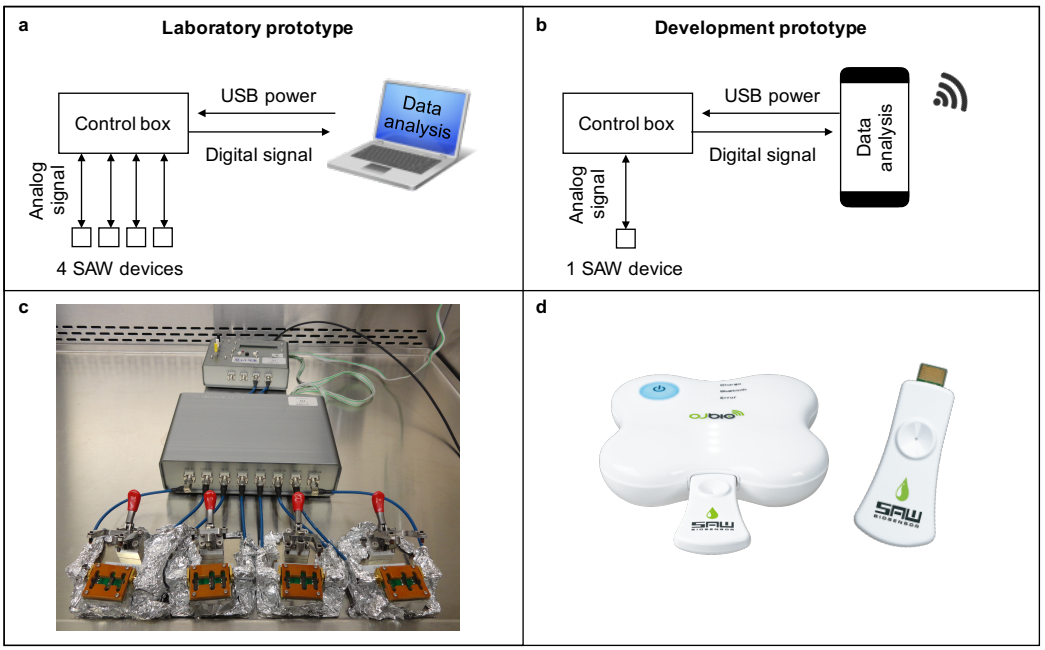

Figure 4.1: SAW biosensor prototype: laboratory and development versions. **a)** Schematic to illustrate the components of the SAW biosensor laboratory prototype. The control box sends/receives an analog signal to/from 4 SAW devices in parallel (one per chip holder), and transmits a digital signal to the laptop. A software processes and analyses the data. **b)** Schematic to illustrate the components of the SAW biosensor development prototype. The control box sends/receives an analog signal to/from the disposable SAW devices, and transmits a digital signal to the smartphone. An app processes and analyses the data, before sending it to public healthcare systems. **c)** Photograph of the laboratory control box and 4 chip holders. **d)** Photograph of the hand-held SAW biosensor development prototype and disposable SAW device.

generated by the control box and sent to the input IDT is characterised by an amplitude of 223mV (see calculations in Chapter 3, equation 38) and a frequency of 251.5MHz.

The elements of the electric circuit used by the control box to extract the phase shift and insertion loss are detailed in Chapter 3. The file ouput by the control box is a .csv file containing the phase shift and insertion loss measured every second, for each SAW device. The SAW device described further on was slotted in the chip holder, and samples were pipetted on and off the surface of the delay line using a manual pipette. An example of the data output by the control box is presented in Figure 4.2.

4.1.2 OJ15 SAW device

The SH-SAW device referred to as OJ15 SAW device was designed using a quartz crystal (36°Y-cut 90°X-propagation). Quartz was chosen over other commonly used substrates

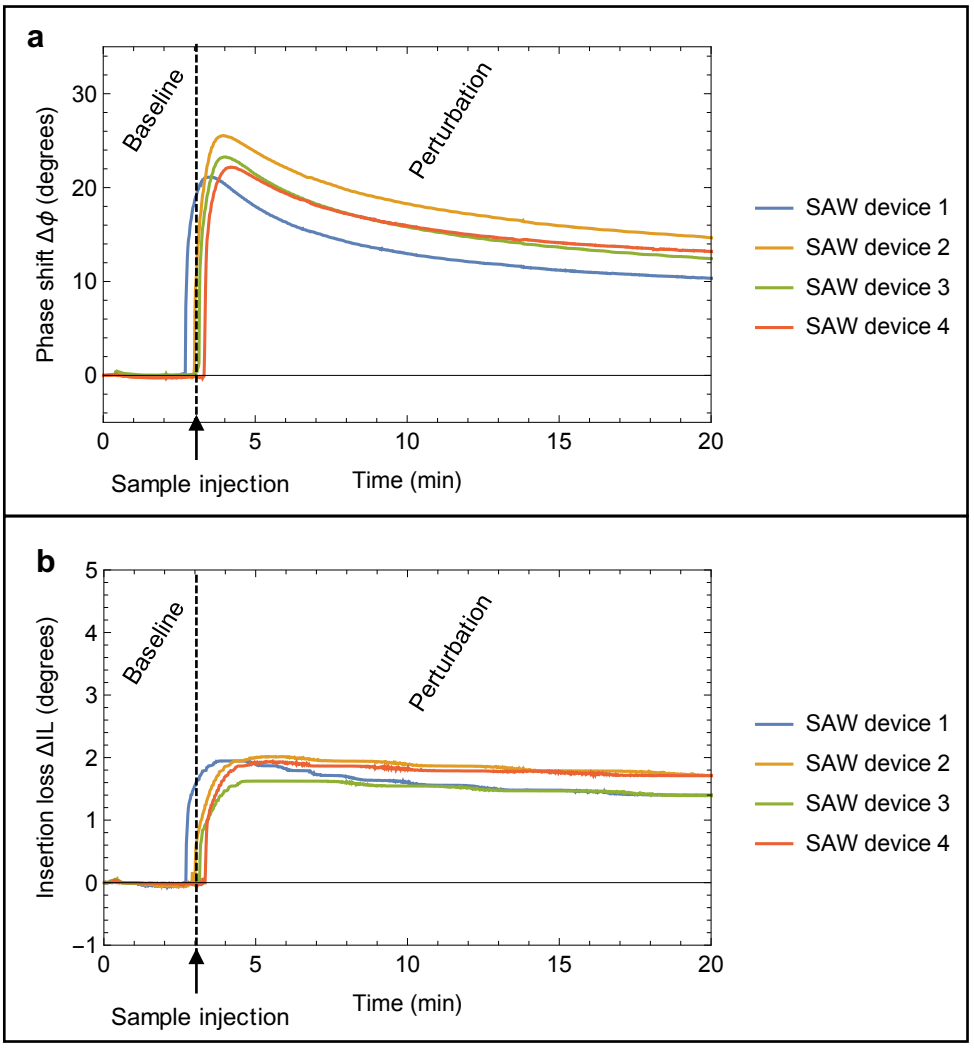

Figure 4.2: Example of data output by the laboratory control box. a) Plot to show the phase shift recorded by the SAW biosensor as a function of time, before and after sample injection. The effect of the perturbation following sample injection can be monitored for four SAW devices in parallel. **b)** Plot to show the insertion loss recorded by the SAW biosensor as a function of time, before and after sample injection. The effect of the perturbation following sample injection can be monitored for four SAW devices in parallel.

(such as lithium niobate or lithium tantalate) as the best compromise between temperature coefficient and the velocity of the acoustic wave travelling through the substrate. The temperature coefficient has to allow for measurements to be reproducible within the range of temperatures of operation. In the case of a PoCT, this corresponds to approximately 0-40°C.

Each OJ15 SAW device comprises two pairs of IDTs, with a delay line in between each pair of IDTs. The gold IDTs were evaporated onto the crystal and consisted of 80 finger pairs

with an aperture of 1mm, exciting a SH-SAW with a wavelength of 20μm at a frequency of 251.5MHz. A 2nm thin film of titanium was evaporated in between the IDTs, followed by the evaporation of a 90nm thin film of gold to form the delay line. The IDTs were protected from liquids by a glass lid and epoxy walls, which were constructed using a photolithography technique as described by Kogai *et al.*[175,176] A schematic of the different components of the final device ($25\times7\times2$ mm^3) is presented in Figure 4.3.

The IDTs were wire bonded to the electrodes at the bottom of the plastic base, which is then put in contact with the electric circuit comprising the control box once slotted into the chip holder.

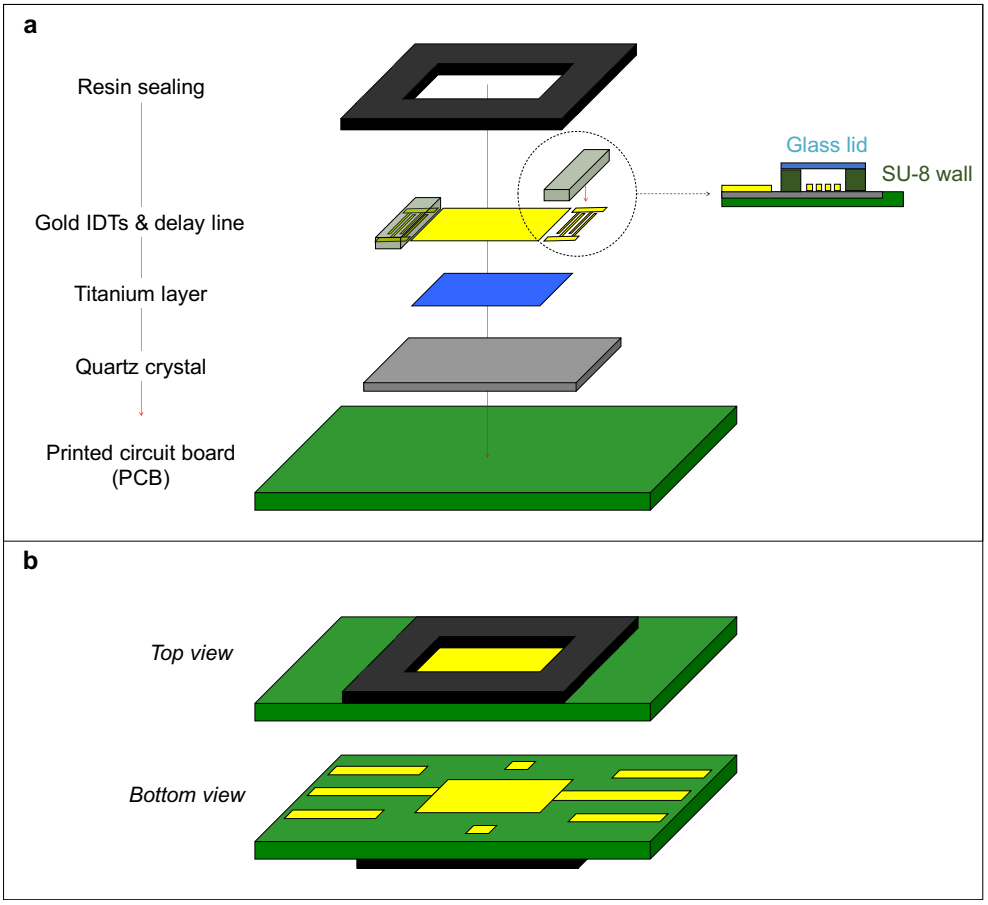

Figure 4.3: OJ15 SAW device components. a) Schematic overview of the different components deposited or formed on top of the quartz substrate. The substrate is fixed to the printed circuit board (PCB) using imyde resin. For clarity, only one pair of IDTs and one delay line are represented. Drawings not to scale. **b)** Schematic to illustrate the top and bottom views of the OJ15 SAW device. The bottom view features the gold electrodes that are used to connect the device to the electric circuit, once placed into the chip holder.

A schematic and photograph of the OJ15 SAW device is provided in Figure 4.4. As can be seen on the schematics in Figure 4.4a, the two delay lines are identical except for the fact

the lower one features a small pattern in its middle. This pattern is created by etching the gold during the same step as the formation of the IDTs. The purpose of this feature is to stop the surface component of the wave. The output IDT of the lower delay line therefore measure the bulk component of the wave only. This signal can be subtracted from the signal measured at the output IDT of the top delay line, in order to consider the surface component of the wave only.

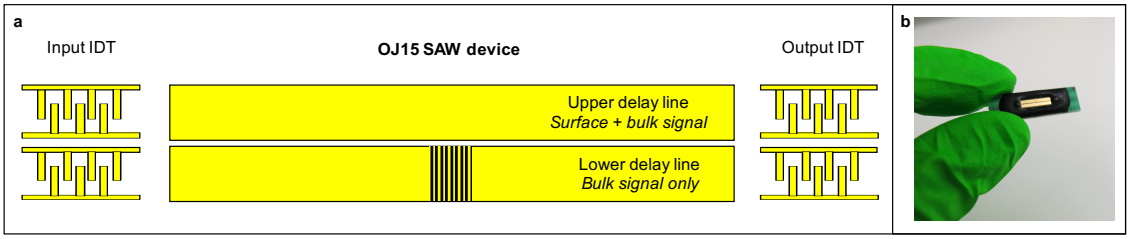

Figure 4.4: OJ15 SAW device. a) Top view schematic of the OJ15 SAW device, featuring two identical IDTs and delay lines. The acoustic wave reflects off a pattern located in the middle of the bottom delay line, leaving only the bulk component of the wave to reach the bottom output IDT. Both the surface and bulk component of the wave reach the top output IDT. **b)** Photograph of OJ15 SAW device measuring $25\times7\times2\text{mm}^3$.

In the following, a SH-SAW device will be referred to as a SAW device, for simplicity. In addition, the SAW *device* described above will be referred to as SAW *biochip* once the surface of the delay line has been functionalised with capture proteins, as described further on.

4.1.3 Different generations of SAW devices

In parallel to the work presented here, industrial partners OJ-Bio Ltd. designed and optimised different generations of devices with better sensitivity, or added features. As a consequence, different SAW devices were used during the course of this work. The results shown in Chapters 5, 6 and 8 were obtained using OJ15 SAW devices, detailed above, whereas the results presented in Chapter 7 were obtained using new generations of SAW devices (OJ24/OJ28/OJ31). A schematic and picture of the latest generation (OJ31) are presented in Figure 4.5.

These new SAW devices differ from OJ15 SAW devices on two main points. Firstly, they feature a reflecting wall at one end of the delay line, off which the acoustic wave bounces before travelling back to the input IDT. This IDT therefore acts both as input and output

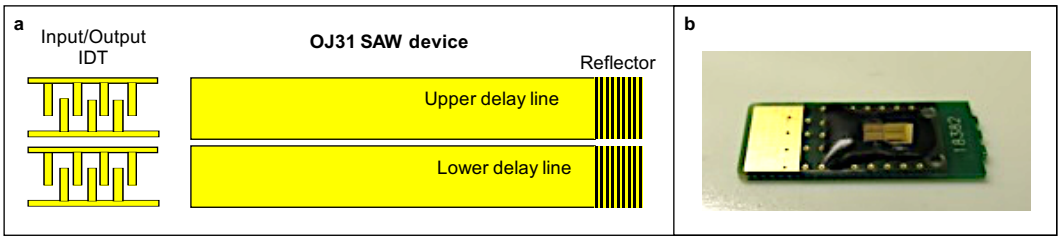

Figure 4.5: OJ31 SAW device a) Top view schematic of the OJ31 SAW device, featuring two identical IDTs and delay lines. The acoustic wave reflects off a pattern located at the end of the delay line, and is directed back to the IDT. A calibration pattern is printed with gold onto the chip, outside of the delay lines and IDTs, to help the automatic spotter find its initial position. **b)** Photograph of OJ31 SAW device.

IDT. The length of the delay line can be divided by two, as the acoustic wave travels along it twice. This makes the SAW device smaller, and the volume of sample required for OJ24/OJ28/OJ31 SAW devices is 6μl where the older OJ15 devices required 20μl.

Secondly, the new generations of SAW devices (OJ24/OJ28/OJ31) feature two identical operational delay lines that can be used as a sensing area, instead of one in OJ15, where the bottom delay line features a reflector to block the propagation of the acoustic wave on the surface. This means that one of the delay lines can be used as a reference channel, provided it is functionalised accordingly. This enables better correction of the signal with regard to non-specific binding and other undesired effects, as it eliminates possible chip-to-chip variation. The importance of this feature will be demonstrated in Chapter 7.

For logistical reasons, the results presented in Chapter 7 were obtained using different generations of SAW biochips. This due to the fact the three generations of SAW biochips were used chronologically, as they were developed by industrial partners OJ-Bio Ltd. The minor differences in design between OJ24 and OJ28 SAW biochips (a slight increase in the IDT aperture length to optimise the air insertion loss, and addition of a printed pattern around the delay lines to help with the calibration of the automated spotting protocol), and between OJ28 and OJ31 (line patterning around the delay lines to prevent the liquid from spreading outside the sensing area) have not been shown to alter the performance (tests performed by industrial partners OJ-Bio Ltd.). This confirmed that the result obtained on the new generations of SAW devices (OJ24, OJ28 and OJ31) could be compared to each other.

Due to the small size and proximity of the two delay lines, the functionalisation process needed to be adapted. With OJ15 SAW devices, a 20μl droplet of capture proteins could

be spread across the whole surface of both delay lines, as the same perturbation needed to occur on both delay lines. With the new generations of SAW devices, however, the one delay line was in most cases used as a control for the non-specific binding, meaning the capture protein had to be different on each delay line. When manual functionalisation using a pipette was experimented at the beginning, it required high dexterity and the chances of contamination of the other delay line were too high. Industrial partners OJ-Bio Ltd. developed an automated functionalisation process specifically for the capture protein functionalisation step. The delay lines were functionalised with DSP following the same protocol described above for OJ15 SAW devices, then a liquid spotter (Musashi Engineering Inc, Shotmaster 300DS-s) was used to deliver a controlled 6μl of capture protein solution on each delay line with high accuracy. The software used to operate the liquid spotter (Mu-CAD) used the patterns on the outside of the lines for initial positioning.

4.2 Surface functionalisation: transforming a SAW device into a SAW biochip

The surface of the delay line of the SAW devices presented above was functionalised with capture proteins in order to detect the target protein in the sample. The functionalisation process is described below. Once functionalised with the relevant capture protein, the SAW devices will be referred to in the following and in Chapters 6 and 7 as SAW *biochips*.

4.2.1 Cleaning the surface of the delay line

5 different cleaning strategies, were used during this work. 4 strategies involved cleaning the surface of the delay line in situ, by adding and removing various solutions from the surface of the biochip whilst docked in the chip reader. The different steps involved are detailed in Table 4.1.

The last cleaning strategy involved soaking the SAW devices in a series of cleaning baths (30min in each of the following solutions, in order: acetone, 70% EtOH solution, 50% EtOH solution, deionised water), before taking them inside a plasma chamber (Air plasma, 2mbar, 5min) and then docking them in the chip holder.

Step #	Action
1	Insert SAW biochip in chip reader.
2	Add a 20μl droplet of deionised water on the surface, leave for 1min.
3	Replace the water by a 20μl droplet of the cleaning solution, leave for 20min.
4	Replace the cleaning solution by a 20μl droplet of deionised water, repeat 10 times.

Table 4.1: Protocol for cleaning the gold surface of SAW devices. The different droplets of liquids are added and removed using a manual pipette. In step #3, the 4 different cleaning solutions testes were: Hellmanex 2% (Hellma Analytics, USA), and 3 solutions of Sodium dodecyl sulphate (SDS) (Sigma, UK) at various weight per volume concentrations: 1%, 2% and 5%.

4.2.2 Chemical linker - DSP

DSP was purchased from Thermo Scientific Pierce, USA (Cat# 22586). it is not soluble in water, the common solvent used to dissolve it is dimethyl sulfoxide (DMSO, Cat# D/4120/PB08, Fischer Chemical, UK). The functionalisation of the surface of the delay line with DSP was done *in situ*. A 20μl droplet of DSP in solution (4mg/ml) was left in contact with the surface of the delay line for 30 minutes. The surface was then cleaned with 5 addition/removal cycles of 20μl droplets of DMSO, then 10 cycles with 20μl droplets of PBS (Cat# 14200-067, Life Technologies, USA, diluted 10x in deionised water). Unless stated otherwise, results presented in Chapters 6 and 7 were obtained using SAW biochips functionalised using DSP following this protocol.

4.2.3 Capture protein

Once the surface of the delay had been functionalised with DSP, a layer of capture proteins was formed above the surface. To do so, a 20μl droplet of solution of capture protein in PBS (100μg/ml) was left in contact with the surface of the delay line for 30 minutes. As mentioned above, primary amine groups on the structure of the proteins in solution react with the active head group of DSP to form a covalent bond between the protein and the DSP molecule. The surface was then cleaned from non-specifically bound protein by 10 addition/removal cycles of 20μl droplets of PBS. A 20μl droplet of TBS-T (Cat# 524753, Calbiochem, USA, dissolved in deionised water and filter through 0.22μm filter system Cat# 431097, Fischer Scientific UK) was then left in contact with the surface for 15 minutes, in

order to block the unreacted DSP molecules: the tris molecule contains a primary amine that reacts with the head group of DSP following the same reaction occurring between DSP and primary amines on the structure of the capture protein. This is to avoid further unspecific binding of any protein presenting a primary amine on its structure. An example of the functionalisation process recorded using the SAW biosensor can be found in Figure 4.6.

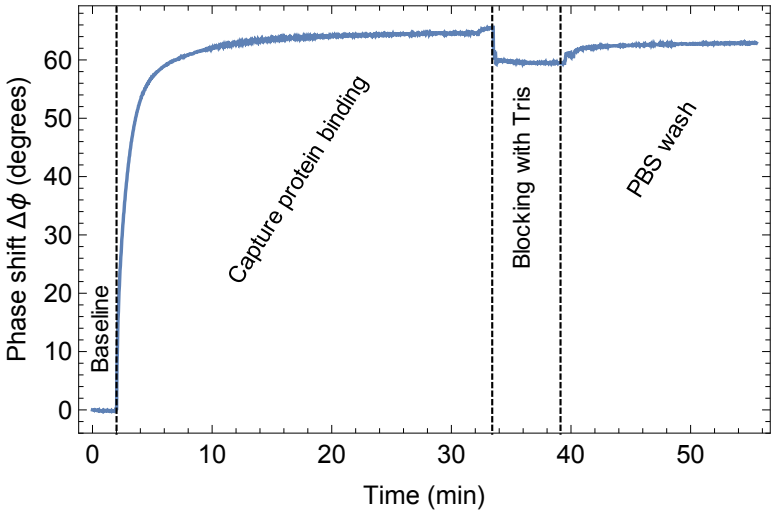

Figure 4.6: Surface functionalisation with capture proteins. Plot to show the phase shift as a function of time, when functionalisation the DSP-coated surface of the delay line of the SAW device. The different steps of the process are indicated on the plot. A baseline was recorded, before injection of the capture solution protein in solution. After incubation to let the capture protein bind to DSP, the delay line was incubated in TBS-T to block the unreacted DSP molecules. The TBS-T was then washed 5 times with PBS.

Table 4.2 lists the various capture proteins used during this work along with the corresponding target protein. The source of each protein is also indicated.

4.3 Anti-p24 llama VHH characterisation

In Table 4.2, 59H10 is an anti-p24 llama VHH used as a capture protein for HIV p24. A representation of the structure can be found in Figure 4.7. 59H10 was produced in-house. A host bacteria (E. Coli TG1) was used to express the llama VHH sequence contained in a plasmid (pCAD51-59H10) gifted for this work by Prof. Weiss at UCL. A more detailed description of the protocol can be found in Appendix A.

Capture protein	Source	Target protein
Anti-HSA	A0433 (Sigma-Aldrich, USA)	HSA
HSA	230-005 (Novozymes Biopharma, USA)	Anti-HSA
HIV p24	AG6054 (Aalto Bio Reagents, UK)	Anti-24
Anti-p24	BC1071 (Aalto Bio Reagents, UK) NIH-3537 (AIDS Reagents Program, USA) [177] NBS500-473 (Novus Biologicals, UK) [85] Capricorn HIV 1/2 (Capricorn Products, USA) C65489M (Meridian Life Science, USA) [85] 59H10 (in house)	HIV p24
Anti-GBP5	Ab89284 (Abcam, UK)	GBP5
HIV gp41	30-AH26 (Fitzgerald, USA)	Anti-gp41
Anti-gp41	AHP2209 (Abd Serotech, USA)	HIV gp41

Table 4.2: List of capture proteins used during this work, and source.

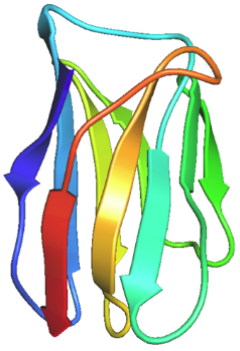

Figure 4.7: Structural homology model of 59H10, rendered to show secondary structure features of the protein (beta-sandwich) in rainbow colouring (blue to red for the N-terminus to the C-terminus). This is a 'side' view orientated to examine the CDR3 (complementary determining region) loop, at the top in orange, which is believed to be integral to p24 'capture'. Image courtesy of Dr. Jenny Brookes.

4.3.1 In solution characterisation using bio-layer interferometry

BLI is a technique used to observe and quantify the binding of a target protein to a surface. In this sense, it is comparable to the gold-standard Surface Plasmon Resonance (SPR), however, BLI is a significantly cheaper technique. The principle of operation is schematised is Figure 4.8. The probe consists of a glass fibre dipped into the sample solution. A bio-compatible optical layer is located at the edge of the probe, and its surface is functionalised with capture proteins. White light is sent through the probe, and is reflected off two

different surfaces: the glass/optical biocompatible layer interface, and the probe/solution interface. A photodetector detects the reflected light waves and breaks the signal down into individual wavelengths signals. The first interface acts as a reference. The reflection off the second interface depends on the surface composition. Analysing the interferences pattern between the light waves reflected off the two interfaces results allows the reconstruction the interferometric profile as a function of time. A shift in the interferometric profile gives an indication of the amount of proteins bound to the surface of the probe.

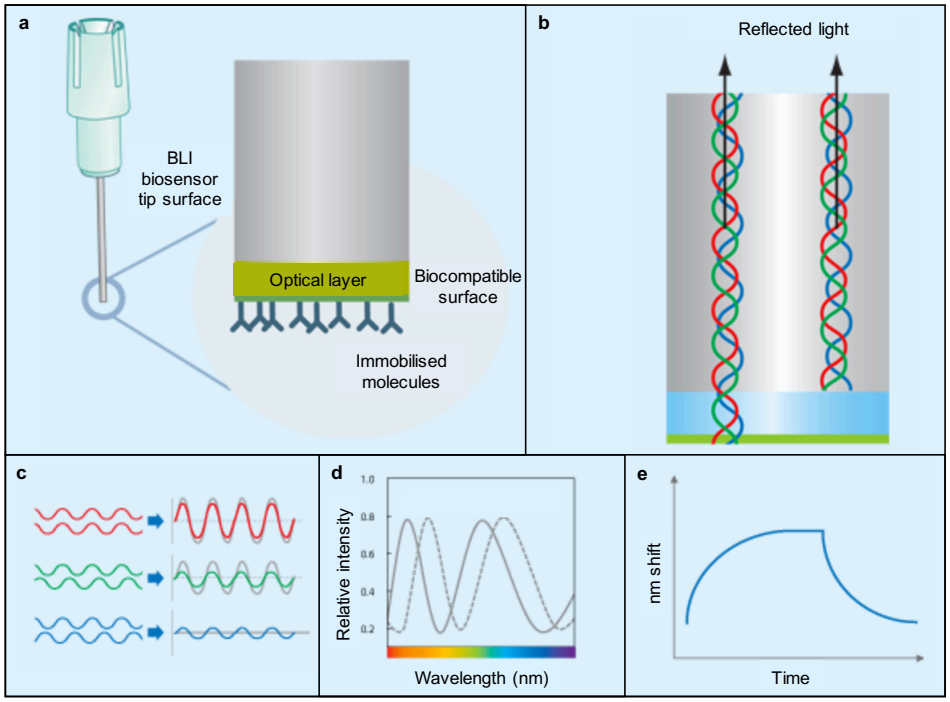

Figure 4.8: BLI principle of operation. **a)** Schematics to illustrate the BLI glass probe, with the optical layer on the edge and surface functionalisation with capture proteins on the outside of the optical layer. **b)** Schematic to illustrate the reflection of the light waves off two different interfaces: glass fibre/optical layer and probe surface/solution. **c)** Schematics to illustrate the interference patterns observed for different individual wavelengths following reflection off both interfaces. **d)** Schematics to illustrate the shift in wavelength observed between interferometric profiles. e) Schematic to illustrate the output of the BLI, the shift in wavelength, which gives an indication of the amount of protein bound to the probe surface, as a function of time. Adapted from [178]

BLI can be used to either qualitatively asses the best binder between two proteins, or to quantify the affinity of one protein for another. Two experiments were conducted to assess which anti-p24 protein to use as the capture protein in the HIV p24 detection assays conducted with the SAW biosensor. The instruments used was the model ForteBio OctetRED96 System (Pall Life Sciences, USA).

To study the relative affinity of llama VHH to p24, four different llama VHH (59H10,37E7, 59H4 and 48G11) were biotinylated using a commercial biotinylation kit (EZ-Link Sulfo-NHS-SS-Biotin, Cat# 21331, ThermoScientific, USA). Streptavidin-coated probes (Streptavidin Biosensors (Tray). Product 18-5019, Pall Life Sciences, USA) were functionalised with different biotinylated llama VHH following the ForteBio designated protocol.

To study binding affinity, BLI probes (Amine Reactive Second Generation (AR2G) Biosensors (Tray). Product no. 18-5092, Pall Life Sciences, USA) were functionalised with each anti-p24 protein using NHS-EDC chemistry following the designated ForteBio protocol, then dipped in solutions of p24 in kinetics buffer (Kinetic Buffer 10X. Product no. 18-1092-dilute in PBS, Pall Life Sciences, USA) at various concentrations.

4.3.2 Functionalised surface characterisation with XPS

XPS is a technique used to analyse the elemental composition of a surface. A beam of X-rays of known energy is focussed on the surface of the sample to analyse. The energy of the irradiating photons excites the electronic state of the atoms on the surface, down to about 20 atomic layers. The excited electrons, ejected from the surface, are then filtered through a hemispherical electron analyser and their kinetic energy is recorded by a detector. The binding energy of the electron before their ejection from the surface is a direct indication of which atoms are present on the surface and how they are bound together. The binding energy is calculated knowing the emitting photon energy, the measured electron kinetic energy, and a factor that depends on the spectrophotometer characteristics. An energy spectra is obtained, which gives the count of electron per second (CPS) as a function of the binding energy. A schematic of the principle can be found in Figure 4.9.

The binding energy of most atoms depending on the chemical bond they are involved in is documented in the literature. The relative percentage of each atom of interested can therefore be estimated by fitting the peaks of energy and comparing it to the literature values. The software that was used to obtain the results below is CasaXPS.

The delay line of the SAW devices characterised with XPS was cleaned and functionalised following the same protocols (described above) used to clean and functionalise the delay line of the SAW devices that were transformed into SAW biochips capable to detect the presence of HIV p24 in solution. After functionalisation, the SAW biochips were immersed

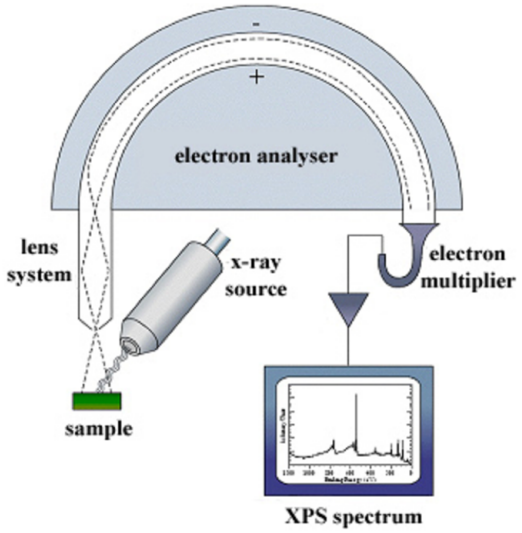

Figure 4.9: XPS principle of operation. Schematics to illustrate the principle of operation of XPS. A beam of X-rays is focussed on sample surface. The excited electrons are ejected from the surface, filtered through the electron analyser and hit a detector which records their kinetic energy. An energy spectra is obtained, which gives the count of electron per second (CPS) as a function of the binding energy. Adapted from [179]

in deionised water and stored at 4°C for 24 hours. Measurements were performed at the NEXUS lab at Newcastle University, UK. The XPS used was the model Theta Probe (Thermo Scientific, East Grinstead, UK) characterized by a monochromatic Al k-alpha X-ray source with a pass energy of 40eV and dwell time of 100ms. The pressure in the chamber was kept at 3.10^{-8}mbar during the measurements. The focused beam hit the sample surface as an elliptical spot of dimensions 400μm$\times 800\mu$m.

4.4 Gold nanoparticles functionalisation with antibodies

1ml of 20nm gold nanoparticles (Cat# 741965, Aldrich Chemistry, USA) were added to a 2ml Eppendorf tube, and mixed with 100μl of a 40μg/ml solution of the antibody of interest (in PBS). The solution was incubated for 20 minutes at 25°C at 650 rpm. 100μl of BSA 1 mg/ml diluted in deionised water were added to the tube. The solution was incubated for 20 min at 25°C at 650 rpm, before being centrifuged at 14000 rpm for 20 min at 4°C. As much of the supernatant as possible was removed manually using a pipette. The functionalised nanoparticles were then resuspended in 300μl of PBS.

4.5 ELISA

PVC microtitres plates (Cat# 655001, GBO GmbH, Germany) were coated with a recombinant protein able to form a complex with the biomarker of interest. The surface was then blocked with a solution of BSA (Cat# B4287, Sigma Life Science, USA) in PBS (2% w/v) to avoid non-specific binding. The unknown sample was injected into the well at this point. Calibration samples containing the biomarker of interest at different known concentrations were run in parallel, in order to generate a calibration curve. After specific binding of the biomarker of interest to the plate, a solution of detection antibody (HRP-tagged anti-human antibody, A8667, Sigma Life Science, USA) was injected into the wells in order to tag the bound biomarkers. Finally, a substrate (TMB solution, Cat# 00-4201-56, eBioscience, Inc. USA) was made to react with the HRP, and the reaction was stopped using a solution of sulphuric acid (0.2M H_2SO_4). The absorbance of the solution in each well was measured for an emission wavelength of 450nm using a SpectraMax i3 (Molecular Devices Ltd., UK). The absorbance of each well was normalised to a blank reading. The linear regression in the linear region of the calibration curve was used to estimate the concentration of unknown samples.

4.6 Clinical pilot studies data processing

As mentioned earlier, the control box outputs a file containing the phase shift and the insertion loss as a function of time, for each SAW device. In the case of the new generations of SAW devices featuring two operational delay lines, the file contains the data for each delay line. When performing the pilot studies presented in Chapter 7 involving testing between one to two hundred samples, the amount of data generated were too big to manually process. An algorithm was therefore written in Wolfram Mathematica to handle these large amount of data. The algorithm essentially imports the output file and processes it to make it easier to visualise it in several ways. The process is described below, and the algorithm can be found in Appendix B.

The first step of the algorithm is an initial loop where each iteration imports and processes a different file. Processing involves:

- Cleaning the data: selecting only the phase shift and insertion loss for each delay line, normalising them to the beginning of the test, i.e. from sample injection, and splitting the table, which contains the data of two or four SAW devices, into two tables of similar dimensions, each one corresponding to one SAW device.
- Subtracting the reference delay line values from the test delay line values, for every time point.
- Extracting the sample name and status (known positive, known negative or calibration sample) from the file name and associating it with the corresponding data.
- Merging all the individual tables obtained into a large one. At this point in the algorithm, the program has in memory a table where each entry contains the sample name and the test data (phase shift and insertion loss as a function of time).

A crucial step of the analysis was to evaluate the threshold used to distinguish between a positive and a negative sample. It was decided to define this threshold using the average and standard deviation of the measurements taken using calibration negative samples (pooled confirmed HIV negative human plasma from LEEBIO Inc., USA). Depending on the number of standard deviations added to the mean, this means that a certain percentage of the measurements performed on negative samples have fallen under this threshold (assuming the data is normally distributed, see Chapter 7). Provided the number of negative samples is sufficiently large (usually about 20 is sufficient to assure normality), this can be expanded to assume that the aforementioned percentage of the true negative samples measured with the test will be correctly declared as negatives. As the calibration samples were run using exactly the same protocol as the actual tests, a threshold value can be defined at every point in time during the test protocol. At this point, it is possible to visualise the data in a variety of ways, illustrated in Figure 4.10:

- Plotting the raw phase shift as a function of time, for any sample (Figure 4.10a).
- Representing the data of the whole pilot study as a barchart where results falling above the threshold are displayed in green bars while those falling below the threshold are displayed in grey bars (Figure 4.10b).
- Plotting the calculated clinical sensitivity and clinical specificity of the test, as a function of time (Figure 4.10c).

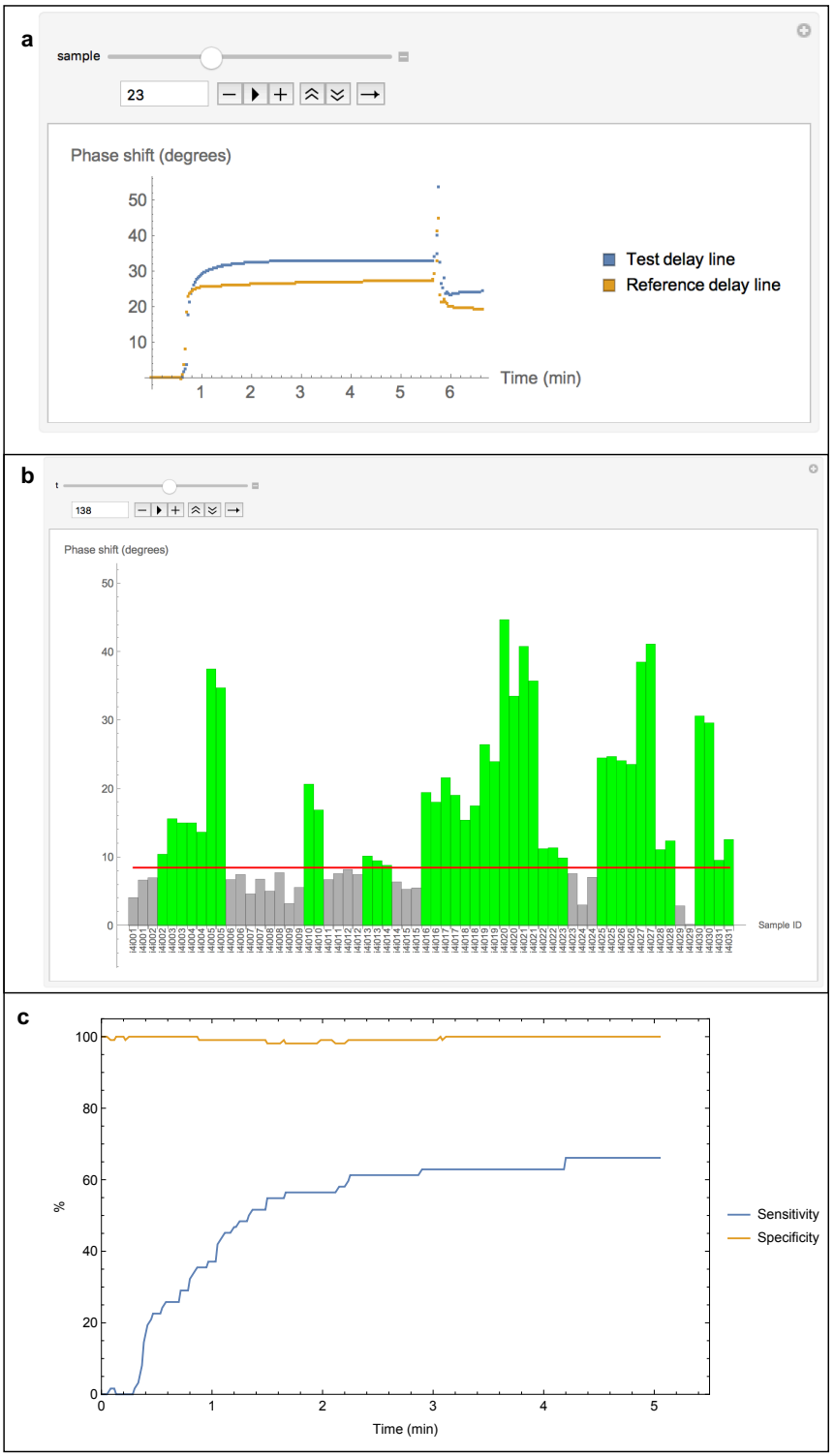

Figure 4.10: Examples of data visualisation. a) Raw phase shift plotted over time for a given sample. Any sample in the study can be visualized individually by selecting its number in the dialog box above the graph. **b)** Example barchart showing the phase shift recorded by the SAW biosensor after a given time (t=138s). Each bar represents one test. For clarity, a colour is associated to each bar depending on whether the recorded value for the differential phase shift is below (grey) or above (green) the threshold for the time considered (represented by the red line). In other words, a grey bar represents a sample declared negative by the test, whereas a green bar represents a positive test. The results can be visualized at any given time using the dialog box above the chart. **c)** Example plot to show that the sensitivity and specificity can be calculated at any point in time.

Chapter 5

SAW Device Characterisation

The theory of perturbation applied to SH-SAW devices was presented in Chapter 3, along with a general introduction to SAW devices and the state of the art of their application as various biosensors. In Chapter 4, the particular prototypes of SAW devices used throughout this work were described, with a particular emphasis on the OJ15 SAW device which was used to obtain the majority of the results presented in the next chapters. In addition, the prototype of control box used to drive the SAW device was presented, along with the details of how it outputs the two main measurement parameters that are the acoustic wave phase and amplitude, which are directly related to the acoustic wave velocity and attenuation, respectively. This chapter presents the careful characterisation of the OJ15 SAW device, a necessary step before using it to obtain all the results presented in the next three chapters. Most of the characterisation results presented here apply to the next generation SAW devices used at the later stages of this work (OJ24 and OJ31). The OJ15 SAW device was characterised from three different approaches, consecutive and complementary to each other. First, it was decided to study the sensitivity of the device from a theoretical point of view, and use this analysis to show experimentally that three of the main characteristics of the device contribute to confer it an optimal sensitivity in the context of being used for biosensing applications. The three parameters studied were the driving frequency, the length of the delay line, and the strategy used to cancel out the bulk component of the signal in order to focus only on the surface component. Then, a second study focussed on assessing the influence of the surface coverage of the delay by the liquid sample on the output signal, and the possible consequences in relation to the future SAW biosensor being

used as a PoCT. Finally, the reproducibility of the measurements taken with the SAW device was assessed, with the idea that each SAW device had to be considered disposable -and was treated as such during this work- as well as the fact the prototype control box used allowed four different measurements to be taken at the same time, therefore introducing a possible variable between measurements.

5.1 Optimising device design to improve sensitivity

The optimal value of some parameters of a SAW device can be estimated theoretically, during the design process and before going into manufacture. The operating frequency, geometry of the IDTs, length of the delay line and strategy used to eliminate of attenuate the impact of bulk wave vibrations on the output signal are all examples of key parameters that influence the device performance. Estimating the optimal conditions when designing the device saves a lot of time and cost associated with a trial-and-error approach, where a lot of different prototypes featuring different values of these key parameters would have to be manufactured, tested and most of them discarded based on the results of these tests. However, the ideal SAW device cannot be modelled perfectly and eventually, a small number of prototypes have to be compared to each other in the lab. It is a common practice to perform simple tests on different prototypes featuring different versions of key parameters, in order to verify the initial hypothesis, optimise the parameters tested and at the same time characterise the device.

5.1.1 Insertion loss and sensitivity

A common target associated with the design of a good SAW device is its sensitivity. The definition of sensitivity can describe different concepts depending on the context in which the term is used: the clinical sensitivity of a PoCT, as presented in Chapters 4 and 7, relates to the proportion of samples in a panel correctly identified as either positive or negative to the biomarker of interest, and has got a very different meaning to the sensitivity of a SAW device.

The following explanations and results focus on the sensitivity of the SAW device, defined as the magnitude of the response the SAW device produces to a given perturbation. This

response takes the form of the attenuation of the acoustic wave amplitude observed between the input IDT and the output IDT, when the wave travels along the delay line (sensing area). This is called the insertion loss (IL) and is, in this context, directly associated with the device sensitivity.

The difference in insertion loss (ΔIL) measured before (IL_0) and after (IL_1) a perturbation occurs on the surface of the delay line was expressed by equation 3.41 in Chapter 3 as:

$$\Delta IL = -\frac{20}{\ln(10)}\Delta\alpha L, \tag{5.1}$$

where L is the length of the delay line and $\Delta\alpha$ the difference in attenuation coefficients before (α_0) and after perturbation (α_1). ΔIL and $\Delta\alpha$ are defined respectively as:

$$\Delta IL = IL_1 - IL_0, \tag{5.2}$$

$$\Delta\alpha = \alpha_1 - \alpha_0. \tag{5.3}$$

Therefore, if we consider the particular case where a sample is added onto the surface of the dry delay line exposed to air, and generates a perturbation, the following general relation can be derived:

$$IL_{sample} = -\frac{20}{\ln(10)}(\alpha_{sample} - \alpha_{air})L + IL_{air}. \tag{5.4}$$

The value of the attenuation coefficient α depends mainly on the characteristic of the sample on the surface of the delay line. The attenuation coefficient in air α_{air} is negligible compared to the attenuation coefficient of any sample. The presence of obstacles such as SU-8 walls or gold on top of the crystal explain the insertion loss observed in air (around -20dB for OJ15 SAW devices). It can be approximated that at a given frequency, IL_{air} is a constant that depends on the design of the device (IDTs and SU-8 walls) but not on the length of the delay line. The following expression of IL_{sample} can therefore be expressed, for any sample other than air:

$$IL_{sample} = -\frac{20}{\ln(10)}\alpha_{sample}L + IL_{air}. \tag{5.5}$$

5.1.2 Theoretical range of values for the insertion loss

The insertion loss only takes negative values. This is confirmed by equation 3.38 in Chapter 3, which gives the expression of the insertion loss as a function of the amplitude measured at the input and output IDT (A_{in} and A_{out} respectively):

$$IL = 20\log_{10}\left(\frac{A_{out}}{A_{in}}\right). \tag{5.6}$$

As the amplitude of the acoustic wave can only be attenuated when the wave travels through the crystal (or in the ideal case of a perfectly designed device, remain unperturbed), the following relation for the ratio of amplitudes is true for any sample:

$$\frac{A_{out}}{A_{in}} \leq 1. \tag{5.7}$$

The theoretical range of values the insertion loss can take is plotted as a function of the ratio in Figure 5.1, confirming that it only takes negative values (or zero in the case of an ideal device, measuring the insertion loss in air).

In the following, references to the size of the insertion loss are made in terms of absolute value of the insertion loss: when comparing two values, the one referred to as the smallest one is the one closest to zero.

5.1.3 Optimal operating frequency: minimising IL_{air}

The first indicator of performance of a SAW device is its ability to minimize the insertion loss in air. If a large insertion loss is required when testing a sample with the SAW device (as it is directly related to the perturbation caused by the sample), a minimal insertion loss is required in air. A crude way to look at it is the smaller the insertion loss in air, the more signal there is to lose when a perturbation occurs on the delay line. This loss of signal is the SAW device response to the perturbation, so the bigger it is, the better.

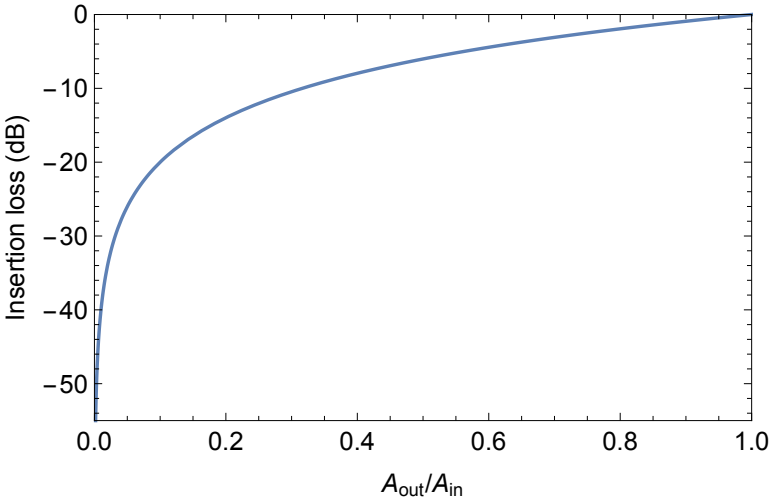

Figure 5.1: Theoretical range of values for the insertion loss IL. Plot to show the theoretical values the insertion loss (measured in dB) can take. The expression of the insertion loss presented in equation 5.6 was plotted as a function of the ratio of amplitudes measured at the output and input IDT, respectively. The insertion loss can theoretically vary from $-\infty$ to zero.

The insertion loss can be measured for a range of different frequencies using a network analyser. This is useful to choose the best operating frequency, i.e. the frequency to use to drive the crystal in order to obtain the minimum insertion loss when operating the SAW device in air. Such measurements were performed on OJ15 SAW devices at Japan Radio Company, (Kamifukuoka, Japan). The network analyser used for the measurements was the model 8753D (Hewlett Packard, USA). The insertion loss is plotted as a function of the driving frequency in Figure 5.2.

Note: As dual channel SAW devices (OJ24 and OJ31) had not been manufactured at the time, it was not possible to perform these measurements on all the types of SAW devices used throughout this work.

As can be seen in Figure 5.2, the frequency chosen to drive the SAW devices (251.5MHz) generates an insertion loss that is very close to the smallest possible (minimum absolute value) for the three SAW devices tested. This frequency was chosen based on the design of the IDTs, but also on the hardware available and compatible with the requirements of the chip reader prototype. The average of the frequencies giving the minimum loss (in absolute value) for each of the three measurements was 251$\pm$0.16MHz, which is very close to the frequency chosen to drive the device.

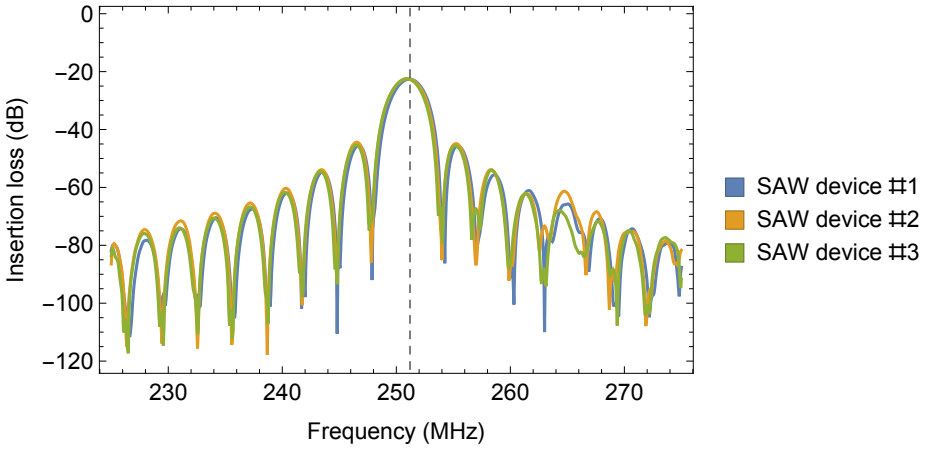

Figure 5.2: Optimising the SAW device operating frequency to minimise IL_{air}. Plot to show the insertion loss (dB) measured as a function of the driving frequency for three different OJ15 SAW devices. Measurements were performed using a network analyser (model 8753D, Hewlett Packard, USA). The surface of the delay lines of the SAW devices was only exposed to air (dry) during the measurement. The dashed line represents the 251.5MHz frequency chosen to drive the SAW devices.

5.1.4 Optimising sensitivity: the role of the different insertion loss

The insertion loss associated to the operating frequency of 251.5MHz (presented in Figure 5.2) was measured in air. The same measurement can be performed with any type of sample on the delay line, and forms the basis of the mode of operation of the SAW biosensor. In Chapter 3, it was presented that the perturbation theory applied to SH-SAW devices shows that the attenuation of the acoustic wave is related to a change in viscosity on the surface proximity. In the following, the relation between the insertion loss measured for samples of different viscosities is studied. The model samples chosen were deionised water, glycerol/water solutions at increasing glycerol content, and pure glycerol.

Note: the following study aims at investigating the effect of a change in the device design (such as the delay line length for example) on the device sensitivity to a pure viscosity perturbation. The study only investigates the performance of different device designs on the insertion loss. Therefore, the results of the following study do not necessarily apply to the results presented in Chapters 6 and 7 which were obtained by measuring the acoustic wave phase shift. They provide, however, a good indication of the fundamental sensitivity of the device to a pure viscosity perturbation, over a range of viscosity regions.

The signal measured at the output IDT has a surface component as well as a bulk component. The latter is due to the fact the SH-SAW is not propagating purely in one direction and

a minor bulk component is observed. The surface component can be removed by adding pure glycerol on the surface of the delay line, leaving only the bulk (and minor spurious component coming from the IDT). In the following, the insertion loss measured with pure glycerol on the surface of the delay line is referred to as IL_{total}.

The sensitivity of a SAW device, when looking at it from the insertion loss angle, is related to three ratios between the insertion loss of different samples:

$$\gamma_1 = \frac{IL_{air}}{IL_{total}}, \tag{5.8}$$

$$\gamma_2 = \frac{IL_{sample1}}{IL_{sample2}}, \tag{5.9}$$

$$\gamma_3 = \frac{IL_{sample}}{IL_{total}}, \tag{5.10}$$

where IL_{sample} is the insertion loss measured for any sample other than pure glycerol or any sample generating the loss of all the surface component of the signal (IL_{total}). The viscosity of sample 2 is higher than the viscosity of sample 1, therefore $IL_{sample2}$ is higher than $IL_{sample1}$. The different insertion loss measurements involved in the expressions of γ_1, γ_2 and γ_3 are shown as an example in Figure 5.3.

Those ratios vary from 0 (in the particular case of the SAW device being ideal and the wave not being perturbed by the sample on the surface this would only be useful in air) to 1 (the insertion loss is the same regardless of sample on surface which is not useful to distinguish between samples). To increase the SAW device sensitivity, it is necessary for each of these ratios to be minimised:

- a small γ_1 means the insertion loss measured in air is small compared to the total insertion loss. This signifies that the design of the device was good, that a minimal amount of signal is lost when the device is exposed to air only, and that there is plenty of signal to allocate for transducing the perturbation caused by the samples.
- a small γ_2 means the perturbation - caused by what distinguishes the two samples - generates a large insertion loss difference. The difference between the two samples

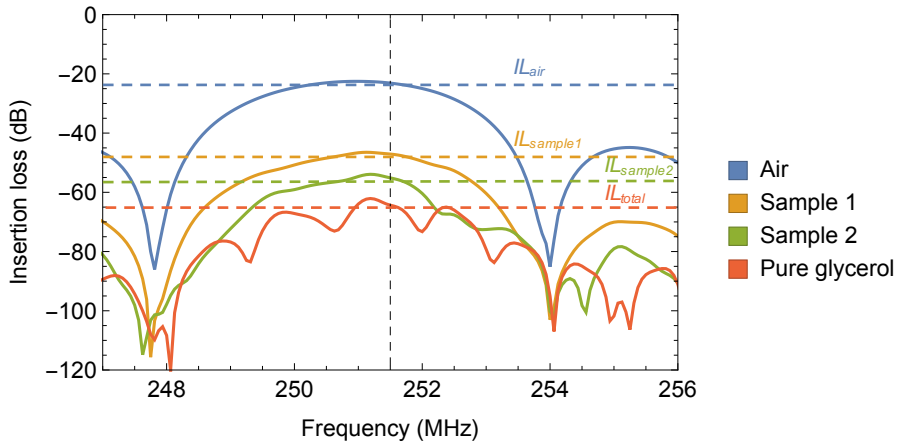

Figure 5.3: Levels of insertion loss. Plot to show the insertion loss (dB) measured with an OJ15 SAW device as a function of the driving frequency, for the 4 different samples indicated in the legend. In the example chosen, Sample 1 and Sample 2 correspond to solutions of glycerol at 10% and 30% (w/w), respectively. The vertical dashed line represents the 251.5MHz frequency chosen to drive the SAW devices. The horizontal dashed lines indicate the insertion loss measured for each sample. Measurements were performed using a network analyser (model 8753D, Hewlett Packard, USA).

here is simply viscosity, but this would equally apply to sample 2 containing the target protein, and sample 1 being the negative control sample or running buffer. A small γ_2 improves the resolution and clarity of the measurements when looking at fine surface perturbations, such as the binding of small proteins of proteins at low concentrations.

- Finally, a small γ_3 corresponds to the fact that any perturbation of interest measured by the SAW device generates an insertion loss far apart in absolute value - from the total insertion loss IL_{total}. IL_{total} represents the upper limit (in absolute value) of what the SAW device can measure in terms of insertion loss. Therefore, the further away the insertion loss of a given sample is from IL_{total}, the more room there is left for measuring greater perturbations, and the larger the range of perturbations the SAW device can measure.

Decreasing the values of γ_1, γ_2, and γ_3 is a design consideration. Regarding γ_1, the thickness of the SU-8 walls (responsible for a constant loss of approximately 3dB on OJ15 SAW devices) and the design of the IDTs play a role in reducing the value of IL_{air}. In addition, different strategies can be used to cancel out the bulk component of the signal measured. Removing the bulk component can also have an effect on decreasing the values of γ_2 and γ_3, as will be shown further on. Finally, tuning the length of the delay line can be used to optimise the device sensitivity, as illustrated in the example below.

The absolute value of IL_{sample} is related to the length of the delay line L (see equation 5.5). As the value of IL_{total} is fixed, γ_3 increases with L. However, equation 5.5 also means that the difference between $IL_{sample1}$ and $IL_{sample2}$ increases with L, and therefore the value of γ_2 decreases when L increases. This is illustrated with an example in Figure 5.4.

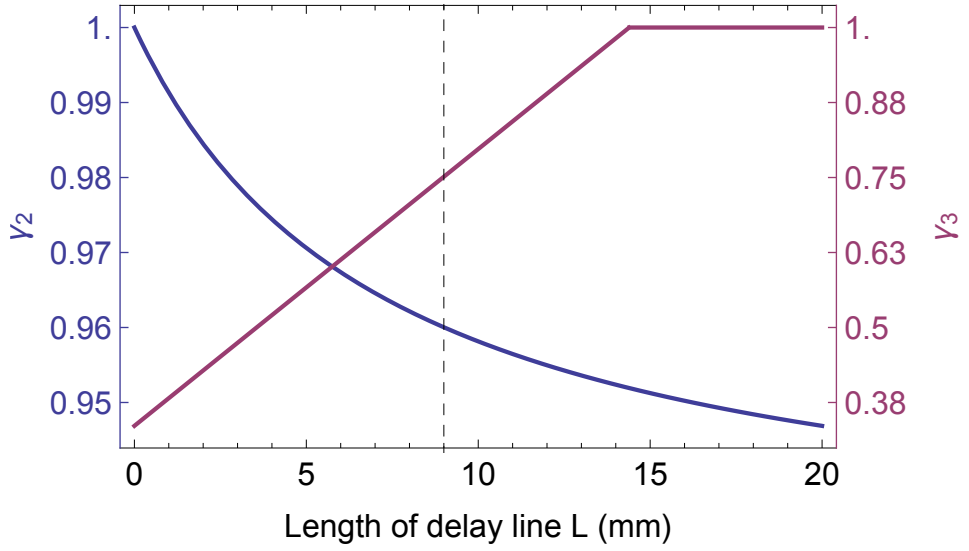

Figure 5.4: Influence of the length of the delay line on γ_2 and γ_3. Plot to show the variation of γ_2 and γ_3 as a function of the length of the delay line L. The ratios γ_2 and γ_3 were calculated using the expression of insertion loss presented in equation 5.5. In the example chosen, sample 1 was deionised water, and sample 2 corresponds to a further loss of 2dB (most perturbations measured during this project gave rise to 1 to 5dB compared to the insertion loss of deionised water). The values of the attenuation coefficients were estimated for each sample based on 5 independent measurements of the insertion loss for the corresponding sample on OJ15 SAW devices (x = 9mm, f = 251.5MHz). The average values used were ILair = -22dB , IL_1 = -47dB, IL_2 = -49dB, IL_{total} = -65dB, α_1 = 0.319dB.mm^{-1} and α_2 = 0.344dB.mm^{-1}. The vertical dashed line indicates the length of the delay line on OJ15 SAW devices (9mm). In this example, all the signal is lost if the length of the delay line is equal or greater than 14.4mm.

5.1.5 Improving SAW device sensitivity by varying the length of the delay line

In the discussion above, the theoretical influence of the length of the delay line on the SAW device sensitivity were studied. The analysis was based on the different expressions of the insertion loss presented in Chapter 3, and the introduction of the three ratios insertion loss ratios γ_1, γ_2 and γ_3. In order to observe the influence of the length of the delay line on the specific case of OJ15 devices, two different prototypes, identical in every aspect except for

the length of their delay line, were tested. A schematic of the two devices is presented in Figure 5.5.

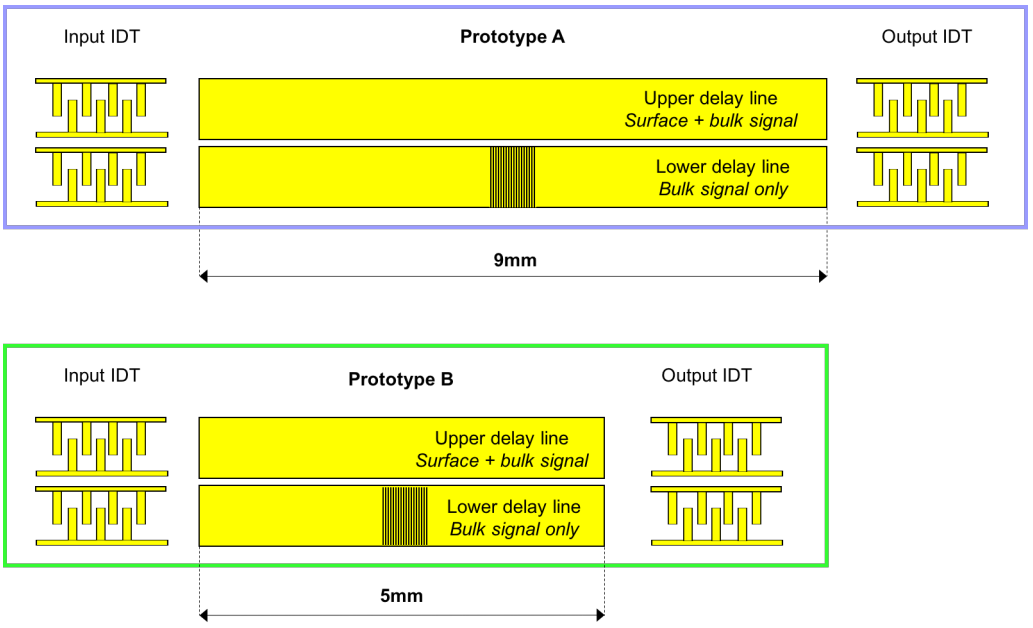

Figure 5.5: Prototypes A and B used to study the influence of the length of the delay line on the SAW device sensitivity. Schematics of the prototypes of SAW device used to study the influence of the length of the delay line on the device sensitivity. The two prototypes are identical apart from the length of the delay line (9mm for prototype A, 5mm for prototype B). Drawings not to scale.

In order to study the influence of the length of the delay line on the device sensitivity, the insertion loss was measured with both devices for 6 different samples: air, deionised water, and water/glycerol solutions at 10%, 20% and 30% (w/w) glycerol, and pure glycerol. Examples of the insertion loss measured and the analysis of the ratios γ_1 (Figure 5.6) and γ_2 and γ_3 (Figure 5.7) are presented below. Glycerol was purchased from Yoneyama Yakhuin Kogyo Co., Ltd., Japan (product number 02272). Measurements were performed at Japan Radio Company, Kamifukuoka, Japan. The network analyser used for the measurements was the model 8753D (Hewlett Packard).

As can be seen in Figure 6b, the ratio γ_1 is very similar between prototypes A and B (0.36 ± 0.015, 0.37 ± 0.001). This indicates that varying the length of the delay line from the reference prototype (OJ15, 9mm delay line) does not influence this particular ratio. This was to be expected, and confirms that when designing the SAW device, the design of the IDTs and the surrounding SU-8 walls may have an impact on γ_1, while the length of the delay line is less likely to.

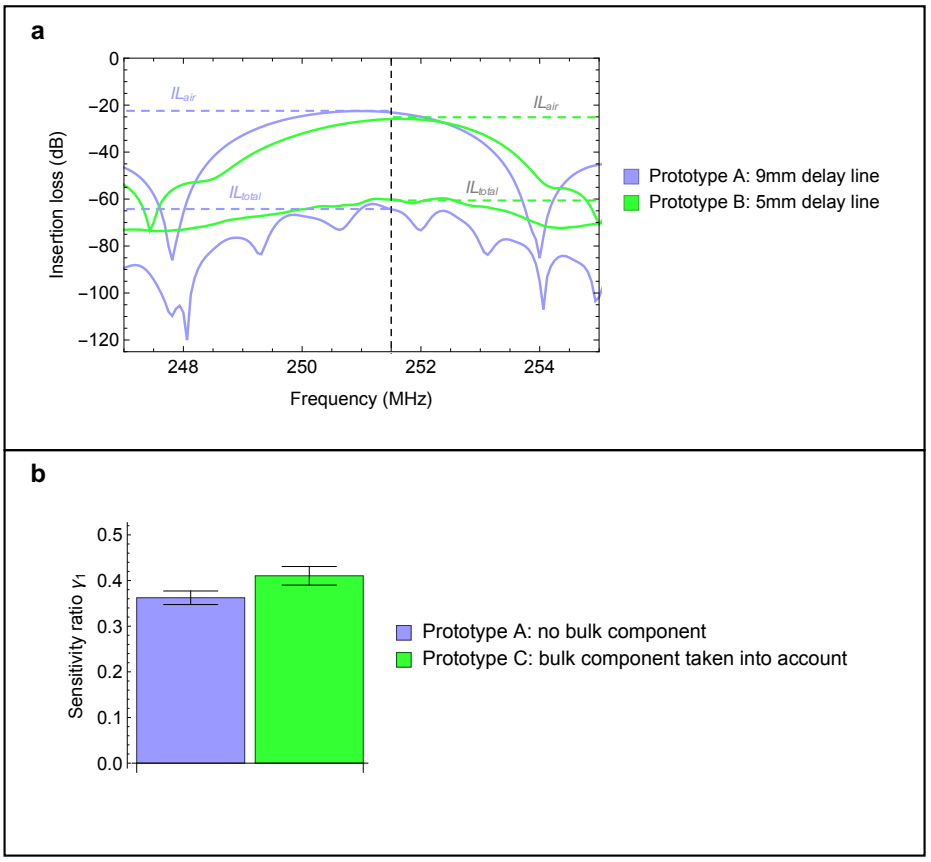

Figure 5.6: Influence of the length of the delay line on the SAW device sensitivity: ratio γ_1. a) Plot to show the insertion loss (dB) measured as a function of the driving frequency on prototype A (blue) and B (green), when the SAW device was exposed to either air or pure glycerol (total loss). The vertical dashed line represents the 251.5MHz frequency chosen to drive the SAW devices. The horizontal dashed lines indicate the insertion loss measured for each sample. **b)** Barchart to show the ratio γ_1 measured for each prototype. Each bar represents the average of 3 independent measurements, error bars represent the standard deviation from the mean.

The analysis of ratios γ_2 and γ_3 presented in Figure 5.7 revealed some useful information. As expected, the ratio γ_3 (which indicates the magnitude of the gap between the insertion loss measured for a sample, and the total insertion loss) was significantly reduced by reducing the length of the delay line from 9 to 5mm, for all samples tested (0.77±0.018 to 0.67±0.011 for deionised water, 0.84±0.019 to 0.70±0.010 for 10% glycerol, 0.92±0.012 to 0.75±0.010 for 20% glycerol and 0.97±0.012 to 0.80±0.007 for 30% glycerol, Figure 5.7c). This confirms the theoretical prediction presented in Figure 5a, showing that γ_3 should decrease with the length of the delay line. Similarly, Figure 5.4 showed that γ_2 should follow the opposite pattern and increase when reducing the length of the delay line. This was confirmed by the experiments conducted as Figure 7b shows that γ_2 was found to be smaller for prototype A than for prototype B in 5 out of 6 cases (0.92±0.004 compared to 0.95±0.002 for deionised

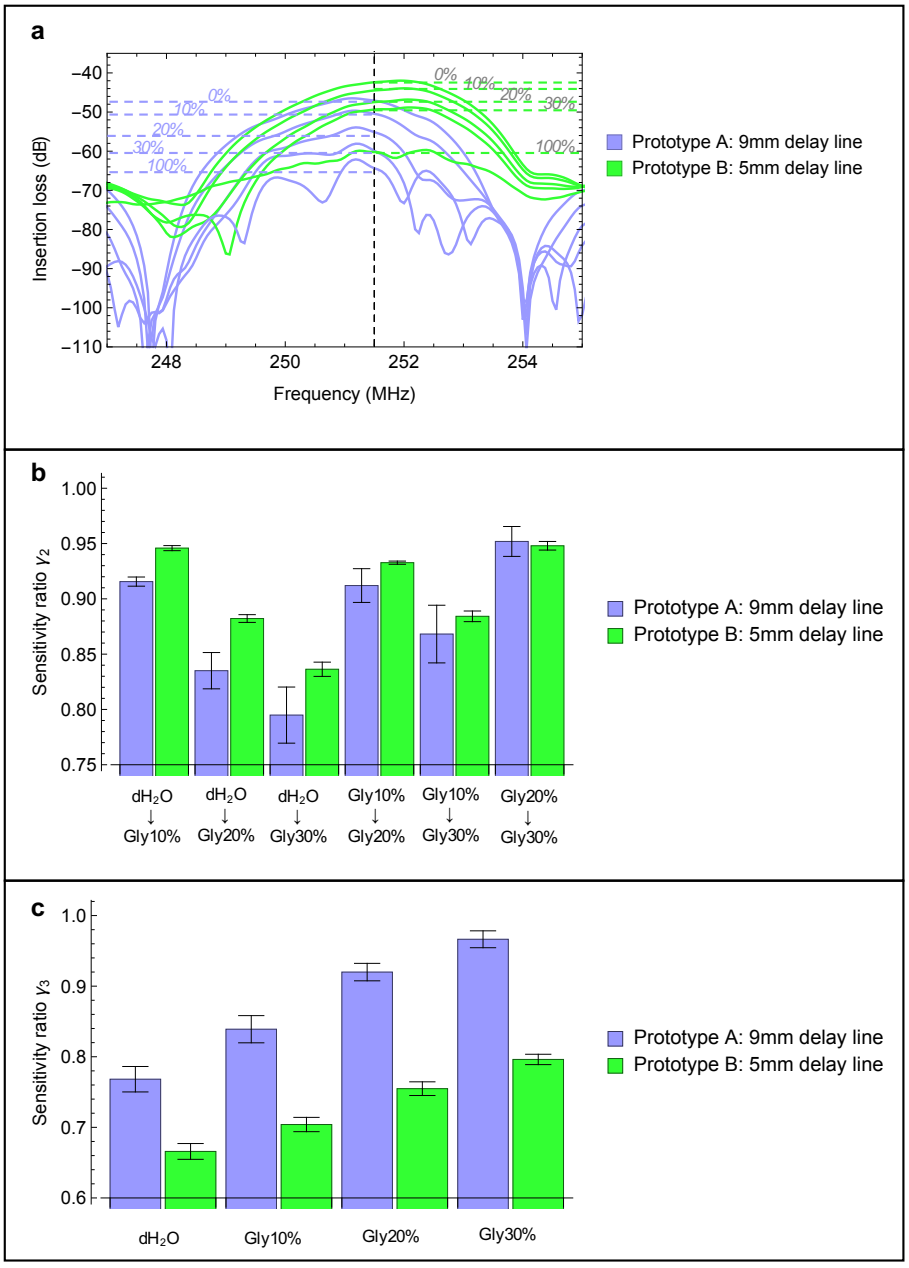

Figure 5.7: Influence of the length of the delay line on the SAW device sensitivity: ratios γ_2 and γ_3. a) Plot to show the insertion loss (dB) measured as a function of the driving frequency on prototype A (blue) and B (green), when the SAW device was exposed to solutions of glycerol at various glycerol content. The glycerol content (v/v) corresponding to each line is indicated on the plot. The vertical dashed line represents the 251.5MHz frequency chosen to drive the SAW devices. The horizontal dashed lines indicate the insertion loss measured for each sample. **b)** Barchart to show the ratio γ_2 measured for each prototype. For each bar, the two samples used to evaluate the ratio are indicated on the chart. Each bar represents the average of 3 independent measurements, error bars represent the standard deviation from the mean. **c)** Barchart to show the ratio γ_3 measured for each prototype. For each bar, the sample used to evaluate the ratio is indicated on the chart. Each bar represents the average of 3 independent measurements, error bars represent the standard deviation from the mean.

water over 10% glycerol, 0.84±0.016 compared to 0.88±0.004 for deionised water over 20% glycerol, 0.79±0.025 compared to 0.84±0.006 for deionised water over 30% glycerol, 0.91±0.015 compared to 0.93±0.001 for 10% glycerol over 20% glycerol and 0.87±0.026 compared to 0.88±0.005 for 10% glycerol over 30% glycerol), the only exception being the ratio of insertion loss measured for the most viscous solutions (0.95±0.014 compared to 0.95±0.004 for 20% over 30% glycerol). However, the larger error bars observed for all measurements involving 30% (v/v) glycerol solutions indicate that the SAW devices are less suited to operate in this viscosity region, as they do not offer the same reproducibility observed for samples of lower viscosities.

As explained above, a SAW device presenting a small γ_2 ratio can be used to distinguish two samples that are only differenced by a fine perturbation, while γ_3 gives an indication on the range of perturbations the SAW device can measure. In the particular case of the application of biosensing, all perturbations of interest will be very fine and therefore the γ_3 ratio matters less than the value of γ_2: the ideal SAW device should present the smallest possible γ_2 ratio in the region of viscosity that corresponds to the viscosity of the samples tested. A 10% (v/v) glycerol solution has a viscosity of 1.21mPa.s at 25°C, which corresponds roughly to the viscosity of blood plasma at 37°C, estimated to be in the region of 1.10-1.30mPa.s.[180] As all the biological samples tested throughout this project were either based on aqueous buffer solutions (for which the viscosity is comparable to that of deionised water) or human blood plasma, the ideal criteria for the SAW device was to present a small γ_2 ratio for the water to 10% glycerol solution and 10% glycerol to 20% glycerol transitions. As can be seen in Figure 5.7b, prototype A is better than prototype B in that respect. A length of 9mm for the delay line is therefore preferable over 5mm, when considering that the SAW device is going to be used as a biosensor. For other applications, however, such as a pure viscosity sensor operating over a large range of viscosities, reducing the length of the delay line would have proved beneficial.

5.1.6 Improving SAW device sensitivity by cancelling out the bulk component of the signal

One of the features of the OJ15 SAW device prototype, as explained in Chapter 4, is the use of a second delay line to cancel out the bulk component of the signal measured at the output IDT. When the acoustic wave is generated at the input IDT, most of it propagates along

the surface of the delay line, but a small bulk component is still observed. By introducing a reflector on the lower delay line, the surface component of the wave is blocked on its way to the output IDT, and therefore only the bulk component is measured. This can then be subtracted from the upper delay line (the one used for sensing purposes) in order to only consider the surface component of the signal. The effect of this feature on the device sensitivity was studied by testing the two prototypes presented in Figure 5.8, which only differ by the presence or not of the reflector on the lower delay line: in other words, one prototype (prototype A) does not subtract the bulk component of the signal whereas the other one (prototype C) does.

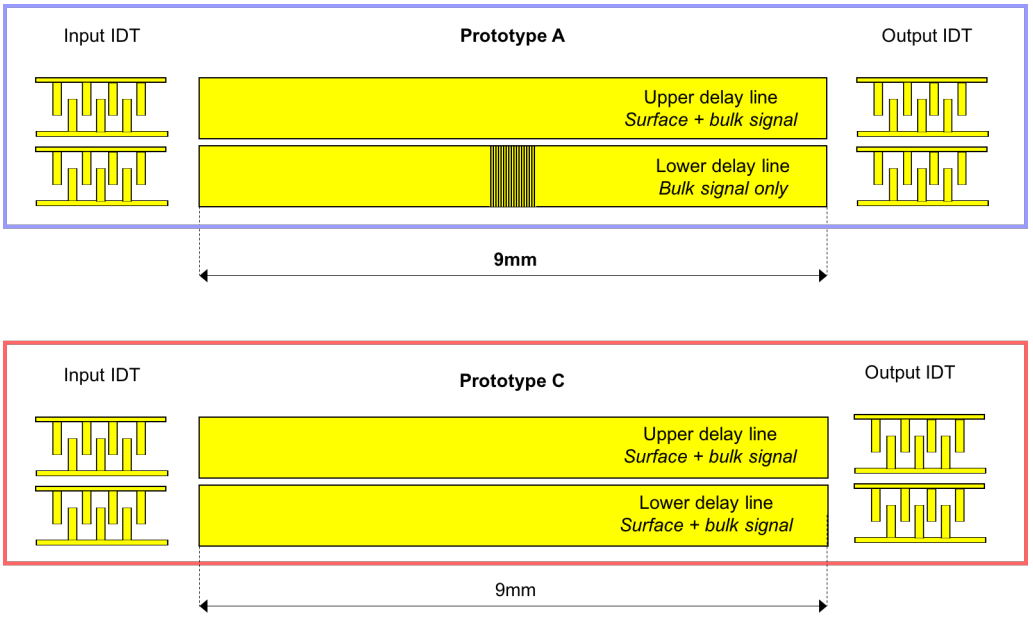

Figure 5.8: Prototypes A and C used to study the influence of cancelling out the bulk component of the signal on the SAW device sensitivity. Schematics of the prototypes of SAW device used to study the influence of cancelling out the bulk component on the device sensitivity. The two prototypes are identical apart from the presence (prototype A) or absence (prototype C) of a feature on the lower delay line to cancel out the surface component. Drawings not to scale.

The same experiments presented above when studying the effect of the length of the delay line on the device sensitivity were conducted. The insertion loss of different glycerol/water solutions was measured, and the ratios γ_1, γ_2 and γ_3 analysed. Results are presented in Figure 5.9 and 5.10.

As can be seen in Figure 5.9, the ratio γ_1 was slightly decreased by the cancellation of the bulk component of the signal: 0.36±0.015 to 0.41±0.020. This insertion loss measured for prototype C is reduced (in absolute value) by the presence of the bulk component. While it

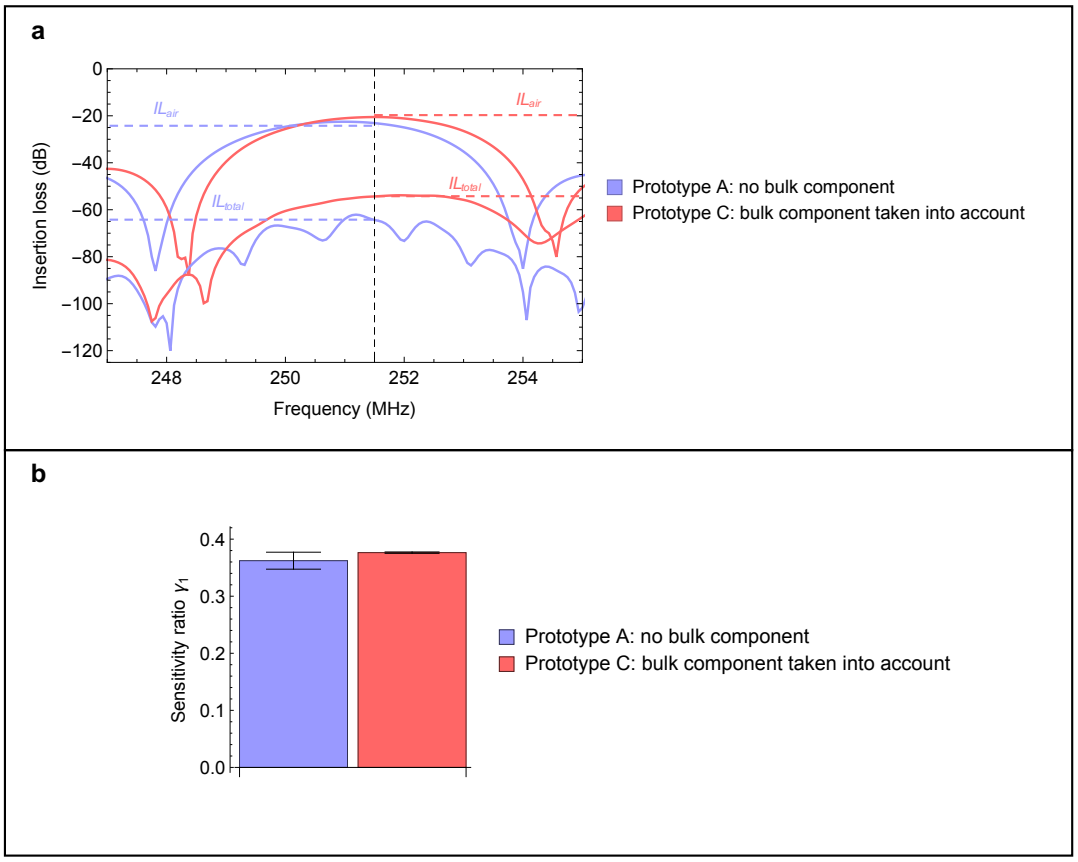

Figure 5.9: Influence of cancelling out the bulk component of the signal on the SAW device sensitivity: ratio γ_1. a). Plot to show the insertion loss (dB) measured as a function of the driving frequency on prototype A (blue) and C (red), when the SAW device was exposed to either air or pure glycerol (total loss). The vertical dashed line represents the 251.5MHz frequency chosen to drive the SAW devices. The horizontal dashed lines indicate the insertion loss measured for each sample. **b)** Barchart to show the ratio γ_1 measured for each prototype. Each bar represents the average of 3 independent measurements, error bars represent the standard deviation from the mean.

is not fully understood how the bulk component of the signal varies with the perturbation occurring on the surface of the delay line, it appears that cancelling it out it has a positive impact on the ratio γ_1, and therefore on the SAW device sensitivity.

As for the ratios γ_2 and γ_3, the same observations that were made above about Figure 5.7 apply to Figure 5.10. The presence of the reflector on the lower delay line, cancelling out the bulk element of the signal and only focusing on the surface component appeared to help reducing γ_2 for all the combination of samples tested, while increasing γ_3 (as expected when decreasing γ_2) for all the samples tested. Once again, with the application as biosensor in mind, prototype A was therefore considered to be more relevant than prototype B, as it proved to be more sensitive to fine perturbations (smaller γ_2), particularly around the

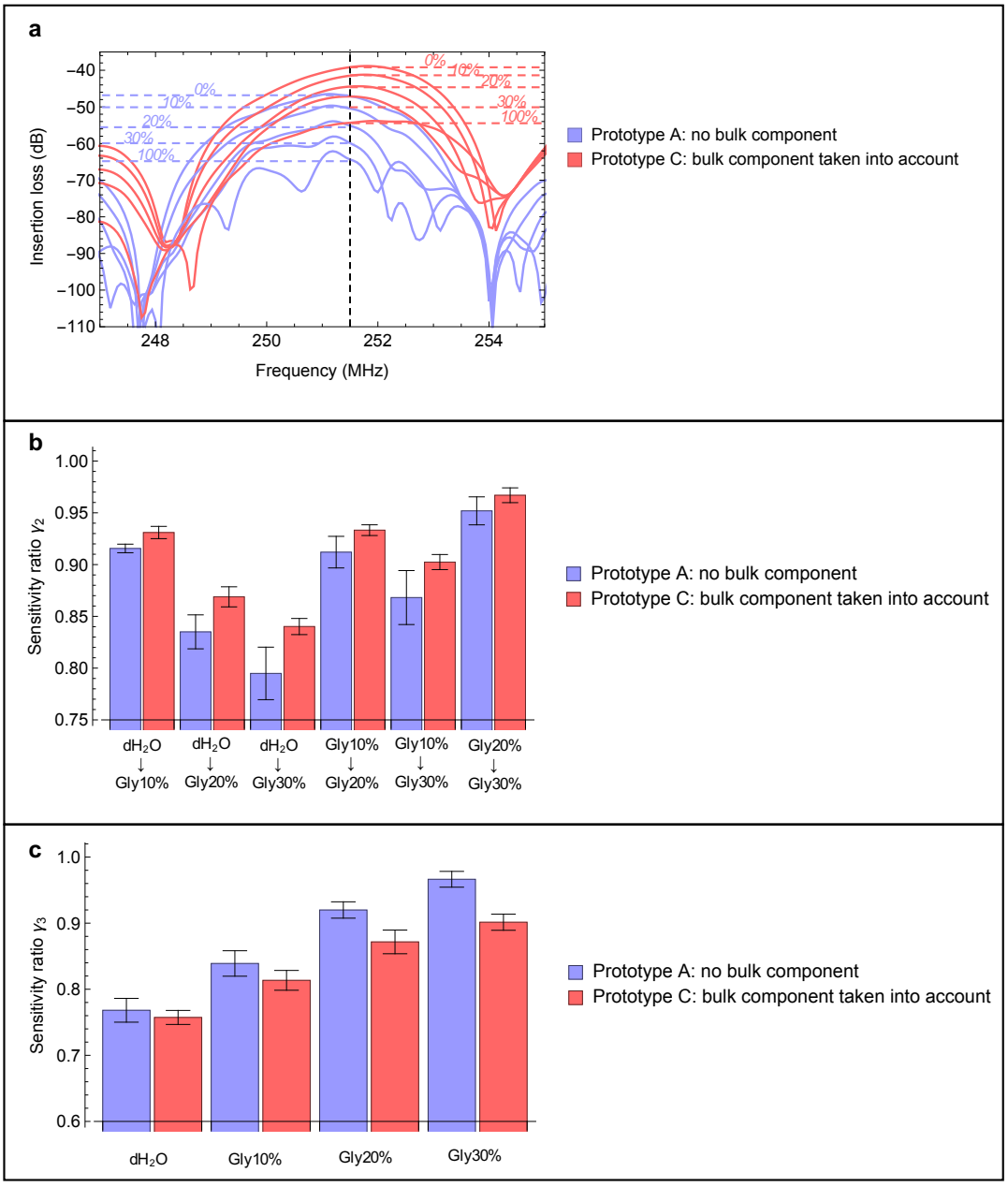

Figure 5.10: Influence of cancelling out the bulk component of the signal on the SAW device sensitivity: ratios γ_2 and γ_3. a) Plot to show the insertion loss (dB) measured as a function of the driving frequency on prototype A (blue) and C (red), when the SAW device was exposed to solutions of glycerol at various glycerol content. The glycerol content (v/v) corresponding to each line is indicated on the plot. The vertical dashed line represents the 251.5MHz frequency chosen to drive the SAW devices. The horizontal dashed lines indicate the insertion loss measured for each sample. **b)** Barchart to show the ratio γ_2 measured for each prototype. For each bar, the two samples used to evaluate the ratio are indicated on the chart. Each bar represents the average of 3 independent measurements, error bars represent the standard deviation from the mean. **c)** Barchart to show the ratio γ_3 measured for each prototype. For each bar, the sample used to evaluate the ratio is indicated on the chart. Each bar represents the average of 3 independent measurements, error bars represent the standard deviation from the mean.

viscosity region of interest (0.91±0.004 compared to 0.93±0.006 for deionised water over 10% glycerol, and 0.91±0.015 compared to 0.93±0.005 for 10% glycerol over 20% glycerol).

Prototype A, corresponding to the OJ15 SAW device presented in Chapter 4, was therefore shown to offer the best guarantees for offering a good sensitivity as a biosensor testing either human blood plasma or aqueous buffer based mock samples. The combination of a 9mm long delay line (instead of a shorter 5mm delay line) and the presence of a reflector on the lower delay line to cancel out the bulk component of the signal proved to give prototype A the edge over prototypes B and C. This study could be used in the future to make further refinement of the sensitivity of the SAW device, if the focus changes to testing whole human blood instead of human blood plasma, as the viscosity of blood is higher than that of plasma.

5.2 Influence of surface coverage of the delay line on output signal

Having established the ideal parameters to give OJ15 SAW devices the optimal sensitivity in the context of a biosensor, it was decided to study the influence of the surface coverage of the delay line on the output signal. This was motivated by the observation that a signal was still measured despite the sample not covering the entire area of the delay line. In addition, the situation when the sample did not instantly spread across the entire surface of the delay line occurred fairly frequently and was identified as a potential future problem for the SAW device being a key component of a PoCT.

One of the main characteristics to focus on when designing a PoCT is the simplicity of use. Ideally, the test would be designed to be performed by non-trained staff, with the simple instructions coming with the test proving enough to make virtually anyone be able to use the device and perform the test. It is crucial, however, to identify the possible mistakes that could be made by the person performing the test and assess whether they would have an impact on the test result or even on its validity. A 2014 study in Kenya and South Africa has shown that prototypes of HIV self PoCT were used incorrectly by more than 75% of the lay users involved in the study, leading to invalid results.[24]

Most PoCT for HIV are lateral flow tests, and the most common mistake that can be made by the test user and lead to an incorrect result is a misinterpretation of a faint line. This comes down to a combination of differences in eyesight and personal judgement, and there is hardly a perfect solution to this problem. In the case of the biosensor presented here, the readout is electronic and the analysis is performed by smartphone, avoiding any human judgement and potential for misinterpretations. One step of the assay, however, was identified as a potential source of error. When loading the sample onto the surface of the SAW biochip, it is possible to leave a certain fraction of the surface uncovered by any liquid and left exposed to air. This is due to the relative hydrophobicity of the surface which sometimes leads to the small volume of liquid sample forming a droplet instead of spreading evenly across the sensing area. An example is shown in Figure 5.11.

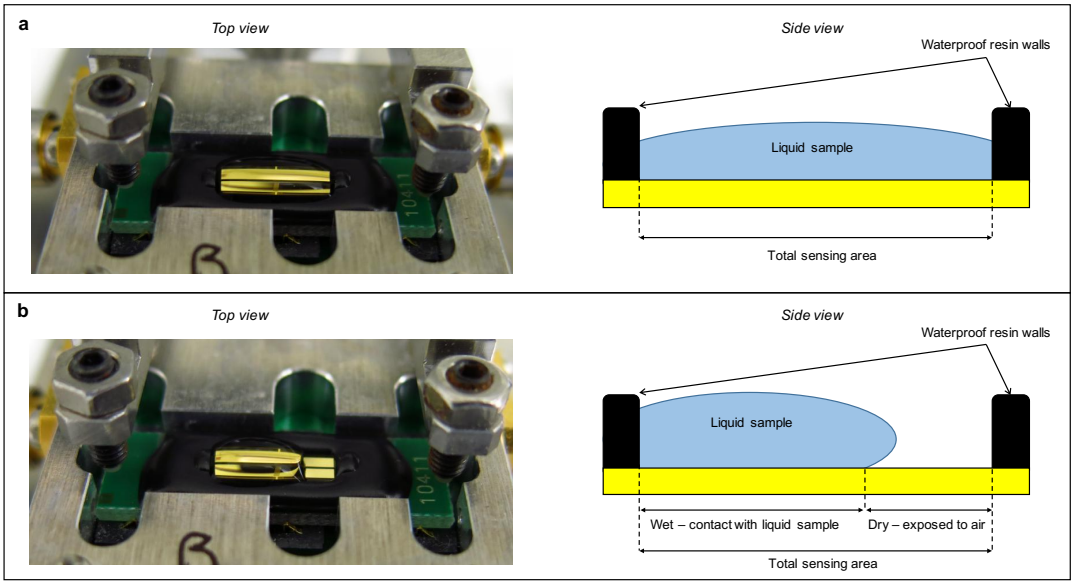

Figure 5.11: Loading of liquid sample onto the SAW biochip. a) Picture taken from the top of the SAW biochip (left) showing the 20μl droplet of deionised water covering the whole surface of the sensing area, and side view schematics associated (right). Drawings not to scale. **b)** Picture taken from the top of the SAW biochip (left) showing the 20μl droplet of deionised water covering a fraction of the surface of the sensing area, instead of spreading out across the whole surface, and side view schematics associated (right). Drawings not to scale.

It was decided to investigate whether a mishandling of the liquid sample, resulting in uneven coverage of the sensing area of the SAW biochip, had direct consequences on the performance and validity of the test. To do so, a fraction of the sensing area of a SAW biochip was put in contact with liquid, while the remaining dry fraction remained exposed to air. This was achieved by carefully pipetting a 20μl droplet of deionised water onto

the clean surface of the SAW biochip, and purposely making sure the liquid would form a droplet instead of spreading out evenly across the surface. The change in phase shift and amplitude loss was measured before and after deposition of the droplet. The surface was then cleaned and dried before a new droplet was deposited. The process was repeated 76 times. The phase shift and insertion loss measured upon addition of each droplet are presented on the barchart in Figure 5.12.

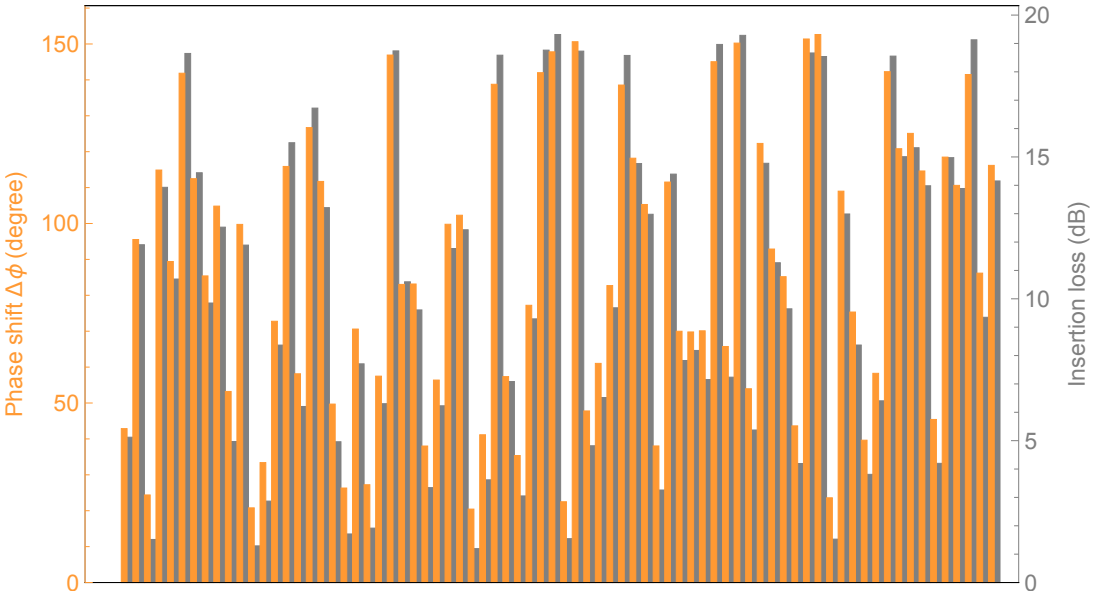

Figure 5.12: SAW biosensor response to liquid droplets loading. Barchart to show the signal measured by the SAW biosensor upon addition of 76 20μl droplets of deionised water on the surface of the dry sensing area. Each orange bar corresponds to one independent measurement and represents the phase shift (left axis) measured upon addition of one droplet. The green bar directly to its right represents the corresponding amplitude loss (right axis) measured for the same droplet.

As can be seen in Figure 5.12, all 76 droplets of liquid on the dry surface of the sensing area were detected by the SAW biosensor, as all measurements show at least a small response in both the phase shift and the amplitude loss. There is also a good correlation between the phase shift and the amplitude loss measured for each droplet. This shows that the SAW biosensor has the ability to show a response despite potential incorrect handling of the sample from the person performing the test.

It is important to note however, that despite all droplets being the same volume (20μl), the signals measured for each of the 76 droplets vary quite a lot (phase shift as low as 20 degrees and as high as 152 degrees, insertion loss varying from 1 to 19dB). As the hydrophobicity of the surface of the sensing area varied slightly between each measurement, in addition to the fact the manual pipetting technique is not perfectly reproducible, the shape of the droplet changed between each measurement, therefore the fraction of the sensing area in contact with liquid (referred to as θ_L below) was different for each measurement. It was therefore possible to study the influence of the signal output as a function of θ_L. The estimation of θ_L was based on pictures of the SAW device taken from the top, and an image recognition software written in Mathematica, which compared the area of the sensing area and the area of the droplet. As the pictures were taken from the top, the angle the droplet edges formed with the surface (see Figure 5.11b) was not taken into account, and the value of θ_L was slightly overestimated as a consequence. The results from this study are therefore not exact, but as the process of image recognition was automated and applied to each picture in the same way, they can be considered consistent relative to each other. They were separated in three categories, depending on whether the droplet was in contact of the left hand side of the sensing area (directly after the input IDT), the right hand side (directly next to the output IDT) or simply sitting at the centre, not in contact with either sides. Examples are shown in Figures 5.13. The phase shift and amplitude loss are plotted as a function of θ_L in Figure 5.14.

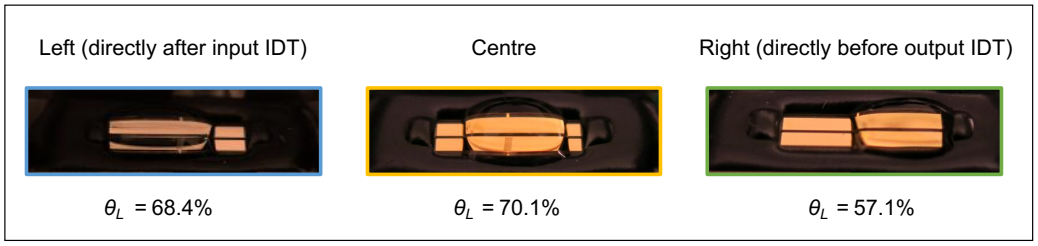

Figure 5.13: Examples of incorrect liquid sample loading onto the sensing area of the SAW device. Three cases of liquid sample were studied, characterised by the position of the droplet with respect to the IDTs: left hand side (blue), centre (orange) and right hand side (green). All pictures were taken from the top of the SAW devices, with the input IDT on the left hand side and the output IDT on the right hand side. In each case, the estimated percentage of the surface covered in liquid (θ_L) is indicated underneath the picture.

As can be seen in Figure 5.14, a very good correlation can be observed between θ_L and both signal outputs (phase shift and insertion loss). Both in Figures 5.14a) and 5.14b), the similarity observed between each set of data (left hand side, right hand side or centre, with

respect to the IDTs) show that the portion of the sensing area left dry does not influence the amount of output signal lost. However, they also show and this is confirmed by the linear regression performed on the whole data (black line, Figure 5.14a and 5.14b) - that the magnitude of the output signal does depend directly and proportionally on the percentage of surface covered (θ_L).

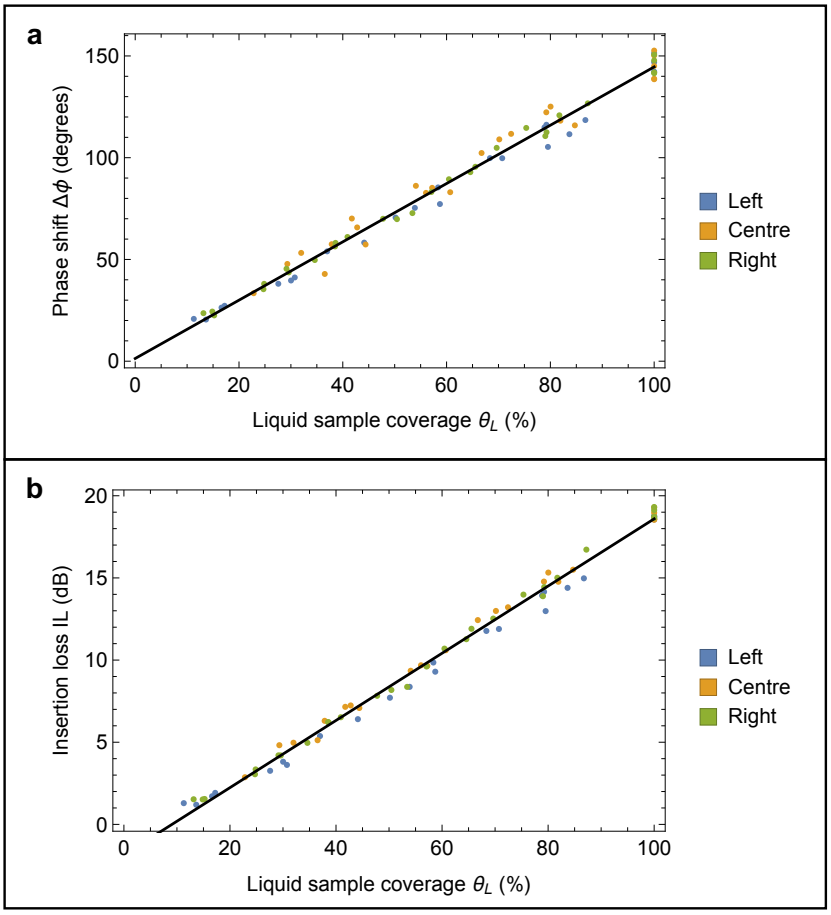

Figure 5.14: Influence of liquid sample coverage of the sensing area on the loss of output signal. a) Plot to show the phase shift measured upon addition of 20μl droplets of deionised water on the surface of the SAW device. Each point represents one measurement. The black line represents the linear regression ($1.4x + 1.33, R^2 = 0.987$) performed on the whole data set, all three categories combined. **b)** Same as **a)**, for the insertion loss. The black line represents the linear regression ($0.2x - 1.9, R^2 = 0.993$) performed on the whole data set, all three categories combined.

This small study demonstrated the importance of correct handling of the sample by the test operator. Despite the SAW biosensor being capable of giving a response upon addition of a droplet of sample leaving a fraction of the sensing area dry, it was demonstrated that the magnitude of this response was directly proportional to the fraction of the surface in contact with liquid. In other words, a fraction of the magnitude of the signal is lost when the

sample does not spread evenly across the whole sensing area. As the test response would have been calibrated against results obtained with a fully wet sensing area, not making sure the samples covers the whole sensing area would make the test result invalid. This key conclusion will have to feature, in the future, in the instructions of use designed to help non-trained staff to correctly use the test.

Additionally, it can be envisaged to implement a built-in test validity criterion within the algorithm processing the data, as the amplitude loss measured will always have to be greater than a minimal threshold value corresponding to the addition of deionised water on a dry chip. Any other sample would be more viscous or contain proteins that can potentially adsorb or bind to the surface, therefore leading to a greater perturbation. All results presented in this thesis were obtained with the sensing area fully covered by the liquid sample measured.

5.3 Statistical analysis of reproducibility and repeatability OJ15 SAW device measurements

The SAW devices used throughout this work were considered as disposable devices, as in only one measurement per device was made. The idea behind this was that ultimately the SAW device would be the only component of the biosensor in contact with human blood and therefore would have to be disposable. It was necessary to treat each SAW device as such when optimising it. However, to do so, a careful statistical analysis was conducted, in order to assess whether measurements made with different SAW devices could be compared with confidence. As the lab control box had the capacity to drive 4 different SAW devices using the 4 different holders at the same time, the agreement between the measurement performed by each of the holders was studied.

As presented in Chapter 4, the prototype of the control box used to perform all the measurements presented in Chapter 6 and 7 features 4 individual holders, each used to run a test with a different SAW device. Most of the results presented later were obtained by making use of this and either running an identical test on all 4 devices, or using some of them as reference for the others. In both cases, relying on a good agreement between the measurement performed by all 4 holders was crucial.

As all 4 holders were always used at the same time as part of the same run, it was decided to use the data obtained on runs where all 4 SAW devices were used to measure the same sample. In order to study the agreement between the holders as accurately as possible, the sample that was measured the most times was selected: the measurement of the insertion loss corresponding to the addition of deionised water on the surface of the dry delay line of the SAW device.

The method chosen was the Bland-Altman method.[181] It is commonly used to assess the reproducibility of a measurement performed on the same sample using two different instruments or methods.[182] Here, each holder was considered to be a different instrument and the agreement between each pair of holders was studied, which corresponds to six cases: if the 4 holders are called A, B, C and D, the six pairs are AB, AC, AD, BC, BD and CD. The idea behind studying each possible pair was that if there is reasonable agreement between the measurements performed on any pair of holders, any holder could be used as a valid reference for the test running on another holder. Similarly, any test could be run in duplicate on another holder and be compared with confidence.

The Bland-Altman method relies on studying the difference measured between the two measurements of the sample by two different methods (here, each holder in the pair considered). The data was checked for normality with a Q-Q plot, and no evidence of non-normality was found. The differences between two measurements are plotted against the mean of the two measurements in Figure 5.15, for each pair of holders considered. Each point represents the difference between two measurements run at the same time, on two different holders.

The disparity observed in the mean of the measurements (from 37 to 43dB approximately) can be explained by the fact the dataset includes runs taken over a long period of time (three years), during which some settings that may affect the measurements are likely to have taken place. These include the lab temperature, the sample temperature, the model of prototype control box used (three different models were used) and the amplifier settings used in the control box. None of these adjustments matter with regards to this study, however, as each data point is associated to measurements taken at the same time and therefore with everything being equal apart from the holder used.

On each plot, the solid red line on the plot indicates the mean of the differences, and the dashed red lines the limits of agreement lim_1 and lim_2. The limits of agreement give a

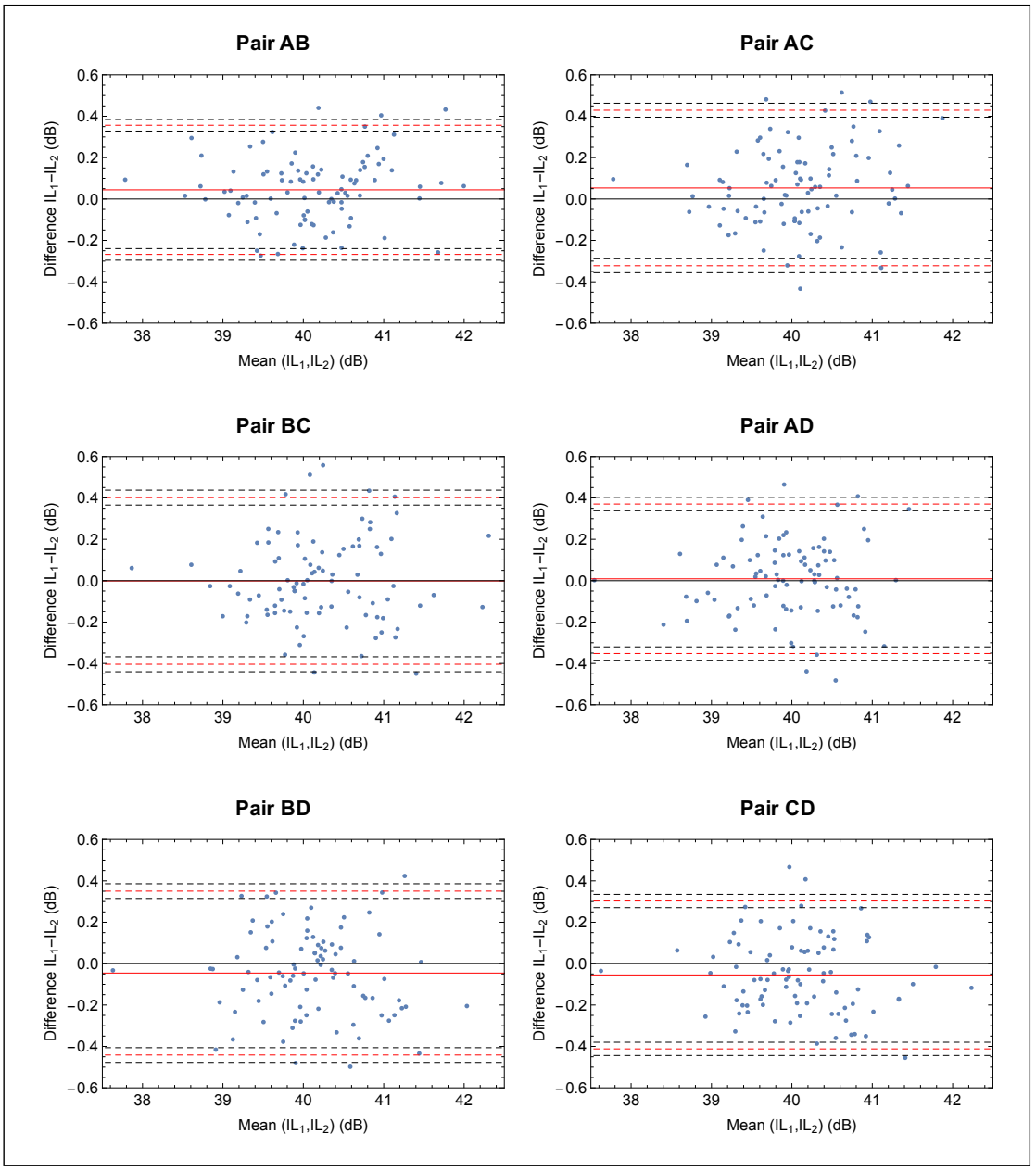

Figure 5.15: Reproducibility of measurements taken using different holders as part of the same run. Blant-Altman plots of measurements of insertion loss (deionised water) taken with two different holders as part of the same run. For each pair (indicated above the plot), the difference in insertion loss measured between the first and second holder (in alphabetical order) is plotted as a function of the mean of the two measurements. On each plot, the red solid line indicates the mean of the differences, the red dashed line indicates the limits of agreement of the mean (lim_1 and lim_2), and the black dashed lines indicate the 95% confidence of interval around each limit of agreement. Each plot represents 91 independent measurements.

range within which 95% of future differences in measurements between the two methods are expected to lie. The limits of agreement [183] are calculated as:

$$\begin{cases} lim_1 = Mean(differences) + 1.92SD(differences) \\ lim_2 = Mean(differences) - 1.92SD(differences), \end{cases} \tag{5.11}$$

where $SD(differences)$ is the standard deviation from the mean for the set of differences.

Finally, a 95% confidence interval (CI) is calculated around each limit of agreement, as these are estimated and also need their own limits of agreement. [183] It is calculated as follows:

$$CI = \frac{1.71SD(differences)}{\sqrt{n}}, \tag{5.12}$$

where n is the number of elements in the data set. On each plot in Figure 5.15, the dashed black lines indicate the 95% confidence interval around each limit of agreement.

The limits of agreements used in the Bland-Altman theory only give an indication on how far apart two measurements are expected to be for 95% of all measurements made using the two methods tested. They do not indicate whether this is acceptable in the specific case of measuring the insertion loss of deionised water with two SAW device holders, this has to be determined with regards to the context in which future measurements will be made. [181–183] The limits of agreement (and associated 95% confidence interval) are summarised in Table 5.1.

The largest theoretical disagreement between two measurements corresponds to pair BD (-0.48dB). Given that the measurement studied here is lies between 38 and 42dB, it means that even in the worst case, 95% of all measurements will differ by no more than 1.3% of the measured insertion loss. The insertion loss measured in this study corresponds to quite a large perturbation (air to deionised water). Such a small error in between two measurements taken on different holders is therefore acceptable. The four holders were considered to be equivalent and were used throughout this thesis interchangeably for reference or duplicate tests run in parallel to the main test.

Pair	lim_1	lim_2	CI	$lim_2 - 1.96\,CI$	$lim_2 + 1.96\,CI$	$lim_1 - 1.96\,CI$	$lim_1 + 1.96\,CI$
AB	0.36	-0.27	0.014	-0.30	-0.24	0.33	0.38
AC	0.43	-0.32	0.017	-0.36	-0.29	0.40	0.46
AD	0.40	-0.40	0.018	-0.44	-0.37	0.37	0.44
BC	0.377	-0.35	0.017	-0.38	-0.32	0.34	0.40
BD	0.35	-0.44	0.018	-0.48	-0.41	0.31	0.39
CD	0.30	-0.41	0.016	-0.44	-0.38	0.27	0.33

Table 5.1: Limits of agreement between two measurements. Table to summarise, for each pair of holders, the limits of agreement around the mean (lim_1 and lim_2), the 95% confidence interval CI and the subsequent four limits obtained by adding and subtracting CI from lim_1 and lim_2. For each pair of holders, the highest and lowest disagreement between measurements are highlighted in red.

5.4 Discussion

The SAW device used to obtain the results presented in the next chapters was manufactured by partner company Japan Radio Company (JRC, Japan). In this chapter, the device was carefully characterised from three different yet complimentary approaches.

It was shown that the sensitivity of the device was optimal in the context of the device being used to measure small perturbations in the viscosity region corresponding to that of human plasma, or aqueous buffer which were used extensively to optimise the surface chemistry, as will be described in the next chapter. The optimal sensitivity was shown to be achieved by tuning three key parameters of the device: (i) driving the SAW device at a frequency of 251.5MHz, corresponding to the closest achievable frequency from the ideal frequency, which was shown to be 251±0.16MHz; (ii) having a delay line of 9mm instead of 5mm, which gives the device the ability to distinguish between fine perturbation in the viscosity of interest with greater precision; (iii) cancelling out the bulk component of the signal, to measure only the surface component which is more directly influenced by the perturbations occurring on the surface. Once again, it was shown that doing so gives the SAW device a greater ability to sense small perturbations occurring in samples of viscosity close to that of either human plasma or aqueous buffer.

During the course of this work, numerous measurements were performed to either optimise the transformation of the SAW device into a SAW biochip, or to run a test on an optimised SAW biochip. It was observed that sometimes, the sample pipetted onto the delay line had to be forced to spread across the whole surface, as it sometimes formed a droplet on top of

the relatively hydrophobic surface. It was also noted that in this situation, an output signal was still delivered by the control box. The influence of the surface coverage of the delay line by the liquid sample was studied, and it was shown that a strong correlation existed between the fraction of the area of the delay line covered by liquid and the magnitude of the output signal. This was identified as a key information in the context of turning the SAW device into a component of a PoCT, as one of the main characteristics of a POC is to be designed to avoid as many operator mistakes as possible. Knowing that the performance of the test is directly related to a correct handling of the sample (a maximum signal is obtained when the sample spread across the entire surface of the delay line) will be a key factor in designing both the disposable SAW device, and also the test instructions.

Each device was considered to be disposable and, in the vast majority of cases, was used only once to perform a single run of measurements. This was justified by the fact the SAW device would ultimately be turned into a key component of the SAW biosensor, and that it would be the only component in contact with human fluids and therefore would have to be disposable. The fact that the results of each run of measurement performed with OJ SAW devices were obtained from four independent holders connected to the same prototype control box was studied, and it was shown that the variable introduced by performing a similar measurement on independent pieces of equipment did not influence their reproducibility. The Blant-Altman method was applied to measurements performed in parallel using four independent holders. In the example, the insertion loss caused by the addition of deionised water on the delay line was measured an example chosen for the high amount of relevant data available. It was shown that each holder could be used interchangeably and that the results obtained with any holder could be used as a reference for another test run at same time using a parallel holder. Similarly, any test could be run in duplicate at the same time using a parallel holder.

This careful characterisation of the SAW device paved the way for transforming it into a SAW biochip capable of detecting the presence of a specific target protein in a sample. Indeed, the process of optimising the SAW biochips required a high sensitivity across a large number of independent measurements. All the results obtained with the SAW biochips, as well as the process of optimisation, are presented in the next two chapters.

Chapter 6

Detecting Model Proteins and HIV Markers of Infection

The objective of this chapter was to optimise the performance of the SAW biosensor assays for highly sensitive, specific, robust and rapid detection of HIV biomarkers. Initial work focused on a model protein assay based on human serum albumin (HSA) and anti-HSA antibodies. This assay was used to optimise the thiol linker chemistry, the loading concentration of capture proteins on the SAW biochips and the response to different target antibody concentrations in solution. It was then decided to systematically optimise the assay parameters for HIV biomarkers of interest, including (i) the response of different antibodies and specificity testing using a non-specific antibody (negative control), (ii) reproducibility of measurements on a single SAW biochip, (iii) the detection of clinically relevant concentrations of anti-HIV antibodies; (iv) reducing the time to result for ultra-rapid testing; (v) proof of concept detection of the HIV p24 antigen; (vi) benchmarking to a benchtop quartz crystal microbalance (QCM) and (vii) signal amplification strategies using gold nanoparticles. Highlight results include the detection of anti-p24 antibodies at clinically relevant concentrations, proof of concept of result delivery within 10 seconds of sample injection, and detection of HIV p24, the key target protein for fourth generation PoCT for HIV.

6.1 Proof of concept using a model protein complex: HSA/anti-HSA

6.1.1 Cleaning the surface of the delay line

In the interest of trying to get the best possible response out of the SAW biochip when performing an assay, every step of the functionalisation process that could potentially be optimised was studied. It was first identified that the strategy used to clean the gold surface prior functionalisation could have consequences on the quality of the capture protein layer, and therefore on the response of the sensor to the target protein detection. In order to assess the best way to clean the gold surface of the delay line of OJ15 SAW devices before functionalising it, a systematic study was conducted. Several SAW devices were cleaned with 5 different strategies (described in Chapter 4), after which antibodies were allowed to adsorb on the surface by incubating the surface in a sample of antibodies in PBS at a constant concentration (25μg/ml).

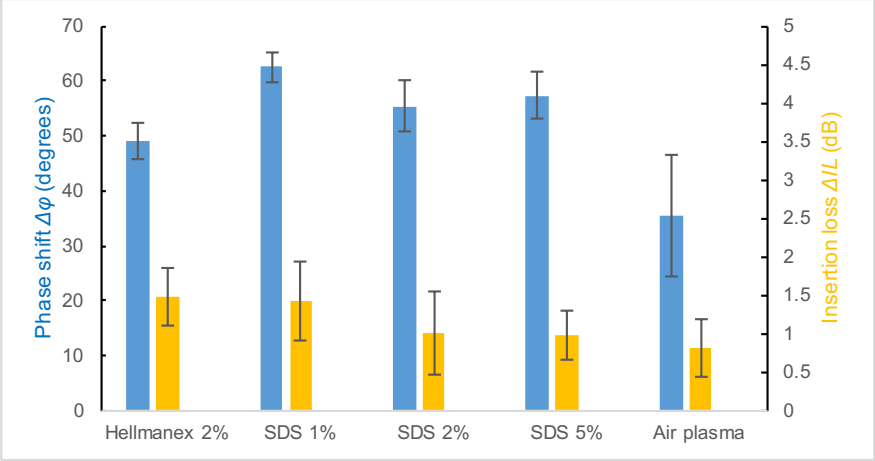

Figure 6.1: Influence of strategy used to clean the gold surface of the delay line. Barchart showing the change in phase shift (in blue) and insertion loss (in orange) measured following the adsorption of anti-HSA antibodies on the gold surface of the delay line. Each bar represents the average of at least 6 independent measurements, the error bars represent the standard deviation from the mean. The strategy used to clean the gold surface prior to antibody adsorption is specified on the horizontal axis. Values recorded 30min after sample injection.

As can be seen in Figure 6.1, the insertion loss measured when adsorbing antibodies on the surface of the delay line does not seem to be greatly dependent on the cleaning strategy used. For all strategies, the error bars are relatively large compared to the value of the

average. With that in mind, the two cleaning strategies that gave the highest reading are Hellmanex 2% (1.5±0.5dB) and SDS 1% (1.4±0.6). This trend is confirmed, and more pronounced, when looking at the phase shift recordings. Using the SDS 1 % cleaning strategy leads to the highest phase shift when adsorbing antibodies (62.6±2.1 degrees).

It is interesting to note that the air plasma cleaning strategy gave the worst results of all strategies tested (0.8±0.4dB and 35.5±10.6 degrees), despite being in theory the most efficient way to clean the gold surface out of all the strategies tested. This is likely to be due to the fact that the antibody adsorption could only be performed about 10 minutes after the surface had been cleaned, for logistical reasons. A more common practise is to functionalise the gold surface straight after it comes out of the plasma chamber, as the top layer of gold atoms is still very reactive following oxidation. In addition, using an air plasma is not as efficient as a dedicated oxygen plasma for example. A plasma created in a pure oxygen environment could potentially have helped to oxidise the top layer of gold atoms more efficiently, making the surface ore reactive and therefore making the subsequent functionalisation of the surface more efficient. Unfortunately, this equipment was not available at the time of the study. Unless stated otherwise, the surface of the delay line of all the SAW biochips that contributed to results presented in this thesis was cleaned with a solution of SDS 1%.

6.1.2 Model assay: HSA detection

Initial proof of concept work focused on HSA as a model, to demonstrate the proof of concept and optimise the assay parameters on the new SAW system. By way of background, HSA is a protein found in human blood plasma. It is produced in the liver, and constitutes about half of the blood serum protein, making it the most abundant protein in plasma. HSA is a major protein of the circulatory system, one of its function being the transport of hormones, fatty acids, and other low molecular weight compounds, as well as a number of drugs.[184,185] As both HSA and anti-HSA antibodies were cheap and easily accessible, it was decided to use the HSA/anti-HSA complex as a model protein for studying the detection of proteins using the SAW biosensor. The test assay is schematised in Figure 6.2. The gold surface of OJ15 SAW biochips was functionalised with anti-HSA antibodies, and this platform was used to detect HSA at various concentrations.

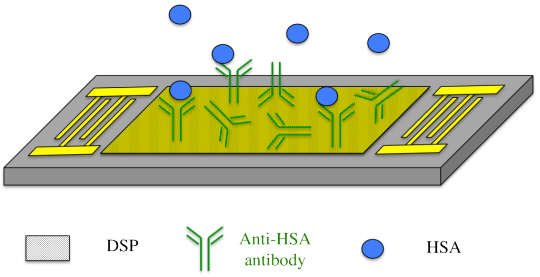

Figure 6.2: HSA assay schematic. The surface of the SAW biochip is coated with anti-HSA antibodies via DSP linker chemistry to the gold surface of the delay line. HSA proteins in the sample are detected when they form a complex with the capture proteins on the surface of the SAW biochip.

6.1.3 Influence of chemical linkers on SAW detection signal

The various proteins or antibodies that may be used as the first capture layer of the immunoassay cannot bind strongly to the gold surface on their own. There is therefore a need for an intermediate layer, strongly linking the proteins or antibodies of interest to the gold surface. Once cleaned, the surface of the delay line was functionalised with a chemical linker. A study of the best linking strategy is presented below. The results of this study pointed at Dithiobis[succinimidyl propionate] (DSP, also known as Lomants Reagent) as the best option as an intermediate to bind proteins to the gold surface.

DSP is an amine-reactive cross linker with NHS-ester reactive ends and a cleavable disulphide bond in the middle of its 8-carbon spacer arm ($12\mathring{A}$).[186] There are two main reasons why DSP is an ideal candidate for functionalising the gold surface in the prospect of creating a thin film of antibodies or other proteins. Firstly, the cleavable disulphide bond yields two identical thiols once cleaved, which happens on contact with gold.[187] Thiols are very good candidates for binding to gold as the formation of a strong non-covalent bond between the gold and the sulphur is very favourable. This is schematised in Figure 6.3. Secondly, DSP contains an amine-reactive N-hydroxysuccinimide (NHS) ester at each end of the spacer arm (i.e. at the end of each thiol once DSP has been cleaved). NHS esters react with primary amines at pH 7-9 to form stable amide bonds, along with release of the N-hydroxysuccinimide leaving group.[186] Given that proteins usually have several primary amines available on their structure, amine reactions are likely to occur, thus resulting in the formation of a capture protein layer above the surface.

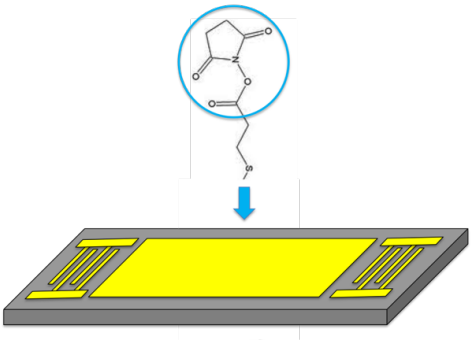

Figure 6.3: Gold functionalisation with DSP. The sulphur at the tail forms a strong non-covalent bond with the gold on the surface (blue arrow) while the NHS head group (circled in blue) will be used to react with primary amines on the outside of the protein or antibody structure.

DSP was chosen as the linker between the gold surface and the capture protein for all the protein detection assays conducted throughout this thesis. This was motivated by a first study on the effect of the nature of the linker on the protein detection signal. In this study, OJ15 SAW biochips were functionalised with anti-HSA antibodies using different linking strategies. HSA proteins were then detected from a sample solution of HSA proteins in TBS-T at 10nM. The different linking strategies are presented in Figure 6.5a. Three different linkers were tested: DSP, DTSSP (3,3 -dithiobis[sulfosuccinimidylpropionate], Thermo Scientific, UK) - which is very similar to DSP except for the fact it is sulfonated and therefore water soluble, see Figure 6.4 - and ORLA85, a protein designed by Orla Protein Technologies Ltd to bind to gold surface on one end and to the Fc portion of IgG molecules (constant fragment of the heavy chain) on the other end, theoretically improving the antibody orientation.

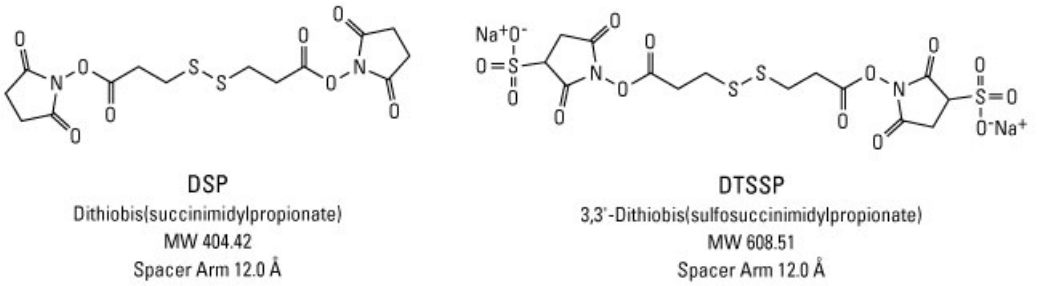

Figure 6.4: Chemical linkers tested to anchor the capture protein to the surface. Chemical structure of DSP and DTSSP. The two molecules are similar except for the fact DTSSP is sulfonated, which makes it soluble in water. DSP is soluble in DMSO. Courtesy of www.thermofischer.com

With both DSP and DTSSP thiol linker chemistries, the gold-sulphur bond drives the formation of a relatively well defined self-assembled monolayer and the terminal reactive ester group forms a covalent bond to the lysine residues on the protein used as the capture protein (here anti-HSA antibody). Finally, allowing the anti-HSA antibodies to simply adsorb onto the gold surface directly was also tested. The average phase shift measured when functionalising the surface, and when subsequently detecting HSA, are presented in Figure 6.5b and 6.5c respectively.

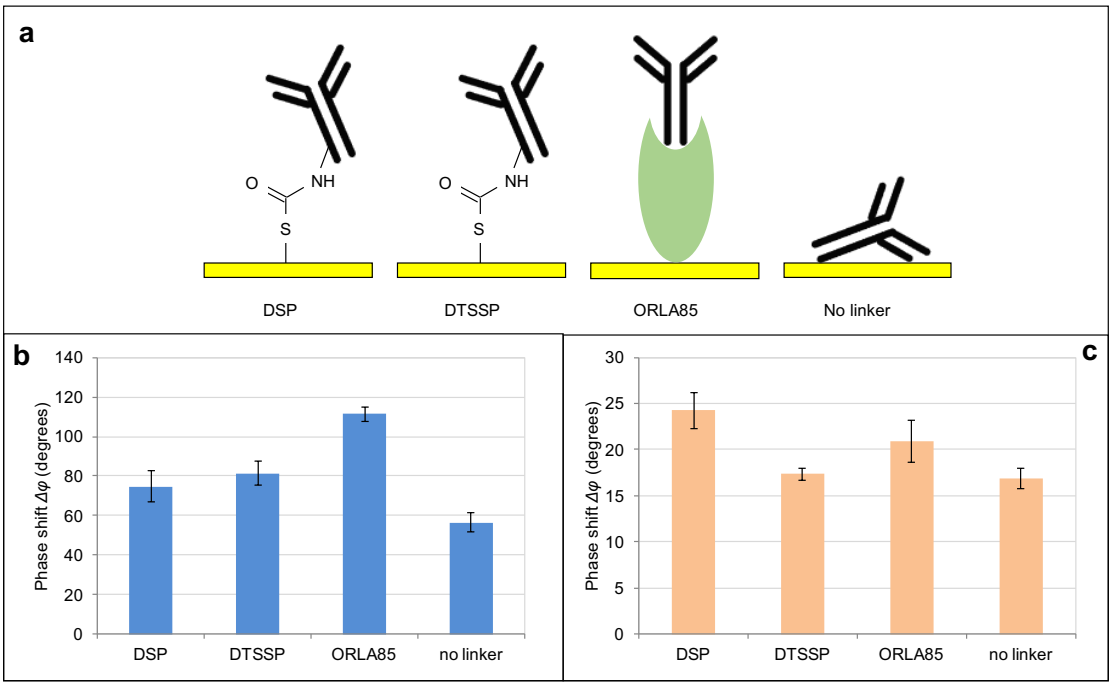

Figure 6.5: HSA test assay: influence of linker on detection signal. a) Schematics to show the different strategies used to link the anti-HSA antibody (in bold black) to the gold surface. **b)** Barchart to show the phase shift recorded 30minutes after injection of anti-HSA (100μg/ml in TBS-T). Each bar represents the average of at least 3 independent measurements normalised to a buffer only equivalent measurement, error bars represent the standard deviation of the mean. **c)** Barchart to show the phase shift recorded 30minutes after injection of HSA (10nM in TBS-T). Each bar represents the average of at least 3 independent measurements normalised to a buffer only equivalent measurement, error bars represent the standard deviation of the mean. The highest reading is observed for SAW biochips functionalised with DSP.

As can be seen in Figure 6.5b, not using any linker and simply allowing the antibodies to adsorb on the gold surface leads to the smallest phase shift (57±5.3 degrees), two similar linker molecules DSP (74.7±5.1) and DTSSP (81.5±4.9) give similar measurements and ORLA85 (111.3±3.2) gives the highest phase shift in the context of linking the capture anti-HSA antibodies to the gold surface. However, in the context of optimising the biosensor, the parameter that matters the most is the phase shift recorded when detecting the target

protein. As can be seen in Figure 6.5c, the trend observed for linking antibodies to the surface does not apply to the detection of the target protein. The highest phase shift is consistently given by SAW biochips functionalised with DSP as a linker for the capture protein (24.2±2.6). DSP was therefore considered to be the best candidate as a linker between the gold surface and the capture protein, and was used throughout the thesis to link any capture protein, in the interest of consistency and comparing different results.

6.1.4 Influence of capture protein density on detection signal

In order to observe the effect of the density of the capture protein on the detection signal, different concentrations of anti-HSA antibodies were used to functionalise OJ15 SAW biochips. Samples of HSA in TBS-T at a fixed concentration (10nM, equivalent to 670ng/ml) were then tested. The phase shift recorded during HSA detection on biochips functionalised with different densities of anti-HSA antibodies (from 0.1μg/ml to 1mg/ml) can be seen in Figure 6.6.

The general trend is that the higher the anti-HSA concentration used during functionalisation, the higher the phase shift recorded after 30 minutes. The phase shift recorded increases with the density of anti-HSA on the surface. An important difference in phase shift can be observed between anti-HSA densities of 10μg/ml (6.5±2.2 degrees) and 100μg/ml (15±3.3 degrees). However, increasing the concentration of anti-HSA antibodies on the surface past 100μg/ml does not greatly improve the detection signal, as a concentration is ten times greater (1mg/ml) yields a similar detection signal (18±1 degrees).

This presumably could be because at higher antibody concentrations the surface is too densely packed with antibodies and antigen binding is sterically hindered. The results suggest that using a concentration of 100μg/ml of capture protein when functionalising the SAW biochip is a good compromise to achieve the highest detection signal when subsequently detecting the target protein, while preserving costly reagents. In the context of optimising a point-of-care biosensor, this is important as some capture protein can be expensive or not easily accessible, and using the optimal amount can prove crucial both in terms of performance but also manufacturing costs.

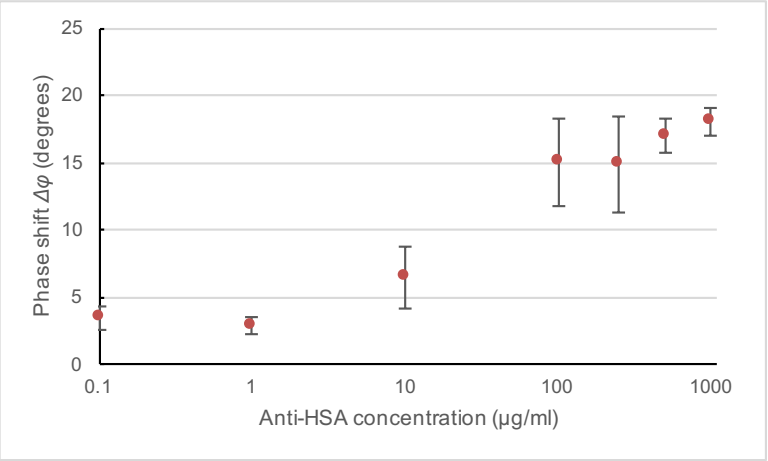

Figure 6.6: HSA test assay: influence of concentration of capture layer antibodies on the detection of target protein. Plot to show the change in phase shift recorded when detecting HSA proteins in TBS-T buffer at 10nM, on OJ15 SAW biochips functionalised with different concentrations of anti-HSA antibodies. Each point represents the average of at least 4 independent measurements normalised to a buffer only equivalent measurement. Error bars represent the standard deviation from the mean. The higher the anti-HSA concentration used during functionalisation, the higher the phase shift recorded when detecting HSA. The improvement in detection signal is found to be more important anti-HSA concentrations of 10μg/ml and 100μg/ml than between anti-HSA concentrations of 100μg/ml and 1mg/ml.

6.1.5 HSA titration using OJ15 SAW biochips

After having optimised the surface functionalisation by studying the impact of both the nature of linker and the concentration of capture proteins used on the detection signal, it was next decided to study the relationship between the concentration of target protein in the sample and the phase shift measured by the SAW biosensor. The gold surface of OJ15 SAW biochips was functionalised with DSP, and a capture layer of anti-HSA antibodies was created by incubating a 100μg/ml solution of anti-HSA antibodies in PBS on the surface of the DSP functionalised gold for 30min. Samples containing HSA in TBS-T at various concentrations were then loaded onto the chip and the change in phase shift was recorded 5 minutes after sample injection. The phase shift is plotted as a function of the HSA concentration in Figure 6.7.

As can be seen in Figure 6.7, the phase shift measured 5min after sample injection depends on the concentration of target protein in the sample. A sharp increase can be seen in the range 0-6nM, where the phase shift recorded after 5min increases from 1.8±0.1degrees for a 1nM sample to 8.5±0.2degrees for a 5nM sample, while for concentrations higher than

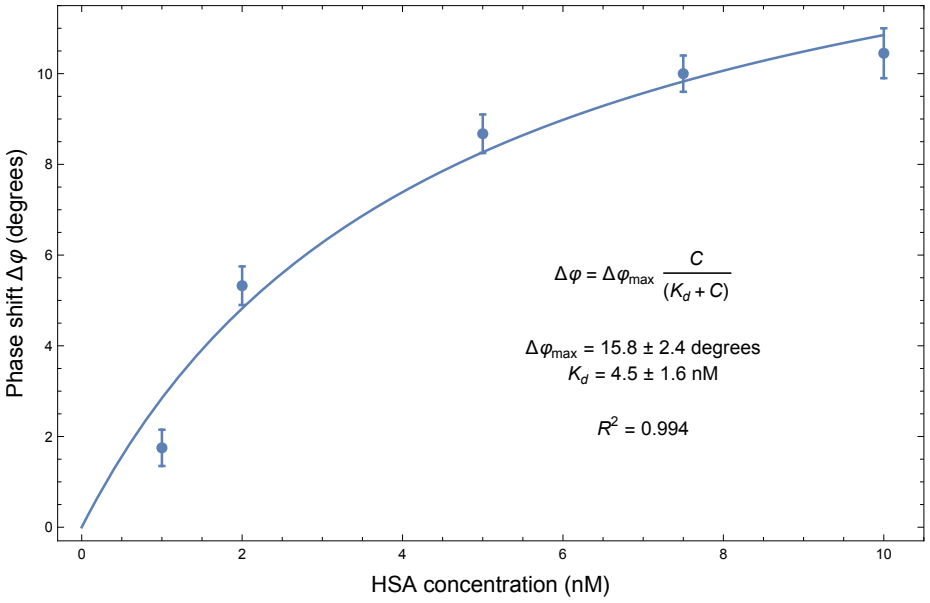

Figure 6.7: HSA titration curve on OJ15 SAW biochips. Plot to show the phase shift recorded 5min after injecting HSA samples at different concentrations in PBS on OJ15 SAW biochips functionalised with anti-HSA antibodies. Each point represents the average of at least 3 independent measurements normalised by subtracting the signal of a buffer only equivalent measurement. Errors bars represent the standard deviation from the mean. The blue line is a fit of the data, using the Langmuir equation displayed on the plot. The dissociation constant K_D and maximum phase shift $\Delta\phi_{max}$ extracted from the Langmuir adsorption model are displayed on the plot.

5nM, the change in phase shift remains relatively constant (10nM HSA sample leads to a phase shift of 10.1±0.2 degrees). The data obtained was fitted using a Langmuir adsorption model[188] (equation displayed on the plot in Figure 6.7). The dissociation constant K_D of 4.54±1.6nM extracted from the fit is in accordance with literature values.[189]

6.2 Detection of anti-HIV antibodies

6.2.1 Anti-p24: proof of concept of detection using the SAW biosensor

Anti-HIV antibodies are the most common target in PoCT for HIV infection and this immunological response is typically detected several weeks after exposure to the virus. As an initial proof of concept, and following the protocol optimised with the model HSA/anti-HSA complex, the detection of anti-HIV antibodies raised against envelope proteins (gp120) was achieved using OJ15 SAW biochips functionalised with recombinant HIV gp120 capture ligands (data not shown). However, it was decided to focus on the detection of antibodies

raised against the viral capsid p24, one of the most conserved and abundant proteins found in HIV. This was achieved using SAW biochips functionalised with recombinant HIV p24 capture ligands (Figure 6.8a) via DSP thiol linker chemistry. As for anti-envelope antibody detection, a 20μl drop of buffer was incubated for 2.5 minutes to establish a stable baseline, before loading the sample. Three different antibodies were tested: two antibodies raised against HIV p24 (BC1071 and 3537) and one antibody raised against a different protein with no known affinity for p24 used as a non-specific control antibody (anti-GBP5). The phase shift recorded 5minutes after sample injection is presented in Figure 6.8b below, for the different samples tested.

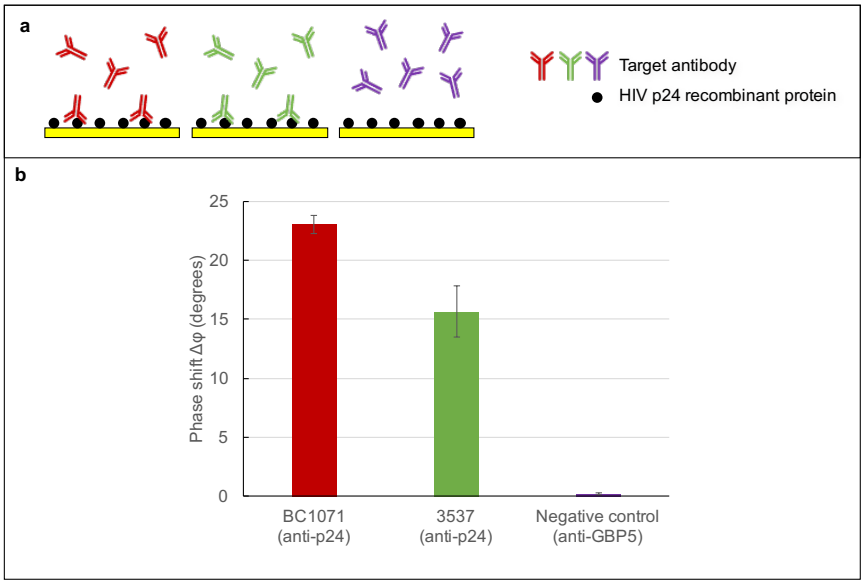

Figure 6.8: Detection of different anti-p24 antibodies on OJ15 SAW biochips. **a)** Schematics at the top represent the surface of the SAW biochip functionalised with recombinant HIV p24, and the different target antibodies in solution whereby colours corresponds to the bars on the barchart. **b)** Barchart to show the phase shift recorded 5min after injecting antibody samples at 100nM in PBS on OJ15 SAW biochips functionalised with recombinant HIV p24. Each bar represents the average of at least 3 independent measurements normalised to a buffer only equivalent measurement. Errors bars represent the standard deviation from the mean.

As can be seen on Figure 6.8b, the phase shift recorded after 5min for both anti-p24 antibody samples (23±0.7 degrees for BC1071, 15.6±2 degrees for 3537) is significantly higher than the one given by the non-binding control (0.2±0.1 degrees). The fact that one anti-p24 antibody sample (BC1071) gives a higher reading than the other one (3537) might suggest that the antibody has a higher affinity for the recombinant HIV p24 used to functionalise the surface. Another factor that might play a role in explaining this difference is the availability of the epitope on the recombinant HIV p24 that is recognised by the

different anti-p24 antibodies tested. Each anti-p24 antibody has a different binding site that binds individual epitopes on HIV p24. DSP molecules on the gold surface bind to primary amines of the lysine residues present on the HIV p24 protein. Depending on the spatial location of the primary amines involved in the chemical bond with DSP, the epitope will be left more or less available to form a complex with the corresponding anti-p24 antibody. In the following experiments where anti-p24 is the target protein, BC1071 was therefore the anti-p24 antibody used, unless otherwise stated.

6.2.2 Anti-p24: reproducibility of detection results

After having established the optimal conditions for the anti-p24 assay on OJ15 SAW biochips, and before performing a titration of anti-p24 using this assay (see below), the number of OJ15 SAW biochips was limited for logistical reasons for a short period of time. Instead of trying out new combinations of proteins and having to dispose of biochips afterwards regardless of the outcome of the experiments, it was decided to study the reproducibility of the results obtained when performing the same experiments with one biochip, while trying to regenerate the surface in between two assays. The assay presented in Figure 6.8 to detect BC1071 was performed on a unique SAW biochip 28 times, with a wash sequence in between each assay. The wash sequence consisted of an acid wash (HCl solution 100nM) in between two buffer washes, in order to remove the anti-p24 antibodies bound to the surface by disrupting the complexes formed with HIV p24. The phase shift recorded 5min after each new addition of the 100nM anti-p24 antibody sample is presented in Figure 6.9b.

As can be seen in Figure 6.9b, the reproducibility of the results of the assay is good. The phase shift reading was found to be consistent over the 28 repetitions of the assay (24.8$\pm$1.9 degrees), with a low variation over the first 7 assays (26.8$\pm$0.8 degrees). While it was known that many different biochips were able to give a consistent result when being used to perform an identical assay, it showed that a single biochip can give a fairly reproducible result several times. This is equally good from a manufacturing point of view. The experiment also gave a good indication that the capture layer of recombinant HIV p24 created on the gold surface of the biochip was very resistant. This is important in the context of the optimisation of the test, even though future work should focus on the sustainability of the biochip to time and other factors such as humidity and temperature, in addition to chemical resistance. Even if this conclusion was not directly not helpful in terms of optimising the assay in the

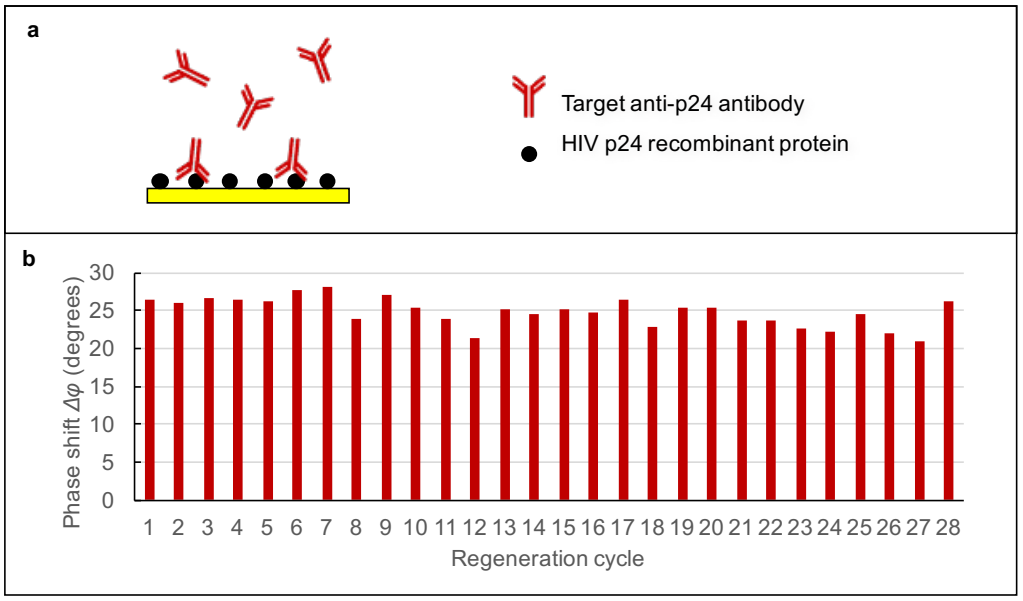

Figure 6.9: Reproducibility of the detection of anti-p24 antibodies on one OJ15 SAW biochips. a) Schematic to represent the surface of the SAW biochip functionalised with recombinant HIV p24, and the target antibody in solution binding to the surface. **b)** Barchart to show the phase shift recorded 5min after injecting an antibody sample at 100nM in PBS on one OJ15 SAW biochip functionalised with recombinant HIV p24. Each bar corresponds to one independent measurement, and represents the phase shift normalised to a buffer only equivalent.

context of PoCT (as in this cases the SAW biochips used would have to be disposable), it was still interesting.

6.2.3 Anti-p24: titration: detection of anti-p24 antibodies at clinically relevant levels

Having shown the proof of concept detection of anti-p24 antibodies using OJ15 SAW biochips, it was decided investigate the relationship between the phase shift $\Delta\phi$ measured as an indication of the formation of anti-p24/complex on the surface of the biochip, and the concentration of anti-p24 antibodies in solution at clinically relevant levels. OJ15 SAW biochips were functionalised with recombinant HIV p24 using DSP as a linker, and samples of anti-p24 antibodies at different concentrations were tested. A 20μl drop of buffer was incubated for 2.5 minutes to establish a stable baseline, before loading the sample. The assay is schematised in FIgure 6.10, and the phase shift is plotted over time in Figure 6.10b, for the different samples tested.

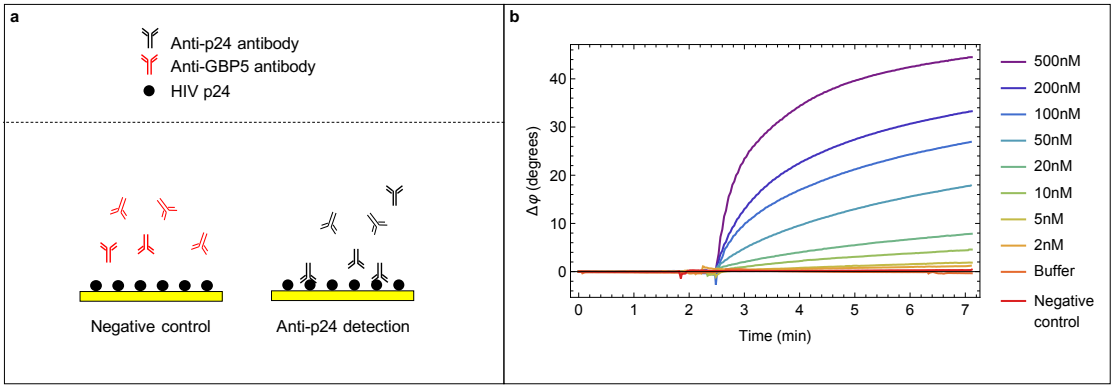

Figure 6.10: Anti-p24 antibody detection using a SAW biochip functionalised with HIV p24 recombinant proteins. a) Schematic to illustrate the specific binding of anti-p24 HIV antibodies to p24 coated biochips, and a negative control using an antibody with no affinity for p24 (anti-GBP5 antibody) which shows no binding to the biochip. **b)** Overlaid raw data plots to show the phase shift recorded between input and output IDTs as a function of time. The sample containing the anti-p24 antibody is injected at t=0. Each sample trace was normalised with the reference assay (containing buffer only, orange line).

As can be seen in Figure 6.10b, the injection of 500nM (75μg/ml) anti-p24 antibodies triggers a rapid increase in the measured phase shift leading to a total phase shift of 46degrees after just five minutes. This phase shift indicates a change in mass and/or viscosity at the surface proximity associated with the specific binding of anti-p24 antibodies to p24 capture proteins on SAW biochips. The other anti-p24 samples at lower concentrations give rise to a smaller phase shift following a similar pattern. However, the series of control tests confirmed the specificity of the SAW signals to anti-p24 over anti-GBP5: an injection of buffer only shows no significant change in phase shift (orange trace, Figure 6.10b and a sample containing 500nM (75μg/ml) of anti-GBP5 shows a negligible response (negative control, red trace Figure 6.10b).

The measurements presented in Figure 6.10b were repeated in triplicate, and the average phase shift measured 5 minutes after sample injection was plotted as a function of the anti-p24 antibody concentration. This is shown in Figure 6.11 below.

The data were found scaled to a Langmuir adsorption model, $R^2 = 0.994$ (Figure 6.11a). At low antibody concentrations (5-20nM, which corresponds to 0.75-3μg/ml), the phase shift increases linearly from 4±0.1 to 22±0.6 degrees, $R^2 = 0.964$ (Figure 6.11b). Above 20nM (3μg/ml) the signal begins to plateau, presumably when all the available binding sites on the surface are occupied. Testing three independent biochips, anti-24 antibodies

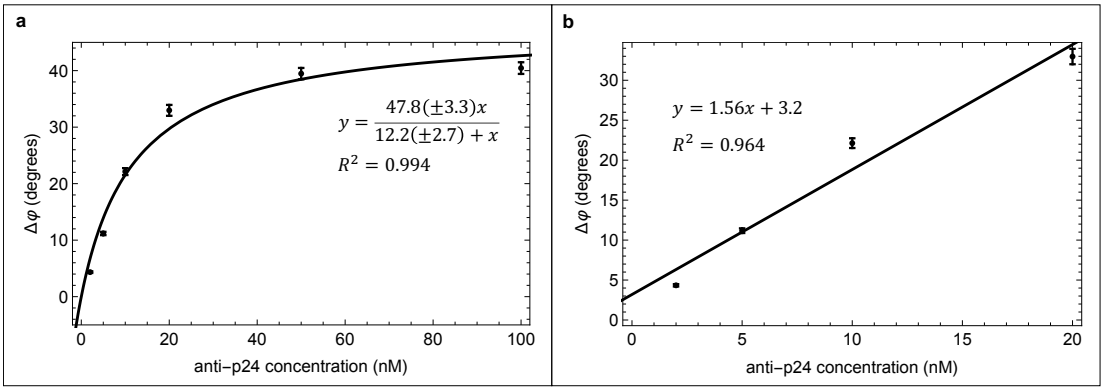

Figure 6.11: Titration of anti-p24 antibody detection in buffer using SAW biochips. a) Graph to show the total phase shift recorded after 5 minutes, plotted as a function of anti-p24 antibody concentration. Each measurement was repeated 3 times; error bars shows the standard deviation of the mean. Black line: Langmuir adsorption model, equation displayed on plot. **b)** Zoom of linear regression in the range 2-50nM, equation displayed on plot.

could reproducibly be detected down to 2nM (300ng/ml) within 5 minutes. The small error bars reflect the high reproducibility of these assays between different biochips and functionalisation steps. This results show comparable performance and even slightly better than leading commercial lateral flow tests such as the Alere Determine which were found to be able to detect 10-30nM (1.5-4.5μg/ml) (E. Gray, personal communication).

6.2.4 Testing times: ultra-fast diagnosis of HIV infection within seconds

Having established that SAW biosensors can detect antibodies at clinically relevant levels, it was decided to test how quickly results could be delivered. This was motivated by the observation that the phase shift measured within the first few seconds after sample injection changes at a very fast rate (Figure 6.10b). In addition, as the SAW biosensor is designed to ultimately be operated with a smartphone with computing processing power capable to analyse the phase shift in real-time, it opens up possibilities of fine, fast, automated signal analysis with the potential to produce results much faster than human readings and interpretation could ever achieve.

The data presented in Figure 6.10b is reproduced in Figure 6.12a, aligned with the corresponding first derivative in Figure 6.12b. The first derivative represents the rate at which the phase shift changes. As can be seen, at high antibody concentrations, this rate can

be as high as a few tens of degrees per minute within the first few seconds after sample injection. It was therefore decided to investigate the phase shift measured within the first few seconds after sample addition. Figure 6.12c shows the average phase shift (for three biochips) recorded shortly after sample injection, for the range of antibody concentrations tested. Two samples can be distinguished from one another if the error bars surrounding their respective average measurement do not overlap. As all values have been normalised to a reference negative sample, a sample can be considered positive if the error bars of the corresponding point do not overlap with the zero horizontal black line. As can be seen, clinically relevant HIV antibody concentrations can be detected and distinguished just 10 seconds after injection down to 50nM (7.5μg/ml).

While these results were obtained in buffer, this is the fastest reported HIV test and is more than 100 times faster than commercially available tests such as the Alere Determine lateral flow test, which exhibits a similar limit of detection to the same biomarker but requires at least 20 minutes between loading the sample and reading the results out by eye (manufacturers guidelines).

6.3 Detection of recent HIV infections using recombinant p24 detection

Building on the detection of HIV antibodies on SAW biochips, it was next decided to investigate whether SAW biochips could detect a virological marker of infection, namely p24 antigen. This is a key virological biomarker of acute HIV infections and is used in combination with antibody detection in gold-standard fourth generation HIV diagnostic assays in centralised laboratories. However, this protein is only present in human blood in minuscule levels, around a million-fold lower concentrations than its antibody counterpart[82,83,89,190–192] and a billion times lower than human serum albumin, presenting a major challenge for PoCT diagnostics. As mentioned in Chapter 2, the clinically relevant concentrations of p24 are very low (0.1-1000 pg/ml). Fourth generation p24 PoCT are beginning to emerge but their performance in the field has been suboptimal, and this has been attributed to a number of factors including the difficulty of interpreting lateral flow tests by non-healthcare workers.[17] The first proof of concept for detection of p24 using the SAW biosensor is presented below.

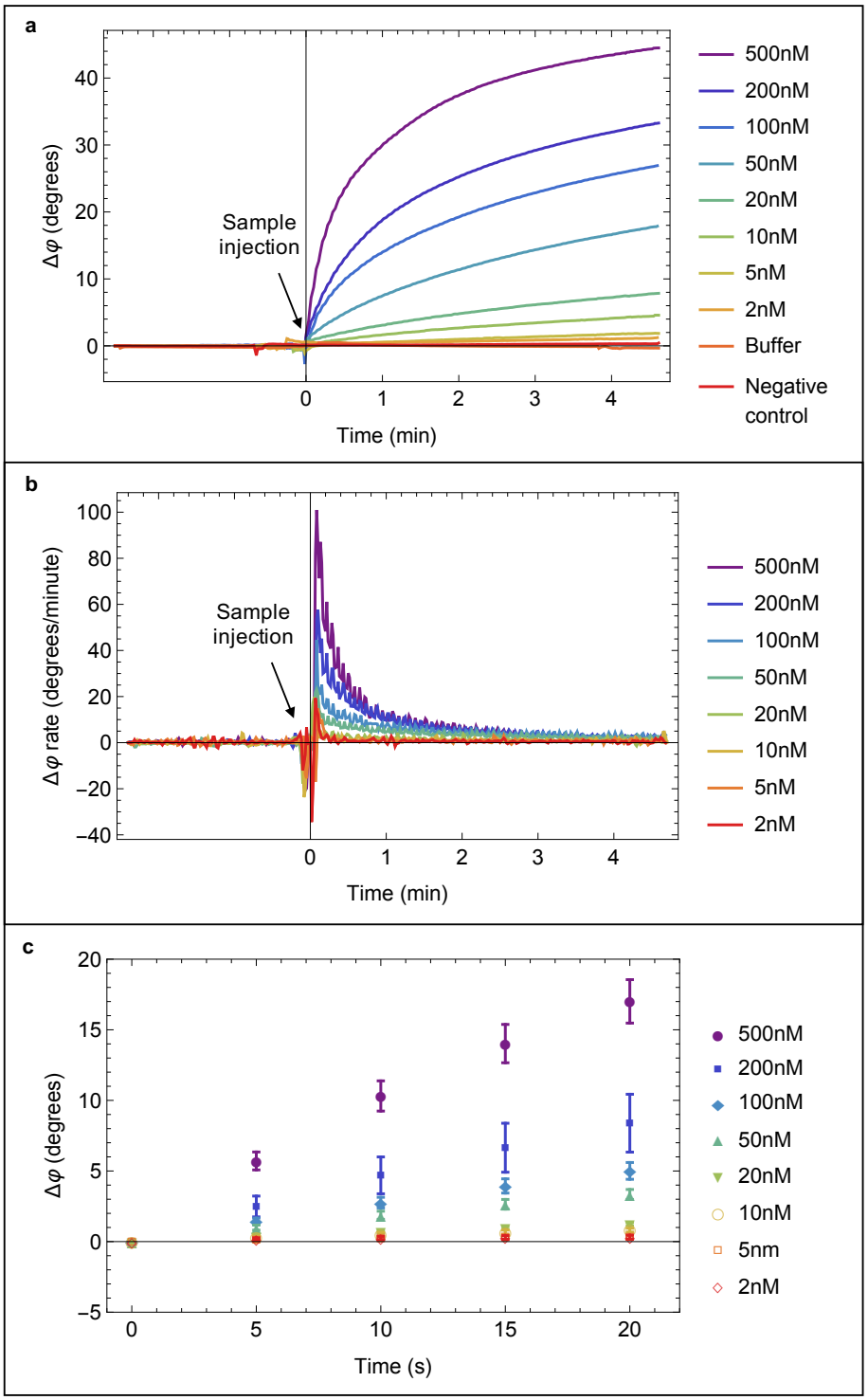

Figure 6.12: Ultra-fast detection of anti-p24 antibodies at clinically relevant concentrations. a) Reprodcution of Figure 6.10b. Overlaid raw data plots to show the phase shift recorded between input and output IDTs as a function of time. The sample containing the anti-p24 antibody is injected at t=0. Each sample trace was normalised with the reference assay (containing buffer only, orange line). **b)** First derivative of the data plotted in **a)**. Note: the first derivative appears wiggly as it is the direct derivative of raw data recorded at discrete time intervals. **c)** Plot to show average phase shift recorded every 5 seconds during the first twenty seconds after injection. Each point represents the average of three measurements, errors bars represent the standard deviation from the mean. Samples of different concentrations (from 50nM (7.5μg/ml) and above) can be distinguished from one another 10 seconds after sample injection.

6.3.1 Anti-p24 llama VHH characterisation

SAW biochips were functionalised with novel capture ligands engineered from anti-p24 llama antibodies. These novel capture ligands are llama VHH (the Variable region of the heavy chain of heavy chain-only antibodies), and are one-tenth the size of conventional antibodies,[193] as schematised in Figure 6.13. Their small footprint means that VHH can access hidden clefts which are inaccessible to larger proteins and in principle they can be packed into dense arrays of capture ligands for diagnostic applications. They have remarkable temperature stability,[194] have shown strong affinity to p24[195] and are therefore ideal candidates for capture ligands on SAW biochips.

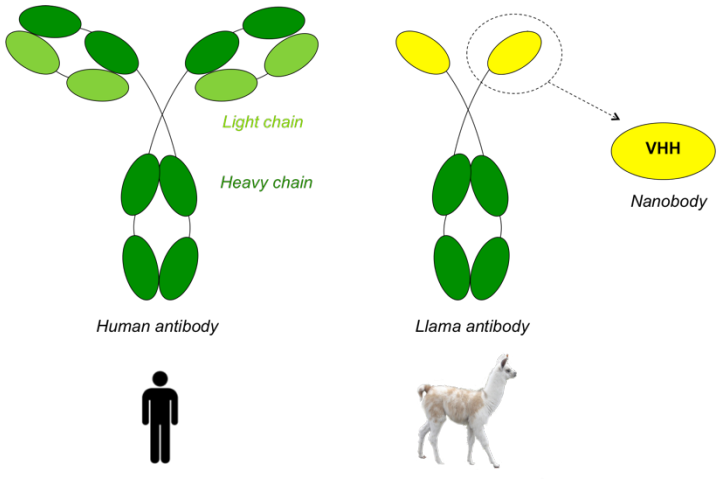

Figure 6.13: Llama VHH. Schematics to illustrate the llama VHH, or nanobodies, used in this thesis. Unlike human antibodies which consist of two heavy chains and two light chains, llama antibodies consist of two heavy chains only. The VHH is the variable part of one of these heavy chains.

Three anti-p24 llama VHH (59H10, 37E7, 59H4) were initially available, each raised against a different epitope on p24. In addition, a fourth VHH was generated in the lab (work done by Dr. E. Gray) by mutating one amino acid in the complementary determining region of the 59H10 sequence. Mutations occurring in this region are not thought to affect the general structure of the protein. Bio-layer interferometry (BLI) was used to assess which anti-p24 protein available (either antibody or llama VHH) was the best binder to p24. Two experiments conducted using BLI showed that one particular VHH (59H10) had a better affinity for p24 than other VHH to conventional mouse anti-p24 antibodies. They are described below.

In the first experiment, streptavidin-coated probes were functionalised with four different biotinylated VHH (59H10,37E7, 59H4 and 48G11) and the relative affinity of the different llama VHH was observed by dipping the different functionalised probe in a 50nM solution of HIV p24. Results are presented in Figure 6.14. BLI data shows that 59H10 is the best binder to p24, out of all four llama VHH available.

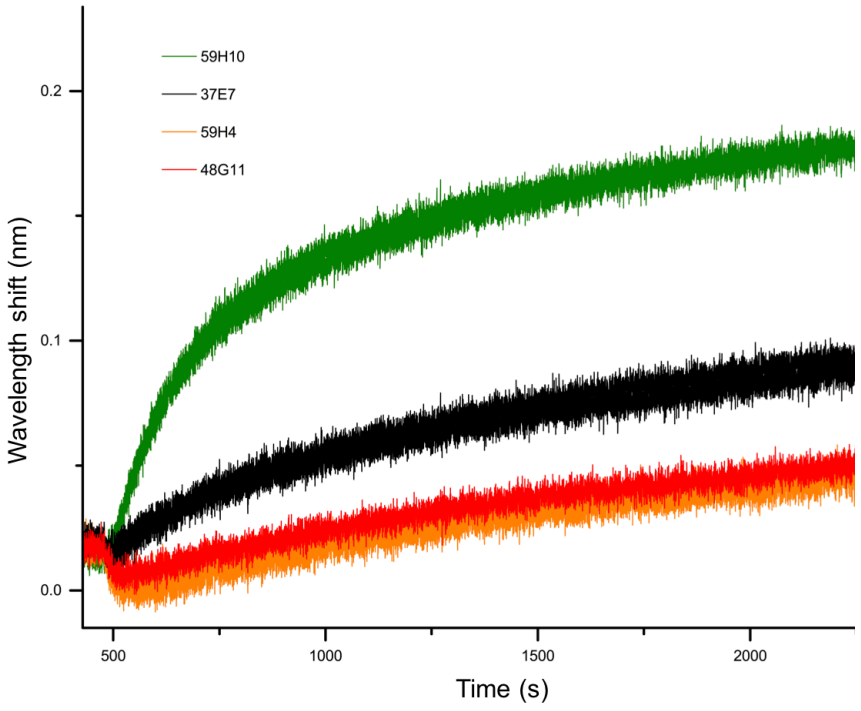

Figure 6.14: Relative affinity of different llama VHH to HIV p24. Plot to show the BLI binding data of 50nM p24 over 30 minutes. Each p24- binding curve was normalized to a reference control of the same llama VHH without p24 in the buffer. Data are combined from experiments performed in triplicate.

In the second experiment, the binding affinity of three different anti-p24 proteins (two mouse antibodies, NIH-3537 and Capricorn HIV 1/2 and the anti-p24 llama VHH, 59H10) to HIV p24 was compared. The BLI binding data is shown in Figure 6.15 and results are summarised in Table 6.1. The results show that 59H10 has a better affinity to the recombinant p24 protein used in the p24 detection assays presented in this chapter.

Protein	NIH-3537	Capricorn HIV 1/2	59H10 llama VHH
K_D	1.2×10^{-8}	1.6×10^{-9}	6.9×10^{-10}

Table 6.1: Dissociation constant estimated with BLI for three anti-p24 proteins.

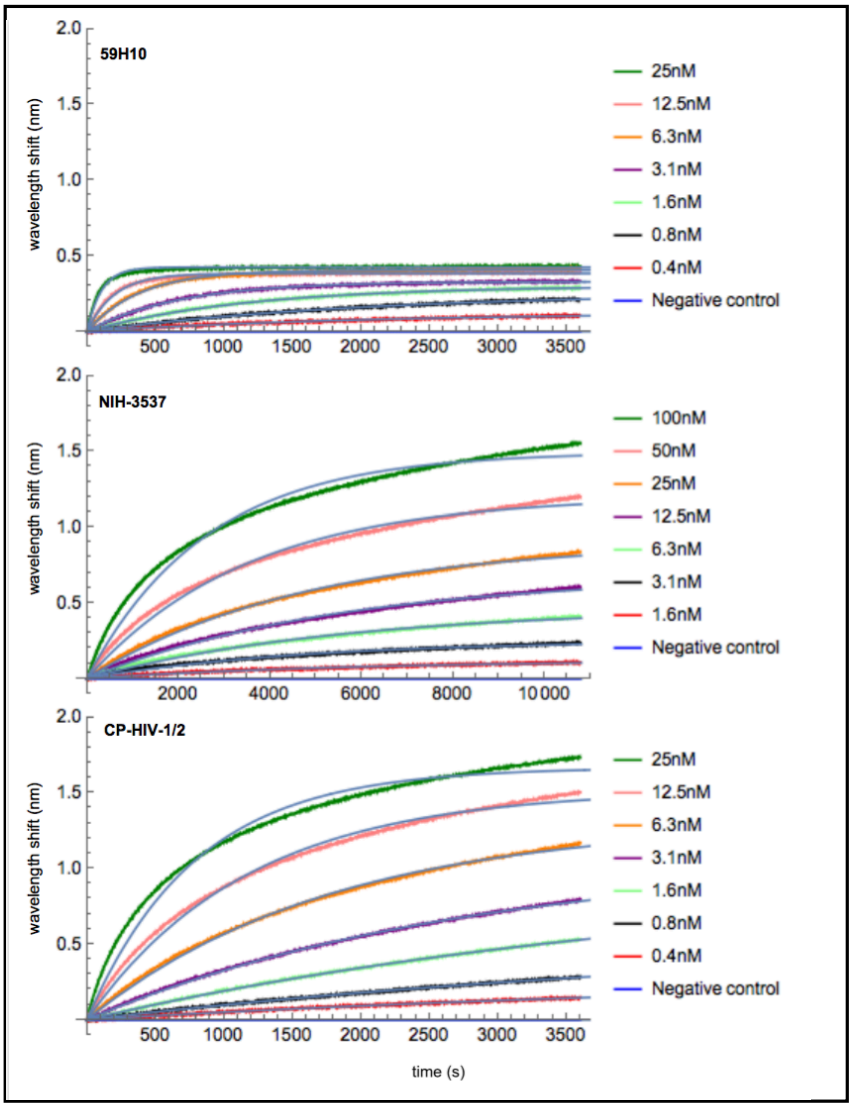

Figure 6.15: BLI association curves of the three different anti-p24 proteins to recombinant p24. Data were acquired through binding of anti-p24 proteins in solution, on BLI sensors functionalised with recombinant HIV p24, over at least 1 hour before dissociation. Each curve was normalized to the signal recorded for buffer without added anti-p24 protein. The plateau value, estimated using the limit to infinity of the fitted function of the different was used to estimate the dissociation constant K_D using the Langmuir adsorption model. Results are presented in Table 6.1.

The surface of the delay line was characterised using X-ray photoelectron spectroscopy (XPS) at each step of the functionalisation process with 59H10 anti-p24 llama VHH. The three steps are detailed in Figure 6.16a. An example of the XPS survey obtained at each of the three steps of the functionalising process is shown in Figure 6.16b. The relative atomic percentage of the four elements studied (Au, C, N and S) is presented in Figure 6.16c. The relative ratios of C:N:S could then be calculated. These ratios were also modelled in parallel by finding the planar density of fcc (111) gold (the surface of the delay line) and a self-assembled monolayer of DSP density and assuming geometrical constraints when the anti-p24 llama VHH is modelled as a cuboid. As can be seen in Table 6.2, the ratios C:N:S measured using XPS compare favourably to the calculated relative percentage of atoms on the surface. Characterisation by XPS provides evidence of monolayer coverage of anti-p24 llama VHH, which, using the model described, was estimated to be around 0.11 VHH/nm^2.

Element	**XPS (%)**	**Calculation (%)**
C	86.1±10.5	76.7
N	11.8±2.8	18.6
S	2.0±0.6	4.6

Table 6.2: C:N:S ratios measured with XPS and estimated theoretically. The ratios measured with XPS compare favourably to the calculated relative percentage of atoms on the surface. The ratios of C:N:S where calculated by finding the planar density of fcc (111) gold (the SAW biochip surface) and a $\sqrt{3}\sqrt{3}R30°$ SAM DSP overlayer density and assuming geometrical constraints when the llama VHH is modelled as a $32.2\times28.2\times48.91\mathring{A}^3$ cuboid.

6.3.2 Proof of concept and signal amplification strategies

As for the previous assays, the llama VHH were immobilised on SAW biochips using DSP chemistry. This time, instead of simply using PBS as the running buffer, the target protein p24 was diluted in pseudoserum, a solution of BSA diluted in TBS-T at 2% (w/v). Because it contains a large amount of proteins, this running buffer is a better approximation of the samples that the SAW biosensor would ultimately need to be able to test, i.e. human blood. It also meant that normalising the readings to a negative control (reading from a pseudoserum only sample tested on identical SAW biochips) was even more important as it would remove non-specific contributions, such as BSA adsorption on the surface, from the test reading.

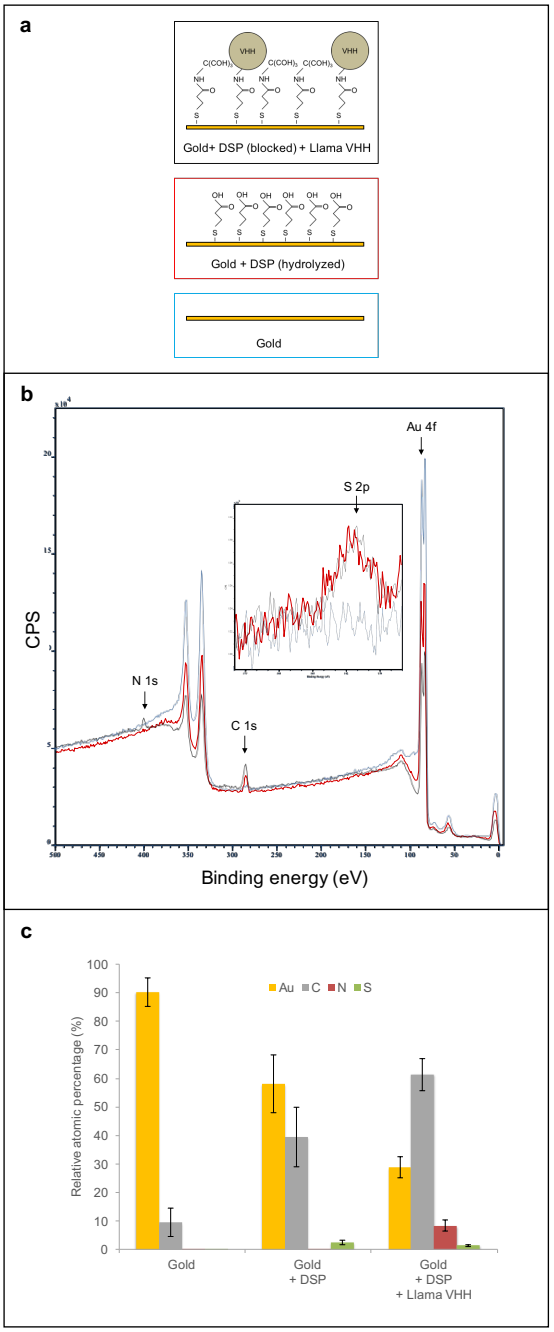

Figure 6.16: XPS characterisation of SAW biochips functionalisation. a) Schematics to illustrate the different stages of the functionalisation process analysed by XPS: bare gold surface, after DSP functionalisation (and hydrolysis), after llama VHH functionalisation (and blocking of unreacted DSP with Tris). **b)** XPS spectrum survey. CPS (count of electrons per second) as a function of the binding energy. Four elements were selected to analyse the surface composition: Au, C, N and S. One example for each step is plotted. Inset: Zoom on the sulphur peak region. **c)** Relative atomic percentage for the four elements analysed at the different stages of the functionalisation process. A minor amount of impurities on the surface explain the presence of carbon atoms on the bare gold surface. Each bar represents the mean of five independent measurements. Error bars represent the standard deviation of the mean.

Figure 6.17a below shows direct p24 detection on SAW biochips coated with anti-p24 llama VHH. A sample of 4nM (96ng/ml) p24 gave rise to a phase shift of only 1.2 degrees, even after waiting for 20 minutes. Since p24 is only one-sixth the mass of an antibody, a strategy of signal amplification was required to achieve detection of p24 through the creation of a larger immuno-sandwich, corresponding to a six-fold increase in mass per antigen. Five combinations of detection antibodies were tested, using antibodies from commercial sources and the AIDS Reagent Program. All antibodies used in Figure 6.17 are described in Table 6.3.

Sample	**HIV p24**	**Detection antibody**	**Binding to HIV p24**
1 (control)	Yes	-	-
2	Yes	BC1071 (Aalto Bio Reagents, UK)	Yes
3	Yes	NIH-3537 (AIDS Reagent Program, USA) [177]	Yes
4	Yes	NBS500-473 (Novus Biologicals, UK) [85]	Yes
5	Yes	Capricorn HIV 1/2 (Capricorn Products, USA)	Yes
6	Yes	C65489M (Meridian Life Science, USA) [85]	Yes
7 (control)	-	NIH-3537 (AIDS Reagent Program, USA) [177]	Yes
8 (control)	Yes	ab89284 (Abcam, UK)	no (anti-BGP5)

Table 6.3: Samples used for HIV p24 detection assay optimisation. For all samples, the proteins listed were diluted in TBS-T buffer containing 2% (w/v) BSA. When HIV p24 is present (column 2), the concentration is 10nM. When a mouse IgG is present (column 3), the concentration is 200nM.

It was found that the largest phase change was measured for a combination of llama VHH capture ligand and the NIH-3537 detection antibody (labelled immune-complex 3 in Figure 6.17b. Figure 6.17b shows that this combination generated a 5.5 degrees phase shift in response to 4nM (96ng/ml) p24 within 20 minutes. This corresponds to a five-fold increase in signal generated by the larger mass of the immune-sandwich complex although additional factors such as surface viscoelastic changes may also contribute to this enhancement. To test the specificity of this signal, a series of control experiments were performed, including a sample with no p24 and injecting non-p24-targeting detection antibodies (Figure 6.17c). The phase shift measured was significantly smaller than when detecting a p24/anti-p24 immuno-sandwich, indicating that the immuno-sandwich complex gave specific and sensitive detection of p24.

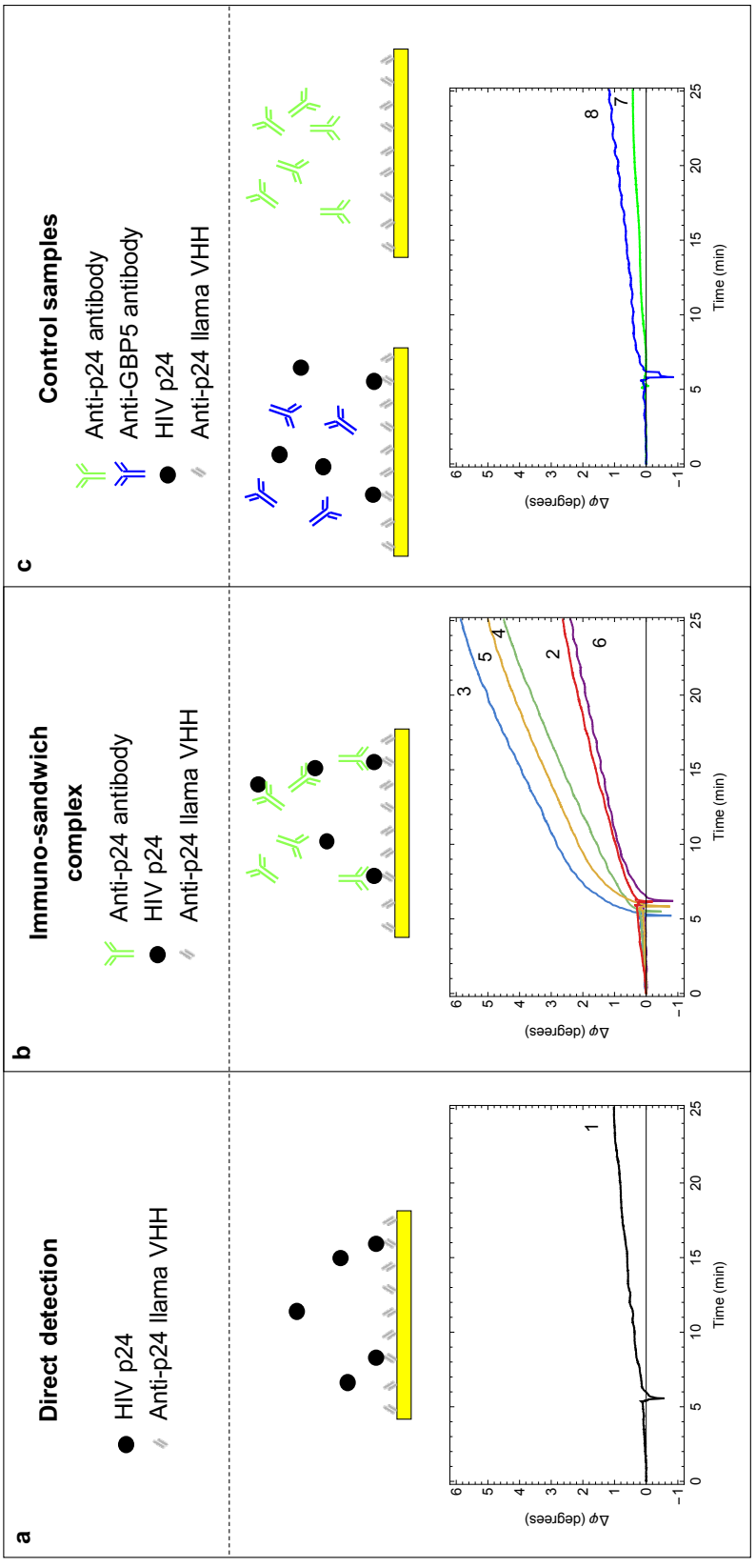

Figure 6.17: HIV p24 detection in buffer using a SAW biochip functionalised with anti-p24 llama VHH. Schematic to show the immuno-sandwich used to detect HIV p24 (the chip is coated with anti-p24 llama VHH) and the resultant phase shift recorded between the input and the output IDT as a function of time. The numbers shown on the graphs refer to different immuno-sandwich complexes formed using the anti-p24 antibodies listed in Table 6.3. Samples injected at t=0. **a)** Direct HIV-p24 detection (llama VHH capture + p24 only). **b)** Immuno-sandwich p24/anti-p24 complexes are formed in the sample and bind to the functionalised surface. The largest signal is seen for immuno-complex 3. **c)** Control samples, where no p24/anti-p24 complexes are formed.

6.3.3 Titration of HIV p24 using the SAW biosensor

It was then decided to titrate the concentration of p24 while keeping the anti-p24 antibody fixed and in excess (200nM - 30μg/ml). The best assay from Figure 6.17b involved detecting HIV p24 via the immunosandwich, which constituted of the anti-p24 llama VHH on the surface and NIH-3537 anti-p24 antibody. It was repeated with different concentrations of HIV p24. The phase shift was recorded after five minutes and is plotted in Figure 6.18 .

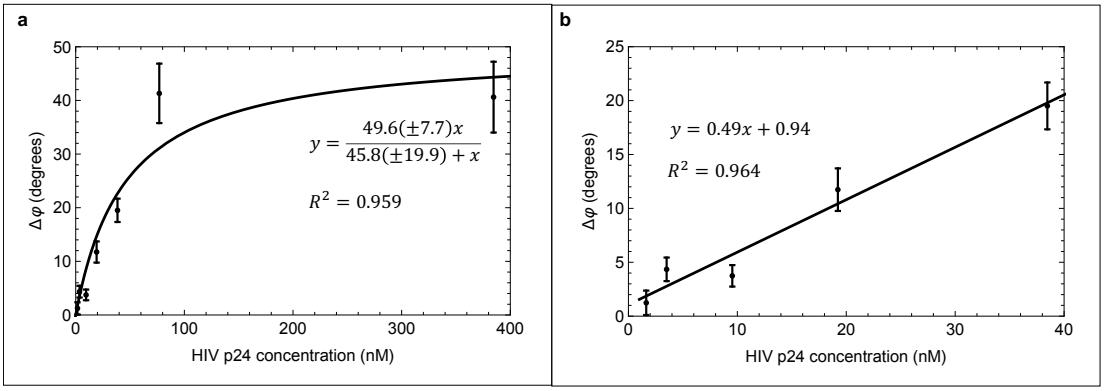

Figure 6.18: Reproducible detection of HIV p24 antigen titration curves. a) Titration of HIV-p24 using optimised immuno-sandwich with NIH-3537 anti-p24 antibody (number 3 in Table 6.3). The phase shift was recorded 5 minutes after sample injection. Black line shows Langmuir adsorption model, equation displayed on plot. Data shown are the combined results from three measurements and error bars show standard deviation of the mean. **b)** Zoom on the 0-40nM region and fitted with a linear regression model (black line), equation displayed on plot. Data shown are the combined results from three measurements and error bars show standard deviation of the mean.

A linear relationship can be observed in the range 2-40nM (48-960ng/ml) p24 (Figures 6.18a-b) followed by plateauing of the signal - closely fitting a Langmuir adsorption model (Figure 6.18b solid black line fit, $R^2 = 0.96$). This demonstrates the ability of the SAW biosensor to detect HIV p24 proteins down to low nanomolar concentrations in the presence of other background proteins at one million fold higher concentrations (2% w/v or 20mg/ml BSA).

6.3.4 Benchmarking QCM study

A benchmarking study using a quartz crystal microbalance (QCM) was used to validate the p24 assay using the immunosandwich anti-p24 llama VHH/NIH-3537 anti-p24 antibody. QCM was chosen for its robustness, fairly low running cost and the fact it was easily

accessible. It is also regarded as a gold standard method to observe and analyse the formation of protein-protein complexes. In a similar way to the SAW biochips presented here, the piezoelectric quartz crystal of a QCM chip is submitted to an electric potential, generating mechanical vibration through the crystal. The frequency is monitored as protein-protein complexes are formed on the surface, and the drop in frequency has been shown to be proportional to the mass of protein binding to the surface of the chip, following the Sauerbrey relation mentioned in Chapter 3.[131]

Typically, QCM crystal operate at a frequency of a few megaHertz to a few tens of megaHertz, operational frequencies much lower than for SAW biochips. The QCM chips used here (QSX 301, Biolin Scientific, UK) operate at 5MHz. They were cleaned and functionalised with DSP offline, using the same protocol as the one used for the SAW biochips, then inserted into the system (Q-sense E4, Biolin Scientific, UK) to be functionalised with llama VHHs of similar molecular weight. VHH1 does not have affinity for p24 and is used as a control, while VHH2 is the one used in the assay described in the study to detect p24. The surface of both chips was then blocked with BSA, before samples containing an excess of NIH-3537 anti-p24 antibodies (200nM - 30μg/ml) and an increasing concentration of p24 were tested. The change in frequency is plotted against time in Figure 6.19.

As can be seen in Figure 6.19a, both llama VHH generate a similar change in frequency when binding to the surface of the chip (about 18Hz for VHH1 and about 15Hz for VHH2). The two chips then also react in a similar way to the addition of BSA (about 25Hz for VHH1 and about 23Hz for VHH2). However, Figure 6.19b shows that only the chip coated with the anti-p24 llama VHH presents a significant frequency shift upon loading of the sample with a high (1μg/ml) concentration of p24, indicating that this VHH has the ability to capture p24/anti-p24 complexes. Moreover, this same chip does not show any significant frequency shift upon addition of the previous less concentrated sample, despite the presence of BSA and anti-p24 antibodies at high concentrations. This indicate the ability of the anti-p24 VHH to specifically bind to p24. The results of the study suggest that with identical surface chemistries, the SAW biosensor offers a 20-fold signal enhancement (about 50ng/ml compared to 1μg/ml).

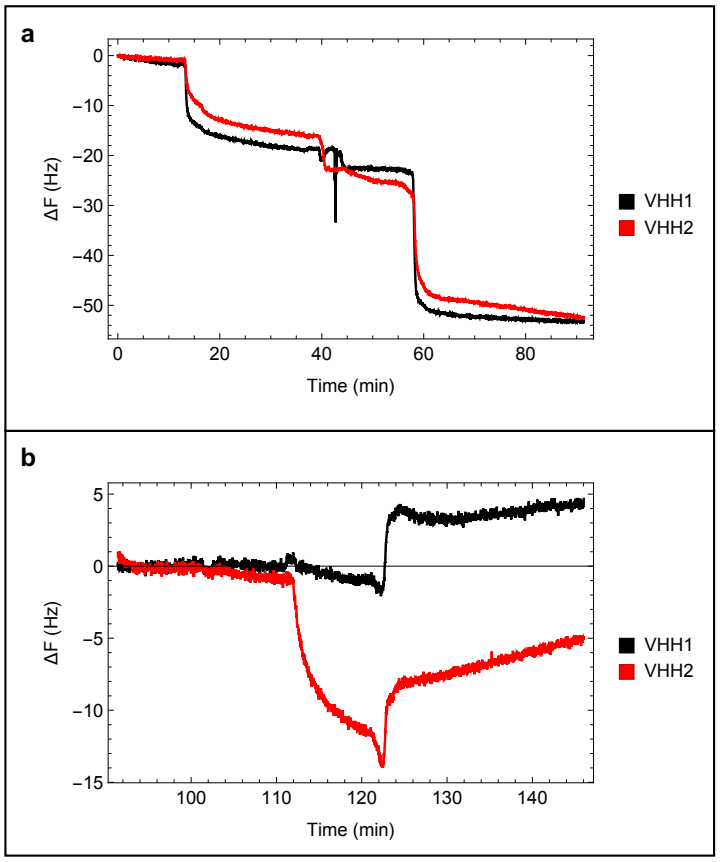

Figure 6.19: HIV p24 detection assay using QCM. a) Frequency shift plotted over time as the llama VHHs are injected in the system, and the functionalised surface blocked with BSA (2% w/v in PBS) to avoid non-specific binding during the assay. **b)** Frequency shift plotted over time as samples containing a mixture of p24 (increasing concentration, as labelled on graph), anti-p24 (NIH-3537) (200nM) and BSA (2% w/v) in PBS buffer is loaded in the system.

6.3.5 Improvement of the limit of detection with gold nanoparticles

As described earlier, the signal measured following the formation of a p24/anti-p24 complex on the surface of the SAW biochip can be used to reliably detect p24 in a sample at concentrations down to about 50pg/ml. This is not sensitive enough to detect the presence of p24 at clinically relevant concentrations (0.1-1000pg/ml). A promising strategy to enhance the sensitivity involved the creation of an immunosandwich, whereby the added mass of the complex leads to a bigger measured phase shift, and lowers the limit of detection of the target protein.

In a bid to enhance the signal further, an improvement to this strategy was tested, involving the use of gold nanoparticles. Gold nanoparticles are much denser and therefore have a much higher molecular weight than proteins (3 to 5 orders of magnitude higher depending

on the size of the nanoparticle). They can easily be functionalised with proteins on their surface, either via simple protein adsorption on the surface or using more complex linking chemistries.[196,197] They are notably used in lateral flow tests as a colour marker of protein complex formation.[198,199] Herein, gold nanoparticles were functionalised with antibodies by simple adsorption, as described in Chapter 4. They were then used in the HIV p24 detection assay to form enhanced protein complexes. An example is schematised in Figure 6.20a, where an immunosandwich is formed between the anti-p24 llama VHH on the surface of the SAW biochip, the target protein HIV p24 and an anti-p24 functionalised gold nanoparticle. An additional gold nanoparticle functionalised with anti-Mouse antibodies binds to the Mouse anti-24 antibodies on the surface of the first gold nanoparticle. The idea was to test whether the gold nanoparticles could enhance the sensitivity of the assay compared to direct detection and help lower the limit of detection of the HIV p24 assay to levels much closer to clinically relevant concentrations. The phase shift measured during the assays is plotted over time in Figure 6.20b. 6 different assays were run, with a concentration of 50pg/ml of HIV p24 for three of them (bright green traces), and 100pg/ml for the remaining three (dark green traces). Because of the presence of dense gold nanoparticles in steps two and three, the phase shift was normalised with a control signal measured with a solution containing nanoparticles functionalised with a non-specific antibody.

As can be seen in Figure 6.20b, the normalised phase shift recorded during the various assays run does not reveal the formation of protein complexes on the surface during steps one and two. In fact, as the phase shift is slightly positive in step two, it seems to suggest that biological mass is removed from the surface. This could be due to the much denser gold nanoparticles dislodging loosely and non-specifically bound BSA proteins from the surface. However, upon addition of the solution containing the anti-Mouse functionalised gold nanoparticles, a significant change in phase shift can be observed. Depending on the concentration of HIV p24 initially injected, the phase shift observed was around 5 degrees (50pg/ml) or 11 degrees (100pg/ml) 10 minutes after the injection of the second solution of nanoparticles. This is likely to be due to non-specific binding of the dense gold nanoparticles to the exposed surface, following the dislodging of BSA in step two.

More work was needed to optimise the conditions of use of the gold nanoparticles, mainly to avoid the alteration of the surface observed in step two. However, despite observing consistency in the measurement during the first 10 repetitions of the assay, it became

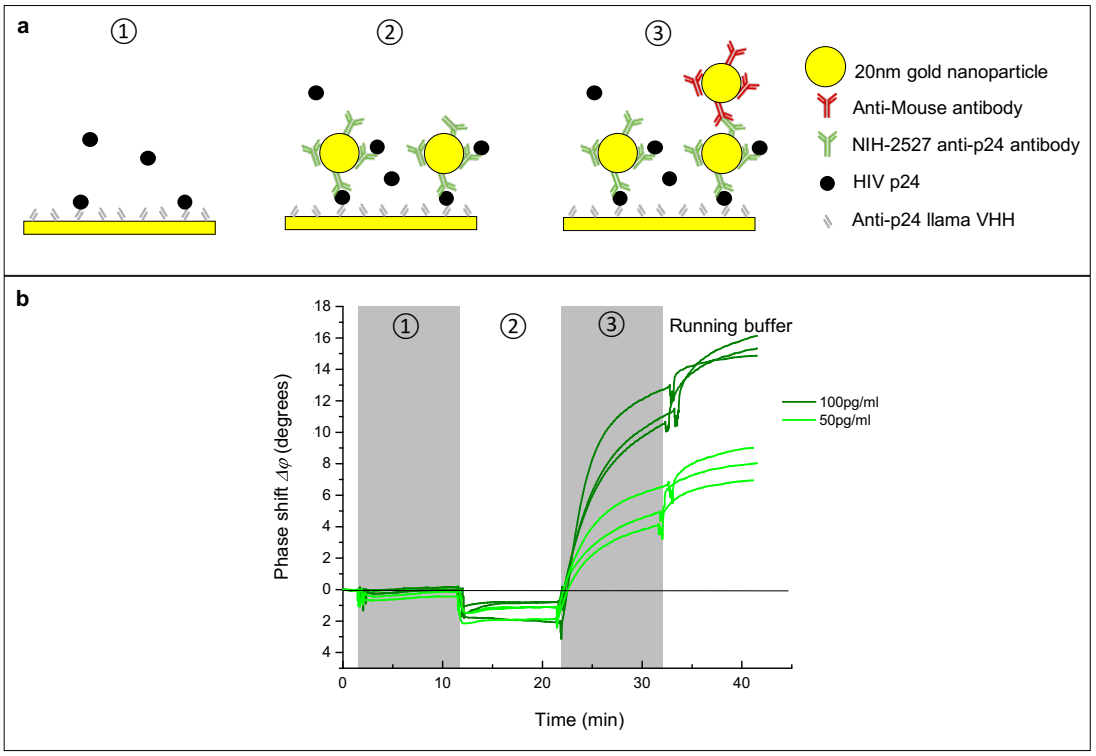

Figure 6.20: Improvement of the HIV p24 detection assay with gold nanoparticles. a) Schematics to represent the different steps of the HIV p24 assay. First, the target protein binds to the anti-p24 llama VHH coated surface of the SAW biochips. Then, gold nanoparticles (20nm diameter) functionalised with Mouse anti-p24 antibodies bind to the p24 on the surface to form the enhanced immunosandwich around the target protein. Finally, gold nanoparticles functionalised with anti-Mouse antibodies bind to the mouse-anti-24 antibodies. **b)** Plot to show the phase shift recorded during the assays, as a function of time. Each trace was normalised with the relevant control measurement (pseudoserum only in step 1, and gold nanoparticles functionalised with a non-specific antibody for steps 2 and 3).

impossible to obtain reproducible results using gold nanoparticles. It was therefore decided to investigate the possible causes of the sudden change observed.

6.3.6 Troubleshooting non-reproducible nanoparticle assay results: antibody affinity

The first possible source of problem that was identified was the functionalisation of the gold nanoparticles with the anti-p24 antibody. Physisorption is one of the most common methods of functionalising gold nanoparticles, however, it is relatively poorly understood and uncontrolled. If any step in the process had gone wrong, or if the antibody had unfolded

in the process of adsorbing to the surface of the gold nanoparticle, then the complex [anti-p24 / gold nanoparticle] could be inactive and unable to bind to the target protein p24. It was therefore decided to characterise the nanoparticles with Dynamic Light Scattering (DLS). The size of the bare 20nm gold nanoparticles was first measured, then the same nanoparticles after being functionalised with either NIH-3537 or Capricorn HIV 1/2 anti-p24 antibodies. The estimated size is shown on the barchart in Figure 6.21.

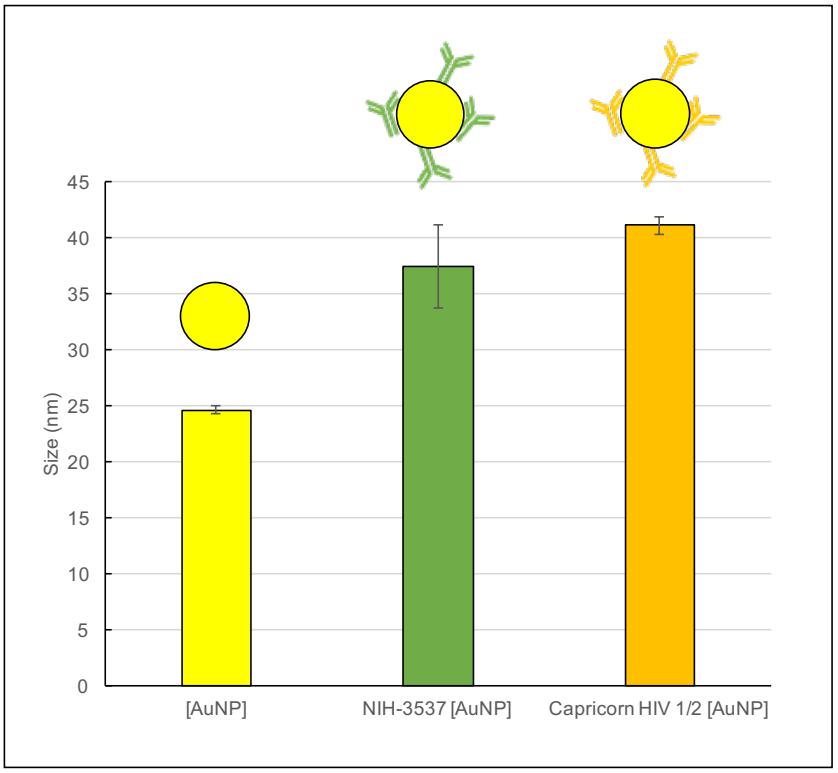

Figure 6.21: Dynamic Light Scattering measurement of functionalised gold nanoparticles. Barchart to show the estimate size of bar gold nanoparticles and gold nanoparticles functionalised with anti-p24 antibodies. Each bar represents the average of 5 independent measurements, error bars represent the standard deviation from the mean.

As can be seen in Figure 14, the average size measured for the bare gold nanoparticle was close to their theoretical size of 20nm in diameter (24.6±0.4nm). Since DLS measures the hydrodynamic radius and takes into account the interaction of the particle with solvent molecules, it is known to slightly overestimate the actual size of the particle measured. Therefore, these results are in good agreement with the theoretical size of the gold nanoparticles. The same measurement performed on nanoparticles functionalised with anti-p24 antibodies gave higher readings (37.5±2.6nm for NIH-3537 and 41.2±0.8nm for Capricorn HIV 1/2). The difference measured between the bare gold nanoparticles and the functionalised ones was therefore about 13 and 17nm for NIH-3537 and Capricorn HIV 1/2,

respectively. Once again, as the theoretical size of the long axis of an IgG is about 10nm, these results are in good agreement with the assumptions that antibodies are present on the surface of the nanoparticle after functionalisation. This did not, however, give any indication as to whether the antibodies are functional and retain their affinity for the target protein HIV p24 after being adsorbed on the gold surface of the nanoparticle.

If for some reason (fridge failure, protein unfolding) the antibody had lost its functionality and affinity for the target, then it would not have been able to form a complex with the p24 bound to the surface. In order to test this hypothesis, it was decided to perform a series of assays using the ELISA technique. As can be seen in the schematics in Figure 6.22a, the plate was functionalised with anti-p24 llama VHH, then HIV p24 was bound to the plate at variable concentrations. The anti-p24 antibody - either alone or adsorbed onto a gold nanoparticle was then added to complete the immunosandwich, before an HRP-tagged anti-Mouse antibody was bound to the resulting complex in order to reveal the results of the ELISA. Two different anti-p24 antibodies were tested: NIH-3537 (used during the successful nanoparticle assays) and Capricorn HIV 1/2, which was successfully used previously in the process of optimising the p24 immunosandwich. Results are presented in Figure 6.22b.

As can be seen in Figure 6.22b, both antibodies, when used on their own, seems to bind to the target protein p24 and these assays led to the detection of p24 at around 100pg/ml and above. A very similar result can be observed for the assay involving gold nanoparticles functionalised with Capricorn HIV 1/2 anti-p24. However, the assay performed with gold nanoparticles functionalised with NIH-3537 was unsuccessful, as only a very small increase in the absorbance can be observed at a concentration of 10,000pg/ml. These results show that neither of the anti-p24 antibodies had lost their affinity for the target protein HIV p24, and that the process of adsorbing the antibodies on gold nanoparticles did not affect the ability for Capricorn HIV 1/2 to bind to HIV p24, as the results of this assay were very much comparable to the one performed with the same antibody alone. However, the functionalisation of the gold nanoparticles with NIH-3537 may have affected the ability for the anti-p24 antibody to bind HIV p24.

These results suggest that, despite both antibodies undergoing the exact same process to adsorb onto the surface of gold nanoparticles, one of them seems to have lost its ability to bind to HIV p24 as a result. Unfortunately, it was not possible to perform the same ELISA with the batch of gold nanoparticles that were used during the first few successful

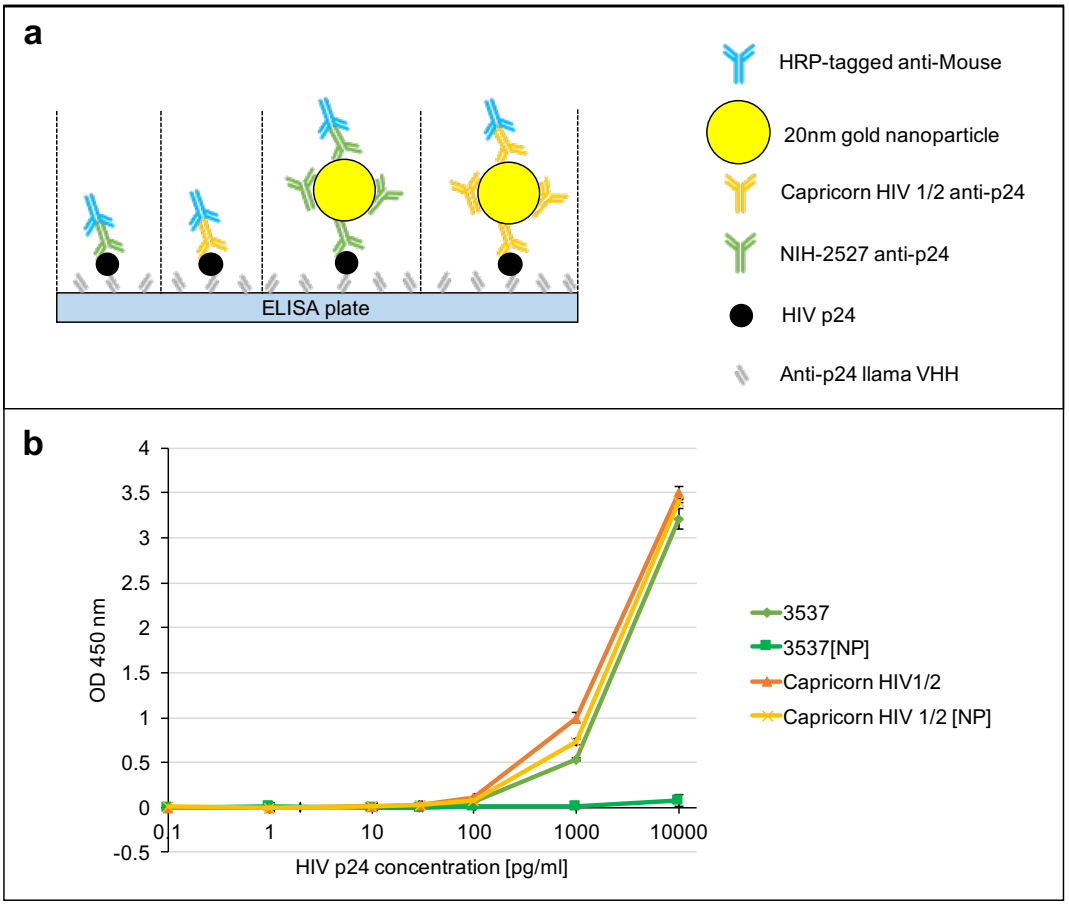

Figure 6.22: Testing antibody activity with ELISA. a) Schematics to illustrate the different assays performed. The plate was coated with anti-p24 llama antibodies, onto which HIV p24 was bound at different concentrations. Four different strategies were tested to complete the immunoasandwich, involving two different anti-p24 antibodies alone or bound to a gold nanoparticle. A HRP-tagged anti-Mouse antibody was used to reveal the amount of complexes left on the plate after washing. **b)** Plot to show the measured absorbance at 450nm at the end of the assay, as a function of the HIV p24 concentration. Each point represents the average of 7 independent measurements, normalised to a negative control. Error bars represent the standard deviation of the mean.

assays on the SAW biosensor. In addition, further attempts to use gold nanoparticles as a single enhancement failed despite using Capricorn HIV 1/2 to functionalise the nanoparticle instead of NIH-3537. While using ELISA confirmed the capability of the anti-p24 antibodies to bind to their target protein, it was not conclusive in terms of explaining what went wrong with the nanoparticles assays.

6.3.7 SAW biochips insertion loss consistency

As the investigation of the reproducibility of the nanoparticles functionalisation process using ELISA was not conclusive, and the confirmation that the antibodies used still had an affinity for their dedicated target protein ruled out any reagent fault, it was decided to look into the insertion loss of the SAW device before functionalisation. Each SAW device is characterised by its insertion loss in air, with no liquid in contact with the surface and nothing attached or adsorbed to the gold surface. This was triggered by the observation that not all SAW devices had the same initial insertion loss.

The insertion loss of all the SAW devices used for various assays during the period January 2013-June 2014 is plotted in Figure 6.23 below. The SAW devices used to perform assays involving gold nanoparticles are identified by crosses. A green cross indicates that the nanoparticle assay was successful, i.e. a significant improvement was observed compared to a similar assay ran without nanoparticles. A red cross indicates that no significant improvement compared to a similar assay without nanoparticles was observed.

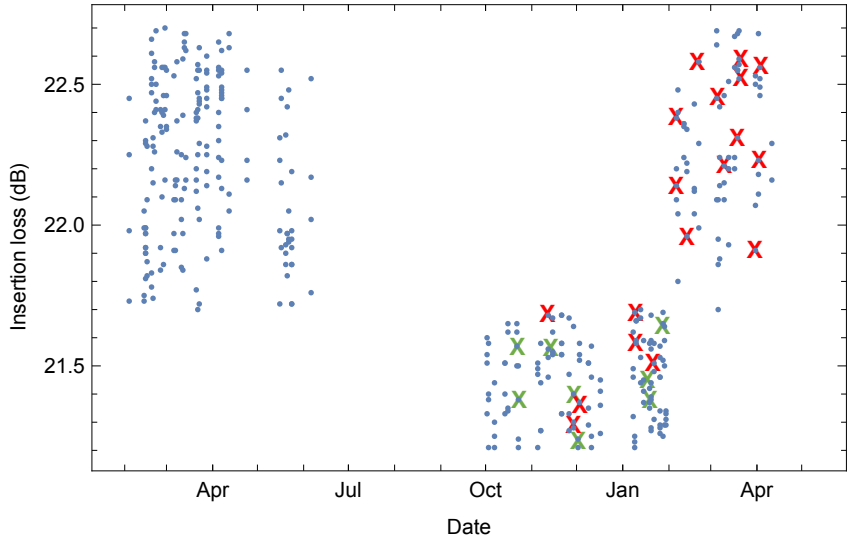

Figure 6.23: Troubleshooting non-reproducibility of gold nanoparticle assays: OJ15 SAW devices insertion loss. Plot to show the insertion loss of various OJ15 SAW devices. Each blue dot represents a unique SAW device, and its insertion loss is plotted against the date it was used to perform an assay. The crosses highlights devices used to perform an assay involving gold nanoparticles to enhance the signal. A green cross indicates that the gold nanoparticles used during the assay enhanced the signal obtained with a control experiment (identical assay without gold nanoparticles), a red cross indicates the nanoparticles did not improve the control signal.

As can be seen in Figure 6.23, the SAW devices can be distinguished by their initial insertion loss in two distinct groups. The SAW devices used between January and July 2013, and between February and May 2014 all had an insertion loss comprised within the interval [21.7-22.7]dB, while the SAW devices used between October 2013 and January 2014 were all characterised by an insertion loss comprised within the interval [21.2-21.7]dB.

Another observation is that all the successful assays (green crosses) involving gold nanoparticles were performed between October 2013 and January 2014, which corresponds to one of the distinct groups in terms of insertion loss. The unsuccessful assays were performed from November 2013 to April 2014, which corresponds to SAW devices from both groups. While this observation is not conclusive enough in itself, it is interesting to note that all successful nanoparticles assays are characterised by a specific parameter. While some assays were unsuccessful using SAW devices from the same insertion loss group, all the assays involving gold nanoparticles performed with SAW devices from the other insertion loss group were unsuccessful. Unfortunately, it was not possible for logistical reasons to reproduce the successful assays on SAW devices presenting an insertion loss lower than 21.7dB. However, these observations are a good starting point for carrying on the troubleshooting of the gold nanoparticle assays in the future.

6.4 Discussion

The SAW biosensor presented in this thesis comprises of different elements, of which the SAW biochip was the main focus. The optimisation of structural parameters that influence its performance such as the gold surface thickness were presented in Chapter 5. Another aspect of the optimisation process is the surface functionalisation of the sensing area. As the target proteins in the sample are detected when they form a complex with the capture protein on the surface, designing the best capture surface is key to the biosensor performance.

The challenge consisted in finding a combination between finding the best protein to form a complex with the target protein, and the best conditions to attach this protein to the gold surface, in order to get the best signal output when detecting the target protein. It was first decided to use a model protein-antibody complex to optimise the functionalisation of the gold surface. The HSA/anti-HSA complex was chosen as both proteins were easily

accessible. Several strategies were investigated to link the anti-HSA antibody to the gold surface, and it was shown that using DSP as a chemical linker was the option that led to the highest subsequent detection signal. DSP forms a stable bond with the gold surface and a covalent bond with the lysine residues of the capture protein. It was also shown that the ideal concentration to use when functionalising the DSP-coated surface with capture proteins was 100μg/ml, which is the best combination between good detection signal and protein economy (some capture proteins can be rare and/or expensive).

It was then shown that the immunoassay designed to detect anti-p24 antibodies, a common marker of HIV infection, could be optimised enough to reproducibly detect the target protein at clinically relevant concentrations within 5 minutes. A careful analysis of the first few seconds after sample injection revealed that concentrations as low as 50nM of anti-p24 antibodies could be detected within just 10 seconds, opening up the possibility for ultra-fast results. This was motivated by the fact the signal can be analysed in real time by the computing power of modern smartphones, which form part of the SAW biosensor. In addition, reducing the time to deliver a test result is crucial for its utility within a typical primary healthcare setting, allowing treatment and care to be given on the spot, overcoming the need for multiple visits and reducing the risk that patients may not return to receive their results. The faster the test can be delivered the more time will be available for post-test counselling and care. The Foundation for Innovative Diagnostics target product profile for a HIV self-test for use in the home underlines the need for results in under 5 minutes. [31] More work is needed to confirm these results in real test conditions, using complex samples that make the signal analysis more challenging because of the large amount of non-specific binding of proteins to the surface of the biochip.

A series of experiments were performed to optimise the immunoassay aiming at detecting HIV p24, a key biomarker of early infection. The strategy of an immunosandwich, with anti-p24 llama VHH on the surface acting as the capture protein, and NIH-3537 anti-p24 antibody at the top, was found to be the option that gave the best results. This working immunoassay was confirmed by a benchmarking study using QCM. A titration performed using the best combination showed that the antigen could reproducibly be detected in pseudoserum at concentrations down to low nanomolar concentrations. More work needs to be done in this direction, at these concentrations are still significantly higher than clinically relevant concentrations needed to be detected by an early fourth generation PoCT for HIV.

The challenge with the detection of HIV p24 is the relatively small size of the protein compared to antibodies (24kDa compared to around 150kDa), and its presence at very low concentrations in human blood. One way to overcome these barriers is to try and amplify the signal obtained when detecting the antigen.

A further investigation into possible ways to amplify the signal using gold nanoparticles as a signal enhancer was conducted. The target protein, once bound to the anti-p24 llama VHH on the surface, was used as an anchor for gold nanoparticles functionalised with Mouse anti-24 antibodies, which in turn were used as a target for nanoparticles coated with anti-Mouse antibodies. A number of ways to optimise the process were identified and opened up possibilities of lowering the detection limit of the assay to clinically relevant levels. However, the initial measurements, despite being consistent, were not conclusive and they could not be reproduced after the first initial attempts. The troubleshooting steps performed in order to explain this change in results were presented. While DLS measurement confirmed the presence of the antibodies on the surface of the gold nanoparticle after functionalisation, a series of ELISA highlighted the loss of activity, after being adsorbed on gold nanoparticles, of the anti-p24 antibody used during the initial successful SAW assays (NIIH-3537). However, another anti-p24 antibody retained his activity after undergoing the same functionalisation process. Both antibodies were confirmed to have an affinity for HIV p24, ruling out a possible unfolding of the protein due to a fridge failure for example. Finally, an investigation into the SAW biochips insertion loss revealed the possibility of a link between a successful assays involving gold nanoparticle enhancement, and the SAW biochip initial insertion loss in air. More work is needed to explore the potential of enhancing the p24 detection signal, which could take the SAW biosensor a step closer to becoming the fastest and first smartphone-connected fourth generation PoCT for HIV. Suggestions are presented in the Conclusion and Future Work at the end of this thesis.

Chapter 7

Clinical Pilot Studies: Testing Real Patient Samples

The previous chapter established the feasibility of detecting key biomarkers of HIV infection at clinically relevant concentrations in mock samples (i.e. buffer samples spiked with both the biomarker of interest and large amounts of serum albumin) using the SAW biosensor. The natural next step forward was to investigate the ability of these biosensors to detect HIV biomarkers in real patient samples. A proof of concept study was first conducted, using human serum spiked with biomarkers of HIV infection at known concentrations. This was followed by two pilot clinical studies using real HIV-positive patient samples, which were conducted in order to assess the sensitivity and specificity of the SAW biosensor as a diagnostic test for HIV. Care was taken to fit the test within an 8-10 minute time frame, which is the approximate duration of a typical doctors appointment in the UK.[20] The process of going from proof of concept studies to pilot studies testing real patient samples was accompanied with an evolution of the materials and methods used to run the tests. Various improvements were made in order to achieve the ultimate goal of being able to run a large scale clinical study testing patient samples with the cheapest, most accurate and most easy-to-use prototype of SAW biosensor. Along the way, the SAW biochips used were optimised to feature an in-built reference channel, as opposed to two individual biochips, thus requiring smaller sample volumes, making the testing easier, and the potential cost even smaller. The functionalisation of the SAW biochips was also automated in collaboration with industrial partners OJ-Bio Ltd., using an automated liquid spotter in order

to increase the chip to chip reproducibility as well as to prepare for the potential large scale manufacturing process. Finally, it was necessary to develop a software using Wolfram Mathematica to automate data analysis, therefore removing any potential user bias associated with manual data analysis. The software also opened up opportunities to go further in the analysis of the results of the pilot studies conducted, and helped preparing for the potential next step large scale studies.

This chapter presents the proof of concept of detecting biomarkers of HIV in real patient samples, as well as the design, results and analysis of the two pilot studies conducted using SAW biosensors. All the results presented in this chapter were obtained in collaboration with Dr Eleanor Gray (UCL) and Dr Vicki Lawson (OJ-Bio Ltd.).

Ethics statement: The University College London Hospital Research Clinical Microbiology Department reviewed and exempted the HIV-positive samples used in the following pilot studies from ethics review because it was an assay development, and waived the need for consent due to the fact the patient material used was fully anonymized. HIV-negative samples were obtained from UCL staff and students who gave full informed consent. The study was reviewed by UCL Ethics Board and given study number 6109/001.

7.1 Proof of concept of detecting biomarkers of HIV infection in human plasma samples

7.1.1 Proof of concept using single-channel OJ15 SAW biochips

In Chapter 6, it was established that SAW biochips have the ability to rapidly detect both virological and immunological biomarkers of HIV infection with high reproducibility down to low nanomolar concentrations using model samples in buffer with 2% (w/v) BSA. As a next step towards the proof of concept of their clinical utility, the performance of the SAW biochips was tested in human plasma. Due to the presence of many different proteins and other components like lipids, fats or metabolites at concentrations of around 70mg/ml, plasma has a higher viscosity than buffer, increasing the amount of non-specific binding on the surface of the biochip. With these high - and variable - viscosities, it is essential to differentiate the contribution of the biomarker binding to the surface from the larger non-specific contributions. Therefore, for each sample type a reference SAW biochip was run

in parallel, as can be seen in Figure 7.1a. Using OJ15 SAW biochips, this reference takes the form of a physically different sensor chip. The signal recorded by the reference SAW biochip was then subtracted from the test SAW biochip chip signal, in order to remove the effect of non-specific binding to the surface.

In these experiments three different types of SAW biochips, each characterised by a different capture coating, were used. Two were coated with p24 and gp41 capture ligands to detect anti-p24 and anti-gp41 antibodies respectively, and are referred to as test biochips. A reference biochip was functionalised with non-animal protein (NAP) to account for non-specific signals, as NAP has no affinity for any human protein.[200] The SAW biochips were incubated in buffer for 30 seconds to record a stable baseline. Two human plasma samples were then tested: one HIV positive sample, and the other was negative for anti-HIV antibodies. The HIV-positive sample was obtained from The University College London Hospital Research Clinical Microbiology Department (see ethics statement below), while the HIV-negative sample was obtained from a healthy UCL student who gave full informed consent.

The phase shifts of both the reference and the tests biochips are plotted against time in Figures 7.1b and 7.1c. Upon addition of the plasma samples, the phase shift of both the test and reference biochips immediately shifts by approximately 20 degrees. This is due to differences in viscosity between buffer and plasma. Moreover, within seconds, the phase shift of the test and reference biochips have clearly separated for the HIV positive sample, whilst remaining at similar levels for the HIV negative sample. The differential signal calculated by subtracting the reference signal from the test signal is shown in Figure 7.1d, and indicates that the binding of the biomarker to the test capture ligand occurs with high specificity. For both HIV biomarkers - anti-p24 and anti-gp41 - the differential phase change was found to be 65 and 35 degrees respectively for the HIV-positive plasma sample. By contrast a much smaller response was seen for the HIV-negative plasma sample which gave rise to 7 and 12 degrees respectively. These findings show that SAW biosensors could potentially be able to detect the presence of both anti-HIV antibodies in human plasma samples. This feasibility study warranted a larger pilot study with more patient samples.

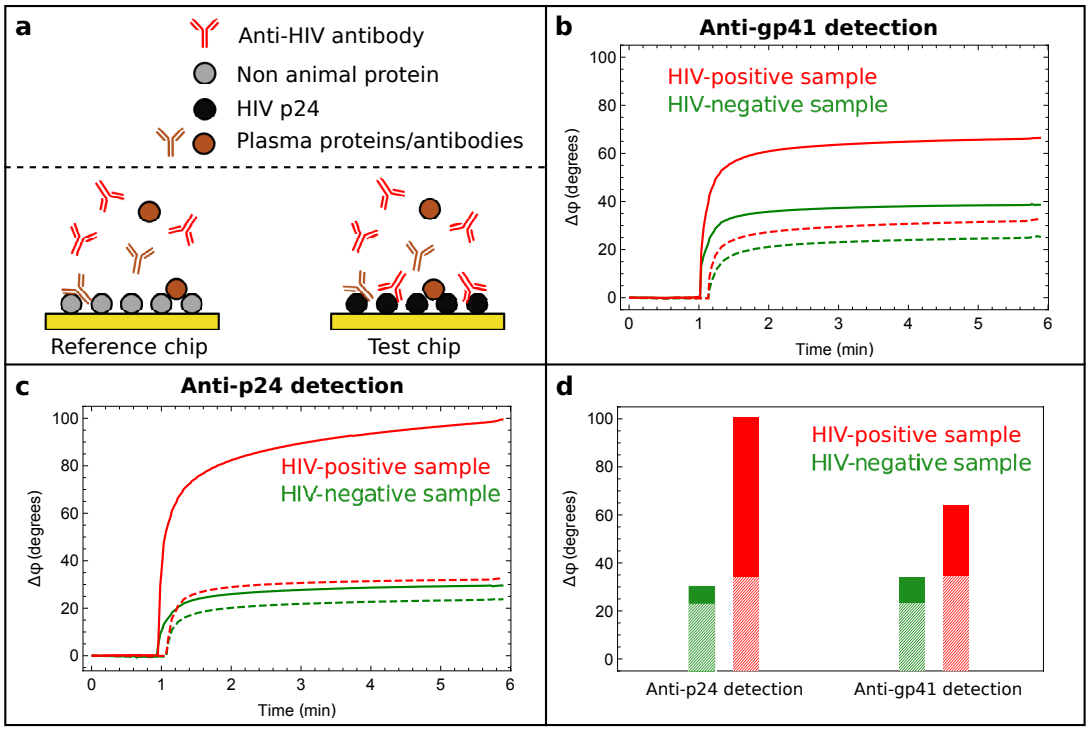

Figure 7.1: Detection of anti-HIV antibodies in a plasma sample from a patient with HIV using OJ15 SAW biochips. a) Schematic of the reference chip functionalised with non-animal protein (NAP), and test chip functionalised with recombinant HIV protein corresponding to the biomarker (HIV p24 or HIV gp41). Non-specific binding of various plasma proteins and antibodies occurs on both chips, but the biomarker (anti-p24 or anti-gp41) only binds specifically to the test chip. **b)** Anti-gp41 detection. Phase shift plotted as a function of time for two different samples (HIV-positive in red and HIV-negative in green). Dashed lines represent the reference chips, and the solid lines the test chips. **c)** Anti-p24 detection. Phase shift plotted as a function of time for two different samples (colours and lines allocation as for (**b**). **d)** Barchart to show the differential response of test and reference chips for anti-p24 and anti-gp41 detection in patient samples, recorded 5 minutes after sample injection. The differential test readout represents the change in phase shift due the specific binding of the biomarker to the SAW biochip, and removes the effect of other non-specific perturbations such as the difference in viscosity between buffer and plasma.

7.1.2 New generation of SAW biochips (OJ24/OJ28/OJ31)

During the course of this work, new generations of SAW biochips (OJ24/OJ28/OJ31) were designed in collaboration with industrial partners OJ-Bio Ltd. and Japan Radio Company. In essence, the new SAW biochips feature an in-built reference channel to help suppress the background noise in the signal due to non-specific adsorption of unwanted proteins and other viscosity effects. They require less sample volume (6μl instead of 20μl). For these reasons, and in the context of aiming to develop the best SAW biosensor for use as a PoCT, it was decided to move from single channel (OJ15) to dual channel (OJ24/OJ28/OJ31) SAW

biochips before conducting the pilot study. A new proof of concept study was therefore required and is presented below. As described in Chapter 4, only minor differences distinguish the three generations of SAW biochips. In the context of the proof of concept or pilot studies presented below, it was assumed that using either of the new generations of SAW biochips would not have an impact on the studies conducted.

7.1.3 Proof of concept using dual-channel OJ24 SAW biochips

The proof of concept study using OJ24 SAW biochips was very similar to the one conducted using single-channel OJ15 chips, with the main difference being the functionalisation of the biochip with the relevant proteins. With single-channel chips, a manually pipetted droplet of solution containing the relevant capture protein could be left to incubate on the whole surface of the sensing area, after this had been functionalised with DSP. With the dual-channel chips, care had to be taken to functionalise each channel with a different protein, and to avoid cross contamination between the channels. This was first achieved by carefully pipetting 1μl of capture protein solution onto one channel, and covering up the chip with a lid during the fifteen-minute incubation period. While this protocol seemed to work (see proof of concept results), it required a lot of dexterity and in the context of developing a reliable biosensor, reproducibility of this step of the process would have been an issue. It was therefore decided to move to an automated functionalisation, using a liquid spotter. This process is described in Chapter 4 (Materials and Methods) and was optimised by industrial partners OJ-Bio Ltd.

In this experiment two types of SAW biochips were designed. The test channel on the sensing area was coated with the relevant recombinant protein (p24 or gp41) used as capture ligand to detect the corresponding antibody (anti-p24 or anti-gp41). The reference channel was functionalised with non-animal protein (NAP) to account for non-specific signals, as NAP has no affinity for anti-HIV antibodies (Figure 7.2a). The SAW biochips were incubated in buffer for 1 minute to record a stable baseline. Three types of mock samples (all based on human serum H4522 AB male, Sigma, UK) were then tested: two positive samples spiked with either polyclonal human anti-p24 antibodies or polyclonal anti-gp41 antibodies at a clinically relevant concentration of 100μg/ml, and the other was negative for anti-HIV antibodies, i.e. serum only. The negative samples were tested on SAW biochips functionalised with p24 as well as on SAW biochips functionalised with gp41. The

average differential phase change recorded after five minutes is represented on the barchart in Figure 7.2b.

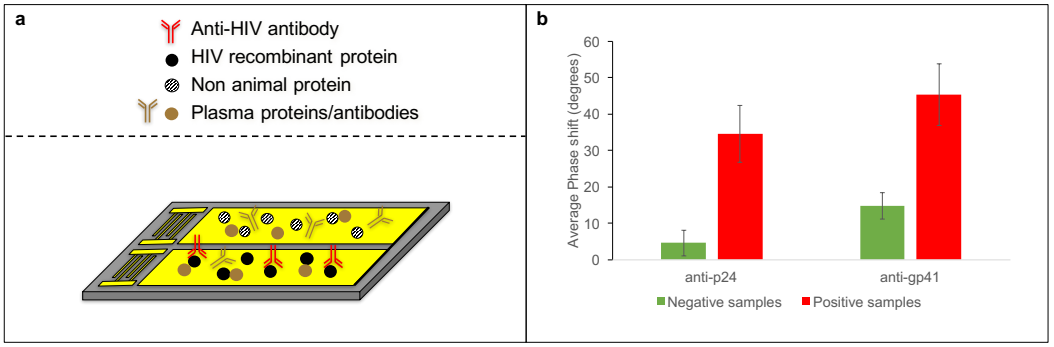

Figure 7.2: Detection of anti-HIV antibodies in a plasma sample from a patient with HIV using OJ24 SAW biochips. a) Schematic of the reference channel functionalised with non-animal protein (NAP), and test channel functionalised with recombinant HIV protein corresponding to the biomarker (HIV p24 or HIV gp41). Non-specific binding of various plasma proteins and antibodies occurs on both chips, but the biomarker (anti-p24 or anti-gp41) only binds specifically to the test chip. **b)** Barchart to show the average differential response of test and reference channels for anti-p24 and anti-gp41 detection in mock samples, recorded 5 minutes after sample injection. Each bar represents the average of 6 independent measurements. Error bars show the standard deviation from the mean.

It was found to be 35±8 degrees on average for the anti-24 positive serum sample, while a much smaller response was seen for the negative samples which on average gave rise to 4±3 degrees. Similarly, the differential phase shift was found to be 45±8 degrees on average for the anti-gp41 positive serum samples, and 15±3 degrees for the negative samples. This confirmed that dual-channel SAW biochips were able to detect the presence of anti-HIV antibodies in human serum samples, and could distinguish between a positive and a negative sample.

7.2 Clinical pilot studies: Method

7.2.1 Diagnostic test performance indicators

The pilot study can be seen as a binary classification test, where for each sample tested, there are only two possible answers: either positive or negative to HIV. As the SAW biosensor is the system that performs the test and outputs the answer, it is necessary to assess its performance statistically. When it comes to defining the performance of such a test, there are a number of parameters that can be considered (examples). In the context

of a diagnostic test, two parameters are most commonly used: the test sensitivity and specificity.

The clinical sensitivity is defined as the ratio between the number of true positives (TP) and the sum of TP and false negatives (FN):

$$Sensitivity = \frac{TP}{TP + FN}. \tag{7.1}$$

A TP refers to a sample which is known as being positive (the reference being a gold-standard test) and is correctly declared positive by the diagnostic test. A FN is defined by a sample known as positive but declared negative by the diagnostic test. Therefore, the sum TP+FN is the total number of sample known as being positive, and the sensitivity can be defined as the proportion of positive samples that are correctly identified by the diagnostic test.

The clinical specificity is defined as a mirror image of the sensitivity, for negative samples. It is defined as the ratio between the number of true negatives (TN) and the sum of TN and false positives (FP):

$$Specificity = \frac{TN}{TN + FP}. \tag{7.2}$$

A TN refers to a sample correctly identified by the diagnostic test as negative, as opposed to a FP which is declared positive by the diagnostic test despite being negative. Therefore, the sum TN+FP is the total number of negative samples, and the specificity measures the proportion of negative samples correctly declared as such by the diagnostic test.

Both the clinical sensitivity and the clinical specificity are important in the context of a diagnostic test: a test with a high sensitivity is only useful if the specificity is also high, otherwise the test will declare most samples as positives and be wrong about the negative samples. Similarly, a test with high specificity and low sensitivity will correctly identify the negative samples but could not be trusted to identify the positive samples. While an ideal test would be 100% sensitive and 100% specific, a trade-off has to be found, that can vary slightly depending on the test application. For instance, when performing a screening test,

it is necessary for the test to have a high sensitivity, while the specificity can be slightly lower. Indeed, false negative results cannot be tolerated, as the patient would not only not get access to treatment but also be likely to pass on the infection. [66] False positive results are less problematic as a second confirmatory test is usually performed after a positive result by the first diagnostic test. In some extreme cases, a confirmatory test is not easily available and even false positives cannot be tolerated. This was the case in the recent Ebola outbreak, as Ebola is highly contagious and people declared as positive were put in contact together, therefore making it likely for a healthy patient to become infected. In these extreme cases, both the sensitivity and the specificity ideally need be as close as possible to 100%.

7.2.2 Clinical Sample Types

Three types of samples were run during the pilot studies:

- Fully anonymized HIV positive samples, obtained from The University College London Hospital Research Clinical Microbiology Department (see ethics statement below).
- HIV-negative samples, obtained from healthy UCL staff and students who gave full informed consent.
- Calibration samples. The calibration samples were a commercial pooled human plasma (screened for biomarkers of HIV infection) and were used to validate the assay with known levels of spiked anti-HIV antibodies. Some calibration samples were not spiked with HIV biomarkers and run as negatives, or zeros, to define the threshold between positive and negative samples.

7.2.3 Protocol: doctor appointment model

In order to reproduce, as much as possible, the conditions of a real diagnostic test, the protocol used to test each sample was designed to fit within an 8-10 minute time frame, which is the approximate duration of a typical doctors appointment in the UK. [20] About a minute was allowed to turn the control box on, insert the SAW biochip in its holder and

load a 6μl drop of TBS-T buffer on the surface of the SAW biochip. The buffer was then replaced with an equal volume of sample, and a 5-minute detection period was recorded, before washing off the sample with buffer (this last step was only performed out of interest and would not have been necessary in the context of a real diagnostic test). Therefore, a few minutes out of the 8-10 minute appointment duration could have been used to welcome the patient, collect the sample, and then deliver and explain the result.

7.3 Processing/Analysis software

A software was written using Mathematica (Wolfram language) to process and analyse the result of the pilot study as a batch rather than require each individual result to be analysed separately, which would be time consuming. In addition to saving time and repetitive effort, this approach made it easier to perform further statistical analysis of the pilot study, such as a time-dependent study of the diagnostic test performance indicators and removed any potential user bias from data interpretation. As a result of this form of analysis, some valuable information could be extracted, about how fast the SAW biosensor can operate while keeping the required level of performance in terms of sensitivity and specificity. The method of analysis is amenable to a mobile phone app which could interpret test results. The principle of the software is presented in Chapter 4.

One of the main advantages of the software developed to analyse the results of the pilot study as a batch is time. The algorithm takes about 3 seconds to compile (2.8s, average of 10 measurements, with a standard deviation of 0.8s), which compares favourably with the 2-3 hours (approximately) required to manually process each file individually, and to plot the results. In addition, the test performance in terms of sensitivity and specificity would also normally have to be calculated separately after processing all the test data. The software incorporates these calculations and therefore makes the analysis of the pilot study easier and more complete.

The time-dependent visualization of the test performance (see Chapter 4) provides very useful information about how fast the test can reliably be performed. The key requirements of PoCT according to the WHO aside from low cost, sensitivity and specificity, ease of use and transportability, is the capacity to provide the test result to the patient quickly.[56] Rapid HIV testing has been proven to increase the return rate of patients to receive confirmatory

results of HIV testing and other sexually transmitted infections.[201] The target product profile for an HIV self-test underlines the need for results in under 5 minutes.[31] Diagnostic test performances are traditionally evaluated after a defined time period post sample injection, as they rely on a human reading that cannot be performed continuously (like the interpretation of the colour of a line on a lateral flow test for example). The advantage of this SAW biosensor, combined with the analysis software, is that a data point is recorded every second, and the test performance can therefore be assessed in a continuous way from the sample injection. This enables very fine estimation of how long the test needs to be run for, in order to perform with the required sensitivity and specificity, rather than a more traditional approximation.

Finally, the analysis software, once written and optimised, can be saved and re-used for the next pilot study without further work needed. As part of the final optimisation of the SAW biosensor, a number of pilot and/or clinical studies might have to be performed. While the end user of the PoCT would ultimately only need a single test readout, the software analysis can prove to be a useful tool in the various stages of product optimisation.

7.4 Preliminary blind clinical pilot study

A preliminary blind study was conducted with ten patient samples: 5 HIV positive samples, and 5 HIV negative samples. They were blinded to the operator with labels A to J. This was done by a third party who also retained the blinding details until post-analysis. Dual channel OJ24 SAW biochips were functionalised with recombinant HIV p24 proteins (test channel) and NAP (reference channel), and were used to conduct the tests.

7.4.1 Calibration

In order to define a threshold between negative and positive samples, calibration negative samples were tested on the SAW biosensor first. 6 samples of pooled plasma (LEEBIO Inc, USA) were tested, and the mean (+3SD) of the differential phase shift recorded 5 minutes after sample injection was used as the test threshold.

7.4.2 Summary of results, test performance indicators

Each of the 10 patient samples was tested 3 times independently on the SAW biosensor. The differential phase shift was recorded 5 minutes after sample injection. It was decided that a sample would be considered positive if the sum of the mean and the standard deviation of the 3 measurements was greater than the threshold value obtained with the calibration samples. Results are presented in Figure 7.3.

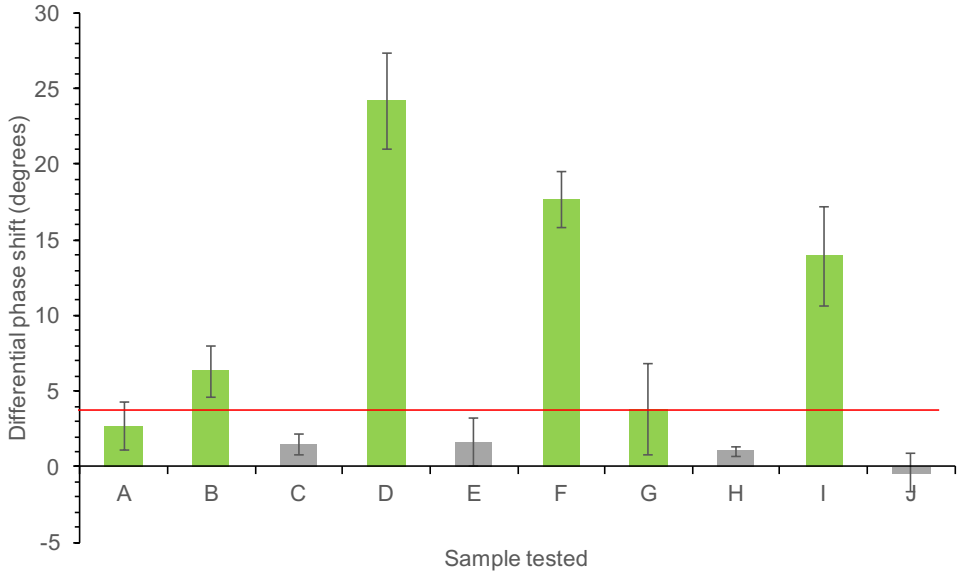

Figure 7.3: Preliminary blind pilot study: readings 5 minutes after sample injection. Differential phase shift measured 5 minutes when testing the 10 unknown samples. The red line represents the threshold value (4.9 degrees), defined as the mean (+3SD) of the negative calibration samples measurements. Error bars represent standard deviation from the mean. For each samples, the bar is coloured green if the mean (+SD) is greater than the threshold value (i.e. if the top of the positive error bar is above the red line), and grey if not. Samples A, B, D, F, G and I returned a positive response from the test. Samples C, E, H and J were declared negative.

As can be seen on Figure 7.3, six samples (A, B, D, F, G and I) were declared positive by the test, while the remaining 4 (C, E, H and J) were declared negative. A summary of the results after comparison with the blinding details is presented in Tables 7.1 and 7.2.

After comparison with the real status of the samples tested, it was found that all positive samples were declared positive by the test, giving a sensitivity of 100%. 4 out of the 5 negative samples were correctly identified as negative, giving a clinical specificity of 80%. Only 1 sample gave a false positive result (sample G).

Sample	**A**	**B**	**C**	**D**	**E**	**F**	**G**	**H**	**I**	**J**
True status	+	+	-	+	-	+	-	-	+	-
Test prediction	+	+	-	+	-	+	+	-	+	-
Result	TP	TP	TN	TP	TN	TP	FP	TN	TP	TN

Table 7.1: Preliminary blind pilot study results. Table listing, for each sample, the known status, the test prediction and the consequent result (True Positive, True Negative, False Positive or False Negative). Only sample G resulted in an incorrect result.

+ samples			**- samples**			**Sensitivity**	**Specificity**
Total	TP	FN	Total	TN	FP		
5	5	0	5	4	1	100%	80%

Table 7.2: Preliminary blind pilot study: summary of results.

7.4.3 Discussion

The results of this preliminary pilot blind study were very encouraging. Using the threshold defined by the measurements of negative calibration samples, the SAW biosensor was able to correctly identify 9 out of the 10 samples tested. The specificity was found to be 80%, and the sensitivity 100%. A more accurate threshold value could have been achieved by testing a higher number of negative calibration samples. of patient samples and investigating the performance indicators of the SAW biosensor. In addition, some of the SAW biochips used in the study were dropped on the lab floor by accident just before being used to conduct the test. The surface of the sensing area was cleaned with dehydrated water and dried with nitrogen straight away. While the SAW sensors are designed to be resistant to being dropped on the floor, no investigation has been conducted at this point about the sensing area, i.e. after the sensor have been turned into SAW biochips. This incident can be seen as encouraging though, as results were still very good despite the biochips being dropped on the floor before being used. Nonetheless, these results made a strong case for larger pilot studies, testing a higher number of samples. It was therefore decided to move on to the second clinical pilot study.

7.5 Second pilot clinical study

This time, the samples were not blinded, but the study involved testing all the samples available (31 HIV-positive samples, 6 HIV-negative samplessee clinical samples types above).

All samples were tested on OJ28 SAW biochips functionalised to detect either anti-gp41 or anti-p24 antibodies. Most SAW biochips were functionalised with an automated liquid spotter (see Chapter 4). The protocol that was optimised to functionalise the SAW biochips, and that was used to obtain the results presented in Chapter 6, was adapted to be used with the automatic liquid spotter. Due to a failure of the automatic liquid spotter during the functionalisation process, a small number of SAW biochips had to be functionalised manually.

7.5.1 Calibration

A series of control samples were tested on the SAW biosensor before moving on to patient samples. They consisted of pooled plasma (LEEBIO Inc, USA) spiked with commercially available anti-HIV antibodies. The control samples were tested on OJ28 SAW biochips functionalised to detect either anti-p24 or anti-gp41, at least 4 times for each concentration. The differential phase shift is plotted against the concentration of the biomarker in Figure 7.4, for both biomarkers tested.

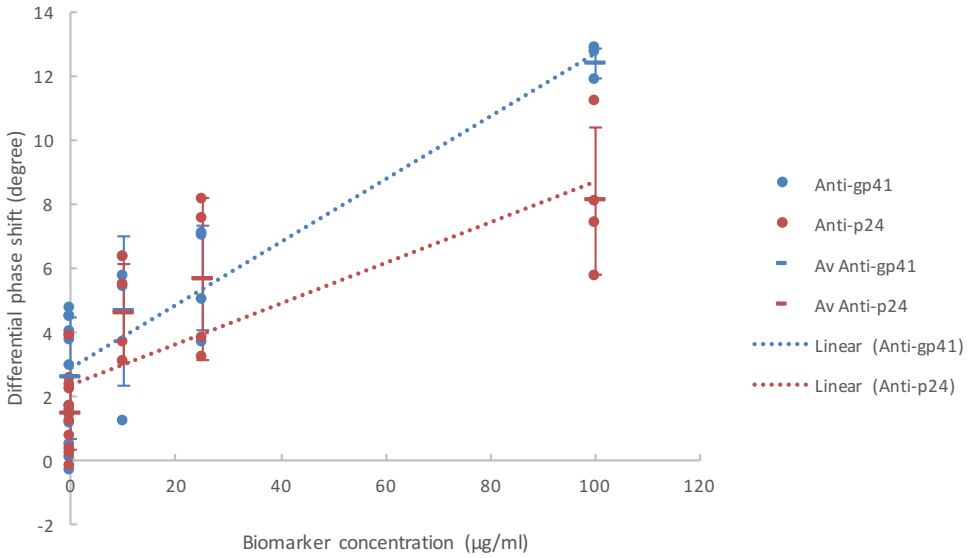

Figure 7.4: Second pilot study: validation of the assay using mock samples of known concentration. Differential phase shift measured after 5 minutes when testing mock samples with known concentration of anti-HIV antibody. Anti-gp41 results are presented in blue, anti-p24 in red. Each dot represents the value of one test, the line represents the average of all measurements for one concentration, with the error bars representing the standard deviation of the average. The dotted line represents the linear regression of the averages values.

The Pearson product-moment correlation coefficient (PPMCC) was evaluated for both data-sets. A PPMCC value close to +1 or -1 indicates a strong correlation between the two data sets, while a value close to 0 (or more generally in the -0.5 / +0.5 interval) indicates a very weak correlation. A good correlation was observed between the biomarker concentration and the differential phase shift (PPMCC of 0.898 for anti-gp41, and 0.76 for anti-p24). The assay was therefore validated and it was decided to move on to testing of patient samples.

7.5.2 Summary of results, test performance indicators

A summary of all the data obtained during this study is presented in Figure 7.5 and Table 7.3. Each sample was tested in duplicate for both biomarkers (anti-gp41 and anti-p24). In other words, each sample was tested on 4 different disposable SAW biochips. It was therefore decided to consider all measurements to be independent when estimating the sensitivity and selectivity of the test. The sensitivity and selectivity presented in Table 2 were calculated for each biomarker independently, and as a combined test. This reflects the fact that, under real test conditions, the detection of only one of the two biomarkers would prove sufficient to rank the sample as being positive. The differential phase shift was read 5 minutes after sample injection, and compared to the threshold value defined as the mean (+3SD) of the negative calibration samples measurements.

	+ samples			**- samples**			**Sensitivity**	**Specificity**
	Total	TP	FN	Total	TN	FP		
Anti-gp41	62	58	4	12	12	0	93.5%	100%
Anti-p24	64	30	34	12	12	0	46.9%	100%
Combined	62	59	3	12	12	0	95.2%	100%

Table 7.3: Second pilot study: summary of results. Each sample tested was assigned to one of the 4 categories (TP, FN, TN, FP), depending on the nature of the sample (known positive or negative) and the value of the phase shift recorded after 5 minutes in comparison with the threshold value, defined as the mean (+3SD) of the negative calibration samples measurements. The test sensitivity and specificity were calculated for both biomarkers separately. A combined sensitivity and specificity is also presented, which reflects the fact that the detection of one of the biomarkers only would be enough to conclude on the positivity of a sample.

58 out of the 62 tests performed on samples from patients with HIV gave a positive reading for anti-gp41 detection, giving a sensitivity of 93.5%. Anti-gp41 is usually the first antibody to appear after HIV infection and therefore a key immune marker of HIV infection. [81] For anti-p24 detection, 30 tests (out of 64 two samples were tested three times instead of two)

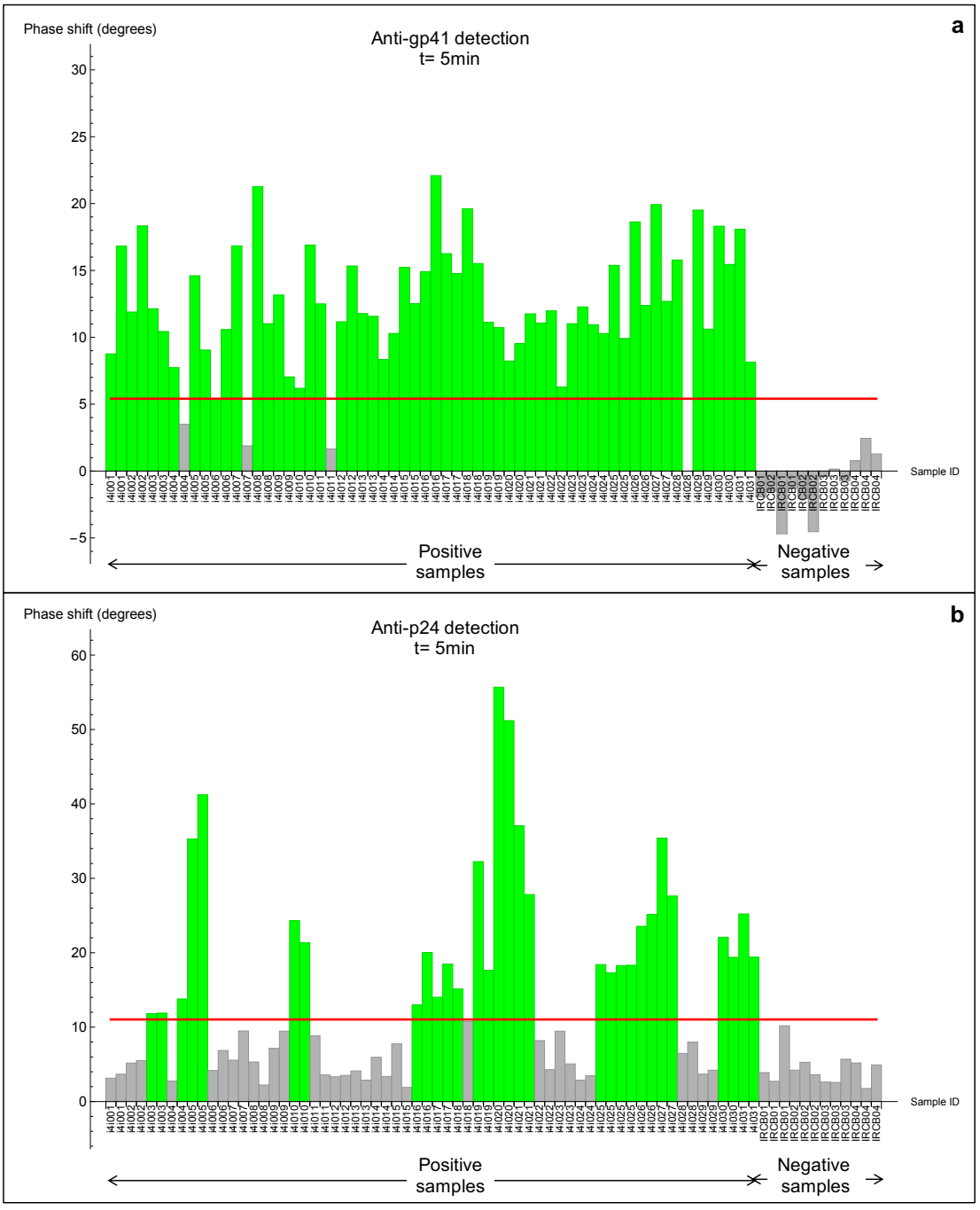

Figure 7.5: Second pilot study: readings 5 minutes after sample injection. **a)** Barchart showing the differential phase shift recorded by the SAW biosensor after 5 minutes. Each bar represents one test. Two tests were conducted for each sample. The red line indicates the threshold value defined to discriminates between positive and negative values. The nature of the sample (known positive, known negative or calibration sample) is indicated at the bottom of the barchart. A grey bar represents a sample declared negative by the test, whereas a green bar represents a positive test. (**b)** As in (**a**), but for Anti-p24 detection.

gave a true positive reading, giving a sensitivity of 46.9%. The combined sensitivity of the test (at least one biomarker detected) was found to be 95.2%. Neither marker was detected in any of the healthy volunteer samples, giving a specificity of 100% of detection for both antibodies, though this is based on only 6 samples (with multiple readings).

7.5.3 Comparison with ELISA

All the samples tested in the pilot study were used in another study, aiming at estimating the concentration of the two biomarkers (anti-gp41 and anti-p24). The SAW biosensor fulfils the requirement of a PoCT for HIV in the context of diagnostics, by simply distinguishing between a positive and a negative sample. However, being able to estimate the actual concentration of a given biomarker could potentially be useful in the context of monitoring. The calibration results presented in Figure 7.4 demonstrate the clear correlation between the phase shift recorded by the SAW biosensor and the biomarker concentration in mock samples. The purpose of this parallel study was to investigate the extension of this conclusion to real patient samples.

The estimated concentration of a biomarker was compared to the magnitude of the signal recorded by the SAW biosensor, and the possibility of a correlation between the two was investigated. The concentration of the HIV biomarkers in each sample was estimated using ELISA (enzyme-linked immunosorbent assay). The principle of the assay is described in Chapter 4. As the concentration of human IgG in a patient sample is very high (around 10mg/ml) compared to the concentration of the biomarker of interest, there is a high risk of non-specific adsorption of any human IgG to the plate. In order to avoid such complications, which would lead to a misleading assay conclusion, a number of extra washing steps (with buffer) were incorporated into the protocol, between each binding step. In addition, each assay was performed using a dilution range of the original samples, from the undiluted sample down to a dilution of 1 to 4000.

Each of the 31 HIV-positive patient samples was tested in triplicate, at 4 different dilutions. For each dilution, the average absorbance reading was injected in the equation of the linear regression of the calibration curve to estimate the concentration of the biomarker at this specific dilution. The result was multiplied by the dilution factor to obtain the final estimation of the concentration of the biomarker in the sample. Out of the final

estimated concentrations, only those who fell in the linear part of the calibration curve were considered. The results are presented on the barchart in Figure **??**, along with the SAW results. As can be seen, the estimated concentration of antibodies in the negative samples (empty bars, on the far right) is high. For anti-gp41, the 4 samples tested were estimated to present a concentration of antibody higher than 100μg/ml. When tested for anti-p24 levels, 2 of these negative sample also presented high concentrations of antbody (higher than 10μg/ml). These values are quite a lot higher than expected for negative samples that should not present any anti-HIV antibodies. This was likely to have been triggered by non-specific adsorption of any human antibodies onto the plate before addition of the tagged anti-human antibody used at the end of the assay to reveal the amount of biomarker bound to the plate. This is probably due to the inability of the blocker used to efficiently prevent non-specific adsorption of human antibodies, and was subsequently confirmed as part of another project. More work would therefore be needed on the estimation of concentrations of biomarkers using ELISA to pursue the study of a possible correlation between the two techniques.

7.5.4 Discussion

Overall, the second pilot study conducted using SAW biosensors showed very promising results. It showed that the SAW biosensor was able to detect key biomarkers of HIV infection in patient samples with very high sensitivity and specificity. However, during the course of this first pilot study, a problem arose in the process of functionalising the SAW biochips with the recombinant protein using the automated liquid spotter. A number of SAW biochips had to be functionalised manually. The fact that two different techniques were used to functionalise the SAW biochips, and that the manual pipetting cannot be assumed to be as reproducible as the automated technique, meant that the results of this second pilot study had to be considered with caution. In addition, there was a doubt as to whether all the SAW biochips that were functionalised manually had been prepared following a similar protocol. The reference and the test channel may have been inverted on some SAW biochips, which were used only to test negative samples for precaution. Those doubts led to the conclusion that a third pilot study had to be conducted, with SAW biochips functionalised solely using the automated spotter.

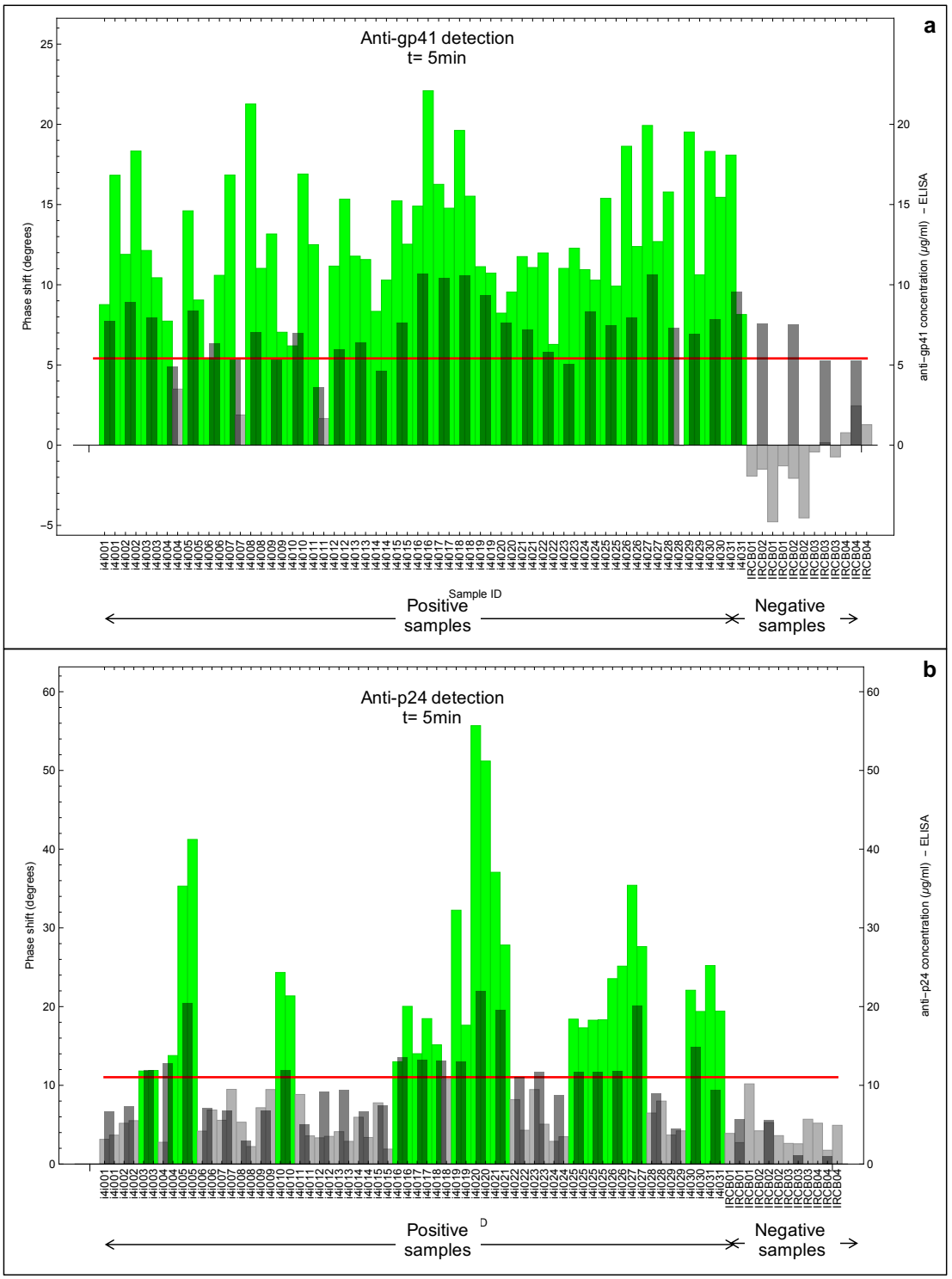

Figure 7.6: Second pilot study: comparison between SAW biosensor results and estimated biomarker concentration. a) Superimposed barcharts to show the comparison between SAW biosensor and ELISA results. Left axis scale: Phase shift recorded by the SAW biosensor (green and light grey bars, colouring as in figure 7.5a. Right axis scale: Concentration of Anti-gp41 (dark grey bars). The concentrations were estimated using ELISA. The phase shift was recorded after 5 minutes. **b)** As in **a)**, but for Anti-p24.

7.6 Third clinical pilot study

This third pilot study was conducted following a very similar protocol to the one used for the second pilot study, with the exception that all SAW biochips were functionalised using the automated protocol. The SAW biochips used for this study are called OJ31 and are described in more details in Chapter 4.

7.6.1 Calibration

As for the previous pilot studies, a series of control samples (pooled plasma spiked with anti-HIV antibodies) were tested on the SAW biosensor before moving on to patient samples. The differential phase shift is plotted against the concentration of the biomarker in Figure 7.7, for both biomarkers tested (anti-p24 and anti-gp41). The PPMCC was evaluated for each data set and was found to be 0.978 for anti-gp41 ($R^2 = 0.958$) and 0.9666 for anti-p24 ($R^2 = 0.934$), indicating a good correlation between the phase shift recorded by the SAW biosensor and the concentration of the biomarker. These are both improved when compared to the calibration results from the second pilot study (0.898 for anti-gp41 and 0.76 for anti-p24) and probably relate to improved performance and reproducibility using automated biochip functionalisation. However, it is interesting to note that the intercept of the linear regression is close to 0 (0.2) for anti-gp41, but not for anti-p24 (3.5). One would expect the intercept to be close to 0, as the interaction of the sample with both the test channel and the reference channel is supposed to be similar in the absence of the biomarker of interest. This interaction is indeed mainly non-specific adsorption of proteins onto the functionalised gold surface, with no specific interaction with the capture protein. A non-null intercept might therefore indicate that the capture protein chosen for the reference channel is not ideal when used in combination with the recombinant gp41 used on the test channel.

7.6.2 Measurement reproducibility

Each sample was tested on two independent prototypes of the SAW biosensor. While the two prototypes are designed to be identical, the question of reproducibility and reliability of the measurements taken was investigated. The phase shift measured by the different SAW biosensors (labelled 1 and 2) is plotted in Figure 7.8. The dots corresponding to

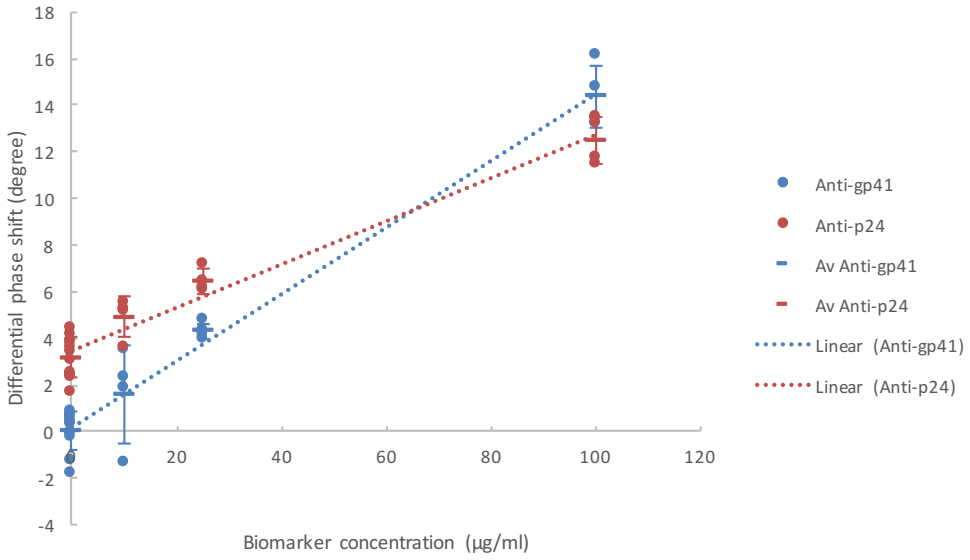

Figure 7.7: Third pilot study: validation of the assay using mock samples of known concentration. a) Differential phase shift measured after 5 minutes when testing mock samples with known concentration of anti-HIV antibody. Anti-gp41 results are presented in blue, anti-p24 in red. Each dot represents the value of one test, the line represents the average of all measurements for one concentration, with the error bars representing the standard deviation of the average. The dotted line represents the linear regression of the averages values.

the same sample are linked with a line. If one of the prototypes was consistently giving a higher reading than the other one, the joining lines would all follow the same direction (either upwards or downwards depending on which prototype gives the higher reading). The absence of any obvious similarities in the joining lines indicates there is no calibration issues between the two prototypes.

In addition, the dependence of the measurement on the user was investigated. That is, looking at whether the person operating the SAW biosensor influences the result of the test. For each type of SAW biosensor (designed to detect anti-gp41 or anti-p24), each of the two operators (data acquired with Dr. Eleanor Gray) tested the same negative calibration sample six times. This sample was not spiked with any of the biomarkers. It was tested on both SAW biosensors (anti-p24 and anti-gp41 detection SAW biosensors). The average phase shifts recorded after 5 minutes for the calibration sample are reported in Table 7.4, and indicates no user dependence.

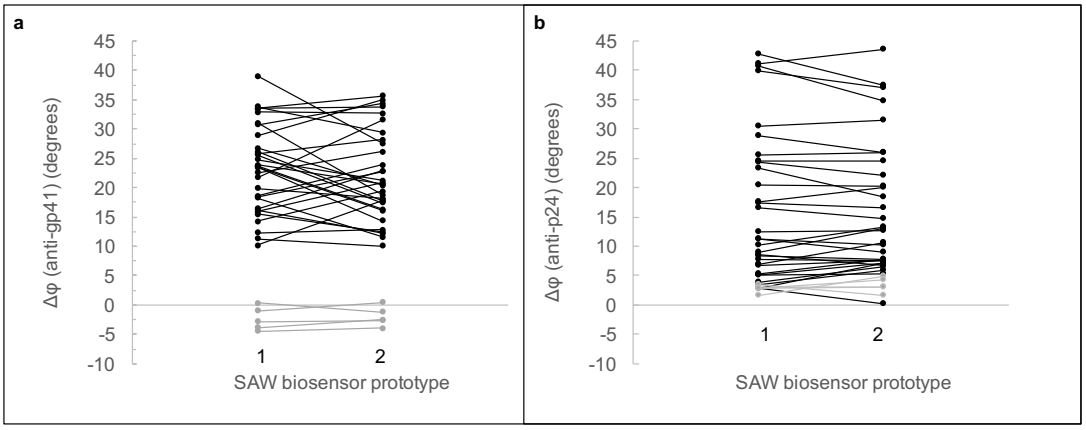

Figure 7.8: Independence of the measurement on prototype used. Plot to show the absence of dependence on the prototype of SAW biosensor used for the measurement. The measurements (differential phase shift recorded after 5 minutes) taken using prototype number one are plotted next to the measurements taken by prototype number 2. Two measurements corresponding to the same sample are joined with a line. **a)** Anti-gp41 detection. **b)** Anti-p24 detection.

	Average phase shift (degrees)	
	User 1	User 2
Anti-gp41	1.1 ± 1.2	2.2 ± 2.1
Anti-p24	2.9 ± 1.7	1.9 ± 1.1

Table 7.4: Third pilot study: Summary of calibration sample measurements. A calibration negative sample (pooled plasma not spiked with anti-HIV antibodies) was tested 6 times by each user, on both SAW biosensors. Results indicates no apparent user dependence.

7.6.3 Investigating correlation between biomarkers (anti-gp41 and anti-p24)

For each sample, the correlation between the two biomarkers of interest was investigated. The levels of anti-p24 and anti-gp41 in HIV-infected patients blood are not known to be dependent, and therefore the two were not necessarily expected to be correlated in this study. The phase shift values recorded by the SAW biosensor for each biomarker are plotted against each other in Figure 7.9.

By eye, this seems to suggest that there is no obvious correlation for the HIV-infected patient samples (plotted in blue). However, the negative samples (in green) seem to show some correlation, which is to be expected as they should both generate a consistent, nearly zero phase shift. The PPMCC was evaluated for the whole data set, but also for the positive samples only, as well as for the negative samples only. It was found to be 0.4565 (R^2 =

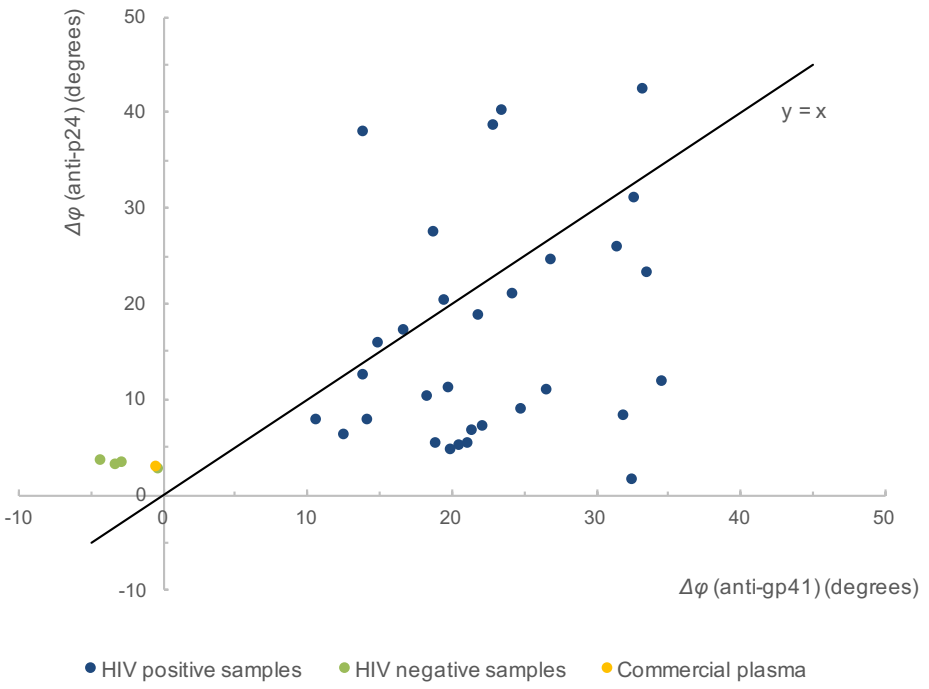

Figure 7.9: Third pilot study: correlation between biomarkers. For each sample, the differential phase shift recorded by the SAW biosensor for anti-p24 detection is plotted against the value recorded for anti-gp41 detection. Negative samples are plotted in green, positive samples in blue. The yellow dot represents the commercial pooled plasma tested. The PPMCC was evaluated for the negative samples and the positive samples separately, as well as for the whole data set. There was no evidence of correlation between the biomarkers in terms of signal recorded by the SAW biosensor, unless the sample was negative.

0.2084) for the whole data set, 0.2364 ($R^2 = 0.0559$) for the positive samples and -0.8183 ($R^2 = 0.6696$) for the negative samples. As expected, there is therefore no evidence of correlation between the phase shift recorded by the SAW biosensor for the two different biomarkers in the same sample, unless it is a negative sample.

7.6.4 Summary of results, test performance indicators

A summary of all the data obtained during this third clinical pilot study is presented in Figure 7.10 and Table 7.5. As for the second pilot study, each sample was tested twice, on two different disposable SAW biochips and all measurements were considered to be independent when estimating the sensitivity and selectivity of the test. The differential phase shift was read 5 minutes after sample injection, and compared to the threshold value established as the mean (+3SD) of the negative calibration samples measurements.

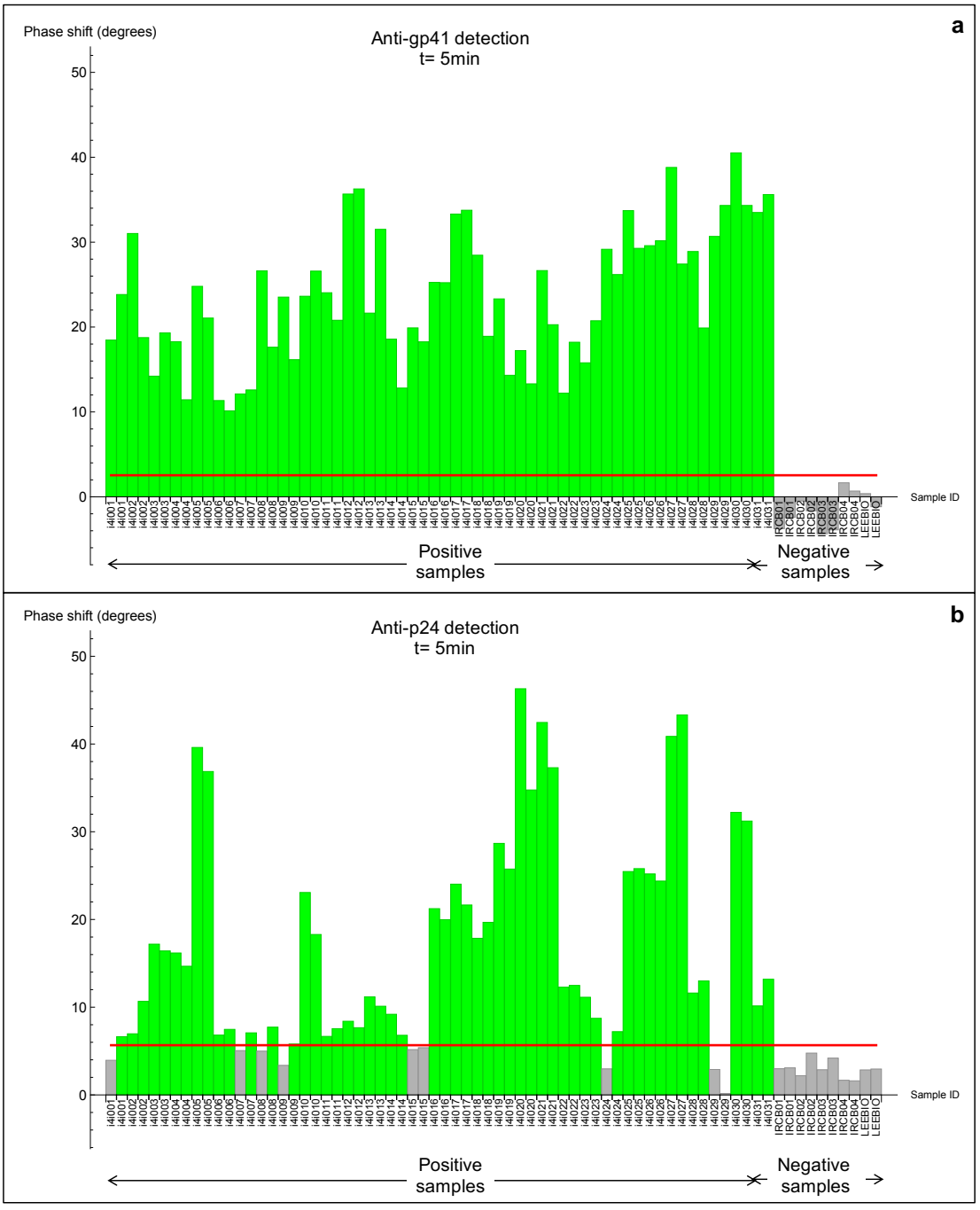

Figure 7.10: Third pilot study: readings 5 minutes after sample injection. **a)** Barchart showing the differential phase shift recorded by the SAW biosensor after 5 minutes. Each bar represents one test. Two tests were conducted for each sample. The red line indicates the threshold value defined to discriminate between positive and negative values. The nature of the sample (known positive, known negative or calibration sample) is indicated at the bottom of the barchart. A grey bar represents a sample declared negative by the test, whereas a green bar represents a positive test. (**b)** As in (**a**), but for Anti-p24 detection.

	+ samples			- samples			Sensitivity	Specificity
	Total	TP	FN	Total	TN	FP		
Anti-gp41	62	62	0	12	12	0	100%	100%
Anti-p24	62	53	9	12	12	0	85.5%	100%
Combined	62	62	0	12	12	0	100%	100%

Table 7.5: Third pilot study: summary of results. Each sample tested was assigned to one of the 4 categories (TP, FN, TN, FP), depending on the nature of the sample (known positive or negative) and the value of the phase shift recorded after 5 minutes in comparison with the threshold value defined as the mean (+3SD) of the negative calibration samples measurements. The test sensitivity and specificity were calculated for both biomarkers separately. A combined sensitivity and specificity is also presented, which reflects the fact that the detection of one of the biomarkers only would be enough to conclude on the positivity of a sample.

All of the samples taken from patients with HIV gave a true positive reading for anti-gp41 detection, giving a sensitivity of 100%. For anti-p24 detection, 53 out of the 62 samples gave a true positive reading, giving a sensitivity of 85.5%. The combined sensitivity of the test (at least one biomarker detected) was found to be 100%. Neither marker was detected in any of the healthy volunteer samples, giving a preliminary specificity of 100% of detection for both antibodies, though only 6 samples were tested (with multiple readings).

7.6.5 Comparison with competing diagnostics technologies

The samples from the patients with HIV were obtained at the stage of discard by the laboratory, and had been kept at 4°C for three weeks. It is unclear what effect this might have on the samples although degradation, rather than the opposite, is probable. In order to validate the results obtained, the samples were therefore also run on two commercially available PoCT currently in use in the UK. The OraQuick Advance is available over the counter in the United States, and the Alere HIV-1/2 Ag/Ab Combo is currently the only available PoCT with p24 antigen detection, although the performance of the precursor Alere Determine HIV 1/2 Ag/Ab test in the field has been variable.[115,116,202] The results of these rapid tests with the samples used in this study are shown in Table 7.6.

All HIV-positive samples gave clear positive antibody readings on both the Alere HIV-1/2 Ag/Ab Combo and the OraQuick Advance tests. None of the samples gave a positive antigen reading using the Alere HIV-1/2 Ag/Ab Combo test. The two rapid tests both detect anti-gp41, which was also positive in all samples by the SAW assay. These results verified the validity of the results obtained using the SAW biochips.

Sample	**SAW biosensor**	**OraQuick Advance HIV-1/2**	**Alere HIV-1/2 Ab/Ag Combo**	
Antibody/Antigen (Ab/Ag)	Ab	Ab	Ab	Ag
All HIV-positive samples (31)	+	+	+	-
All healthy volunteer samples (5)	-	-	-	-
Pooled donor plasma (1)	-	-	-	-

Table 7.6: Third pilot study: summary of PoCT comparison results. Each sample tested was assigned to one of the 4 categories (TP, FN, TN, FP), depending on the nature of the sample (known positive or negative) and the value of the phase shift recorded after 5 minutes in comparison with the threshold value defined as the mean (+3SD) of the negative calibration samples measurements. The test sensitivity and specificity were calculated for both biomarkers separately. A combined sensitivity and specificity is also presented, which reflects the fact that the detection of one of the biomarkers only would be enough to conclude on the positivity of a sample.

7.6.6 Discussion

This third pilot study demonstrated once again the ability of the SAW biosensor to detect key biomarkers of HIV in patient samples. The 100% combined sensitivity and specificity achieved in this small trial cannot be improved, though testing with an increased number of samples was needed to confirm these results, particularly control samples from health volunteers (at this stage only 6). In addition, this small study used samples (from HIV patients) that were at the stage of discard from the diagnostic laboratory, had been stored for three weeks between receipt and discharge, and were therefore not fresh upon use on the SAW biosensor. It is not known at which stage of infection the patients were at the time of sampling, though as they had uncontrolled viral load (at >5,000c/mL) it is not probable that they were taking effective antiretroviral therapy and it is formally possible that they were recently diagnosed. All samples were negative for the HIV-1 antigen p24, which can be detected using the Alere Determine HIV-1 Ag/Ab Combo test, suggesting that samples were not taken during the stage of acute infection, though the performance of the antigen component of this test is poor, so this is not conclusive.[203,204] Given these caveats, therefore, the levels of sensitivity achieved are exceptional and warrant a further, larger trial with fresh samples.

7.7 Fourth clinical pilot study

A final pilot study was conducted following the same protocol as the one used for the third pilot study. An additional 100 confirmed negative samples were tested, in order to refine the test performance indicators. For logistical reasons, the confirmed positive samples could not be tested again and the results from the third pilot study were used. A total of 28 negative calibration samples were run. In addition, the threshold value was adjusted separately for each biomarker, to achieve the best test performance indicators, as described below.

7.7.1 Threshold value adjustment

In the previous three clinical pilot studies, the cut-off value used to discriminate between a positive and a negative sample was defined as the mean +3SD of the measurements performed on negative calibration samples (pooled plasma from confirmed healthy individuals). This meant that statistically, 95% of the future potential true negative samples tested would be expected to give a reading below this threshold value and count as true positives. The decision to define the threshold as this value was arbitrary, and did not necessarily reflect on the specific results recorded by the test with confirmed negative samples.

Ideally, the threshold should be defined so that it lies in between the highest reading recorded for a confirmed negative sample, and the lowest reading recorded for a confirmed positive sample. If there is an overlap, it should be adapted to exclude most false positives and false negatives. This method can only be applied, however, if a large amount of test results is available. In previous studies, only 6 confirmed negative samples were tested (in duplicate), therefore the statistical approach was more justified than this empirical method. For this fourth pilot study, as the number of confirmed negative samples was significantly increased (over a hundred), it was decided to consider the differences observed between samples (confirmed positive versus confirmed negative) to define the optimal threshold for the test.

7.7.2 Summary of results, test performance indicators

A summary of all the data obtained during this fourth clinical pilot study is presented in Figures 7.11, 7.12 and Table 7.7. The differential phase shift was read 5 minutes after

sample injection, and compared to a threshold value specific to each biomarker. For anti-gp41, the mean (+4SD) of the negative calibration samples measurements was used, for anti-p24, the mean (+5SD) of the negative calibration samples measurements was used.

	+ samples			**- samples**			**Sensitivity**	**Specificity**
	Total	TP	FN	Total	TN	FP		
Anti-gp41	62	62	0	106	106	0	100%	100%
Anti-p24	62	41	21	106	106	0	66.1%	100%
Combined	62	62	0	106	106	0	100%	100%

Table 7.7: Fourth pilot study: summary of results. Each sample tested was assigned to one of the 4 categories (TP, FN, TN, FP), depending on the nature of the sample (known positive or negative) and the value of the phase shift recorded after 5 minutes in comparison with the threshold value. The test sensitivity and specificity were calculated for both biomarkers separately. A combined sensitivity and specificity is also presented, which reflects the fact that the detection of one of the biomarkers only would be enough to conclude on the positivity of a sample.

Using these respective thresholds, all the confirmed negative samples tested gave a negative reading, giving a 100% specificity for both antibodies. All samples taken from patients with HIV gave a true positive reading for anti-gp41 detection, giving a sensitivity of 100%. For anti-p24 detection, 41 out of the 62 samples gave a true positive reading, giving a sensitivity of 66.1%. The combined sensitivity of the test (at least one biomarker detected) was found to be 100%.

7.7.3 Reducing test waiting time

As the calibration samples were run following the exact same protocol as the test samples, it was possible to define a discriminative threshold value as a function of time. It was then possible to compare each test value to a threshold value at any point in time, and therefore count the number of TP, FN, TN, and FP, starting from sample injection and all the way to the end of the 5 minutes measurement, and to evaluate the sensitivity and the specificity of the test as a function of time. The results are presented in Figure 7.13.

This study was very instructive as it revealed that there was no need to wait for 5 minutes after sample injection to achieve high levels of performance. As can be seen in Figure 7.13a, the test only requires 1 min to declare a sample as true positive with a 100% sensitivity, and only 4 minutes and 30 seconds to declare a sample as true negative with a 100% specificity. This shows that, with further development, the SAW biosensor has great potential to deliver

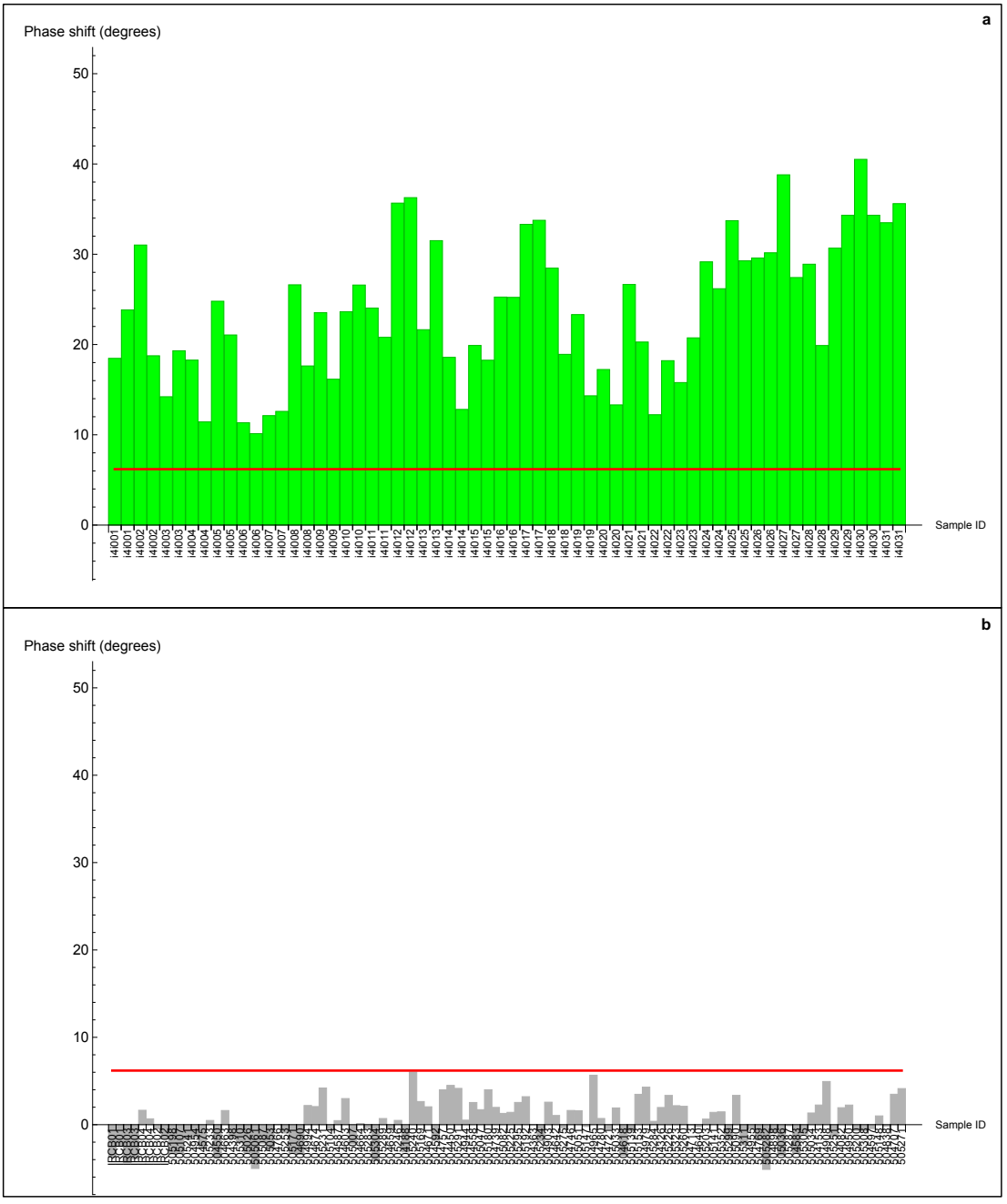

Figure 7.11: Fourth pilot study: readings 5 minutes after sample injection. Anti-gp41 a) Barchart showing the differential phase shift recorded by the SAW biosensor after 5 minutes, for confirmed positive samples. Each bar represents one test. Two tests were conducted for each sample. The red line indicates the threshold value defined to discriminate between positive and negative values. A grey bar represents a sample declared negative by the test, whereas a green bar represents a positive test. **b)** As in **a)**, but for confirmed negative samples detection.

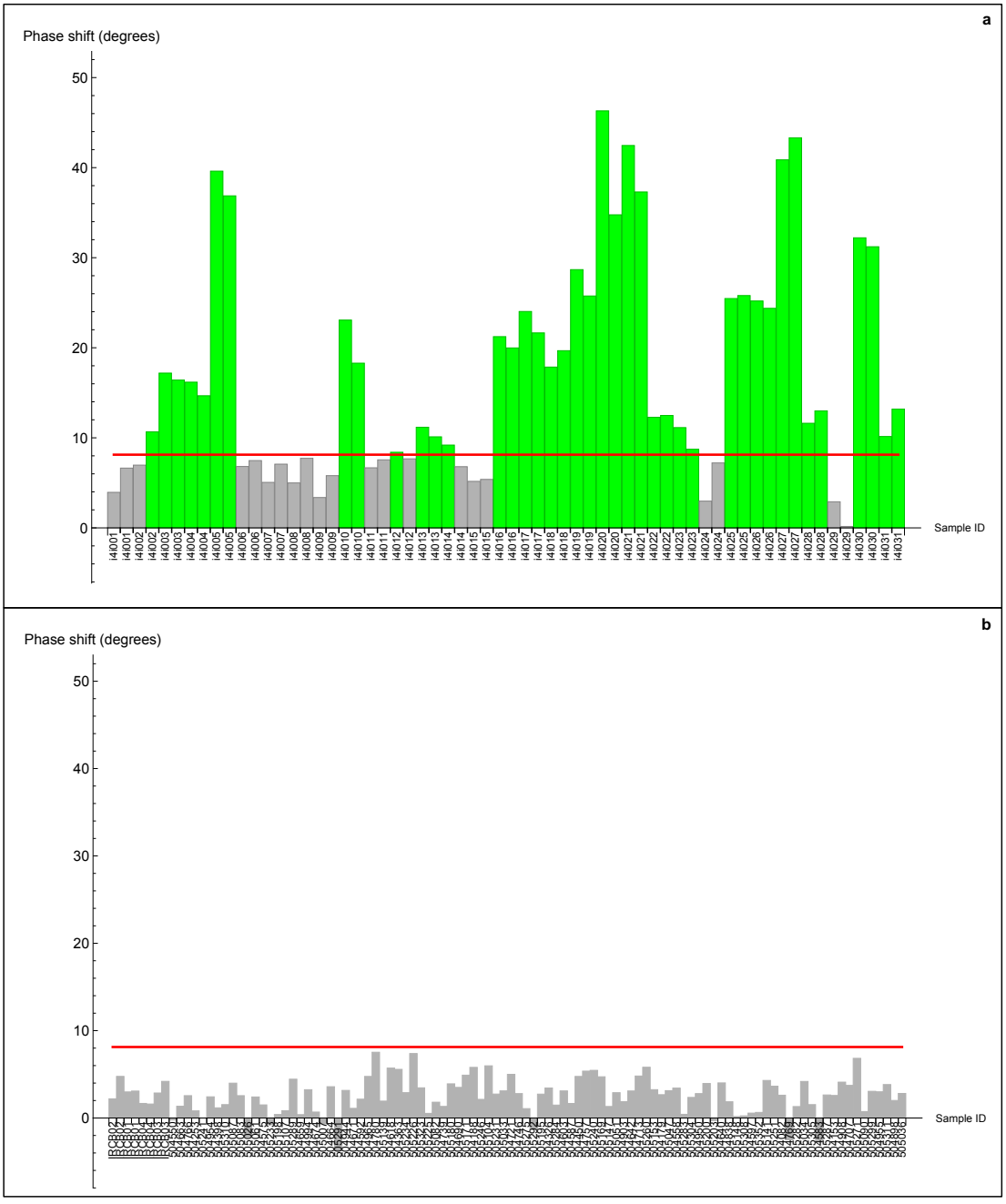

Figure 7.12: Fourth pilot study: readings 5 minutes after sample injection. Anti-p24 a) Barchart showing the differential phase shift recorded by the SAW biosensor after 5 minutes, for confirmed positive samples. Each bar represents one test. Two tests were conducted for each sample. The red line indicates the threshold value defined to discriminate between positive and negative values. A grey bar represents a sample declared negative by the test, whereas a green bar represents a positive test. **b)** As in **a)**, but for confirmed negative samples detection.

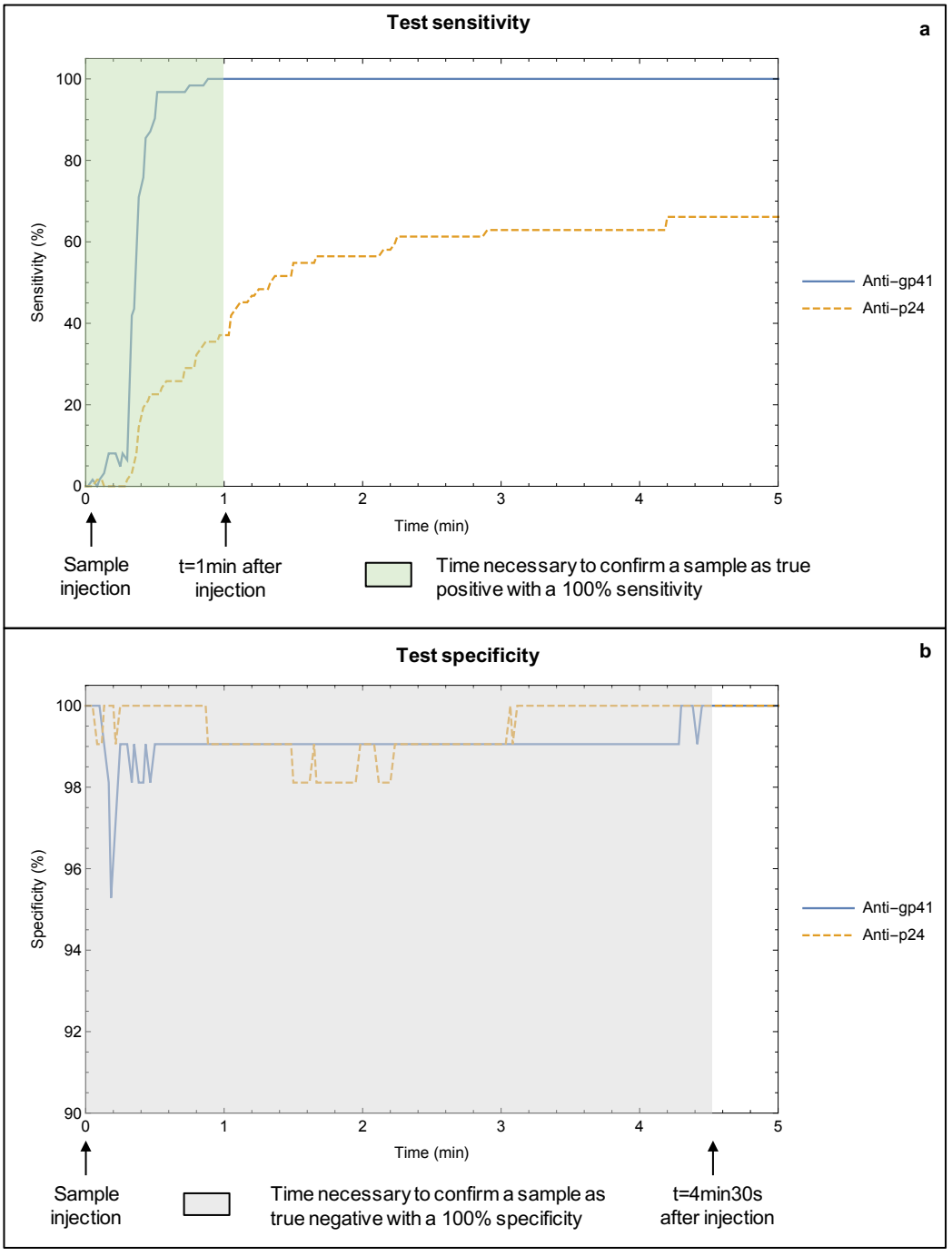

Figure 7.13: Fourth pilot study: sensitivity and specificity of the test over time. a) Plot to show the test sensitivity over time, for both biomarkers. The green window indicates the time necessary to cinfirm a sample as true positive (at least one biomarker detected with a 100% sensitivity). **b)** Plot to show the test specificity over time, for both biomarkers. The green window indicates the time necessary to cinfirm a sample as true positive (both biomarkers detected with a 100% specificity).

results with high levels of sensitivity and specificity within a shorter time frame than all current commercially available PoCT.

7.7.4 Discussion

This final clinical pilot study confirmed the ability of the SAW biosensor to detect both biomarkers of HIV infection with 100% sensitivity and specificity under 5 minutes. A higher confidence in the test specificity was achieved by testing a high number of confirmed negative samples form healthy individuals (106). It was also shown that the it was possible to achieve shorter time to result, the highlight being the ability of the test to declare a true positive result with a 100% sensitivity within a minute from sample injection

7.8 Conclusions

After optimising the characteristics of the SAW biochips and demonstrating their ability to detect the presence of key HIV biomarkers in mock samples, it was decided to move a step closer to real point-of-care conditions, and investigate the performance of the SAW biosensor with real patient samples. Due to logistical considerations, two proof of concept studies using two different types of SAW biochips had to be conducted, and they both showed the SAW biochips were capable of detecting the two biomarkers of HIV (anti-gp41 and anti-p24) in a complex matrix (serum or plasma. It was therefore decided to conduct a series of pilot studies using 31 HIV positive patient samples. Progress was made step by step through the four small pilot studies presented in this chapter, in parallel with the optimisation of the SAW biochips. Reducing the size of the SAW biochip warrants smaller manufacturing costs and enables the test to be run with a minimal amount of patient sample (6μl). The implementation of an in-situ reference channel to account for the high risk of non-specific binding events due to the complexity of the samples tested has made the SAW biosensor even more simple to use and has taken it to the next level of performance. The evolution of the key results of the pilot studies is presented in Table 7.8 below.

The results from the latest pilot study highlight the very good performance of the SAW biosensor as a PoCT. Both the sensitivity and the specificity of the test were found to be 100%, and further analysis showed that only one minute between sample injection and test

Pilot study	**Number of samples tested independently**	**Test performance indicators**	**Highlights and improvements**
1	10 (blind study)	100% sensitivity 80% specificity	First study involving patient samples
2	62 confirmed positives 12 confirmed negative	95.2% sensitivity 100% specificity	Promising results nuanced by SAW biochips functionalisation issues
3	62 confirmed positives 12 confirmed negatives	100% sensitivity 100% specificity	Levels of sensitivity and specificity excellent, larger trials needed
4	62 confirmed positives 112 confirmed negatives	100% sensitivity 100% specificity	High number of confirmed negative samples / time to result reduced to 1min for 100% sensitivity and 99% specificity

Table 7.8: Evolution of the results of the clinical pilot studies.

reading are sufficient to achieve a 100% sensitivity and 99% specificity, which gives the SAW biosensor a competitive advantage over current commercially available PoCT. A summary of the different characteristics and performance indicators of four PoCT is presented in Table 7.9. It shows that it out performs the other experimental smartphone-connected PoCT in terms of sensitivity and specificity. In addition, for a comparable sensitivity and specificity, the SAW biosensor prototype requires a smaller sample volume than the Alere HIV 1/2 Ab/Ag Combo. More importantly, it out performs all other tests in terms of time to result. Finally, it is characterised by its connectivity and possibility of data linkage, which none of the current commercially available PoCT offer at the moment.

These promising results should serve as a platform for larger pilot studies conducted using fresh samples. Testing a large number of healthy volunteers samples would help assessing the test sensitivity and specificity with a higher accuracy. Another step forward would involve testing whole blood instead of blood plasma. This would reduce the number of steps required to perform the test, making it even cheaper, faster and more simple overall. The test could then potentially be performed anywhere and require a very minimal amount of training. Work has already begun on this, using the pore structure of a paper strip to filter out most of the blood cells from the initial drop of blood sample, and at the same time taking advantage of the capillary effect to deliver the plasma sample to the SAW biochip. In order to make the test more versatile, implementing additional channels to the SAW

	SAW biosensor (4th pilot study	**OraQuick Advance HIV-1/2**	**Alere HIV-1/2 Ab/Ag Combo**	**ELISA smartphone dongle**[23]
Sensitivity (limit of detection)	10μg/ml (anti-gp41) 25μg/ml (anti-p24)	10μg/ml (anti-gp41). No anti-p24 detection	5μg/ml (anti-gp41) 100μg/ml (anti-p24)	NP
Clinical sensitivity	100%	100%	100%	92 to 100%
Clinical specificity	100%	100%	100%	79 to 100%
Volume of sample required	6μl	2.5μl	50μl	fingerprick
Time to result	<5min	20-40min	20-30min	15min
Connectivity and data linkage	Yes	No	No	Yes

Table 7.9: Comparison of some key characteristics of four different PoCT. The SAW biosensor has better or comparable sensitivity to two PoCT available in the UK. It requires less sample volume than Alere HIV 1/2 Ab/Ag Combo, and delivers a result faster than the other three currently available PoCT. It is the only one to offer connectivity with the experimental ELISA smartphone dongle, which presents lower levels of sensitivity and specificity. NP = not published.

biochip and functionalising each of them accordingly could allow for multiplexed testing of different biomarkers, and therefore potentially testing for multiple infections with the same SAW biochip. The SAW biochips can be used as a platform for detecting virtually any biomarker, provided the sensing area can be functionalised with the relevant capture protein against the biomarker of interest. Finally, further studies will ideally be conducted using the development hand-held prototype connected to a smartphone, instead of using the laboratory prototype and a laptop.

Chapter 8

Model to Characterise SAW Device Response, Sample and Target Protein Properties

Building on the promising results obtained with the SAW biosensor and presented in Chapters 6 and 7, the aim of this chapter was to characterise the fundamental physical parameters contributing to the signal output measured with the SAW biochips used throughout this thesis. The approach involved applying the model developed by Saha and Gizeli,[38] which relies on the combination of a precise calibration of the sensor and the assimilation of proteins into non-interacting solid particles to disentangle the contribution of different physical parameters contributing to the measured signal. As the method offers a way to characterise some of the parameters defining both the sample and the sensor itself, using this analysis could potentially contribute to optimising the SAW biosensor even further to make it faster, more sensitive and able to answer more questions about a given sample. More generally, the idea behind this work was to potentially be able to predict the characteristics of the output signal based on the type of sample, or to extract useful information other than the presence or the concentration- about the biomarker of interest.

8.1 Introduction

The main results presented in chapters 6 and 7 demonstrate the ability of the SAW biosensor presented in this thesis to differentiate between two samples, based on the comparison of the signal (phase shift or insertion loss) recorded for each sample separately. Using this concept, it was showed that samples characterised by different concentrations of the biomarker of interest could be distinguished from one another. Furthermore, the unknown concentration of a given sample could be estimated using a titration curve created beforehand using mock samples of known concentration. It was also shown that real patient samples could be assessed as being either positive or negative to a given biomarker of HIV. Once again, this was achieved by comparing the recorded signal for the unknown sample to a reference value established beforehand in this case a threshold value determined based on the average signal recorded for a number of known negative samples. The promising results of the three pilot studies conducted are paving the way for larger clinical studies, and contributed to establishing the SAW biosensor as a better alternative to current commercially available PoCT for HIV.

These results all rely on a simple approach: carefully establishing one or several reference values recorded under the same conditions as when the actual test is carried out, and comparing the value recorded for the unknown sample to the reference value(s). This is the general description of the mode of operation of most biosensors. As for any system, understanding the mechanisms leading to a signal change could potentially help optimise the biosensor, and extract absolute information about the sample tested, instead of limiting the analysis to a relative comparison to one or several reference samples.

As mentioned in Chapter 3, the perturbation theory applied to SH-SAW can be used to derive equations describing the wave velocity and attenuation, which relate directly to the change in the phase shift and insertion loss (respectively) measured by a SAW device supporting a SH-SAW. Different sets of equations can be derived depending on the initial assumptions on the nature of the perturbation occurring on the surface of the SAW sensor. An analytical solution can be expressed in two specific cases. The first case is when the viscosity at the surface proximity is altered by changing the solution in contact with the sensor, assuming nothing is adsorbed or binds to the surface and the solutions are Newtonian fluids (see Equations 3.9 and 3.10 in Chapter 3). The second case is when

mass is adsorbed on the surface of the sensor, in the form of a uniform isotropic thin film. The typical example being a thin film of metal grown or evaporated on the surface (see equations 3.11 and 3.12 in Chapter 3).

While these two sets of equations can be very useful in the specific cases where they are valid, there is no current analytical solution to describing the adsorption or binding of proteins to the surface of the sensor. Particles (proteins or nanoparticles for example) binding to the surface lead to a combination of non-ideal perturbations involving mass, viscosity, and possibly a combination of both. Such perturbations are typical in the context of using the SAW sensor as a biosensor. Being able to understand the changes in mass, viscosity and viscoelasticity on the surface proximity, when objects such as proteins bind to the surface of the sensor, could therefore prove to be an essential tool to the development of SAW sensors as biosensors. It was therefore decided to try and characterise as many as possible of the parameters involved in the process of the biosensor giving a response to a given sample: the sensor itself, some of the liquid sample properties and finally some properties of the proteins binding to the surface of the biosensor.

8.2 Review of Saha/Gizeli method

In 2003, a group at Cambridge University proposed a method to evaluate the mass coverage on the surface of their SH-SAW sensor, based on a simple device calibration with glycerol/water solutions, and the assimilation of proteins binding to the surface as non-interacting solid particles.[38] In summary, their method only requires the measure of the insertion loss induced by the perturbation occurring on the surface of the SAW sensor to probe the mass added on the surface of the delay line of the SAW sensor. Along the way, the method estimates different parameters characterising the sample solution (such as density and viscosity), as well as the sensor itself. They reported a good agreement between the surface mass coverage obtained using their method and a gold standard method such as Surface Plasmon Resonance (SPR). As can be seen in Figure 8.1, the device used to generate the SH-SAW and measure its insertion loss is very similar to the SAW devices used throughout this thesis, with two IDTs separated by a delay line on top of a quartz substrate. Despite the fact Saha *et al.* used a polymer film as a waveguide, their device

was considered similar enough, and therefore the Saha/Gizeli method was assumed to be suitable to characterise the SAW device.

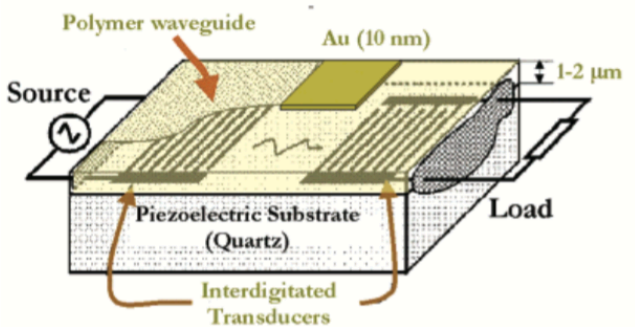

Figure 8.1: SH-SAW device used by Saha/Gizeli.. Schematic to illustrate the SH-SAW device used by Saha/Gizeli. The device consists of two gold IDTs and a gold delay line (used as the sensing area) on top of a quartz piezoelectric crystal. A 1.2m thick polymer film covering the top surface of the crystal, the IDTs and the delay line is used as a waveguide. Adapted from [38]

.

8.2.1 Principle of the Saha-Gizeli method

The principle of the method is presented in Figure 8.2. The main objective of the method is to relate, for a given sample, the **measured insertion loss** ΔIL to the **mass per surface area** M_{norm} added on the surface of the SAW device. The relation between the two is outlined in red in the diagram, and is shown as a dashed arrow to underline the fact the link between the two is indirect. Indeed, the method involves a series different steps and calculations that are inter-dependent.

The authors introduced the concept of glycerol equivalent weight fraction (w_{gly}), which translates the fact that adsorbing proteins on the surface of the SAW device is similar, for viscoelastic purposes, to adding glycerol to the solution until it contains w_{gly} glycerol.

Another concept introduced is the sensing volume V_{sens}, which represents the volume of solution affected by the acoustic wave. It is schematised in Figure 8.3, and is defined as:

$$V_{sens} = \delta A_{sens}, \tag{8.1}$$

where δ is the acoustic penetration depth, and A_{sens} the sensing area. A_{sens} is effectively the surface area of the delay line of the device.

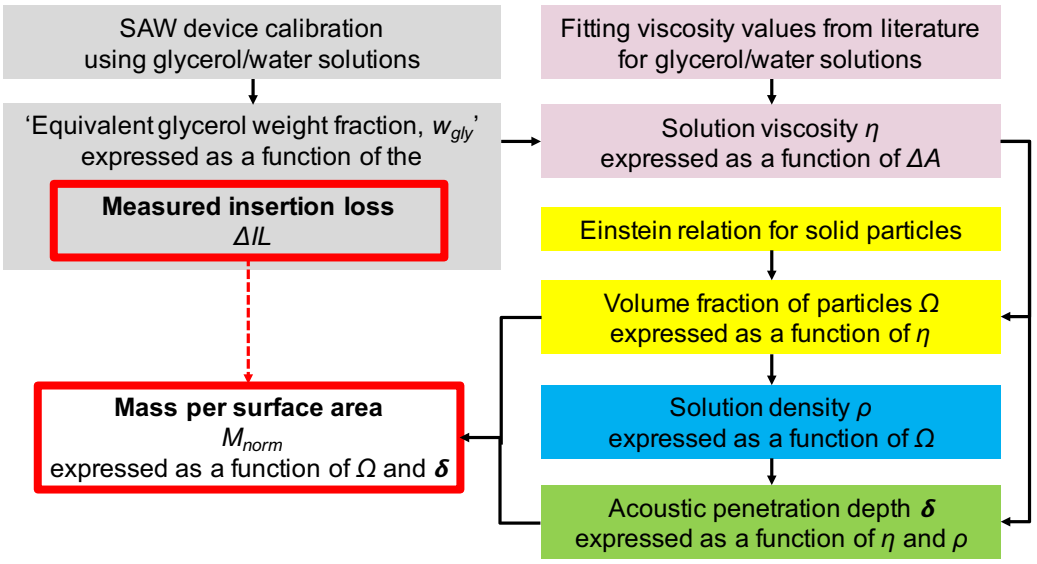

Figure 8.2: Diagram to present the Saha/Gizeli approach. The mass per surface area M_{norm} of proteins binding to the surface of the SAW device is estimated indirectly via the measurement of the insertion loss ΔIL. A calibration of the device using glycerol/water solutions (grey block) is used in combination with an estimation of the solution viscosity from literature values (purple block) to relate the solution viscosity η to ΔIL. Applying the Einstein relation for solid particles gives a relation between the volume fraction of particles Ω and η (yellow block). The solution density ρ can be expressed as a function of Ω (blue block), and the acoustic penetration depth δ can be expressed as a function of ρ and η (green block). Finally, M_{norm} can be expressed as a function of Ω and δ.

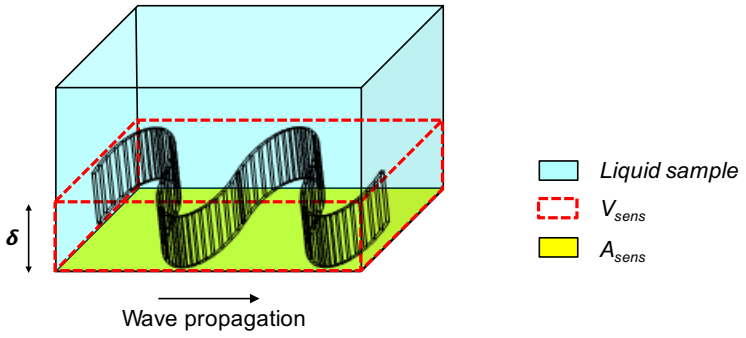

Figure 8.3: Sensing area, penetration depth and sensing volume. Schematics to show the propagation of the acoustic wave through the sensing volume V_{sens} (red dotted volume), defined as the product of the sensing area A_{sens} (yellow area), and the wave penetration depth δ. Any part of the liquid sample that is not included in the sensing volume is not affected by the wave, and therefore only the proteins contained within V_{sens} can be probed by the sensor. Drawing not to scale. *Note*: the acoustic wave is evanescent and its amplitude decreases exponentially as it propagates along the sensing area.

Finally, the method relies on considering the proteins binding to the surface as non-interacting solid particles. This is schematised in Figure 8.4, with the example of antibodies adsorbing onto the surface of the sensor.

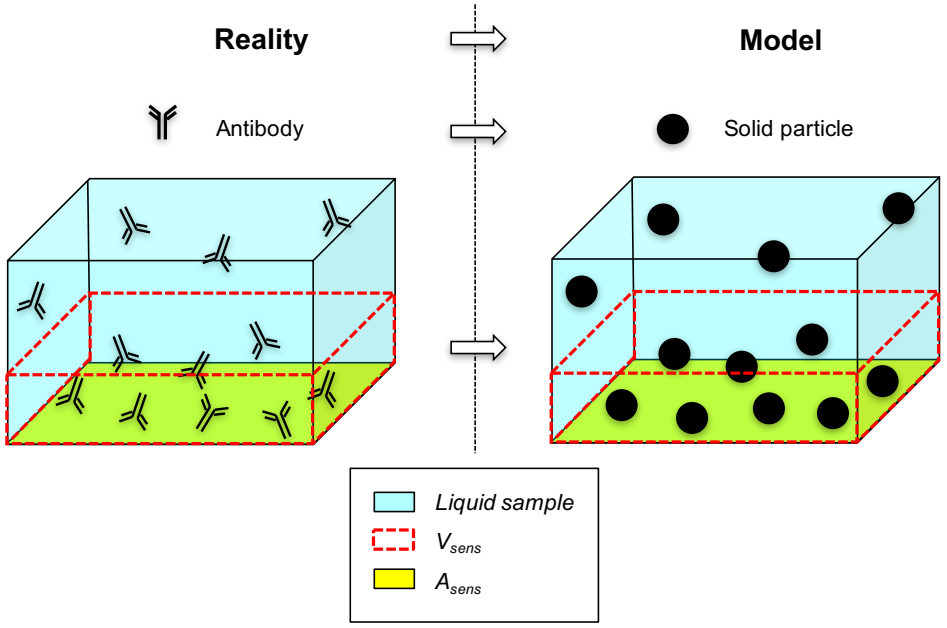

Figure 8.4: Assimilating proteins to non-interacting solid particles. Schematics to show one of the main assumptions involved in the Saha-Gizeli method. Proteins in the sample are assimilated to non-interacting solid particles. In the example shown, antibodies in the sample simply adsorb on the surface of the sensor. Only the particles contained within the sensing volume (red box) can be probed by the sensor. Drawing not to scale

.

The total mass of particles M_{par} contained within V_{sens} therefore relates to M_{norm} as follows:

$$M_{norm} = \frac{M_{par}}{A_{sens}}. \tag{8.2}$$

The volume fraction of particles, Ω is defined as:

$$\Omega = \frac{N_{par} V_{particle}}{V_{sens}}, \tag{8.3}$$

where $V_{particle}$ is the volume of one particle and N_{par} is the number of particles contained within the sensing volume, defined as:

$$N_{par} = \frac{M_{par} N_A}{MW_{particle}}, \tag{8.4}$$

where $MW_{particle}$ is the molecular weight of a particle, and N_A is the Avogadro constant ($6.02 * 10^{23}\text{mol}^{-1}$). By combining equations 8.1, 8.2, 8.3 and 8.4, the following expression for M_{norm} can be derived:

$$M_{norm} = \frac{\delta \Omega MW_{particle}}{V_{particle} N_A}. \tag{8.5}$$

The acoustic penetration depth $\delta$is defined as function of the solution viscosity and density ρ , as well as the device frequency f:[136]

$$\delta = \sqrt{\frac{\eta}{\pi f \rho}}. \tag{8.6}$$

As the device frequency f is known, and both $MW_{particle}$ and $V_{particle}$ are known quantities, the remaining unknown in Equation 5 are the solution viscosity η and density ρ, as well as the volume fraction of particles Ω.

The Einstein relation for solid particles gives a relation between the solution viscosity η (with and without particles) and the volume fraction of particles Ω within the sensing volume V_{sens}:[205]

$$\frac{\eta_2}{\eta_1} = 1 + \nu\Omega, \tag{8.7}$$

where η_1 is the viscosity of the solution without particles, $\eta_2$the viscosity of the solution containing the particles and ν is the particle shape factor (2.5 for a sphere[205]). This relation is only valid if $\Omega \leq 0.2$.

In the following, the model solution will consist of water, or buffer, containing proteins (the model particles). η_1 will therefore be considered as the viscosity of water, or buffer, and $\eta_2$will be the viscosity of the solution defined earlier, η. The only remaining unknowns in Equation 8.5 are therefore the solution viscosity η and density ρ.

The solution density ρ is defined as the ratio between the mass and volume of solution that is affected by the wave. The mass of solution affected by the wave can be expressed as the sum of the mass of water within the sensing volume (Mwater), and the mass of particles contained within the sensing volume (M_{par}). Therefore, the solution density can be expressed as:

$$\rho = \frac{M_{par} + M_{water}}{V_{sens}} = \frac{M_{par}}{V_{sens}} + \rho_{water}, \tag{8.8}$$

which using Equation 8.5, can be expressed as:

$$\rho = \frac{\Omega MW_{particle}}{V_{particle} N_A} + \rho_{water}. \tag{8.9}$$

The only unknown remaining in Equation 8.5 is therefore the solution viscosity η. It is estimated using the following method.

Firstly, a calibration of the SAW device is performed, using different glycerol/water solutions of known weight percentage of glycerol. A direct proportional relationship is observed, with a slope γ. This yields the following relation between the glycerol weight fraction w_{gly}, and the normalised insertion loss ΔIL_{norm}(measured insertion loss ΔIL divided by the device sensing area A_{sens}):

$$\Delta IL_{norm} = \frac{\gamma}{A_{sens}} w_{gly}. \tag{8.10}$$

Then the solution viscosity η is expressed as a function of w_{gly} by fitting the literature values of the viscosity of glycerol/water solutions based on their glycerol weight fraction. Combining Equation 8.10 and the fitted function yields a direct relationship between the measurement of ΔIL and the solution viscosity η. It is therefore possible to estimate the mass per surface area adsorbed on the surface of the SAW device, M_{norm}, using the measurement of ΔIL.

8.2.2 Advantages and limitations of the model

The main advantage of the approach presented by Saha *et al.* is its simplicity. Once the device calibration with glycerol/water solutions is done, the function expressing the viscosity η as a function of the measured insertion ΔIL can easily be expressed. From this point, one only requires to input the values of ΔIL into a series of equations to estimate the mass of protein binding to the surface, the solution viscosity and density, and the acoustic wave penetration depth amongst other parameters. The method can also be used to characterise the sensor and therefore predict its response in terms of insertion loss, to perturbations due to particles of different size, weight and shape.

The method can also be used stepwise, to estimate the mass of protein binding to the surface at different stages. For example, it is possible to apply the method twice, starting with a simple adsorption of antibodies on gold, then considering the antibody-coated gold surface as a new starting point to estimate the mass of antigen binding to the layer of antibodies.

Finally, the authors report a good agreement between their estimations and the measurement of mass binding to the surface of a gold chip using the gold-standard Surface Plasmon Resonance (SPR), as can be seen in Figure 8.5.

The possible limitations of such an approach reside in the initial assumptions made. By considering the proteins binding -or adsorbing- to the surface as non-interacting solid particles, it is possible to apply the Einstein relation for solid particles. This ultimately solves the problem of not being able to directly measure certain quantities that would be necessary to estimate the mass added on the surface, by expressing this as a function of the solution viscosity. However, depending on their nature, as well as the concentration on the surface, some particles might interact between one another to form a network, and effectively contribute to altering the viscoelasticity within the sensing volume. Therefore, this assumption might not be true for all systems, making the model inapplicable in some cases, for examples non-Newtonian fluids. Other more advanced versions of the model exist, which take those interactions into account.

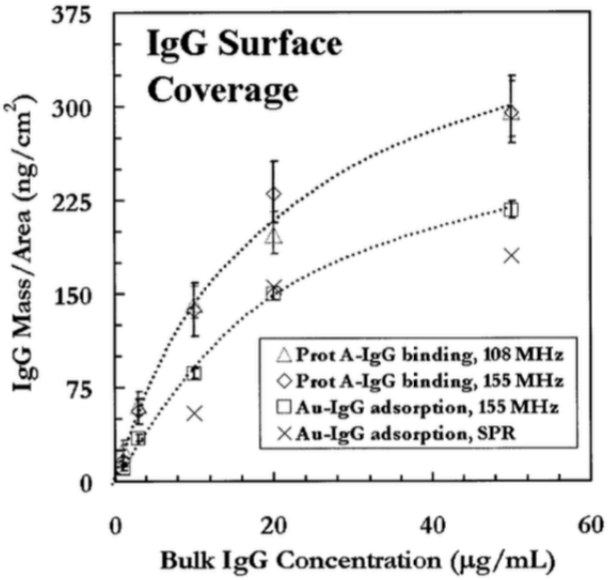

Figure 8.5: Validation of the Saha-Gizeli method: comparison of the results with equivalent gold standard method (SPR). The mass per surface area of IgG adsorbed on the bare gold surface of a 155MHz SAW sensor was estimated using the Saha-Gizeli method. Results are plotted as a function of the IgG concentration in solution (square markers). Measurements of the mass per surface area of IgG on bare gold SPR sensors were performed using the same solutions of IgG, and the results are plotted on the same graph (cross markers). There is a good correlation between the estimated results obtained using the method, and the measurement performed using the gold standard SPR method. Plot reproduced from Saha *et al.*[38]

8.3 OJ15 SAW device calibration and characterisation

Two different SAW devices were used in the method presented by Saha *et al.* They both have a very similar design to the SAW biochips used throughout this thesis. Both are based on a quartz piezoelectric crystal supporting a SH-SAW propagating along a delay line located between two sets of IDTs. Both sets of IDTs, as well as the delay line, are made of a thin film of gold deposited on the surface of the piezoelectric crystal. The devices used operate at a frequency of 108MHz and 155MHz, respectively. The following results were obtained using OJ15 SAW biochips operating at 251.5MHz, also based on a quartz piezoelectric crystal supporting a SH-SAW generated using gold IDTs and propagating along a gold sensing area.

8.3.1 OJ15 SAW device glycerol/water calibration studies

OJ15 SAW devices were calibrated using glycerol/water solutions of known weight fraction of glycerol, ranging from 0 to 0.72. The different solutions were put in contact with the sensing area of the biochip for 5 minutes, after which the sensing area was washed with deionised water. The real time insertion loss and phase shift of the SAW device calibration are presented in Figure 8.6.

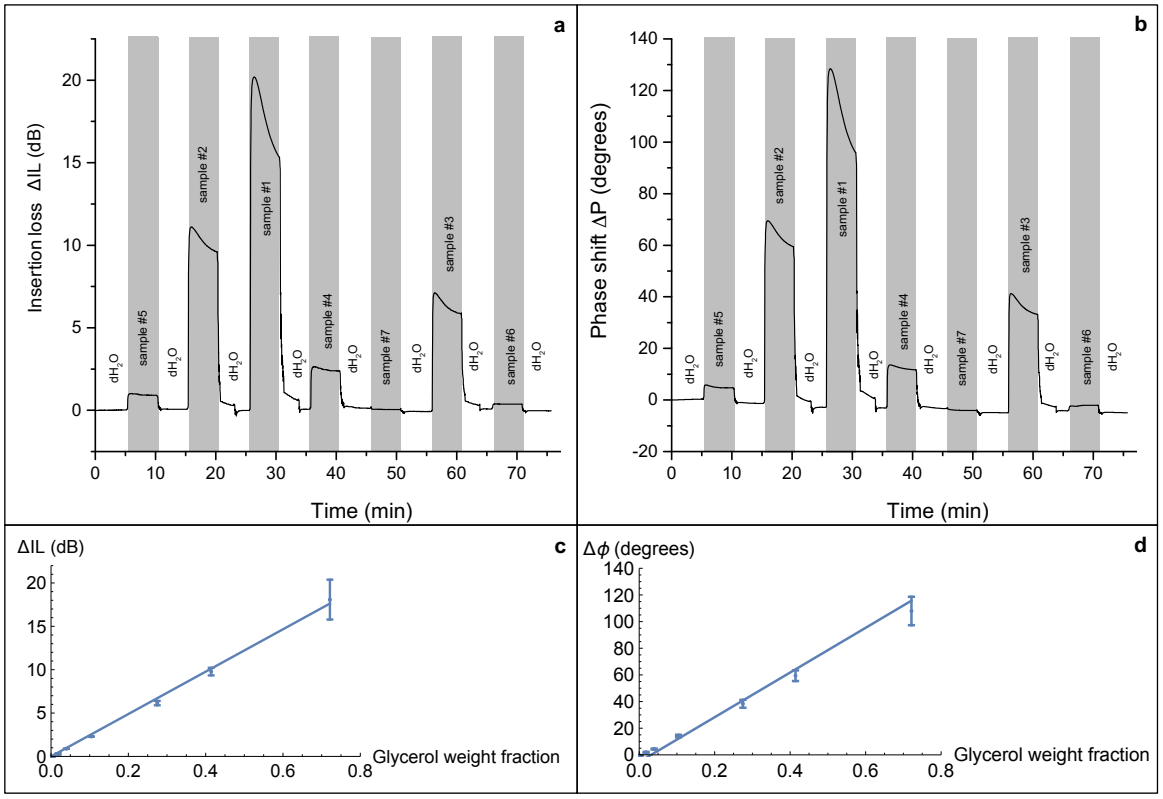

Figure 8.6: OJ15 SAW device calibration. **a)** Plot to show the evolution of the insertion loss ΔIL over time, as various glycerol/water solutions are added and left to incubate over the surface of the SAW device. The surface was washed with deionised water after each incubation. The seven different solutions were tested in a random order, as indicated on the plot (sample #1 to #7, in decreasing weight fraction of glycerol). **b)** Plot to show the insertion loss ΔIL as a function of the glycerol weight fraction. The insertion loss was recorded 5 minutes after sample injection. Each point is the average of 4 independent measurements, error bars represent the standard deviation of the mean. The blue line represents the linear regression $y = 24.4x, R^2 = 0.998$. **c)** Same as a, for the phase shift $\Delta\phi$. **d)** Same as b, for the phase shift $\Delta\phi$. The linear regression yields the equation $y = 147x, R^2 = 0.999$.

As can be seen in Figures 8.6b and 8.6d, a linear relationship was found between the signal output by the SAW biosensor and the solution glycerol weight fraction, for both the

insertion loss ΔIL and the wave phase shift $\Delta\phi$. The R-squared of the linear regression was found to be 0.998 and 0.999 for ΔIL and $\Delta\phi$ respectively.

8.3.2 Comparison with other SAW sensors

In order to assess the performance of the OJ15 SAW devices in terms of sensitivity to different glycerol/water solutions, the results of the calibration were compared to the ones presented in the Saha *et al.* paper, obtained with different SAW sensors. When a perturbation occurs within the sensing volume of the SAW sensor, the higher the response measured (either ΔIL or $\Delta\phi$), the more sensitive the SAW sensor is. Therefore, a good indication of the sensitivity of a given sensor is the slope of the linear regression performed on the data acquired from the sensor calibration with different glycerol/water solutions. The slopes obtained for both ΔIL and $\Delta\phi$ are presented in Table 8.1, for the two SAW sensors presented by Saha *et al.*, as well as for the OJ15 SAW devices.

	Saha *et al.* 108MHz	Saha *et al.* 155MHz	OJ15 SAW biochip
Insertion loss per percent of glycerol weight fraction (dB)	3.2×10^{-2}	20.8×10^{-2}	$24.4(\pm 0.14) \times 10^{-2}$
Phase shift per percent of glycerol weight fraction (degree)	11.8×10^{-2}	91.1×10^{-2}	$147(\pm 9.1) \times 10^{-2}$

Table 8.1: Sensitivity of different SAW sensors to a given viscosity change. Slope of the linear regression performed on the data obtained with the SAW device calibration using different glycerol/water solutions. The slope of the linear regression represents the insertion loss (or phase shift) recorded by the sensor in response to a change of 1% glycerol weight fraction. For the two Saha et.al. sensors, the slope was estimated using the data available in the paper.[38] For the OJ15 SAW biochips, the slope corresponds to the linear regression of the data presented in Figure 8.6b and 8.6d. The OJ15 SAW biochip has a greater sensitivity to a given perturbation than the other two sensors presented.

As can be seen in Table 8.1, the OJ15 SAW device shows a greater response to a 1% change in glycerol weight fraction than the other two SAW sensors presented, when measuring either ΔIL or $\Delta\phi$. The response was found to be 24.4 $\pm$0.14 dB for the insertion loss and 147 $\pm$9.1 for the phase shift, while out of the two the SAW sensors used by Saha *et. al.*, the one with the greater response to a comparable perturbation gave responses of 20.8dB and 91.1 degrees, respectively. OJ15 SAW devices used throughout this thesis are therefore more sensitive than comparable sensors used by Saha *et al.*

8.4 Characterisation of the liquid sample viscosity and density

8.4.1 OJ15 SAW device calibration curve for sample viscosity

In order to express the sample viscosity as a function of the equivalent glycerol weight fraction w_{gly}, literature values were used.[206] The glycerol weight fraction values and their corresponding solution viscosity values were fitted to a function of the form $y = \eta_{water}(ax^b + 1)$, were y represents the solution viscosity as a function of x, the glycerol weight fraction. The literature values of viscosity of glycerol/water solutions as a function of the glycerol weight fraction are plotted (in blue) in Figure 8.7, along with the fitted function obtained (in red).

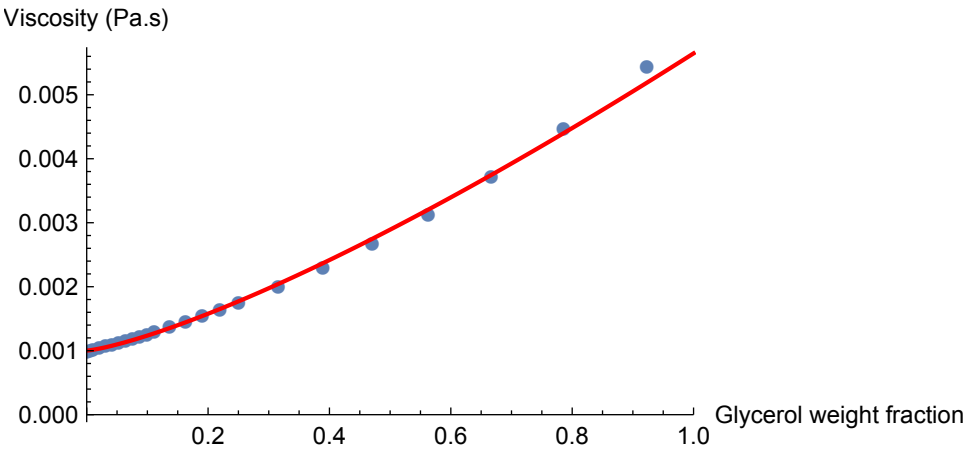

Figure 8.7: Solution viscosity expressed as a function of the glycerol weight fraction. Literature values for the viscosity of glycerol/water solutions,[206] plotted as a function of the glycerol weight fraction. The red line represents the fitted function obtained when fitting the data to the equation $y = \eta_{water}(ax^b+1)$, where the coefficients (a,b) where found to be (4.6, 1.3) and the literature value of η_{water} is 1.002mPa.s.

Using the fitted function in combination with the proportional relation found between ΔIL and w_{gly} following the sensor calibration, the sample viscosity η can be plotted as a function of the measured insertion loss ΔIL. This is presented in Figure 8.8. For clarity, only values up to 20dB are considered as this is the range of insertion loss covering most of the perturbations measured during this thesis. This plot can be seen as a characteristic of operation of the SAW biosensor. It can be used to either estimate the change in viscosity corresponding to a given measured loss in insertion, or to get an idea of the insertion loss when causing a perturbation with a known change in viscosity to the solution.

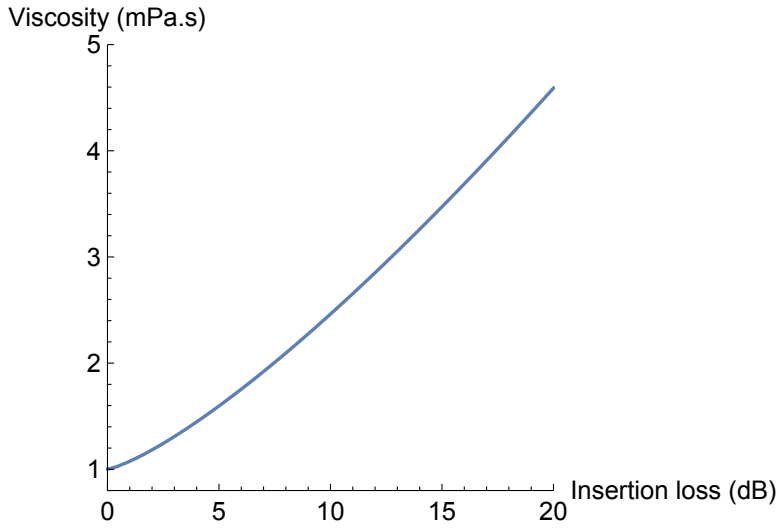

Figure 8.8: Solution viscosity expressed as a function of the measured insertion loss ΔIL. Plot to show the relationship between the insertion loss measured by the OJ15 SAW device and the corresponding solution viscosity. The measured insertion loss for a solution viscosity of 1. 002mPa.s (viscosity of water at 25°C) is 0dB, as the sensor calibration was performed with water as the starting reference point.

8.4.2 Calibration method validation

Key steps of the Saha-Gizeli model which were applied to estimate the mass per surface area are the OJ15 SAW device calibration with glycerol/water solutions, and the estimation of the sample viscosity based on this calibration. In order to validate the calibration, the relationship between the measured insertion loss ΔIL and the estimated sample viscosity η was investigated.

First, the density of glycerol water solutions was expressed as a function of the glycerol water content. Similarly to what was done for the viscosity, theoretical values of density [206] were plotted as a function of the glycerol weight content, and fitted to obtain a relation between the two quantities. This is presented in Figure 8.9.

Weiss *et al.* showed and verified that, when using SH-SAW devices, the relationship between the density-normalised insertion loss and the square root of the solution viscosity was linear. [207] The two quantities are plotted against each other in Figure 8.10. The relationship was indeed found to be linear, with a linear regression correlation coefficient of 0.999, suggesting that the Saha-Gizeli model can be applied to the OJ15 SAW devices, and further analysis involving protein solutions instead of glycerol/water solutions can be undertaken.

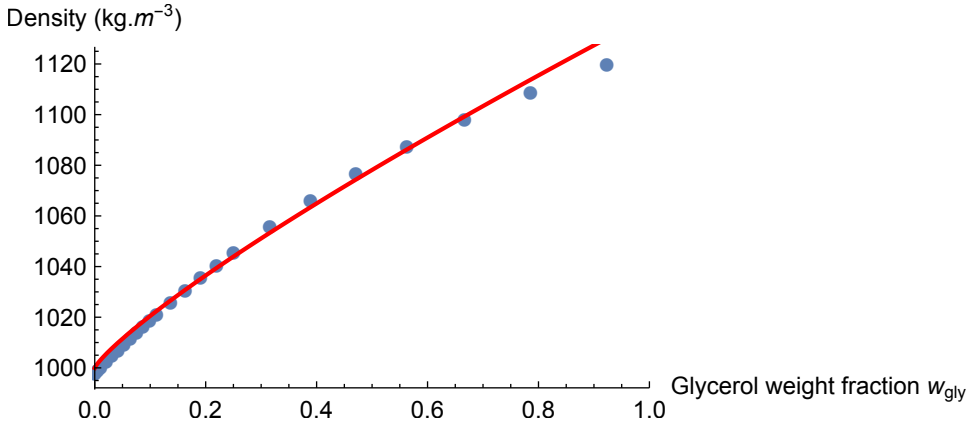

Figure 8.9: Solution density expressed as a function of the glycerol weight fraction. Literature values for the density of glycerol/water solutions,[206] plotted as a function of the glycerol weight fraction. The red line represents the fitted function obtained when fitting the data to the equation $y = \rho_{water}(ax^b+1)$, where the coefficients (a,b) where found to be (0.14, 0.83) and the literature value of $\rho_{water}$is 999.97kg.m^{-3}.

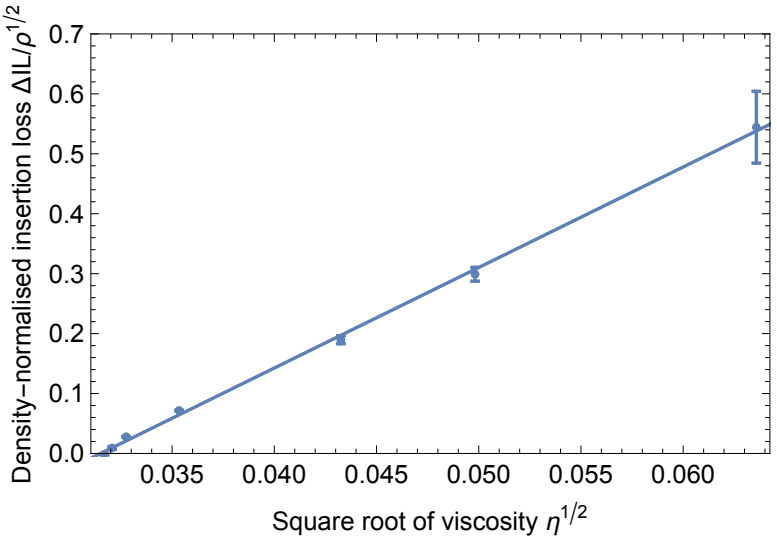

Figure 8.10: Insertion loss viscosity relationship. Plot to show the density normalised insertion loss as a function of the square root of the solution viscosity. Each point represents the average of 4 measurements, error bars represent the standard deviation. The blue line represents the linear regression of the data, with equation $y = 530.3x - 16.7, R^2 = 0.999$.

8.4.3 Using the Saha-Gizeli method to estimate the solution density

Using equations 8.7 and 8.9 presented earlier, the solution density can be expressed as:

$$\rho = \frac{1}{\nu}\left(\frac{\eta_2}{\eta_1} - 1\right)\frac{MW_{particle}}{V_{particle}N_A} + \rho_{water}, \tag{8.11}$$

where in this case η_1 is the viscosity of the running buffer and η_2 the sample viscosity. In the following, the running buffer (PBS, solution without particles) was assimilated to water at 25°C when considering its density and viscosity.

As the viscosity of the sample has been expressed as a function of the measured insertion loss ΔIL, six parameters remain in the equation. Four of them can be found in the literature (Avogadro constant N_A, viscosity of water η_{water}, density of water ρ_{water}, particle shape factor ν), and the remaining two are intrinsic properties of protein probed (molecular weight of the particle $MW_{particle}$, volume of the particle $V_{particle}$). For clarity, they are listed in Table 8.2.

Parameter	**Value**
Avogadro constant N_A	$6.02.10^{23}\text{mol}^{-1}$
Viscosity of water η_{water} at 25°C	1.002mPa.s
Density of water ρ_{water} at 25°C	999.97kg.m^{-3}
Particle shape factor ν	2.5
Particle molecular weight $MW_{particle}$	Depending on protein
Particle volume $V_{particle}$	Depending on protein

Table 8.2: List of parameters involved in the expression of the solution density. The values for the viscosity and density of water at 25°C were taken from the literature.[206] The particle shape factor was set to 2.5 to begin with, which corresponds to particles being modelled as spheres.[205] This coefficient can take different values depending on the particle shape assumptions, as will be discussed below.

In the model presented, the expression of the solution density depends on the nature of the protein. It was therefore decided to plot the solution density as a function of the measured insertion loss ΔIL for different proteins. Different model proteins used throughout this thesis, with different intrinsic characteristics (volume and molecular weight) were chosen as examples: HIV p24, an anti-p24 Llama VHH and an anti-p24 IgG. Table 8.3 summarises the different proteins properties.

Protein	Anti-p24 llama VHH (59H10)	HIV p24	IgG
Protein structure			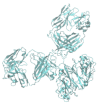
Protein immersed in water sphere			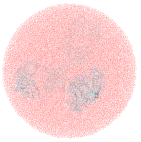
Radius (nm)	2.3	4.5	8.5
Volume (nm^3)	51.6	389	2527
Molecular weight (kDa)	12.47	24	150

Table 8.3: Intrinsic properties of some proteins used as examples. Table to summarise the Radius, volume and molecular weight of three proteins used in the experiments presented in this section. Protein sequences were either obtained in-house for the 59H10 anti-p24 VHH (courtesy of Dr. E. Gray), or from the protein data bank, pdb code 1E6J (p24) and 1HZH (IgG). The proteins were immersed in a water sphere that just contains all the atoms in the protein and the radius calculated. Models are built and rendered using Visual Molecular Dynamics.[208] Modelling structure and protein radius and volume courtesy of Dr. J. Brookes.

In addition, three different protein complexes were considered, each involving the binding of HIV p24 to either one or two anti-p24 antibodies/llama VHH. In these cases, the complex was assimilated to one spherical particle. The molecular weights of the different proteins involved in the complex were added together to express the molecular weight of the complex. Similarly, the radius of the complex was considered to be the sum of the radius of the different proteins involved in the complex. The resulting molecular weights and sizes of the different complexes are listed in Table 8.4.

The solution density is plotted against the measured insertion loss ΔIL in Figure 11 below. As for the sample viscosity, the range 0 to 20dB was considered as it covers the range of perturbations investigated throughout this work.

As with Figure 8.8, Figure 8.11 can be used as an operation characteristic of the SAW biosensor, to either relate a measured insertion loss to a density perturbation, or to predict the insertion loss caused by a given perturbation of the density within the sensing volume. It is interesting to note that for any given change in solution density, the smallest and lightest

Protein complex	Llama VHH + HIV p24	Llama VHH + HIV p24 + IgG	IgG + HIV p24 + IgG
Radius (nm)	6.8	15.3	21.5
Volume (nm^3)	1340	14973	41225
Molecular weight (kDa)	36.47	186.47	324

Table 8.4: Intrinsic properties of some proteins complexes used as examples. Table to summarise the radius, volume and molecular weight of some of the protein complexes used in the experiments presented in this section. Estimations based on the values presented in Table 8.3.

protein (Llama VHH, blue trace) is predicted to give rise to a smaller insertion loss than any other larger and/or heavier protein or protein complex. By contrast, the largest and heaviest protein (two IgGs forming an immunosandwich around HIV p24, brown trace) gives rise to the largest insertion loss for a given perturbation. Similarly, any protein complex gives rise to a larger insertion loss than its individual protein components. However, the larger protein does not always give rise to the larger insertion loss: the complex formed between HIV p24 and the anti-p24 llama VHH (red trace) gives rise to a larger insertion loss than the IgG (green trace) on its own, despite being 4 times lighter (36.47kDa vs 150kDa) and about twice smaller ($1340nm^3$ vs $2527nm^3$). In addition, proteins that are very different in size can give a similar response: the traces representing HIV p24 (orange) and IgG (green) are very close, despite the IgG protein being nearly 6 times heavier (150kDa vs 24kDa) and about 6 times larger than HIV p24 ($2527nm^3$ vs $389nm^3$). This shows that, in the context of optimising the design of the SAW biosensor and aiming for the right protein target, the combination of the structure of the protein and its molecular weight matter more than the molecular weight or volume only. This is confirmed by the expression of the density in Equation 8.8, which depends on the ratio of the molecular weight and the volume of the particle.

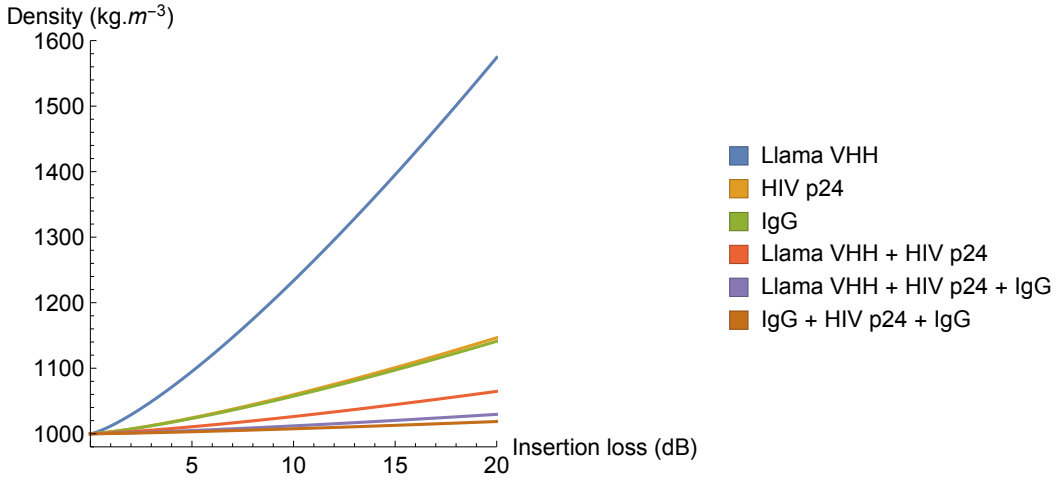

Figure 8.11: Solution density expressed as a function of the measured insertion loss ΔIL. Plot to show the relationship between the insertion loss measured by the OJ15 SAW biochip and the corresponding solution density, for different proteins used throughout this thesis. The measured insertion loss for a solution density of 999.97kg.m^{-3} (density of water at 25°C) is 0dB, as the sensor calibration was performed with water as the starting reference point.

8.5 Characterisation of the proteins adsorbed on the surface of the SAW device

In order to estimate the mass per surface area added onto the surface of the SAW device, a model experiment was conducted. Solutions of anti-HSA at different concentrations in buffer (PBS) were put in contact with the surface of OJ15 SAW devices. The measurement protocol was the same as the one used for the SAW device calibration, except for the fact the glycerol/water solutions were replaced by the antibody solutions, and the pure water by a PBS running buffer in which the antibody was diluted. The insertion loss ΔIL was recorded 15 minutes after sample injection.

In parallel, the theoretical maximum mass adsorbed per surface area was estimated. As the antibodies adsorbed on the surface are modelled as spheres, the method developed by Feder *et al.* could be used. They studied the coverage of a surface onto which discs of constant diameter are disposed, and demonstrate that the theoretical maximum coverage of the surface was 54.7%.[209] Based on this, and on the assumptions that the antibodies form a monolayer at the point where the insertion loss is recorded, a theoretical maximum M_{norm} could be calculated, depending on rparticle.

As mentioned earlier, in the calculations that led to the estimation of the mass per surface area, the particle shape factor ν was set to 2.5, which corresponds to the antibody being modelled as a spherical particle. However, an antibody is not likely to present itself to the surface as a perfect sphere, but more as an ellipsoid. Jeffery [210] estimated the particle shape factor theoretical values for different shapes of ellipsoids, depending on their ellipticity. He showed that the average maximum values for ν were 3.3 and 6, for prolate and oblate ellipsoids, respectively. This corresponds to ellispoids of ellipticity equal to 0.9, and therefore represents extreme cases where the shape of the spheroid is the furthest away from a perfect sphere (either a long thin prolate ellipsoid or a large flat oblate ellipsoid). To investigate whether the model would still be valid with particles being modelled as ellipsoids instead of spheres, the calculations of M_{norm} were run for these different values of ν. Results are shown in Figure 8.12.

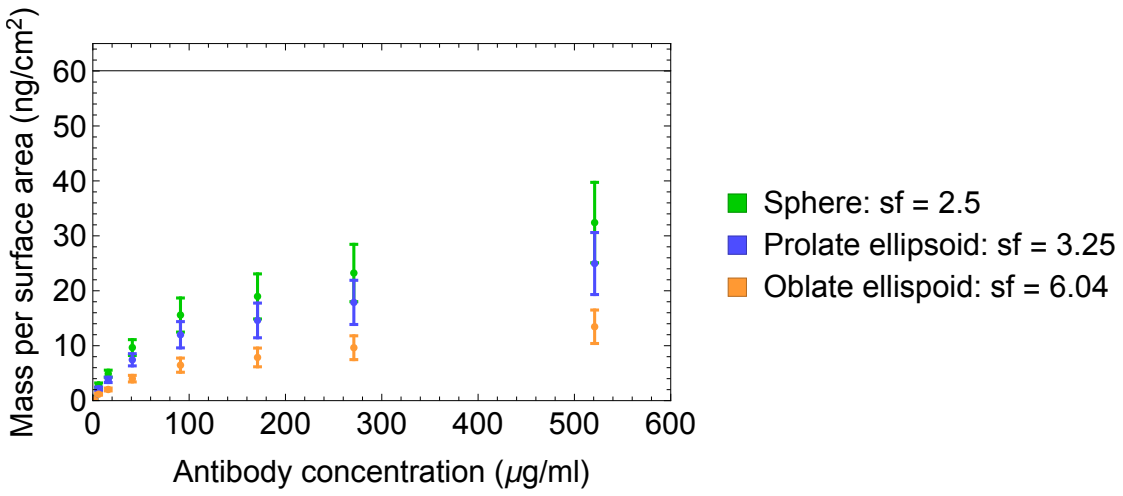

Figure 8.12: Mass per surface area as a function of the antibody concentration. Plot to show the mass adsorbed per surface area M_{norm} as a function of the antibody concentration, for three different shapes of particle. Each point represents the average of 3 measurements. The black line represents the theoretical maximum M_{norm} and was estimated using the Feder method. [209]

Figure 8.12 shows that the surface coverage estimated using the method, was found to be below the theoretical maximum surface coverage calculated by Buijs *et al.*, for all concentrations tested. In this commonly cited study, they estimate the surface coverage when IgG molecules adsorb on a surface based on crystal structure data, and find the maximum values to be in the range 200 to 550ng/cm^2, depending on the arrangement of the molecule on the surface. [211] For each particle shape tested, the estimated M_{norm} does not seem to

plateau even at high concentrations, suggesting that higher antibody concentrations might be needed to achieve a maximum surface coverage.

Note: the volume fraction of particle in the sensing volume does not depend on the volume of the particle. However, it is important to note that within the range of antibody concentration tested, it remained below the threshold of 0.2. Applying the Einstein relation for solid particles therefore stands in this model for the range of concentration used.

8.6 Discussion

The Saha-Gizeli method was used to characterise the OJ15 SAW devices used throughout this work. It was shown that the OJ SAW device has a slightly better sensitivity than comparable SH-SAW devices used by Gizeli *et al.*, in the viscosity region tested. Useful calibration curves were obtained that indicate the relation between sample viscosity and the measured insertion loss.

Using an estimation of the size of some of the proteins used to obtain the results presented in Chapters 6 and 7, the solution density was plotted as function of the insertion loss, for individual proteins as well as protein complexes. This highlighted the need for considering the combination of the structure of the protein and its molecular weight rather than the molecular weight or volume only in the context of optimising the design of the SAW biosensor and aiming for the right protein target. These results have to be nuanced, however, by the fact they were obtained under the initial assumptions required to apply the Saha-Gizeli method, which assimilates the proteins in solution as non-interacting solid particles. At high concentrations especially for the protein used as a capture protein this is unlikely to be exact. Further work will look into refining these results by applying the model in two distinct steps to a surface/protein/protein system, instead of limiting it to the surface/protein system studied to begin with. Target proteins binding to the functionalised surface are more likely to act as non-interacting solid particles.

Similarly, the estimation of the acoustic wave penetration depth (see Figure 8.13) will have to be refined to take into account the difference in density for each layer of proteins, rather than assimilating the proteins in each layer as non-interaction solid particles.

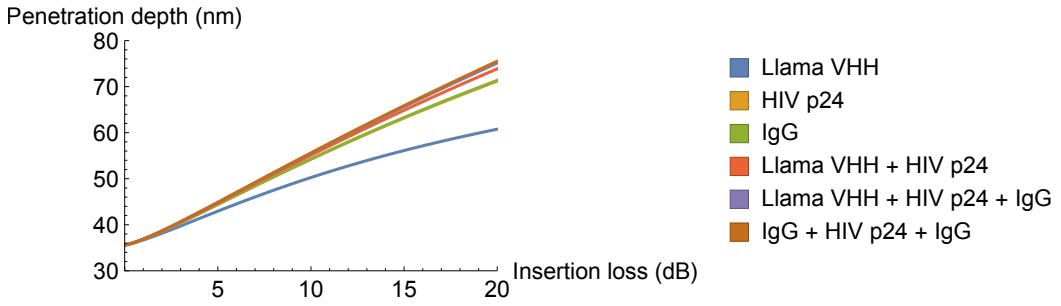

Figure 8.13: Penetration depth expressed as a function of the measured insertion loss ΔIL. Plot to show the relationship between the insertion loss measured by the OJ15 SAW device and the corresponding acoustic wave penetration depth, for different proteins used throughout this thesis. The penetration depth corresponding to an insertion loss of 0dB is that of the running buffer, which in this case was PBS.

Using the Saha-Gizeli method, an estimation of the mass per surface area adsorbed on the surface of the SAW device could also be achieved. One of the key parameters in the model used is the volume of the particle. In Figure 8.12, the value of V_p was set to 2527nm^3, which corresponds to the value estimated using Visual Molecular Dynamics under the assumption that the protein was included in a sphere of water (see Table 8.3). Other modern estimations or observations of single molecule IgG tend towards the representation of IgG molecules as fitting within a sphere of radius 5 to 6nm. This is due to the fact the long axis of the molecule, along which the Fc region is aligned, is approximately 10 to 12 nm. In addition, a study by Foster *et al.*[212] shows that IgG molecules do not undergo important denaturation when adsorbing on bare gold surfaces. They used XPS to look at the ratio between amino acids on the surface over amino acids buried inside the protein, in order to estimate how much denaturation the protein had undergone after adsorbing to the gold surface. As the value of V_p following this technique varies from the initial estimation (about 900 nm^3 compared to 2527nm^3), calculations of the mass per surface area were run again with the alternative value of V_p. However, if the absolute values of M_{norm} increased compared to the values observed in Figure 8.12 at similar concentrations, the general trend was the same as the one observed in Figure 8.12. Even at high concentrations, M_{norm} did not plateau, and for every shape tested, the highest value of M_{norm} did not reach the theoretical maximum (which also increased, at it is dependent on the radius of the particle). Future work will look into testing the model for particles of different sizes, with a better knowledge of their size in order to minimise the uncertainty regarding the parameter of the model corresponding to the particle volume. Similarly, studying the shape of the proteins

with external methods would help with choosing the most appropriate value for the shape factor when applying the Einstein relation, and therefore tend towards a more accurate estimation of the surface coverage.

This powerful and simple method also has the potential to bring new insights into the analysis of protein adsorption on surface, as well as protein protein interactions. Because the SAW device operates at a frequency (251.5MHz) one to two orders of magnitude higher than conventional quartz crystal microbalances (QCM), it probes mechanisms happening within the typical relaxation time of proteins, whereas QCM can typically only give indications on the surface formed after relaxation. Future work will involve investigating this aspect of the probing further.

Chapter 9

Conclusions and Future Work

New, higher performance and better connected PoCT for HIV can contribute to the fight to stop the HIV/AIDS pandemic. Widening access to testing, making tests easier to use, faster and more reliable, and building data sets with information that can be used to monitor and fight the spread of the pandemic are all motivations that drive the design and development of this new generation of PoCT. SAW devices are ideal candidates, as they are low cost, disposable and can easily be integrated in a simple test performed in conjunction with a smartphone. The aims of this thesis were to (i) explain the theoretical concept of biosensing using SAW devices, (ii) contribute to the development of a simple to use, reliable and sensitive SAW biosensor, (iii) show that it can be engineered to rapidly detect key biomarkers of early HIV infection at clinically relevant levels, (iv) assess and optimise its clinical performance indicators and (v) investigate the transduction mechanisms in the hope to further improve its performance.

9.1 Summary of overall thesis conclusions

9.1.1 Chapter 2: HIV diagnostics needs

In 35 years, more than 60 million people have contracted HIV infection, causing nearly 30 million deaths.[1] As an alarming proportion of HIV infected persons (about a quarter in the UK[2]) is unaware of their infection, the need for efficient diagnostics tools is crucial. The recent court ruling in the UK specifying that the NHS has the legal power to commission

pre-exposure prophylaxis (PrEP) is very good news. By blocking HIV from incorporating its genetic material into the hosts genome and therefore preventing infection in healthy individual, the treatment constitutes a welcomed additional tool to limit the spread of the infection.[213] However, the need for effective diagnostic tools is still there, as PrEP is not globally implemented yet, and has not been shown yet to be 100% efficient in the prevention of HIV infection.

Traditional diagnostic tools are very efficient, but are associated with high costs, the need for highly trained staff and modern equipment, and often patients experience delays between their initial visit to the hospital or clinic, follow up appointments and eventually access to care.[8–10] The interest shown in recent years by the WHO towards HIVST[14] has led to reports of global acceptability towards this new form of testing[15] and its recent legalisation in the UK[6]. The conclusions of various studies on the cost effectiveness of the implementation of HIVST at national level in the UK agree in saying that the costs associated with the operation would largely be counterbalanced by the huge savings made by public healthcare providers, and that this trend would carry on year on year.[11–13]

The target product profile set out by PATH to describe the ideal HIVST was presented in Chapter 2. It constituted a point of reference throughout this work, along with the ASSURED criteria recommend by the WHO for PoCT.[18] In relation with the work presented in this thesis, the following criteria were identified as crucial: (i) the test should be simple to use, consisting of only 3 to 5 intuitive steps (ideally just one), (ii) the test should deliver the result under 5 minutes, and (iii) the clinical sensitivity and specificity should be greater than 99%.

A review of the currently available PoCT for HIV infection was conducted, which highlighted the current absence of a perfect test. Some tests were characterised by a limit of detection to a certain biomarker of HIV infection that was too low (based on measurements performed in the lab, which gave different results than the manufacturers claims). Some tests required a time to result exceeding the 5 minute requirements. Most of the available PoCT for HIV are based on lateral flow technology. These tests are notoriously difficult to interpret[8] as they requires the test user to see the apparition of a coloured line on the test, which can sometimes be quite faint if the concentration of the biomarker is low, or if the light conditions are not ideal.

It was also observed that very few current commercially available tests have the ability to record and send the data to health care providers, and most of the ones who do are laboratory-based tests. This feature is crucial to avoid loss of data, and represents a very effective tool for global and local healthcare providers to monitor the spread of the infection, and occasional outbreaks. The connectivity is the key feature of the next generation of PoCT, and their implementation may be facilitated by public healthcare providers who could see in them an opportunity to access and record much needed data that could contribute to stopping the spread of the infection. Some connected tests have been reported, either using a smartphone to interpret existing current commercial lateral flow tests,[22] or fully adapting an ELISA on a USB dongle.[23] However, the first conclusion of this work is that there is still a gap in the field of high performance, simple to use, low cost and connected PoCT for HIV infection.

9.1.2 Chapter 3: Potential of SAW devices for biosensing

One of the aims of this work was to justify the use of SAW sensors for biosensing, as they have the potential to fulfil most of the ASSURED criteria of the ideal PoCT for HIV described by the WHO. The objectives of this section were to understand the theory behind the sensing mechanism of SAW devices, and explain the best options for monitoring the events of interest detected by the sensor.

Acoustic wave based sensors consist of piezoelectric crystals through which an acoustic wave is made to propagate. They make use of the piezoelectric effect to sense perturbations in their surrounding medium. The effect of the perturbations on the acoustic wave, which propagates much more slowly than its electromagnetic wave equivalent, can be monitored *via* the piezoelectric effect. A well-known acoustic wave sensor, QCM, has been used in laboratories since the 1980s to monitor the mass adsorbed on the surface of a gold coated piezoelectric substrate. In 1959, Sauerbrey proposed a direct relationship between the mass adsorbed and the shift in the resonant frequency of the acoustic wave propagating through the crystal and reflected by the surface.[131]

A new form of acoustic wave based sensors emerged at the beginning of the 1980s, with the emergence of the first SAW sensors.[145] Unlike the QCM whereby the acoustic wave

propagates through the crystal twice before being monitored, the acoustic wave propagation is confined, as much as possible, to the surface of the crystal, making SAW sensors theoretically more sensitive to surface perturbations. A necessary initial objective of this work was to review the field of biosensing using SAW devices. Various applications have been reported during the past 40 years or so, ranging from pH sensing[169] to the monitoring of phospholipids[153], antibody[155], or bacteria[157] adsorption on the surface of the sensor. Little has been done, however, in the specific field of using SAW sensors for HIV diagnostics. The proof of concept of detection of biomarkers of HIV infection, such as anti-gp41 antibodies, has been reported by Thompson *et al.*,[30] but with a limit of detection (100μg/ml) too high to be used as a diagnostic test. It transpired that the potential for using SAW devices for HIV diagnostic had yet to be fulfilled.

The particular case of SH-SAW devices was considered, as industrial partners OJ-Bio Ltd. developed a SAW device based on a quartz crystal supporting a SH-SAW sensor, with the capacity to handle liquid samples. IDTs deposited on the surface of the quartz crystal make use of the piezoelectric effect to transduce an electromagnetic wave into an acoustic wave that propagates along the delay line in between the IDTs and back into an electromagnetic wave. This system can be used to monitor the acoustic wave parameters via the electromagnetic wave parameters. The perturbation theory applied to SH-SAW predicts that perturbations occurring on the surface of the delay line of SH-SAW sensors have a direct impact on the acoustic wave velocity and attenuation coefficient. Kondoh *et al.* derived equations to define the impact of specific perturbations, namely a viscosity change and a mass loading on the surface of the sensor, and analysed the implications of viscoelastic perturbations on the same parameters.[173,174]

The perturbations of interest in the context of a biosensor for HIV consist of the binding of target proteins to the functionalised surface of the sensor. They are most likely a combination of all the aforementioned basic perturbations. It was shown that the measurement of two parameters - the electroacoustic wave phase shift and the insertion loss - gives a direct indication of the changes occurring to the acoustic wave velocity and attenuation, respectively. Therefore, monitoring the phase shift and insertion loss when submitting the SAW device to a given sample is the ideal way to detect any perturbation cause by this sample. In other words, when the target protein present in a positive sample binds to the

functionalised surface, this can be detected by monitoring changes in the phase shift and the insertion loss.

9.1.3 Chapter 5: SAW device characterisation

The first objective in relation to the usage of the SAW device developed by industrial partners OJ-Bio Ltd. was to characterise its performance before it goes through the functionalisation process to transform it into a SAW biochip. The performance of the device was looked at from three different angles: the shear sensitivity, the simplicity of use, and the reproducibility of measurements recorded using the laboratory control box. The objectives and corresponding achievements are listed in Table 9.1.

The shear sensitivity of the SH-SAW device to given perturbations was studied and optimised. It was shown that two specific features characterising the device improved its sensitivity, compared to other prototypes of SH-SAW devices. The length of the delay line used (9mm) was shown to bring a higher sensitivity to the perturbations encountered in the context of the use of the device as a biosensor than a shorter delay line of 5mm. Similarly, the presence of a reflector on the lower delay line of the device a feature enabling the monitoring of the surface component of the acoustic wave only, instead of a combination of the bulk and surface components was shown to improve the devices sensitivity.

During the course of this work, it was noted that loading a sample onto the surface of the sensor could easily result in the formation of a droplet, preventing the sample from spreading across the whole area of the delay line. In the interest of developing a PoCT that can be used easily by non-trained staff, a study was performed which showed that the amplitude of the signal output by the control box phase shift and insertion loss was dependent on the fraction of the surface of the delay line covered by liquid. As a smaller signal was still output when the sample formed a droplet, the conclusion was that a correct loading of the sample onto the surface of the sensor was crucial to the validity of the test result.

The SH-SAW devices used throughout this work were considered disposable and were only used for one measurement. The control box used to obtain the measurements featured 4 different SAW devices holders, enabling 4 measurements to be run in parallel. In order to justify the comparison of measurements obtained on different devices, a statistical analysis

Objective	**Achievements**
Assess SAW device sensitivity	• Operational frequency used to drive the device (f = 251.5Mhz) found to be very close to optimal driving frequency (f = 251±0.16MHz). • Length of the delay line used (9mm) generating higher sensitivity in perturbation region of interest than other prototype available (5mm delay line). • Cancelling out the bulk component of the signal using reflector on lower delay line increases overall device sensitivity in perturbation region of interest.
Ensure ease of use of future PoCT product	• Possible user mistake identified: liquid sample forming a droplet on the surface of the delay line instead of spreading across the sensing area. • Signal readout found to be proportional to fraction of surface area in contact with liquid sample.
Measurements reproducibility	• 364 measurements recorded in parallel using laboratory control box and 4 chip holders investigated. • Differences in similar measurements recorded on different holders found to be low enough to consider measurement reproducible (no more than 1.3%). • Confirmation that laboratory control box allows for 4 SAW devices to be used at the same time, allowing for referencing or duplicate runs.

Table 9.1: Objectives and achievements of Chapter 5, in relation to assessing the SAW device performance

of a large number of measurements performed on the same sample were performed. The construction of Bland-Altman plots and associated analysis applied to this specific system concluded that the difference in measurements observed between the 4 different SAW devices holders were small enough to justify intra-holders comparison.

9.1.4 Chapter 6: Detecting model proteins and HIV markers of infection

On the basis of this initial analysis of the SH-SAW device performance, an optimisation of the functionalisation of the gold surface of the delay line was performed, with the aim of turning the SAW device into a SAW biochip with the capacity to detect the presence of key biomarkers of early HIV infection in a sample. The detailed objectives and corresponding achievements are listed in Table 9.2.

It was shown that functionalising the surface with capture proteins via the chemical linker DSP led to the optimal signal readout. Using different capture proteins, the detection of various target proteins could be achieved. Anti-p24 was reproducibly detected down to 2nM (300ng/ml) within 5 minutes of sample injection, and down to the clinically relevant concentration of 50nM (75μg/ml) within 10 seconds. This represents test results about 100 times faster than commercially available tests such as the Alere Determine lateral flow test which requires about 20 minutes between sample injection and valid test result.

A series of experiments helped optimise the detection of HIV p24 antigen, an early marker of HIV infection, using an immunosandwich consisting of novel anti-p24 llama VHH on the surface and mouse anti-p24 antibody on top of the target protein. The use of an immunosandwich was shown to increase the signal readout, enabling reproducible detection of p24 down to 2nM (48ng/ml).

The use of gold nanoparticles to further improve the signal readout for this assay was investigated using two layers of gold nanoparticles functionalised with anti-p24 and anti-mouse antibodies. However, despite careful troubleshooting of the process, the initial results could not be reproduced, and further work related to this assay optimisation is detailed in the Future Work section further on.

Objective	**Achievements**
Optimise surface functionalisation with model protein complex HSA/anti-HSA	• DSP found to be ideal chemical linker to anchor capture proteins on the gold surface of the delay line. • Assessment of optimised concentration to use to functionalise surface with capture proteins (100μg/ml) • Titration curve of HSA detection using SAW biochips yields kinetic constants comparable to literature.
Rapid detection of anti-HIV antibodies at clinically relevant levels (Anti-p24 82 - 1900μg/ml, Anti-gp41 5.4 - 5194μg/ml)	• Proof-of-concept of detection of anti-p24 antibodies using SAW biochips. • Same measurement taken multiple times using one SAW biochip found to be robust, highlighting longevity and resistance of the capture proteins layer. • Titration curve of anti-p24 antibodies obtained. • Reproducible detection down to 2nM (300ng/ml) within 5 minutes of sample injection. • Ultrafast detection down to 50nM (7.5μg/ml), below clinically relevant concentrations.
Rapid detection of HIV p24 antigen at clinically relevant levels (0.1-1000pg/ml)	• Proof-of-concept of detection of HIV p24 antigen using SAW biochips functionalised with anti-p24 llama VHH. • Reproducible detection down to 2nM (48ng/ml). • Benchmarking of detection assay using QCM.
Investigate signal amplification strategies	• Initial results using gold nanoparticle as signal enhancement inconclusive. • Difficulties encountered in reproducing results. • Troubleshooting not giving clear evidence of loss of antibody affinity for its target protein.

Table 9.2: Objectives and achievements of Chapter 6, in relation to the detection of key biomarkers of HIV infection using SAW biochips.

9.1.5 Chapter 7: Clinical pilot studies: Testing real patient samples

After the biosensor was shown to be able to reliably detect biomarkers of HIV infection in mock samples, it was decided to investigate its ability to do so in patient samples, then to conduct a series of pilot studies to assess the clinical performance of the biosensor. In the process of doing so, ensuring a smooth transition between the different generations of SAW biochips became an additional objective. The objectives and achievements associated with the testing of real patient samples are listed in Table 9.3.

Objective	**Achievements**
Moving from detection in mock samples to patient samples	• Proof-of-concept of anti-HIV antibodies (anti-p24 and anti-gp41) detection in human plasma spiked with antibodies. • Established the need for referencing to account for non-specific binding of the many proteins found in plasma.
Transition from single channel SAW biochips (OJ15) to new generations of SAW biochips featuring two operational delay lines (OJ24/OJ28/OJ31).	• Proof-of-concept of anti-HIV antibodies showing similar results with manual functionalisation of each delay line. • Moving a step further towards automatization of manufacturing process using liquid dispenser to functionalise delay lines. delay lines. Increased reproducibility of measurements. • Using one of the two delay lines as an in-built reference channel. Reference delay line functionalised with NAP.
Achieving clinical performance in line with PATH target product profile for HIVST	• Combined clinical sensitivity to anti-gp41 and anti-p24 of 100% (target >99%) • Combined clinical specificity to anti-gp41 and anti-p24 of 100% (target >99%) • Time to result <5min (target <5min)

Table 9.3: Objectives and achievements of Chapter 7, in relation to the assessment of the PoCT clinical performance.

A proof-of-concept study established the need for a reference test to be run in parallel to the sample test, due to the complexity and higher viscosity of plasma samples compared to

aqueous buffer samples. It was shown that both anti-p24 and anti-gp41 antibodies could be detected using SAW devices functionalised with the corresponding recombinant protein (p24 or gp41, respectively). A series of pilot studies was therefore conducted, using a panel of 31 HIV patient samples in addition to over 100 confirmed HIV negative patient samples. An algorithm was developed herein to handle the large amount of data generated by testing these numerous samples multiple times. The automation of the functionalisation process of the SAW devices, conducted by industrial partners OJ-Bio Ltd., helped to perfect the performance of the biosensor. A combined 100% sensitivity and 100% specificity to anti-p24 and anti-gp41 was achieved, the test results being obtained under 5 minutes. The key objectives set out by the PATH target product profile for HIVST were therefore achieved.

9.1.6 Chapter 8: Characterising SAW device response, sample and target protein properties

The last aim of this work was to characterise the response of the SAW device to a known perturbation, the liquid sample viscosity and density, and the mass loading when proteins adsorb on the surface of the sensor. The objectives and corresponding achievements in relation to this characterisation approach are listed in Table 9.4.

A method developed by Gizeli *et al.* was investigated and applied to the OJ15 SAW device. The method relies on a calibration of the sample using solutions of known viscosities, and the assimilation of proteins adsorbed on the surface of the delay line to non-interacting solid particles. Gizeli *et al.* developed this method using SH-SAW devices very similar to the OJ15 SAW device used throughout most of this work.

The calibration of the SAW device with solutions of different viscosities showed that the OJ15 SAW device presented a higher sensitivity to viscosity changes, compared to the two types of devices tested by Gizeli *et al.* The insertion loss response (0.24dB) and phase shift response (1.47degrees) to a change in one percent glycerol weight fraction were both found to be higher than the most sensitive device presented by Gizeli *et al.* (0.2dB and 0.91degrees, respectively).

Calibration curves were generated to describe the response of the SAW device to a given change in sample viscosity and density. For the latter, specific examples were chosen to reflect the properties of some key protein solutions used to obtain the results presented in

Objective	**Achievements**
Finding a new approach to characterise the response of the SAW device to given perturbation	• Literature review which highlighted the concept of the Gizeli *et al.* method, applied to similar SH-SAW devices.
Comparison of performance of OJ15 devices to other SAW devices	• Calibration of the SAW device using solutions of glycerol/water. • Estimated higher sensitivity to viscosity perturbation, compared to similar SH-SAW devices used by Gizeli *et al.*
Characterise the response of the SAW device to given perturbations	• Calibration curve generated to describe the response of the SAW device to a given viscosity perturbation. • Calibration curve generated to describe the response of the SAW device to specific solution densities, corresponding to solutions of proteins used throughout this thesis.
Characterise the mass per surface area deposited on the surface of the delay line	• Applied the model to a simple antibody adsorption on gold system. • Estimation of the mass per surface area correctly found to be below theoretical maximum coverage.

Table 9.4: Objectives and achievements of Chapter 8, in relation to characterising the SAW device response, sample and target protein properties.

previous chapters. More work is needed to make these calibration curves more accurate, taking into account the specific characteristics of the proteins used. They could constitute a potential useful tool to optimise the sensitivity of the biosensor in the future.

The mass per surface area of proteins loaded onto the surface of the delay line was estimated by applying the model to a simple system whereby antibodies were adsorbed on the surface of the delay line. Different values of the shape factor parameter were tested to reflect the uncertainty about the shape of an antibody adsorbed on a surface. The values of mass per surface area were found to be below the theoretical maximum coverage in every case tested, even at high antibody concentrations. The model also opens up exciting opportunities to

optimise crucial parameters of the assay, as will be discussed in the next section.

9.2 Future Work

This work presented in this thesis aimed at contributing to the development of a new, better PoCT for HIV. As detailed throughout the thesis and above, it was shown that a smartphone-connected biosensor could be developed using low cost SH-SAW devices optimised for the rapid detection of key biomarkers of HIV infection in human samples. Building on from this work, multiple aspects of the optimisation of the biosensor can be explored and optimised further.

9.2.1 Further optimisation of the SAW biochip sensitivity

9.2.1.1 Novel capture ligands

In the process of designing the biosensor, one of the key aspects is the surface functionalisation. The work in relation to the functionalisation of the delay line was detailed in Chapter 6. One of the aspects of the functionalisation process that could be explored further is the nature of the capture layer. Conventional antibodies, recombinant proteins and llama VHH were used successfully to bind to key biomarkers of HIV infection in the sample. Various other ligands binding to the target protein can be used, of which one stands out, and could be used to functionalise the delay line of a SH-SAW device: aptamers. Aptamers are synthetic peptides selected or engineered to bind to a specific target molecule.[214] Aptamers have attracted attention in recent years for their flexibility they can theoretically be engineered to bind to any molecule depending on user requirements[215] and thermal stability[216]. Like llama VHH, thermal stability would be a great asset in the prospect of designing a biosensor able to endure important variations of temperature during shipping or storage. Used in combination with recently developed portable PCR systems,[217–219], aptamer-functionalised SAW biochips could be used as molecular probes to detect the presence of viral RNA in a sample, further reducing the detection window for new HIV infections.

9.2.1.2 Multiplexed analysis

The choice of capture protein, and the way it is anchored to the surface directly impact on the biosensors ability to detect the presence of the target protein in the sample. By chosing the appropriate capture protein, it can be envisaged that the biosensor could theoretically be used as a platform to detect any protein. A SH-SAW device featuring multiple delay lines, each functionalised with a different capture protein, could be used as a biosensor to diagnose multiple infections, or to detect multiple strains of the same infection. This could be particularly useful in cases of testing groups of individuals who are at risk of multiple infections, such as injection drug users (IDU). Another example of a benefit brought by a multiplexed detection system would be to prevent the prescription of a particular drug in the treatment of one infection, that would be contraindicated by the presence of infection by a different pathogen. Some drugs used in the treatment of HIV also affect hepatitis B virus (HBV), and can foster resistance if an ineffective HBV monotherapy is then effectively used. This has to be avoided with patients presenting a HIV/HBV coinfection.[220]

9.2.1.3 Improved reference capture coatings

As mentioned in Chapter 7, testing plasma samples requires the use of a reference test, or a reference channel on the same device. This reference test measures the signal generated by the sample on a surface functionalised with proteins that are engineered to not resemble human proteins, and therefore do not bind to the target protein. The ability of this reference test to not bind to the target protein, while behaving as similarly as possible to the normal test, is key to the accuracy of the test result. NAP was used for the reference tests performed as part of the difference pilot studies. The average signal measured for negative samples (both negative calibration samples and true negative samples) was not exactly zero, and different for each biomarker tested (anti-p24 and anti-gp41). It is possible that other proteins, or other strategies, would give a better reference and therefore increase the test accuracy and overall performance.

Poly(L-lysine)-*graft*-PEG (PLL-*g*-PEG) has been widely reported as an efficient system to prevent non-specific adsorption of serum proteins on a surface.[221,222]. However, in the case of the SAW biosensor presented here, it is important that the two delay lines respond to perturbations that are unrelated to the binding of the target protein (such as a change in

viscosity for example), in a similar way, to ensure correct normalisation of the test signal. As the structure and size of Poly(L-lysine)-*graft*-PEG (PLL-*g*-PEG)is quite different to the characteristic of the capture protein used in this work, in is unlikely to be the ideal solution. One way to enhance the effectiveness of the reference delay line is to functionalise it with a protein that is almost identical to the capture protein used on the test delay line, but engineered to not bind the target protein. This could be achieved by mutating a small number of amino acids in the binding site region of the sequence of the capture protein. Another approach would be to investigate multifunctional molecules. Synthetic co-polymers have been engineered to bind to a substrate *via* their poly-(L-lysine) (PLL) backbone, block non-specific adsorption of protein to a surface *via* poly(ethylene glycol) (PEG) on the side chains, while promoting the binding of the cell target via incorporation of a specific peptide to the side chains.[223,224] Using the appropriate backbone to bind to gold, and the appropriate peptide engineered against the target protein, this strategy has the potential to increase the sensitivity of the SAW biochips to biomarkers of HIV while eliminating the need for a reference test.

9.2.1.4 New enhancement strategies

The thousand-fold improvement in the p24 detection assay, obtained using multiple layers of gold nanoparticles and presented in Chapter 6, could not be reproduced and careful troubleshooting did not give clear indications about the possible causes of the problem. The significant improvement observed with the first successful assays, and the fact it takes the level of detection of a key biomarker of early HIV infection down to clinically relevant levels, calls for an in-depth investigation regarding the enhancement of the detection signal.

Other strategies to improve p24 detection assays can be envisaged, one of which being the silver enhancement technique, whereby silver ions in solution nucleate around gold nanoparticles and precipitate as silver metal. This technique is already used to increase the size of small gold nanoparticles for better visualisation in scanning electron microscopy.[225] It would be the natural step forward in the evolution of the signal amplification strategies tested so far, as is schematised in Figure 9.1.

Following the perturbation theory applied to SH-SAW, mass loading on the surface of the delay line of a SH-SAW device directly affects the acoustic wave velocity, which can be

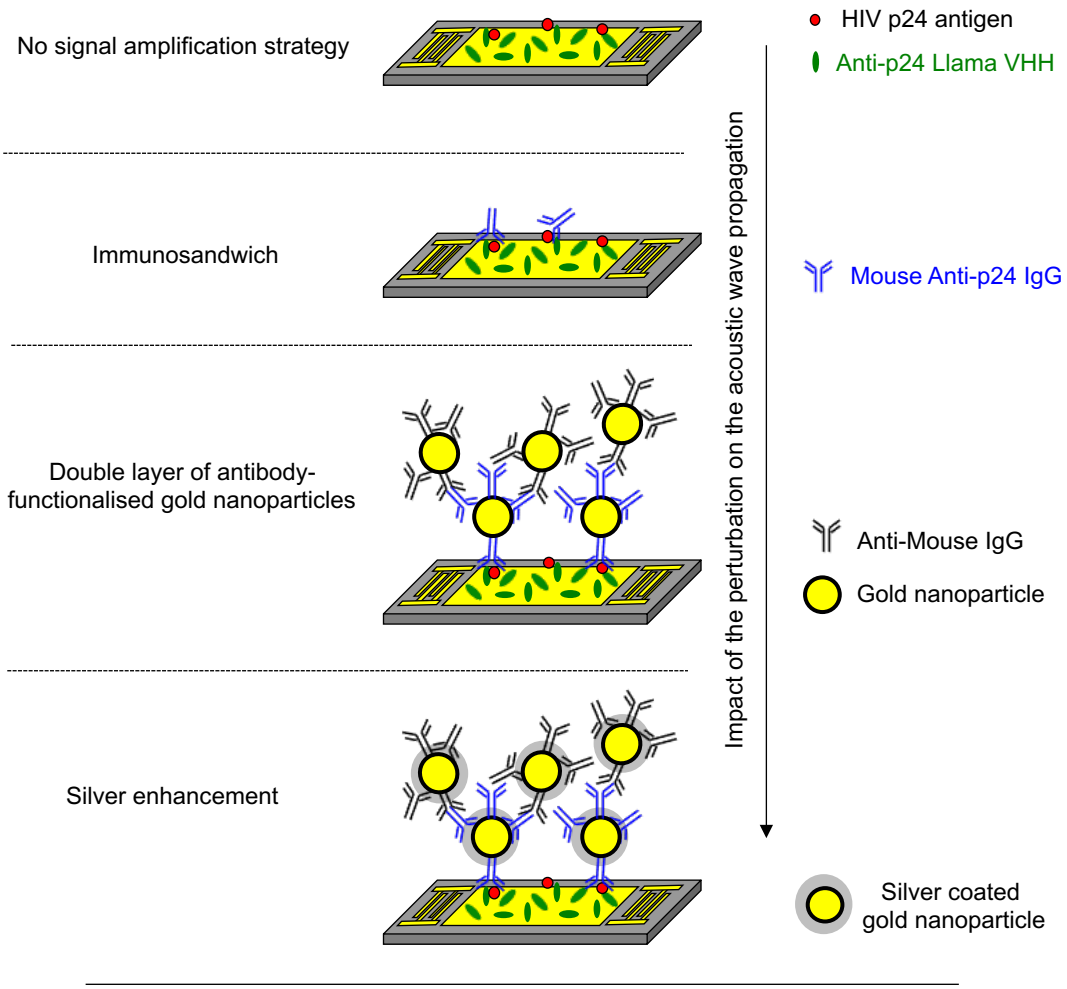

Figure 9.1: Silver enhancement as the next step signal amplification strategy. Schematics to illustrate the different signal amplification strategies used throughout this work in the context of the HIV p24 antigen detection assay. The arrow on the right-hand side indicates the impact the amplification strategy is likely to have on the propagation of the acoustic wave, and therefore on the sensitivity of the assay. The straightforward detection of HIV p24 in solution (top) was improved with the formation of an immunosandwich using mouse anti-p24 antibodies. This strategy was further improved by replacing the mouse antibody by a double layer of antibody-functionalised gold nanoparticles. A potential improvement of this technique could be the nucleation of silver around the gold nanoparticles, increasing the mass loading and therefore amplifying the signal. Drawings not to scale.

monitored *via* the phase shift . Using the silver enhancement strategy, an increase in mass loading would be generated specifically where the target protein is present, therefore improving the sensitivity of the assay.

Similarly, changes in viscoelasticity could be enhanced. The target proteins binding to the surface of the delay line are isolated, as their concentration is usually low. Connecting them using larger structures with an affinity for the target protein (and binding to a different epitope than the capture protein on the surface) would create a net above the surface, capturing more water molecules and generating a larger viscoelastic perturbation at the surface proximity.

9.2.1.5 Maximising the perturbation of the SH-SAW

A method was presented in Chapter 8 to characterise the response of the SAW device to given perturbation, and the potential for modelling certain physical parameters of the samples, the target protein or the sensor itself was investigated. One of the outcomes was the possibility to relate the penetration depth of the acoustic wave in the liquid sample to the characteristics of the particles on the surface, i.e. the complex formed by the capture protein, target protein, and signal amplification objects/proteins. The molecular weight, shape and volume of the particle all contribute to the general effect on the penetration depth. More work is needed to refine this model, notably in terms of characterising the different proteins more accurately. There is a potential to create a very useful tool to optimise the capture protein layer as well as validating the amplification strategy. Indeed, the penetration depth was found to range in the order of a few tens of nanometres. The strategy adopted to perform the assay would only be useful if the combined height of all the elements (capture protein, target protein and any single amplification object) remains below the penetration depth, otherwise perturbations would not be sensed by the acoustic wave. As the capture proteins and target proteins usually range from a few nanometres to a few tens of nanometres, investigating the acceptable boundaries of the penetration depth would prove crucial. This is particularly relevant in the example of the signal amplification strategy involving gold nanoparticles of 20nm diameter. This concept is schematised in Figure 9.2.

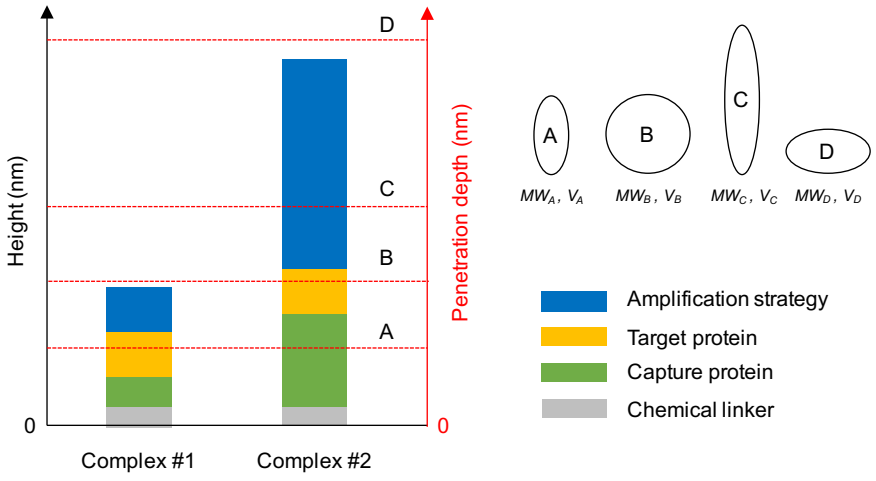

Figure 9.2: Modelling penetration depth to validate the assay and signal amplification strategy. Schematics to illustrate the effect of the choice of the assay elements on the assays success. Two hypothetical complexes of different combined height are represented (Complex #1 and #2) and four different complex characteristics (combination of the molecular weight, volume and shape) are considered (letters A to D). Each complex can be characterised by any of these letters. The penetration depth corresponding to each letter is indicated with a doted red line. For complex #1, B, C and D are efficient assay strategies, while A would mean the signal amplification is useless. For complex #2, the only efficient assay strategy corresponds to D. Drawings not to scale.

9.2.2 Next stage translational strategy

The SAW biosensor presented here already ticks some of the criteria of the ideal PoCT set out by the WHO, and presents some characteristics of the ideal HIVST described by PATH. It is potentially low cost as the disposable SAW devices are already on manufactured, and the successful functionalisation of the delay line with an automated liquid spotter performed by industrial partners OJ-Bio Ltd paves the way for a smooth transition to mass manufacture the optimised SAW biochips. It has also been shown to deliver highly accurate results under 5 minutes form sample injection. Other aspects of the design of the biosensor as a connected PoCT can still be improved, and are detailed below.

Ultimately, the test should be able to work with whole blood samples, to avoid the centrifugation step necessary to extract plasma only from the sample. Ideally, the SAW device would be able to handle the blood sample directly. However, blood being a non-Newtonian fluid, this might complicate the analysis presented in Chapter 3 of the relation between the perturbation and the corresponding output signal. Another potential idea to implement this is the addition of a membrane filter above the surface, with pore size smaller than

typical white and red blood cells. The sample could also be loaded on the membrane and be carried while being filtered to the surface of the sensor using capillary action.

On the front of optimising the ease of use of the test, improvement could be made to the way the sample is loaded onto the surface of the sensor. To avoid the formation of a droplet, the surface could be made more hydrophilic by incorporating polylysine molecules to the surface functionalisation, provided the resulting surface is still able to binding to target proteins in the sample with the same efficiency. Ultimately, the step consisting in the loading of the sample should be carried out by a panel of randomly selected participants to confirm the test is easy enough to be used by non-trained staff. Any other potential user mistakes should be identified and tested by the same panel as well.

As the test will ultimately be used in conjunction with a smartphone, there will be a need to develop an app with the appropriate data processing algorithm. The app interface will also constitute a future exciting challenge, as the simplicity of use of the test will largely depend on it. Ideally, the instructions provided by the app should be clear enough that the eventuality of mistakes by the test user will be very unlikely. In addition, the app will provide a great opportunity to promote access to online patient pathways, which facilitate counselling and linkage to care.

As mentioned earlier, the connectivity of the test is likely to bring the added benefit of convincing public healthcare providers to fund and help with its implementation. The added value of building datasets to monitor the spread of the infection and outbreaks would be of great interest to these organisations. This will come with the absolute requirement that the data is securely transmitted to relevant organisations only. Work will need to be done towards convincing both the end users and public stakeholders they can trust the data generated by the test will remain secure.

9.2.3 Engaging with end users and keeping up to date with their needs

A crucial aspect of the implementation of a new PoCT was not explored in this thesis. The success of a new PoCT for HIV cannot happen without building patient trust, and making sure the test, as well as the handling of the data it produces, is ethical and acceptable to the patients themselves. Ensuring the patients will engage with the test is a key consideration at every step of the design process. The biosensor presented here is designed to be used

with a smartphone, not only for ease of use but also with the idea that any data it produces could be stored and shared with health protection bodies. Work will need to be done to assure patients their data are secured, and that it would only be shared with relevant health protection organisations in order to contribute to the general fight to stop the pandemic.

It transpired during discussions with public healthcare workers that the end user needs may differ from country to country. There is a case, in developed countries like the UK where HIV prevalence is low, for targeting the groups at high risk of HIV infection and making sure that healthy individuals are identified and linked to preventative measures. On the other hand, in countries where HIV prevalence is still very high, such as South Africa, correctly identifying individuals that have contracted the infection remains the priority, focussing on the general population.

With the recent legalisation of self-testing in the UK, end user needs are likely to have to be redefined depending on the context of the test usage. Target product profiles established by and for health care workers may not be relevant to self-testers. Discussions have begun about the concept of designing self-tests in a way that it would be impossible for the user to interpret the test result. Instead, the result would be sent to an online healthcare system that would have the capacity to interpret it and would provide the appropriate counselling within a short time, thereby avoiding the difficult situation of an individual finding out about the reactivity of their test on their own.

9.2.4 Testing the test refining clinical performance indicators by expanding trials

Another aspect of the future work should look into refining the performance indicators of the biosensor clinical sensitivity and specificity to a given biomarker of HIV infection by testing larger panels of samples, ideally a few hundreds to a thousand of samples. The key concept in the assessment of the clinical sensitivity and specificity of the test is the combination between (i) a good knowledge of the amplitude of the signal recorded by the sensor in response to both true positive and true negative samples, and (ii) the threshold value used by the test to discriminate between positive and negative samples. Increasing the number of samples tested, whether they are true positive, true negative, or negative calibration samples, can only help in refining the value of the threshold value and therefore

increases the accuracy of the test. In addition, the higher the number of samples tested, the higher the confidence in the test performance indicators.

In terms of testing patient samples, the next step will be to obtain the authorisation to test fresh samples (i.e. not stored samples). All the patient samples tested in the pilot studies presented in Chapter 7 were at the stage of discard, after having been stored at 4°C for three weeks subsequent to collection. Testing fresh patient samples will provide the last confirmation needed for the test to be ready for field trials, which will constitute one of the most crucial and most exciting stages of development of this PoCT.

Trials should be implemented both in developed countries probably in the UK and low and middle income countries. A current close collaboration with the Africa Centre, the largest HIV diagnostic centre in South Africa, located in the province of KwaZulu-Natal, should provide help in the process of implementing field test trials in a region with one of the highest HIV prevalence in the world.

*

The work presented in this thesis was undertaken in the hope that it would bring a contribution to the development of a diagnostic system with the potential to bring major economic and human benefits. If more work will be needed to perfect all aspects of the biosensor, progress was made towards this exciting and challenging target.

Appendix A

Expression of VHH in *E. coli* TG1 cells

The following describes the principle and the protocol used to produce and purify the anti-p24 llama VHH 59H10 from bacteria transformed with the original plasmid. The protocol detailed below was optimised by Dr. Laura McCoy and colleagues. [226,227]

General principle

Plasmid and host cell

The general principle is to use a host bacteria to express the VHH sequence encoded by a plasmid. The original plasmid used in this protocol, pCAD51-59H10, was a gift from Professor Weiss. It encodes antibiotic resistance, and the 59H10 sequence inserted into a multiple cloning site using restriction enzymes (SfiI and BstEII), adjacent to a promoter under the control of the lac operon. The VHH sequence includes an N-teminal His-tag that is used to purify the VHH during the production process, as well as a Myc-tag. The host bacteria used in that process is a commercial *E. coli* called TG1, produced by several suppliers. *E. coli* TG1 is a competent cell, which means it is primed for transformation.

Bug stock

The first step is transformation, that is forcing the plasmid into the host bacteria. This is schematised in Figure 1. There are two main techniques to integrate a plasmid into a cell, depending on the cell characteristics. A competent cell can either be electrocompetent

or chemically competent. In both cases, the idea is to disturb the cell wall to make the bacteria transiently permeable to plasmids. If the cell is electrocompetent - which is the case of *E. coli* TG1 - this is done by submitting it to electric pulses in the presence of the plasmid, a process called electroporation. If the cell is chemically competent, then a simple temperature shock (typically 42°C for 30 seconds) will make the cell walls transiently permeable to the plasmid.

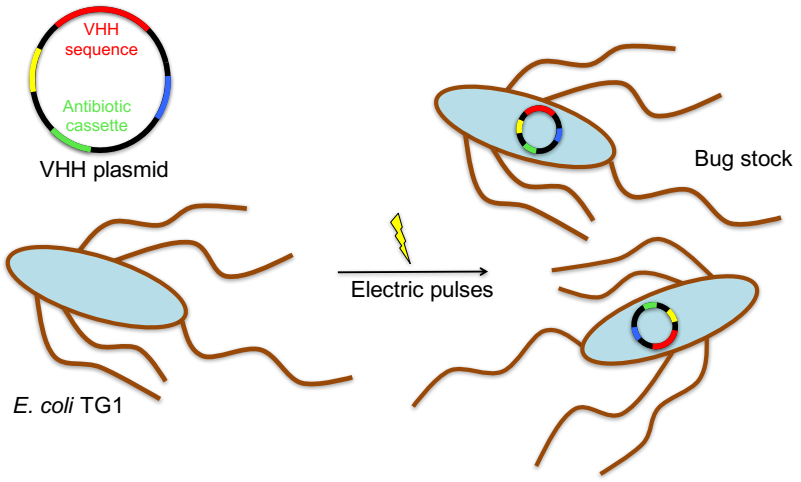

Figure 1: Electroporation process schematic. Electrocompetent *E. coli* TG1 cells are submitted to electric pulses in the presence of a VHH plasmid, making the cell wall transiently permeable to plasmids and therefore resulting in the incorporation of the plasmid into the bacteria.

After the host cell transformation, the cells are plated out on agar in a selective medium containing an antibiotic called ampicillin. The plasmid sequence includes constitutive expression of an antibiotic resistance cassette, to produce a protein whose function is to make the host cell resistant to ampicillin. Therefore, *E. coli* TG1 containing the plasmid are resistant to ampicillin, and they can use the rich medium to grow while all the other bacteria are killed by the ampicillin. A colony is selected for growth in liquid media overnight. Once prepared, the bug stock can be stored in 20-50% glycerol-LB broth at -80°C. However, the stock degrades with each freeze/thaw cycle, hence the need to prepare it fresh from time to time.

First *E. coli* growing process

In order to isolate the transformed bacteria from any contamination (e.g. other bacteria coming from the environment, pipette tips or the edges of the containers) before expressing

the VHH sequence, a toothpick of the bug stock is mixed with ampicilin, in a environment suited for cell growing (rich medium consisting of LB broth and glucose). The cell growing rate follows a well defined pattern illustrated in Figure 2. There are three main phases:

- a *lag* phase where cells start dividing slowly. The absolute number of cells increases slowly..
- an *exponential growth* phase, where the number of cells is now high enough for the cell number to increase quickly and significantly after each division process
- a *stationary* phase where the number of cells saturates, and cells stop dividing, partly because of the lack of glucose, but also because of a phenomenon called quorum sensing, where the cell population autoregulates its number to stay at equilibrium.

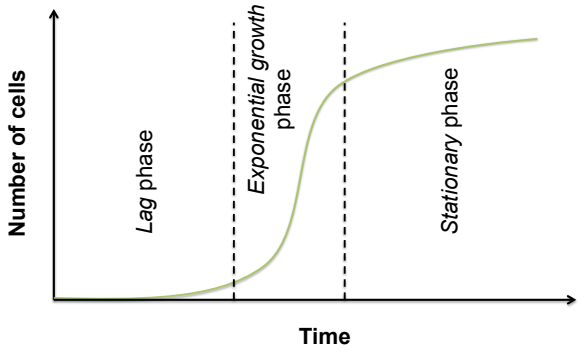

Figure 2: *E. coli* typical growth rate *E. coli* typical growth curve featuring the *lag*, *exponential growth* and *stationary* phases.

Cell growth follows this general pattern, making this plot a useful tool to control the number of cells or to estimate the optimal time to start protein production. The growth rate depends on different parameters, including the initial volume of bug stock and the media.

During this first growth process, the growth rate and the number of cells does not need to be thoroughly controlled, as the main objective is to grow a significant number of host bacteria and to make sure that only these are grown, as schematised in Figure 3. The initial volume added to the media is not measured exactly, and the cells are left growing for long enough to reach the stationary phase. At this point, it is referred to as the starter culture.

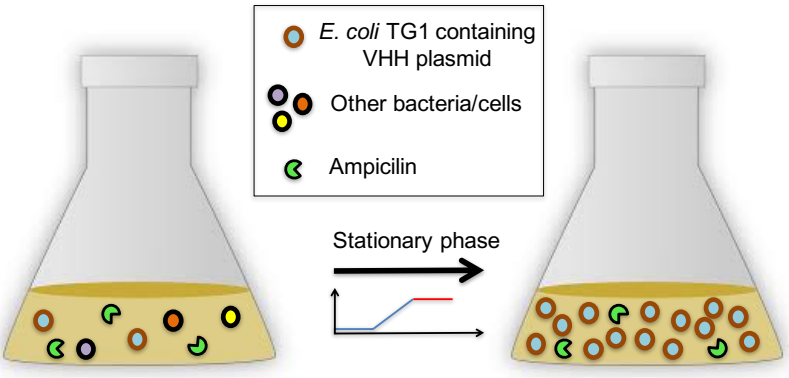

Figure 3: First *E. coli* TG1 growth process. The transformed cells are grown in a selective rich medium until they reach stationary phase

Second *E. coli* growing process, VHH expression

Once the host bacteria has been isolated from other impurities, it can be grown with more control. A defined volume of the starter culture (usually measured as a dilution, in this case 1:100) is added to a second growth medium with ampicilin (in order to prevent contamination). The new medium consists of a different broth (2xYT) and a smaller content of glucose, making it an ideal media for protein production as well as cell growing. As the important parameters are now under control, it is possible to estimate the start and finish of the exponential growth phase. Triggering the protein production with a gene inducer during the exponential growth phase is ideal, as the system is working at full speed and the whole machinery for protein production is in place. There is also an ideal number of bacteria without them having reached overpopulation. When cells are roughly in the middle of this phase (OD_{600} 0.6-0.8) a gene inducer (IPTG) is added to the culture. This is schematised in Figure 4.

VHH extraction and purification

The next step is to extract the VHH from the bacteria and purify it. Extracting VHH from the *E. coli* TG1 is simply done by lysing the bacteria walls using freeze/thaw cracking (see schematics in Figure 5). The culture is centrifuged and the resulting pellet is left at -80°C for at least an hour. In order to get rid of the lysed bacteria debris, the pellet is then resuspended in PBS and centrifuged again. As the lysed bacteria are much heavier than

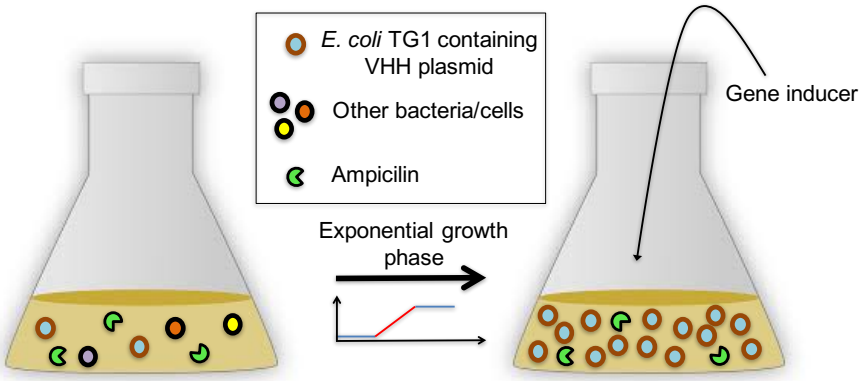

Figure 4: Second *E. coli* TG1 growth process. The transformed cells are grown in a selective rich medium until they reach the middle of the exponential growth phase, at which point the gene inducer IPTG is added to the culture

single proteins, the supernatant contains the VHH and all the other bacterial proteins from the lysed cells.

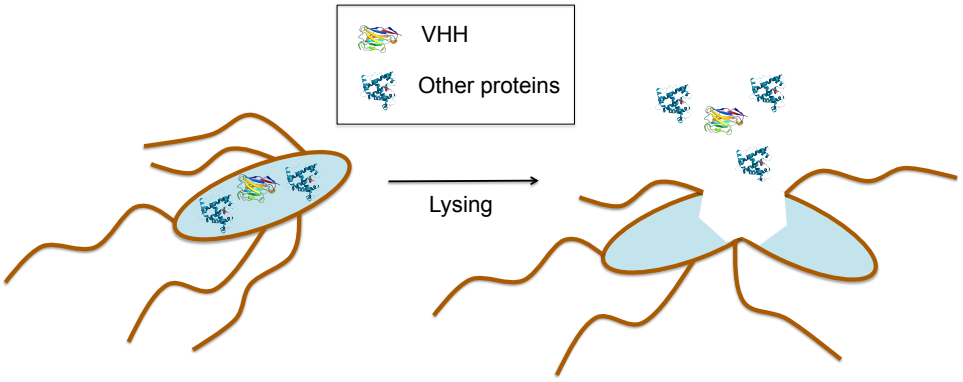

Figure 5: *E. coli* TG1 lysing process schematic. A freeze/thaw cracking breaks open the bacterial membrane, releasing the bacterial proteins in the medium

Purifying the VHH from those proteins is done using an affinity resin, specific for His-tagged proteins. This resin consists of cobalt-coated beads, to which the His_6 tag binds. As mentionned earlier, the VHH sequence contains an hexa His (HIS_6)-tag, which means that a series of six consecutive histidine amino acids are added at one end of the protein when it is produced. This chain of six amino acids binds strongly to the cobalt, therefore allowing for a selection of the VHH over the other proteins. Indeed, some of the other proteins may have histidine amino acids in their sequence, but one or two histidine will bind much less strongly to cobalt than the His-tagged VHH. Washing in a column helps getting rid of the other weakly bound proteins.

The VHH is then released from the resin in the column using an elution buffer containing imidazole, which disturbs the His-Co bond. During this elution stage, a Bradford Colorimetric Assay (BCA) is performed in order to assess whether a protein was released from the resin. Fractions of eluate are collected after each addition of elution buffer, and a small sample of each of those fractions is used in the BCA. The principle of the assay is based on the absorbance shift of a dye (Coomassie Brilliant Blue G-250) which appears green or purple under acidic conditions depending on the presence of the protein being assayed. The dye is mixed with the different samples as well as a few controls.

The fractions of solution that exhibited the presence of protein in the BCA are dialysed against PBS to get rid of the imidazole.

Finally, the concentration of the dialyzed proteins in solution is assessed using BCA.

Protocol

Culture media

2x Tryptone/yeast (YT) medium	1.6% (w/v) tryptone 1.0% (w/v) yeast extract 0.5% (w/v) NaCl
Lysogeny broth / Luria-Bertani (LB) medium	1.0% (w/v) tryptone 0.5% (w/v) yeast extract 0.5% (w/v) NaCl

VHH TALON purification

Materials required:

- Prepare buffers (see below)
- Plastic Bio-Rad columns
- TALON resins in solution: 50% TALON, 20% EtOH (+ 0.1% NaN_3)
- Dialysis cassette: MWCO 3500Da
- PBS (10X PBS)

Buffer composition (native buffers)

- 1x Equilibration buffer (pH 8.0): 50mM sodium phosphate, 300mM NaCl
- 1x Pre-elution buffer (pH 7.0): 50mM sodium phosphate, 300mM NaCl, 10mM imidazole
- 1x Elution buffer (pH 7.0): 50mM sodium phosphate, 300mM NaCl, 150mM imidazole

Buffer	1M NaH_2PO_4 (ml)	1M Na_2HPO_4 (ml)	3M NaCl (ml)	Imidazole (g)
Equilibration (1l)	4.2	46.6	100	0
Pre-elution	Dilute elution buffer 1 in 15 with equilibration buffer			0
Elution (50ml)	Add imidazole to 50ml equilibration buffer			0.51

Components

- TALON resin Cat 635503 Takara Biotech (Clontech)
- Slide a Lyzer Cat 66330 Thermo Scientific
- Polyprep Columns Cat 731-1550 BioRad

Protocol (4 days)

Day 1

- 1. Prepare 2X YT medium, autoclave.
- 2. Inoculate 5ml (1/10th of expression volume) of LB medium containing 100 μg/ml of ampicillin (or carbenicillin) and 2% (w/v) glucose with *E. coli* TG1 cells containing the desired VHH/pCAD51 constructs (from a single colony).
- 3. Incubate overnight at 37°C and 200-250rpm.

Day 2

- 4. Use a 5-10ml aliquot to inoculate 500ml of 2X YT medium containing 100 μg/ml of ampicillin and 0.1% (w/v) glucose. If expressing in a smaller volume of 2X YT medium, inoculate with a smaller volume (corresponding to at least a 1:100 dilution of the overnight culture).
- 5. Incubate at 37°C and 250rpm until an OD600 of 0.6-0.8. under 3H
  Collect pre-induced sample 500μl in eppendorf.
- 6. Induce VHH expression with 1 mM of IPTG (stock = 200mg/ml, = 839mM, = 596μl for 500ml)
- 7. Incubate overnight at 30°C at 250rpm.

Day 3

PLACE EQUILBRATION BUFFER AT 56°C, PRE-COOL CENTRIFUGE

- 8. Pellet bacteria in 2 x 250ml aliquots at 5000rpm in centrifuge for 10min
- 9. Freeze pelleted bacteria min 1h at -80°C
- 10. Thaw pellets and resuspend in 2 x 25ml of STERILE 1x PBS with long pipette and vortex.
- 11. Centrifuge at 5000rpm in centrifuge for 30min at 4°C
- 12. Collect and pool supernatants (the VHH-containing *E. coli* lysate). Take pre-purification sample (500μl into eppendorf)
- 13. Take 2ml 50% TALON suspension, bang to resuspend first. Use approximately 1ml of TALON resin (corresponding to 2ml of TALON suspension) for 3mg of anticipated His-tagged protein per 50ml of supernatant.
  - a. Centrifuge at 2000rpm for 2min at 4°C. Remove and discard supernatant
  - b. Resuspend TALON in 25-50ml equilibration buffer, pH 8.0
  - c. Centrifuge at 2000rpm for 2min at 4°C
  - d. Repeat steps a-c (i.e. wash twice)
- 14. Add *E. coli* clarified lysate (supernatant only!) to the TALON resin.

  - a. Incubate for 20-60min on rotating wheel at room temperature.
  - b. DO NOT LEAVE FOR >1h!
  - c. Centrifuge at 2000rpm for 2min at 4°C.

- 15. Remove and discard supernatant (= non-bound sample, collect 500μl in eppendorf). Wash the TALON resin twice with 25-50ml of equilibration buffer, pH 8.0, spin for 2min to repellet and wash again, then spin again.

- 16. Resuspend the TALON resin in equilibration buffer, pH 8.0, in a total volume of approximately 10ml.

- 17. Pack the TALON resin into the column.
  - a. Wash the column twice with equilibration buffer, pH 8.0, using a wash volume equal to 1x the bed volume.
  - b. Pre-elute with 1x the bed volume of pre-elution buffer. Keep the eluted fraction for analysis COLLECT FRACTIONS
  - c. Elute once with elution buffer, pH 7.0. Elution volume = 0.5x the bed volume.
  - d. Elute further five times with elution buffer, pH 7.0. Elution volume = 0.5x the bed volume - COLLECT FRACTIONS

- 18. Do quick BCA assay: 10μl of each fraction to flat 96 well plate, PBS ctl, 10μl of standard 100ng and 250ng. Add 100μl of reagent A + B mixture (make up just before 50:1) to each well, place at 37°C for half an hour.

- 19. Dialyse the passed-through fractions which are positive for protein against 4l of STERILE PBS overnight, change PBS first thing in morning, and again after 2h, after another 2 hours collect fractions from dialysis cassettes

- 20. Run full BCA to assess protein concentration in including control samples (25μl in triplicate plus 200μl of reagent A+B at 50:1 ratio)

- 21. Run SDS PAGE gel with pre-induction sample, pre-purification sample, unbound sample, final purified sample and stain with Coomassie blue.

Steps 5.a, 12 and 15: include in full BCA to troubleshoot where protein may have been lost.

Appendix B

In[52]:=
```
dir1 = SetDirectory[
    "/Users/valerianturbe/Desktop/Work post backup/Analysis/Clinical
      pilot study merge/Anti-p24/data/Calibration samples/"];
dir2 = SetDirectory["/Users/valerianturbe/Desktop/Work post
      backup/Analysis/Clinical pilot study
      merge/Anti-p24/data/Positive samples/"];
dir3 = SetDirectory["/Users/valerianturbe/Desktop/Work post
      backup/Analysis/Clinical pilot study
      merge/Anti-p24/data/Negative samples/"];
dir = {dir1, dir2, dir3};
```

In[56]:=
```
cal = FileNames["*cal000_EDITED*.csv*", dir1];
c1 = Table[rawdat = Import[cal[[k]]];
   c0 = Transpose[rawdat[[2 ;; -1]]]
   , {k, 1, Length[cal]}];
c2 = Join[Table[c1[[i, 3]] - c1[[i, 2]], {i, 1, Length[c1]}],
   Table[c1[[i, 5]] - c1[[i, 4]], {i, 1, Length[c1]}]];
limit = Table[Mean[Table[c2[[i, t]], {i, 1, Length[c2]}]] +
    5 * StandardDeviation[Table[c2[[i, t]], {i, 1, Length[c2]}]], {t, 1, 229}];
```

In[60]:=
```
values = Table[
   files = FileNames["**_EDITED.csv", dir[[z]]];
   d3 = Table[rawdat = Import[files[[k]]];
     d1 = Transpose[rawdat[[2 ;; -1]]]
     , {k, 1, Length[files]}];
d4 = Join[Table[d3[[i, 3]] - d3[[i, 2]], {i, 1, Length[d3]}],
     Table[d3[[i, 5]] - d3[[i, 4]], {i, 1, Length[d3]}]];
d5 = Flatten[Table[{d4[[i]], d4[[i + Length[files]]]},
      {i, 1, Length[d4] - Length[files]}], 1]
   , {z, 1, Length[dir]}];
```

In[61]:=
```
start1 = {141, 142, 138};
start2 = {148, 149, 145};
samples = Table[
   files = FileNames["**_EDITED.csv", dir[[z]]];
   Flatten[Table[{StringTake[files[[i]], {start1[[z]], -19}],
      StringTake[files[[i]], {start2[[z]], -12}]}, {i, 1, Length[files]}]]
   , {z, 1, Length[dir]}];
```

2 | *barchart antip24 merge for Appendix.nb*

In[64]:=
```
TP = Table[Count[values[[2, All, t]] - limit[[t]], _?Positive], {t, 1, 200}];
FN = Table[Length[values[[2]]] - TP[[t]], {t, 1, 200}];

TN = Table[Count[limit[[t]] - values[[3, All, t]], _?Positive], {t, 1, 200}];
FP = Table[Length[values[[3]]] - TN[[t]], {t, 1, 200}];

s1 = Table[100 * TP[[t]] / (TP[[t]] + FN[[t]]), {t, 1, 200}];
s2 = Table[100 * TN[[t]] / (TN[[t]] + FP[[t]]), {t, 1, 200}];

sensitivity = Table[{c1[[1, 1, i]] - c1[[1, 1, 19]], s1[[i]] // N}, {i, 19, 200}];
specificity = Table[{c1[[1, 1, i]] - c1[[1, 1, 19]], s2[[i]] // N}, {i, 19, 200}];

plot = ListLinePlot[{sensitivity, specificity},
  PlotLegends → PointLegend[{"Sensitivity", "Specificity"}],
  Frame → True, FrameLabel → {"Time  (min)", "%"}, ImageSize → 500,
  LabelStyle → Medium, PlotRange → {{0, 5.5}, {0, 105}}]
```

Out[72]=

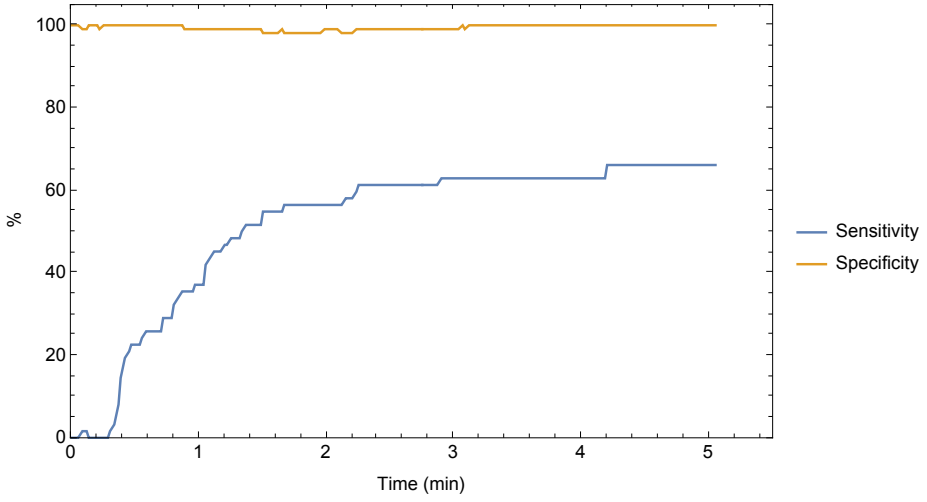

In[73]:=
```
(*Export["/Users/valerianturbe/Desktop/Bim/Word/Chapter
   4/Figures chapter 4/sensspechapt4.pdf",plot]*)
```

In[74]:=
```
Calibration = Manipulate[
  Show[{BarChart[
     Table[values[[1, i, t]], {i, 1, Length[values[[1]]]}]
     , ChartLabels → Placed[Table[samples[[1, i]],
        {i, 1, Length[samples[[1]]]}], Axis, Rotate[#, Pi / 2] &]
     , PlotRange → {-5, 50}
     , AxesLabel → {"      Sample ID", "Phase shift (degrees)"},
     LabelStyle → Medium
     , ColorFunction → Function[{height}, If[height > limit[[t]],
        Green, Lighter[Black, 0.7]]], ColorFunctionScaling → False]
    , Graphics[{Red, Thick, Line[{{1, limit[[t]]},
        {Length[samples[[1]]], limit[[t]]}}]}]}]
   , ImageSize → 500]
  , {t, 10, 229, 1}]
```

Out[74]=

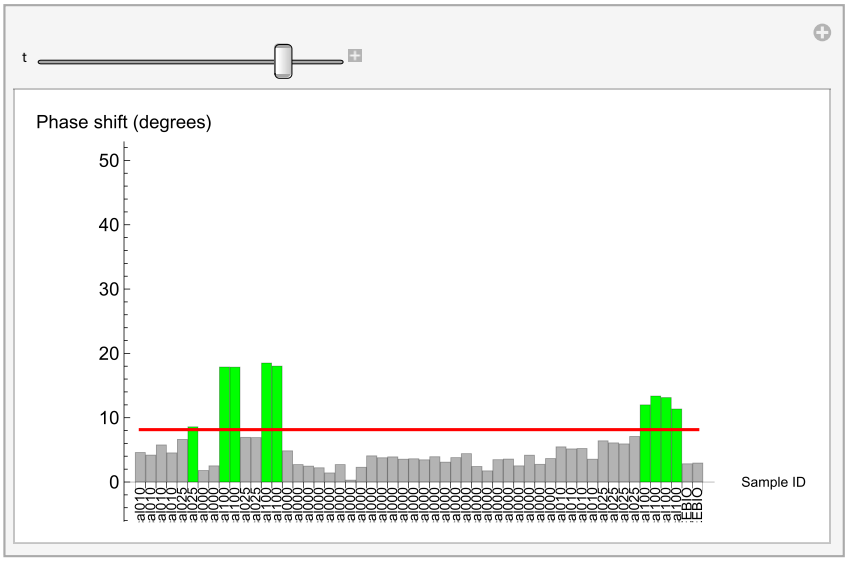

4 | *barchart antip24 merge for Appendix.nb*

In[75]:=
```
PositiveS = Manipulate[
  Show[{BarChart[
     Table[values[[2, i, t]], {i, 1, Length[values[[2]]]}]
     , ChartLabels → Placed[Table[samples[[2, i]],
        {i, 1, Length[samples[[2]]]}], Axis, Rotate[#, Pi / 2] &]
     , PlotRange → {-5, 50}
     , AxesLabel → {"      Sample ID", "Phase shift (degrees)"},
     LabelStyle → Medium
     , ColorFunction → Function[{height}, If[height > limit[[t]],
        Green, Lighter[Black, 0.7]]], ColorFunctionScaling → False]
    , Graphics[{Red, Thick, Line[{{1, limit[[t]]},
        {Length[samples[[2]]], limit[[t]]}}]}]}
   , ImageSize → 500]
  , {t, 10, 229, 1}]
```

Out[75]=

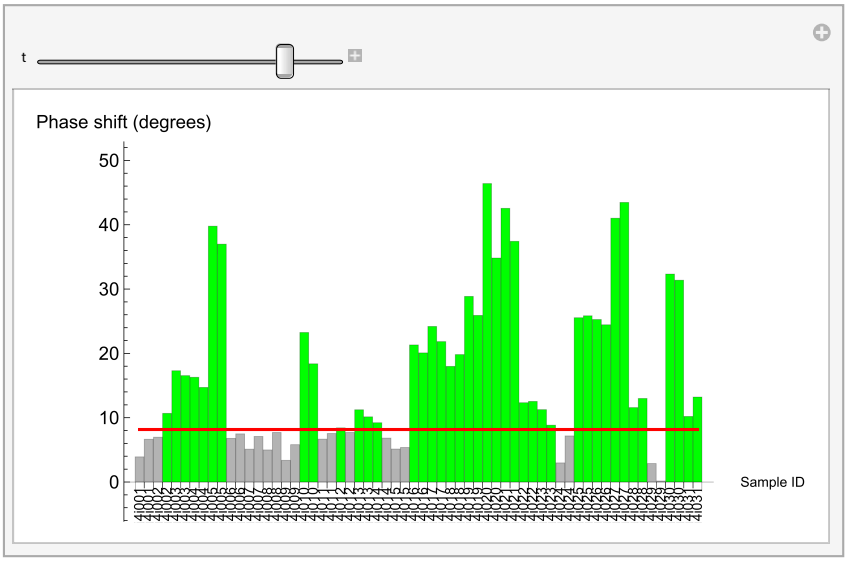

In[76]:=
```
NegativeS = Manipulate[
  Show[{BarChart[
     Table[values[[3, i, t]], {i, 1, Length[values[[3]]]}]
     , ChartLabels → Placed[Table[samples[[3, i]],
        {i, 1, Length[samples[[3]]]}], Axis, Rotate[#, Pi / 2] &]
     , PlotRange → {-5, 50}
     , AxesLabel → {"      Sample ID", "Phase shift (degrees)"},
     LabelStyle → Medium
     , ColorFunction → Function[{height}, If[height > limit[[t]],
        Green, Lighter[Black, 0.7]]], ColorFunctionScaling → False]
    , Graphics[{Red, Thick, Line[{{1, limit[[t]]},
        {Length[samples[[3]]], limit[[t]]}}]}]}]
   , ImageSize → 500]
  , {t, 10, 229, 1}]
```

Out[76]=

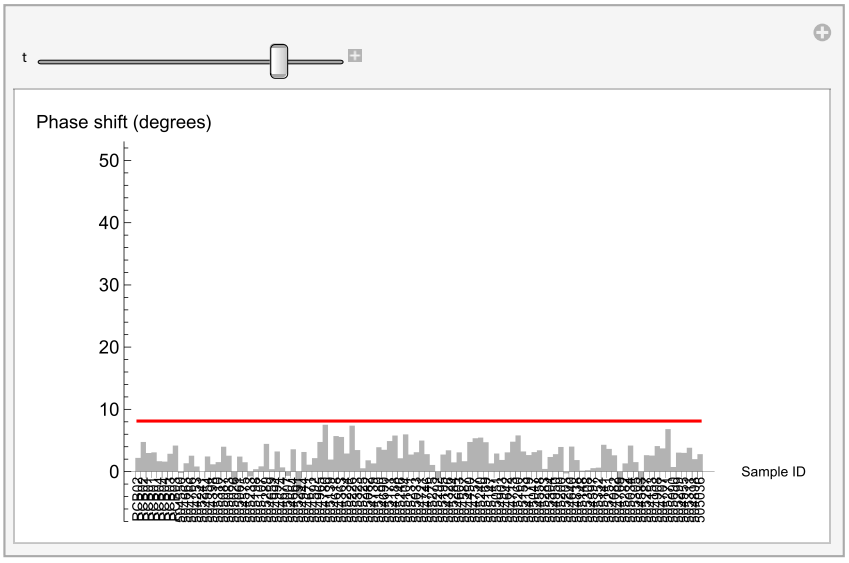

Bibliography

[1] UNAIDS. Global Report: UNAIDS report on the global AIDS epidemic 2013. Technical report, UNAIDS, 2013. URL http://www.unaids.org/en/resources/campaigns/globalreport2013/.

[2] Zheng Yin, Alison Brown, Gwenda Hughes, Anthony Nardone, O.Noel Gill, et al. HIV in the United Kingdom: 2014 Report. *Public Health England*, (November):39, 2013. URL https://www.gov.uk/government/publications/hiv-in-the-united-kingdom.

[3] Audrey Pettifor, Catherine MacPhail, Amy Corneli, Jabu Sibeko, Gift Kamanga, et al. Continued high risk sexual behavior following diagnosis with acute HIV infection in South Africa and Malawi: implications for prevention. *AIDS and behavior*, 15 (6):1243–50, aug 2011. ISSN 1573-3254. doi: 10.1007/s10461-010-9839-0. URL http://www.ncbi.nlm.nih.gov/pubmed/20978833.

[4] Health Protection Agency. Time to test for HIV: Expanding HIV testing in healthcare and community services in England. Technical report, 2011.

[5] House of Lords. House of Lords - Select Committee on HIV and AIDs in the United Kingdom - First Report, 2011. URL http://www.publications.parliament.uk/pa/ld201012/ldselect/ldaids/188/18802.htm.

[6] Department of Health UK. Modernisation of HIV rules to better protect public - Department of Health (UK). Technical report, DoH, 2013. URL https://www.gov.uk/government/news/modernisation-of-hiv-rules-to-better-protect-public.

[7] Sharon Peacock. Health care: Bring microbial sequencing to hospitals. *Nature*, 509 (7502):557–559, may 2014. ISSN 0028-0836. doi: 10.1038/509557a. URL http://www.nature.com/doifinder/10.1038/509557a.

[8] Oscar Grusky, Kathleen Johnston Roberts, and Aimee-Noelle Swanson. Failure to return for HIV test results: a pilot study of three community testing sites. *Journal of the International Association of Physicians in AIDS Care (Chicago, Ill. : 2002)*, 6(1):47–55, mar 2007. ISSN 1545-1097. doi: 10.1177/1545109706297530. URL http://www.ncbi.nlm.nih.gov/pubmed/17329504.

[9] Ronald H Gray, Fredrick Makumbi, David Serwadda, Tom Lutalo, Fred Nalugoda, et al. Limitations of rapid HIV-1 tests during screening for trials in Uganda: diagnostic test accuracy study. *BMJ (Clinical research ed.)*, 335(7612):188, jul 2007. ISSN 1756-1833. doi: 10.1136/bmj.39210.582801.BE. URL http://www.ncbi.nlm.nih.gov/pubmed/17545184.

[10] Christopher D Pilcher, Brian Louie, Shelley Facente, Sheila Keating, John Hackett, et al. Performance of rapid point-of-care and laboratory tests for acute and established HIV infection in San Francisco. *PloS one*, 8(12):e80629, 2013. ISSN 1932-6203. doi: 10.1371/journal.pone.0080629. URL http://www.ncbi.nlm.nih.gov/pubmed/24349007.

[11] National Institute for Health and Clinical Excellence. HIV testing: increasing uptake in black Africans — Guidance and guidelines — NICE. Technical report, NICE, 2011. URL https://www.nice.org.uk/guidance/ph33/documents/new-nice-guidance-to-increase-hiv-testing-in-black-african-communities-in-england.

[12] National Institute for Health and Clinical Excellence. HIV testing: increasing uptake in men who have sex with men — Guidance and guidelines — NICE. Technical report, NICE, 2011. URL https://www.nice.org.uk/guidance/ph34.

[13] Victoria Brennan, Stephen Beard, and Christian Hill. The public health and economic impact of early diagnosis and early HARRT treatment for HIV in the UK. Technical report, 2011.

[14] C. Johnson, R. Baggaley, S. Forsythe, H. van Rooyen, N. Ford, et al. Realizing the Potential for HIV Self-Testing. *AIDS and Behavior*, 18(S4):391–395, jul 2014. ISSN 1090-7165. doi: 10.1007/s10461-014-0832-x. URL http://link.springer.com/10.1007/s10461-014-0832-x.

[15] Vincent Wong, Cheryl Johnson, Elliot Cowan, Matthew Rosenthal, and V Wong. HIV Self-Testing in Resource-Limited Settings: Regulatory and Policy Considerations. *AIDS and Behavior*, 2014. doi: 10.1007/s10461-014-0825-9.

[16] Tawanda Makusha, Lucia Knight, Miriam Taegtmeyer, Olivia Tulloch, Adlai Davids, et al. HIV Self-Testing Could Revolutionize Testing in South Africa, but It Has Got to Be Done Properly: Perceptions of Key Stakeholders. *PLOS ONE*, 10(3): e0122783, mar 2015. ISSN 1932-6203. doi: 10.1371/journal.pone.0122783. URL http://dx.plos.org/10.1371/journal.pone.0122783.

[17] Benjamin J Wolpaw, Catherine Mathews, Mickey Chopra, Diana Hardie, Virginia de Azevedo, et al. The failure of routine rapid HIV testing: a case study of improving low sensitivity in the field. *BMC health services research*, 10(1):73, jan 2010. ISSN 1472-6963. doi: 10.1186/1472-6963-10-73. URL http://bmchealthservres.biomedcentral.com/articles/10.1186/1472-6963-10-73.

[18] David Mabey, Rosanna W Peeling, Andrew Ustianowski, and Mark D Perkins. Diagnostics for the developing world. *Nature reviews. Microbiology*, 2(3):231–40, mar 2004. ISSN 1740-1526. doi: 10.1038/nrmicro841. URL http://dx.doi.org/10.1038/nrmicro841.

[19] WHO. Rapid HIV tests: Guidelines for use in HIV testing and counselling services in ressource-constrained settings. Technical report, 2004.

[20] NHS. GP appointments - The NHS in England - NHS Choices, 2016. URL http://www.nhs.uk/NHSEngland/AboutNHSservices/doctors/Pages/gp-appointments.aspx.

[21] Pragna Patel, Berry Bennett, Timothy Sullivan, Monica M Parker, James D Heffelfinger, et al. Rapid HIV screening: missed opportunities for HIV diagnosis and prevention. *Journal of clinical virology : the official publication of the Pan American Society for Clinical Virology*, 54(1):42–7, may 2012. ISSN 1873-5967. doi: 10.1016/j.jcv.2012.01.022. URL http://www.ncbi.nlm.nih.gov/pubmed/22381919.

[22] Qingshan Wei, Hangfei Qi, Wei Luo, Derek Tseng, So Jung Ki, et al. Fluorescent imaging of single nanoparticles and viruses on a smart phone. *ACS nano*, 7(10): 9147–55, oct 2013. ISSN 1936-086X. doi: 10.1021/nn4037706. URL http://dx.doi.org/10.1021/nn4037706.

[23] Tassaneewan Laksanasopin, Tiffany W Guo, Samiksha Nayak, Archana A Sridhara, Shi Xie, et al. A smartphone dongle for diagnosis of infectious diseases at the point of care. *Science translational medicine*, 7(273):273re1, feb 2015. ISSN 1946-6242. doi: 10.1126/scitranslmed.aaa0056. URL http://stm.sciencemag.org/content/7/273/273re1.full.

[24] Roger B. Peck, Jeanette M. Lim, Heidi van Rooyen, Wanjiru Mukoma, Lignet Chepuka, et al. What Should the Ideal HIV Self-Test Look Like? A Usability Study of Test Prototypes in Unsupervised HIV Self-Testing in Kenya, Malawi, and South Africa. *AIDS and Behavior*, 18(S4):422–432, jul 2014. ISSN 1090-7165. doi: 10.1007/s10461-014-0818-8. URL http://link.springer.com/10.1007/s10461-014-0818-8.

[25] L. Rayleigh. On Waves Propagated along the Plane Surface of an Elastic Solid. *Proceedings of the London Mathematical Society*, s1-17(1):4–11, nov 1885. ISSN 0024-6115. doi: 10.1112/plms/s1-17.1.4. URL http://plms.oxfordjournals.org/cgi/doi/10.1112/plms/s1-17.1.4.

[26] T. Moriizumi, Y. Unno, and S. Shiokawa. New Sensor in Liquid Using Leaky SAW. In *IEEE 1987 Ultrasonics Symposium*, pages 579–582. IEEE, 1987. doi: 10.1109/ULTSYM.1987.199023. URL http://ieeexplore.ieee.org/lpdocs/epic03/wrapper.htm?arnumber=1535963.

[27] E Gizeli, A C Stevenson, N J Goddard, and C R Lowe. A novel Love-plate acoustic sensor utilizing polymer overlayers. *IEEE transactions on ultrasonics, ferroelectrics, and frequency control*, 39(5):657–9, jan 1992. ISSN 0885-3010. doi: 10.1109/58.156185. URL http://www.ncbi.nlm.nih.gov/pubmed/18267678.

[28] Eric V. Olsen, Iryna B. Sorokulova, Valery A. Petrenko, I-Hsuan Chen, James M. Barbaree, et al. Affinity-selected filamentous bacteriophage as a probe for acoustic wave biodetectors of Salmonella typhimurium. *Biosensors and Bioelectronics*, 21(8):1434–1442, 2006. ISSN 09565663. doi: 10.1016/j.bios.2005.06.004.

[29] M. Bisoffi, B. Hjelle, D. C. Brown, D. W. Branch, T. L. Edwards, et al. Detection of viral bioagents using a shear horizontal surface acoustic wave biosensor. *Biosensors and Bioelectronics*, 23(9):1397–1403, 2008. ISSN 09565663. doi: 10.1016/j.bios.2007.12.016.

[30] Sonia Sheikh, Christophe Blaszykowski, and Michael Thompson. Label-free detection of HIV-2 antibodies in serum with an ultra-high frequency acoustic wave sensor. 2011.

[31] Valdez MM Peck RB, Lim JM, Wellhausen JD, Lee AM. Target Product Profile: HIV Self-Test Version 4.1: A White Paper on the Evaluation of Current HIV Rapid Tests and Development of Core Specifications for Next-Generation HIV Tests - PATH. Technical report, 2014. URL http://www.path.org/publications/detail.php?i=2446.

[32] Health Protection Agency. HIV in the United Kingdom: 2012 Report. Technical report, 2012. URL http://www.hpa.org.uk/Publications/InfectiousDiseases/HIVAndSTIs/1211HIVintheUK2012/.

[33] Brian Rice, Jonathan Elford, Zheng Yin, Sara Croxford, Alison Brown, et al. Trends in HIV diagnoses, HIV care, and uptake of antiretroviral therapy among heterosexual adults in England, Wales, and Northern Ireland. *Sexually transmitted diseases*, 41 (4):257–65, apr 2014. ISSN 1537-4521. doi: 10.1097/OLQ.0000000000000111. URL http://www.ncbi.nlm.nih.gov/pubmed/24622638.

[34] Frank H Galvan, Ronald A Brooks, and Arleen A Leibowitz. Rapid HIV testing: issues in implementation. *AIDS patient care and STDs*, 18(1):15–8, jan 2004. ISSN 1087-2914. doi: 10.1089/108729104322740875. URL http://www.ncbi.nlm.nih.gov/pubmed/15006190.

[35] Clinicaltrials.gov. Smart Linkage-to-HIV Care Via a Smartphone App - Full Text View - ClinicalTrials.gov, 2016. URL https://clinicaltrials.gov/ct2/show/NCT02756949.

[36] Stephen Carson, Péter Kersch, Per Lindberg, Elena Fersman, Craig Donovan, et al. Ericsson Mobility Report, may 2015. URL http://www.ericsson.com/mobility-report.

[37] Andrew J Amato-Gauci, Gianfranco Spiteri, and Anastasia Pharris. Understanding the impact of smartphone applications on STI/HIV prevention among men who have sex with men in the EU/EEA. Technical report, 2015. URL http://ecdc.europa.eu/en/Pages/home.aspx.

[38] K. Saha, F. Bender, A. Rasmusson, and E. Gizeli. Probing the Viscoelasticity and Mass of a Surface-Bound Protein Layer with an Acoustic Waveguide Device. *Langmuir*, 19(4):1304–1311, feb 2003. ISSN 0743-7463. doi: 10.1021/la026806p. URL http://dx.doi.org/10.1021/la026806p.

[39] Michael S. Gottlieb, Robert Schroff, Howard M. Schanker, Joel D. Weisman, Peng Thim Fan, et al. Pneumocystis carinii Pneumonia and Mucosal Candidiasis in Previously Healthy Homosexual Men. *New England Journal of Medicine*, 305(24): 1425–1431, dec 1981. ISSN 0028-4793. doi: 10.1056/NEJM198112103052401. URL http://www.ncbi.nlm.nih.gov/pubmed/6272109.

[40] Robin A. Weiss, Angus G. Dalgleish, Clive Loveday, and Deenan Pillay. Human Immunodeficiency Viruses. In *Principles and Practice of Clinical Virology 6th Edition*, pages 721–757. John Wiley & Sons, Ltd, Chichester, UK, 2009. ISBN 9780470020975. doi: 10.1002/0470020970.ch25. URL http://doi.wiley.com/10.1002/0470020970.ch25.

[41] R A Weiss. Special anniversary review: twenty-five years of human immunodeficiency virus research: successes and challenges. *Clinical and experimental immunology*, 152 (2):201–10, may 2008. ISSN 1365-2249. doi: 10.1111/j.1365-2249.2008.03645.x. URL http://www.ncbi.nlm.nih.gov/pubmed/18373700.

[42] F Barré-Sinoussi, J C Chermann, F Rey, M T Nugeyre, S Chamaret, et al. Isolation of a T-lymphotropic retrovirus from a patient at risk for acquired immune deficiency syndrome (AIDS). *Science (New York, N.Y.)*, 220(4599):868–71, may 1983. ISSN 0036-8075. doi: 10.1126/science.6189183. URL http://www.ncbi.nlm.nih.gov/pubmed/6189183.

[43] R C Gallo, P S Sarin, E P Gelmann, M Robert-Guroff, E Richardson, et al. Isolation of human T-cell leukemia virus in acquired immune deficiency syndrome (AIDS). *Science (New York, N.Y.)*, 220(4599):865–7, may 1983. ISSN 0036-8075. URL http://www.ncbi.nlm.nih.gov/pubmed/6601823.

[44] Gary Maartens, Connie Celum, Sharon R Lewin, PM Sharp, BH Hahn, et al. HIV infection: epidemiology, pathogenesis, treatment, and prevention. *Lancet (London, England)*, 384(9939):258–71, jul 2014. ISSN 1474-547X. doi: 10.1016/S0140-6736(14)60164-1. URL http://www.ncbi.nlm.nih.gov/pubmed/24907868.

[45] Steven G Deeks, Julie Overbaugh, Andrew Phillips, and Susan Buchbinder. HIV infection. *Primer*, 1:1–22, oct 2015. ISSN 2056-676X. doi: 10.1038/nrdp.2015.35. URL http://www.nature.com/articles/nrdp201535.

[46] Joseph Anthony Moss. HIV/AIDS Review. *Radiologic technology*, 84(3):247–67; quiz p.268–70, 2013. ISSN 1943-5657. URL http://www.ncbi.nlm.nih.gov/pubmed/23322863.

[47] J. H. L. Playfair and B.M. Chain. *Immunology at a Glance*. John Wiley & Sons, 2009. ISBN 1405180528.

[48] Joris Hemelaar, Eleanor Gouws, Peter D Ghys, Saladin Osmanov, and WHO-UNAIDS Network for HIV Isolation and Characterisation. Global trends in molecular epidemiology of HIV-1 during 20002007. *AIDS*, 25(5):679–689, mar 2011. ISSN 0269-9370. doi: 10.1097/QAD.0b013e328342ff93. URL http://www.ncbi.nlm.nih.gov/pubmed/21297424.

[49] UNAIDS. UNAIDS 2014 - Fact sheet, 2014. URL http://www.unaids.org/en/resources/campaigns/2014/2014gapreport/factsheet.

[50] UNAIDS. UNAIDS — AIDSinfo - HIV prevalence map, 2016. URL http://aidsinfo.unaids.org/.

[51] UNAIDS. Global AIDS Update 2016 — UNAIDS. Technical report, UNAIDS, 2016. URL http://www.unaids.org/en/resources/documents/2016/Global-AIDS-update-2016.

[52] A Mocroft, S Vella, T L Benfield, A Chiesi, V Miller, et al. Changing patterns of mortality across Europe in patients infected with HIV-1. EuroSIDA Study Group. *Lancet (London, England)*, 352(9142):1725–30, nov 1998. ISSN 0140-6736. URL http://www.ncbi.nlm.nih.gov/pubmed/9848347.

[53] Frank J. Palella, Kathleen M. Delaney, Anne C. Moorman, Mark O. Loveless, Jack Fuhrer, et al. Declining Morbidity and Mortality among Patients with Advanced Human Immunodeficiency Virus Infection. *New England Journal of Medicine*, 338 (13):853–860, mar 1998. ISSN 0028-4793. doi: 10.1056/NEJM199803263381301. URL http://www.nejm.org/doi/abs/10.1056/NEJM199803263381301.

[54] M. May, M. Gompels, V. Delpech, K. Porter, F. Post, et al. Impact of late diagnosis and treatment on life expectancy in people with HIV-1: UK Collaborative HIV Cohort (UK CHIC) Study. *BMJ*, 343(oct11 2):d6016–d6016, oct 2011. ISSN 0959-8138. doi: 10.1136/bmj.d6016. URL http://www.bmj.com/cgi/doi/10.1136/bmj.d6016.

[55] Fumiyo Nakagawa, Rebecca K. Lodwick, Colette J. Smith, Ruth Smith, Valentina Cambiano, et al. Projected life expectancy of people with HIV according to timing of diagnosis. *AIDS*, 26(3):335–343, jan 2012. ISSN 0269-9370. doi: 10.1097/QAD.0b013e32834dcec9.

[56] WHO. WHO — Simple / Rapid tests, 2016. URL http://www.who.int/diagnostics{_}laboratory/faq/simple{_}rapid{_}tests/en/(Accessedon10/03/2016).

[57] WHO. WHO — Consolidated guidelines on the use of antiretroviral drugs for treating and preventing HIV infection. Technical report, WHO, 2015.

[58] HIV PrEP Guidelines: Press Release — Newsroom — NCHHSTP — CDC, 2016. URL https://www.cdc.gov/nchhstp/newsroom/2014/PrEP-Guidelines-Press-Release.html.

[59] PrEP HIV drugs: court hears NHS England appeal — Society — The Guardian, 2016. URL https://www.theguardian.com/society/2016/sep/15/prep-hiv-drugs-court-hears-nhs-england-appeal.

[60] UNAIDS. 909090 - An ambitious treatment target to help end the AIDS epidemic — UNAIDS. Technical report, 2014. URL http://www.unaids.org/en/resources/documents/2014/90-90-90.

[61] UNAIDS. Global gains made towards the 909090 targets — UNAIDS, 2016. URL http://www.unaids.org/en/resources/presscentre/featurestories/2016/july/20160717{_}90-90-90.

[62] Public Health England. HIV in the UK Situation Report 2015 - Incidence, prevalence and prevention, 2015.

[63] HIV in the United States — Statistics Overview — Statistics Center — HIV/AIDS — CDC, 2016. URL http://www.cdc.gov/hiv/statistics/overview/ataglance.html.

[64] UNAIDS. The Gap Report — UNAIDS. Technical report, UNAIDS, 2014.

[65] Jacob Bor, Abraham J Herbst, Marie-Louise Newell, and Till Bärnighausen. Increases in adult life expectancy in rural South Africa: valuing the scale-up of HIV treatment. *Science (New York, N.Y.)*, 339(6122):961–5, feb 2013. ISSN 1095-9203. doi: 10.1126/science.1230413. URL http://www.ncbi.nlm.nih.gov/pubmed/23430655.

[66] M.D. Cohen, Myron, S., Ph.D Chen, Ying Q., M.P.H. McCauley, Marybeth, Ph.D Gamble, Theresa, M.D. Hosseinipour, Mina C, et al. Prevention of HIV-1 Infection with Early Antiretroviral Therapy. *The New England Journal of Medicine*, 365(6): 493–505, 2011. ISSN 0028-4793. doi: 10.1056/NEJMoa1105243.

[67] HIV Cost-effectiveness — Guidance — Program Resources — HIV/AIDS — CDC, 2016. URL http://www.cdc.gov/hiv/programresources/guidance/costeffectiveness/index.html.

[68] Fumiyo Nakagawa, Alec Miners, Colette J. Smith, Ruth Simmons, Rebecca K. Lodwick, et al. Projected Lifetime Healthcare Costs Associated with HIV Infection. *PLOS ONE*, 10(4):e0125018, apr 2015. ISSN 1932-6203. doi: 10.1371/journal.pone.0125018. URL http://dx.plos.org/10.1371/journal.pone.0125018.

[69] Alan Engelman and Peter Cherepanov. The structural biology of HIV-1: mechanistic and therapeutic insights. *Nature reviews. Microbiology*, 10(4):279–90, apr 2012. ISSN 1740-1534. doi: 10.1038/nrmicro2747. URL http://www.nature.com/doifinder/10.1038/nrmicro2747.

[70] John M Coffin, Stephen H Hughes, and Harold E Varmus. *Retroviruses*. Cold Spring Harbor Laboratory Press, 1997. ISBN 0879695714. URL http://www.ncbi.nlm.nih.gov/pubmed/21433340.

[71] Lee Ratner, William Haseltine, Roberto Patarca, Kenneth J. Livak, Bruno Starcich, et al. Complete nucleotide sequence of the AIDS virus, HTLV-III. *Nature*, 313 (6000):277–284, jan 1985. ISSN 0028-0836. doi: 10.1038/313277a0. URL http://dx.doi.org/10.1038/313277a0.

[72] B G Turner and M F Summers. Structural biology of HIV. *Journal of molecular biology*, 285(1):1–32, jan 1999. ISSN 0022-2836. doi: 10.1006/jmbi.1998.2354. URL http://www.ncbi.nlm.nih.gov/pubmed/9878383.

[73] Eric O. Freed. HIV-1 Gag Proteins: Diverse Functions in the Virus Life Cycle. *Virology*, 251(1):1–15, 1998. ISSN 00426822. doi: 10.1006/viro.1998.9398.

[74] Bryan R. Cullen and Warner C. Greene. Regulatory pathways governing HIV-1 replication. *Cell*, 58(3):423–426, 1989. ISSN 00928674. doi: 10.1016/0092-8674(89)90420-0.

[75] Anna Aldovini and Richard A Young. Mutations of RNA and protein sequences involved in human immunodeficiency virus type 1 packaging result in production of noninfectious virus. *Journal of virology*, 64(5):1920–1926, may 1990. ISSN 0022-538X.

[76] Françoise Barré-Sinoussi, Anna Laura Ross, and Jean-François Delfraissy. Past, present and future: 30 years of HIV research. *Nature Reviews Microbiology*, 11(12):877–883, oct 2013. ISSN 1740-1526. doi: 10.1038/nrmicro3132.

[77] Alan D. Frankel and John A. T. Young. HIV-1: Fifteen Proteins and an RNA. *Annual Review of Biochemistry*, 67(1):1–25, jun 1998. ISSN 0066-4154. doi: 10.1146/annurev.biochem.67.1.1. URL http://www.annualreviews.org/doi/10.1146/annurev.biochem.67.1.1.

[78] Eric O. Freed. HIV-1 Replication. *Somatic Cell and Molecular Genetics*, 26(1/6):13–33, 2001. ISSN 07407750. doi: 10.1023/A:1021070512287. URL http://link.springer.com/10.1023/A:1021070512287.

[79] UNAIDS. The HIV Life Cycle — Understanding HIV/AIDS — AIDSinfo, 2016. URL https://aidsinfo.nih.gov/education-materials/fact-sheets/19/73/the-hiv-life-cycle.

[80] Hua-Xin Liao, Xi Chen, Supriya Munshaw, Ruijun Zhang, Dawn J Marshall, et al. Initial antibodies binding to HIV-1 gp41 in acutely infected subjects are polyreactive and highly mutated. *The Journal of experimental medicine*, 208(11):2237–49, oct 2011. ISSN 1540-9538. doi: 10.1084/jem.20110363.

[81] Georgia D Tomaras and Barton F Haynes. HIV-1-specific antibody responses during acute and chronic HIV-1 infection. *Current opinion in HIV and AIDS*, 4(5):373–9, sep 2009. ISSN 1746-6318. doi: 10.1097/COH.0b013e32832f00c0.

[82] J M Binley, P J Klasse, Y Cao, I Jones, M Markowitz, et al. Differential regulation of the antibody responses to Gag and Env proteins of human immunodeficiency virus type 1. *Journal of virology*, 71(4):2799–809, apr 1997. ISSN 0022-538X.

[83] A E Brown, M T Vahey, S Y Zhou, R C Chung, N M Ruiz, et al. Quantitative relationship of circulating p24 antigen with human immunodeficiency virus (HIV) RNA and specific antibody in HIV-infected subjects receiving antiretroviral therapy. The RV43 Study Group. *The Journal of infectious diseases*, 172(4):1091–5, oct 1995. ISSN 0022-1899. URL http://www.ncbi.nlm.nih.gov/pubmed/7561186.

[84] G. D. Tomaras, N. L. Yates, P. Liu, L. Qin, G. G. Fouda, et al. Initial B-Cell Responses to Transmitted Human Immunodeficiency Virus Type 1: Virion-Binding Immunoglobulin M (IgM) and IgG Antibodies Followed by Plasma Anti-gp41 Antibodies with Ineffective Control of Initial Viremia. *Journal of Virology*, 82 (24):12449–12463, dec 2008. ISSN 0022-538X. doi: 10.1128/JVI.01708-08. URL http://www.ncbi.nlm.nih.gov/pubmed/18842730.

[85] Eric Y Wong and Indira K Hewlett. HIV diagnostics: challenges and opportunities. *HIV Therapy*, 4(4):399–412, jul 2010. ISSN 1758-4310. doi: 10.2217/hiv.10.29. URL http://www.futuremedicine.com/doi/abs/10.2217/hiv.10.29.

[86] C R Robert George, Peter W Robertson, M Josephine Lusk, Ross Whybin, and William Rawlinson. Prolonged second diagnostic window for human immunodeficiency virus type 1 in a fourth-generation immunoassay: are alternative testing strategies required? *Journal of clinical microbiology*, 52(11):4105–8, nov 2014. ISSN 1098-660X. doi: 10.1128/JCM.01573-14. URL http://www.ncbi.nlm.nih.gov/pubmed/25210068.

[87] Thoai Doung Ly, Catherine Edlinger, Astrid Vabret, Odile Morvan, Beryl Greuet;, et al. Contribution of Combined Detection Assays of p24 Antigen and Anti-Human Immunodeficiency Virus (HIV) Antibodies in Diagnosis of Primary HIV Infection by Routine Testing. *J. Clin. Microbiol.*, 38(6):2459–2461, jun 2000. URL http://jcm.asm.org/content/38/6/2459.full.

[88] M Gilbert, J Kirihara, and J Mills. Enzyme-linked immunoassay for human immunodeficiency virus type 1 envelope glycoprotein 120. *Journal of clinical microbiology*, 29(1):142–7, jan 1991. ISSN 0095-1137.

[89] N L Yates, A R Stacey, T L Nolen, N A Vandergrift, M A Moody, et al. HIV-1 gp41 envelope IgA is frequently elicited after transmission but has an initial short response half-life. *Mucosal immunology*, 6(4):692–703, jul 2013. ISSN 1935-3456. doi: 10.1038/mi.2012.107.

[90] British HIV Association. UK National Guidelines for HIV Testing 2008. Technical Report September, 2008. URL http://www.bhiva.org/documents/Guidelines/Testing/GlinesHIVTest08.pdf.

[91] Bernard M. Branson, H. Hunter Handsfield, Margaret A. Lampe, Robert S. Janssen, Allan W. Taylor, et al. Revised recommendations for HIV testing of adults, adolescents, and pregnant women in health-care settings. Technical Report RR-14, 2006.

[92] Laura Waters, Duncan Churchill, N Ahmed, B Angus, M Boffito, et al. BHIVA guidelines for the treatment of HIV-1-positive adults with antiretroviral therapy 2015. Technical report, BHIVA, 2016. URL https://www.nice.org.uk/about/what-we-do/accreditation.

[93] Autotests de dépistage du VIH — Gouvernement.fr. URL http://www.gouvernement.fr/argumentaire/autotests-de-depistage-du-vih-2862.

[94] Food and Drug Administration. First Rapid Home-Use HIV Kit Approved for Self-Testing, 2012. URL http://www.fda.gov/downloads/ForConsumers/ConsumerUpdates/UCM311690.pdf.

[95] Julie E Myers, Wafaa M El-Sadr, Allison Zerbe, and Bernard M Branson. Rapid HIV self-testing: long in coming but opportunities beckon. *Wolters Kluwer Health*, 2013. doi: 10.1097/QAD.0b013e32835fd7a0.

[96] WHO. WHO — Procurement of HIV diagnostics. Technical report, 2014. URL http://www.who.int/diagnostics{_}laboratory/procurement/hiv/en/.

[97] U.S. Food and Drug Administration. Complete List of Donor Screening Assays for Infectious Agents and HIV Diagnostic Assays. Technical report, 2013. URL http://www.fda.gov/BiologicsBloodVaccines/BloodBloodProducts/ApprovedProducts/LicensedProductsBLAs/BloodDonorScreening/InfectiousDisease/ucm080466.htm.

[98] Alere Determine HIV-1/2 - Alere, 2016. URL http://www.alere.com/en/home/product-details/determine-hiv-1-2.html.

[99] HIV-1/HIV-2 Rapid Antibody Test — bioLytical Laboratories Inc., 2016. URL http://www.biolytical.com/products/instiHIV.

[100] David K Plate. Evaluation and implementation of rapid HIV tests: the experience in 11 African countries. *AIDS research and human retroviruses*, 23(12):1491–1498, 2007. ISSN 0889-2229. doi: 10.1089/aid.2007.0020.

[101] DxDiscovery. Lateral Flow Assay, 2016. URL http://www.dxdiscovery.com/lateral-flow-assay.html.

[102] Dhayendre Moodley, Pravi Moodley, Themba Ndabandaba, and Tonya Esterhuizen. Reliability of HIV rapid tests is user dependent. *South African Medical Journal*, 98 (9):707–709, 2008. ISSN 02569574.

[103] Adrian Carrio, Carlos Sampedro, Jose Luis Sanchez-Lopez, Miguel Pimienta, and Pascual Campoy. Automated low-cost smartphone-based lateral flow saliva test reader for drugs-of-abuse detection. *Sensors (Switzerland)*, 15(11):29569–29593, nov 2015. ISSN 14248220. doi: 10.3390/s151129569. URL http://www.ncbi.nlm.nih.gov/pubmed/26610513.

[104] Nitika Pant Pai, Jigyasa Sharma, Sushmita Shivkumar, Sabrina Pillay, Caroline Vadnais, et al. Supervised and unsupervised self-testing for HIV in high- and low-risk populations: a systematic review. *PLoS medicine*, 10(4):e1001414, 2013. ISSN 1549-1676. doi: 10.1371/journal.pmed.1001414. URL http://www.ncbi.nlm.nih.gov/pubmed/23565066.

[105] David A Katz, Matthew R Golden, James P Hughes, Carey Farquhar, and Joanne D Stekler. Acceptability and Ease of Use of Home Self-Testing for HIV among Men Who Have Sex with Men. *Medicine Biostatistics Public Health Seattle & King County*, 2 (5), 2012.

[106] Charlotte A Gaydos, Yu-Hsiang Hsieh, Leah Harvey, Avanti Burah, Helen Won, et al. Will patients "opt in" to perform their own rapid HIV test in the emergency department? *Annals of emergency medicine*, 58(1 Suppl 1):S74–8, jul 2011. ISSN

1097-6760. doi: 10.1016/j.annemergmed.2011.03.029. URL http://www.ncbi.nlm.nih.gov/pubmed/21684413.

[107] Alex Carballo-diéguez, Timothy Frasca, Curtis Dolezal, Ivan Balan, and Alex Carballo-die. Will Gay and Bisexually Active Men at High Risk of Infection Use Over-the-Counter Rapid HIV Tests to Screen Sexual Partners ? Will Gay and Bisexually Active Men at High Risk of Infection Use Over-the-Counter Rapid HIV Tests to Screen Sexual Partners ? *Journal of Sex Research*, 49(July):37–41, jul 2012. ISSN 0022-4499. doi: 10.1080/00224499.2011.647117. URL http://www.tandfonline.com/doi/abs/10.1080/00224499.2011.647117.

[108] Vernon J Lee, Soon Choon Tan, Arul Earnest, Peck Suet Seong, Hiok Hee Tan, et al. User Acceptability and Feasibility of Self-Testing With HIV Rapid Tests. *JAIDS Journal of Acquired Immune Deficiency Syndromes*, 45(4):449–453, aug 2007. ISSN 1525-4135. doi: 10.1097/QAI.0b013e318095a3f3. URL http://www.ncbi.nlm.nih.gov/pubmed/17554213.

[109] Luis de la Fuente, María Elena Rosales-Statkus, Juan Hoyos, José Pulido, Sara Santos, et al. Are Participants in a Street-Based HIV Testing Program Able to Perform Their Own Rapid Test and Interpret the Results? *PLoS ONE*, 7(10): e46555, oct 2012. ISSN 19326203. doi: 10.1371/journal.pone.0046555. URL http://www.ncbi.nlm.nih.gov/pubmed/23056342.

[110] Augustine Talumba Choko, Nicola Desmond, Emily L. Webb, Kondwani Chavula, Sue Napierala-Mavedzenge, et al. The uptake and accuracy of oral kits for HIV self-testing in high HIV prevalence setting: A cross-sectional feasibility study in Blantyre, Malawi. *PLoS Medicine*, 8(10):e1001102, oct 2011. ISSN 15491277. doi: 10.1371/journal.pmed.1001102. URL http://www.ncbi.nlm.nih.gov/pubmed/21990966.

[111] Damian P. Conway, Martin Holt, Anna McNulty, Deborah L. Couldwell, Don E. Smith, et al. Multi-centre evaluation of the determine HIV combo assay when used for point of care testing in a high risk clinic-based population. *PLoS ONE*, 9(4): e94062, apr 2014. ISSN 19326203. doi: 10.1371/journal.pone.0094062. URL http://dx.plos.org/10.1371/journal.pone.0094062.

[112] Yen T. Duong, Yvonne Mavengere, Hetal Patel, Carole Moore, Julius Manjengwa, et al. Poor performance of the determine HIV-1/2 Ag/Ab combo fourth-generation

rapid test for detection of acute infections in a national household survey in Swaziland. *Journal of Clinical Microbiology*, 52(10):3743–3748, oct 2014. ISSN 1098660X. doi: 10.1128/JCM.01989-14. URL http://www.ncbi.nlm.nih.gov/pubmed/25122853.

[113] Clifford B Jones, Kristin Kuldanek, David Muir, Karen Phekoo, Adam Black, et al. Clinical evaluation of the Determine HIV-1/2 Ag/Ab Combo test. *The Journal of infectious diseases*, 206(12):1947–9; author reply 1949–50, dec 2012. ISSN 1537-6613. doi: 10.1093/infdis/jis617. URL http://www.ncbi.nlm.nih.gov/pubmed/23045627.

[114] William Kilembe, Michelle Keeling, Etienne Karita, Shabir Lakhi, Paramesh Chetty, et al. Failure of A Novel, Rapid Antigen and Antibody Combination Test to Detect Antigen-Positive HIV Infection in African Adults with Early HIV Infection. *PLoS ONE*, 7(6):e37154, jun 2012. ISSN 1932-6203. doi: 10.1371/journal.pone.0037154. URL http://dx.plos.org/10.1371/journal.pone.0037154.

[115] Nora E Rosenberg, Gift Kamanga, Sam Phiri, Dominic Nsona, Audrey Pettifor, et al. Detection of acute HIV infection: a field evaluation of the determine® HIV-1/2 Ag/Ab combo test. *The Journal of infectious diseases*, 205(4):528–34, feb 2012. ISSN 1537-6613. doi: 10.1093/infdis/jir789. URL http://www.ncbi.nlm.nih.gov/pubmed/22207651.

[116] Silvia Faraoni, Andrea Rocchetti, Franca Gotta, Tina Ruggiero, Giancarlo Orofino, et al. Evaluation of a rapid antigen and antibody combination test in acute HIV infection. *Journal of Clinical Virology*, 57(1):84–87, may 2013. ISSN 13866532. doi: 10.1016/j.jcv.2013.01.007. URL http://www.ncbi.nlm.nih.gov/pubmed/23380659.

[117] Vani Chetty, Dhayendre Moodley, and Anil Chuturgoon. Evaluation of a 4th generation rapid HIV test for earlier and reliable detection of HIV infection in pregnancy. *Journal of Clinical Virology*, 54(2):180–184, jun 2012. ISSN 13866532. doi: 10.1016/j.jcv.2012.02.021. URL http://www.ncbi.nlm.nih.gov/pubmed/22445263.

[118] G. Beelaert and K. Fransen. Evaluation of a rapid and simple fourth-generation HIV screening assay for qualitative detection of HIV p24 antigen and/or antibodies to HIV-1 and HIV-2. *Journal of Virological Methods*, 168(1-2):218–222, sep 2010. ISSN 01660934. doi: 10.1016/j.jviromet.2010.06.002. URL http://www.ncbi.nlm.nih.gov/pubmed/20561542.

[119] Miriam Taegtmeyer, Peter MacPherson, Kathy Jones, Mark Hopkins, Jay Moorcroft, et al. Programmatic Evaluation of a Combined Antigen and Antibody Test for Rapid HIV Diagnosis in a Community and Sexual Health Clinic Screening Programme. *PLoS ONE*, 6(11):e28019, nov 2011. ISSN 1932-6203. doi: 10.1371/journal.pone.0028019. URL http://dx.plos.org/10.1371/journal.pone.0028019.

[120] Marieke Brauer, Johanna C. De Villiers, and Simnikiwe H. Mayaphi. Evaluation of the Determine fourth generation HIV rapid assay. *Journal of Virological Methods*, 189(1):180–183, apr 2013. ISSN 01660934. doi: 10.1016/j.jviromet.2013.01.017. URL http://www.ncbi.nlm.nih.gov/pubmed/23391823.

[121] Julie Fox, Helen Dunn, and Siobhan O'Shea. Low rates of p24 antigen detection using a fourth-generation point of care HIV test. *Sexually transmitted infections*, 87 (2):178–9, mar 2011. ISSN 1472-3263. doi: 10.1136/sti.2010.042564. URL http://www.ncbi.nlm.nih.gov/pubmed/21084439.

[122] J Curie and P Curie. Sur l'électricité polaire dans les cristaux hémièdre à faces inclinées. *Comptes rendus de l'Académie des sciences*, 91:383–386, 1880.

[123] Jacques Curie and Pierre Curie. Contractions et dilatations produites par des tensions électriques dans les cristaux hémièdres à faces inclinées. *Comptes-rendus de l'Académie des Sciences*, 93:1137–1140, 1881.

[124] Jacques Curie and Pierre Curie. Phénomènes électriques des cristaux hémièdres à faces inclinées. *Comptes-rendus de l'Académie des Sciences*, 11:245–251, 1882.

[125] W. Wersing, W. Heywang, H. Beige, and H. Thomann. 3. The Role of Ferroelectricity for Piezoelectric Materials. *Piezoelectricity*, 114:37 – 87, 2008. ISSN 0933-033X. doi: 10.1007/978-3-540-68683-5. URL http://link.springer.com/10.1007/978-3-540-68683-5.

[126] Takurō Ikeda. *Fundamentals of piezoelectricity*. Oxford University Press, 1996.

[127] Sara Tombelli, Marco Mascini, Cristiana Sacco, and Anthony P.F Turner. A DNA piezoelectric biosensor assay coupled with a polymerase chain reaction for bacterial toxicity determination in environmental samples. *Analytica Chimica Acta*, 418(1): 1–9, 2000. ISSN 00032670. doi: 10.1016/S0003-2670(00)00943-0.

[128] Thomas M A Gronewold. Surface acoustic wave sensors in the bioanalytical field: recent trends and challenges. *Analytica chimica acta*, 603(2):119–28, nov 2007. ISSN 1873-4324. doi: 10.1016/j.aca.2007.09.056. URL http://www.ncbi.nlm.nih.gov/pubmed/17963831.

[129] Kerstin Länge, Bastian E Rapp, and Michael Rapp. Surface acoustic wave biosensors: a review. *Analytical and bioanalytical chemistry*, 391(5):1509–19, jul 2008. ISSN 1618-2650. doi: 10.1007/s00216-008-1911-5. URL http://www.ncbi.nlm.nih.gov/pubmed/18265962.

[130] Colin Campbell. *2 - Basics of Acoustic Waves and Piezoelectricity*. Academic Press, 1989. ISBN 978-0-12-157345-4. doi: http://dx.doi.org/10.1016/B978-0-12-157345-4.50006-0. URL http://www.sciencedirect.com/science/article/pii/B9780121573454500060.

[131] Günter Sauerbrey. Verwendung von Schwingquarzen zur Wägung dünner Schichten und zur Mikrowägung. *Zeitschrift für Physik*, 155(2):206–222, apr 1959. ISSN 1434-6001. doi: 10.1007/BF01337937. URL http://link.springer.com/10.1007/BF01337937.

[132] Ping Sun, Yadong Jiang, Guangzhong Xie, Xiaosong Du, and Jia Hu. A room temperature supramolecular-based quartz crystal microbalance (QCM) methane gas sensor. *Sensors and Actuators B: Chemical*, 141(1):104–108, 2009. ISSN 09254005. doi: 10.1016/j.snb.2009.06.012.

[133] Qiang Chen, Wei Tang, Dingzhong Wang, Xiaojie Wu, Na Li, et al. Amplified QCM-D biosensor for protein based on aptamer-functionalized gold nanoparticles. *Biosensors and Bioelectronics*, 26(2):575–579, 2010. ISSN 09565663. doi: 10.1016/j.bios.2010.07.034. URL http://www.sciencedirect.com/science/article/pii/S0956566310004094.

[134] Jianqiao Hu, Furong Zhu, Jian Zhang, and Hao Gong. A room temperature indium tin oxide/quartz crystal microbalance gas sensor for nitric oxide. *Sensors and Actuators B: Chemical*, 93(1):175–180, 2003. ISSN 09254005. doi: 10.1016/S0925-4005(03)00186-2.

[135] T Nomura and A Minemura. Behaviour of a piezoelectric quartz crystal in an aquous solution and the application to the determination of minute amount of cyanide. *Nippon Kagaku Kaishi*, 12(10):1621–1625, 1980. ISSN 0369-4577.

[136] K Keiji Kanazawa and Joseph G Gordon. The oscillation frequency of a quartz resonator in contact with liquid, 1985. ISSN 00032670.

[137] Ishida Naoyuki and Simon Biggs. Direct Observation of the Phase Transition for a Poly(N-isopropylacryamide) Layer Grafted onto a Solid Surface by AFM and QCM-D. *Langmuir*, 23:11083–11088, 2007. doi: 10.1021/LA701461B.

[138] Michael Rodahl, Fredrik Hook, Anatol Krozer, Peter Brzezinski, and Bengt Kasemo. Quartz crystal microbalance setup for frequency and Q-factor measurements in gaseous and liquid environments. *Review of Scientific Instruments*, 66(7):3924, 1995. doi: 10.1063/1.1145396. URL http://scitation.aip.org/content/aip/journal/rsi/66/7/10.1063/1.1145396.

[139] Sung-Rok Hong, Hyun-Do Jeong, and Suhee Hong. QCM DNA biosensor for the diagnosis of a fish pathogenic virus VHSV. *Talanta*, 82(3):899–903, 2010. ISSN 00399140. doi: 10.1016/j.talanta.2010.04.065.

[140] R. M. White and F. W. Voltmer. Direct piezoelectric coupling to surface elastic waves. *Applied Physics Letters*, 7(12):314, 1965. ISSN 00036951. doi: 10.1063/1.1754276. URL http://scitation.aip.org/content/aip/journal/apl/7/12/10.1063/1.1754276.

[141] D.S. Ballantine, S.J. Martin, A.J. Ricco, G.C. Frye, H Wohltjen, et al. *Acoustic Wave Sensors and Responses*. Elsevier, 1997. ISBN 978-0-12-077460-9. doi: 10.1016/B978-012077460-9/50003-4.

[142] Ken-ya Hashimoto. *Surface Acoustic Wave Devices in Telecommunications*. Springer Berlin Heidelberg, Berlin, Heidelberg, 2000. ISBN 978-3-642-08659-5. doi: 10.1007/978-3-662-04223-6. URL http://link.springer.com/10.1007/978-3-662-04223-6.

[143] Jared Kirschner. Surface acoustic wave sensors (SAWs): design for fabrication. *Microelectromechanical systems*, 2010.

[144] H. Wohltjen and R. Dessy. Surface acoustic wave probe for chemical analysis. I. Introduction and instrument description. *Analytical Chemistry*, 51(9):1458–1464, 1979. ISSN 0003-2700. doi: 10.1021/ac50045a024. URL http://pubs.acs.org/doi/abs/10.1021/ac50045a024.

[145] H. Wohltjen and R. Dessy. Surface Acoustic Wave Probes for Chemical Analysis. II. Gas Chromatography Detector. *Analytical Chemistry*, 51(9):1465–1470, 1979. ISSN 0003-2700. doi: 10.1021/ac50045a025. URL http://pubs.acs.org/doi/abs/10.1021/ac50045a025.

[146] H. Wohltjen and R. Dessy. Surface acoustic wave probes for chemical analysis. III. Thermomechanical polymer analyzer. *Analytical Chemistry*, 51(9):1470–1475, 1979. ISSN 0003-2700. doi: 10.1021/ac50045a024. URL http://pubs.acs.org/doi/abs/10.1021/ac50045a026.

[147] H. Wohltjen. Mechanism of Operation and Design Considerations for Surface Acoustic Wave Device Vapor Sensors. *Sensors and Actuators*, 5(4):307–325, 1984. ISSN 02506874. doi: 10.1016/0250-6874(84)85014-3. URL http://linkinghub.elsevier.com/retrieve/pii/0250687484850143.

[148] B. A. Krieger, R. E., Auld. *Acoustic fields and waves in soldis*. R.E. Krieger, 1990. ISBN 0898747821.

[149] Jun Kondoh. A liquid-phase sensor using shear horizontal surface acoustic wave devices. *Electronics and Communications in Japan*, 96(2):41–49, feb 2013. ISSN 19429533. doi: 10.1002/ecj.10407. URL http://doi.wiley.com/10.1002/ecj.10407.

[150] A. J. Ricco and S. J. Martin. Acoustic wave viscosity sensor. *Applied Physics Letters*, 50(21):1474–1476, 1987.

[151] S.J. Martin, A.J. Ricco, G.C. Frye, T.M. Niemczyk, and I. Adhihetty. Sensing in liquids with SH plate mode devices. In *IEEE 1988 Ultrasonics Symposium Proceedings.*, pages 607–611. IEEE, 1988. doi: 10.1109/ULTSYM.1988.49449. URL http://ieeexplore.ieee.org/lpdocs/epic03/wrapper.htm?arnumber=49449.

[152] R. M. White and S. W. Wenzel. Fluid loading of a Lamb-wave sensor. *Applied Physics Letters*, 52(20):1653, may 1988. ISSN 00036951. doi: 10.1063/1.99047.

[153] Fabrice Martin, Michael I Newton, Glen Mchale, Kathryn A Melzak, and Electra Gizeli. Pulse mode shear horizontal-surface acoustic wave (SH-SAW) system for liquid based sensing applications. *Biosensors and Bioelectronics*, 19:627–632, 2004. doi: 10.1016/S0956-5663(03)00257-4.

[154] Marc D. Schlensog, Thomas M.A. Gronewold, Michael Tewes, Michael Famulok, and Eckhard Quandt. A Love-wave biosensor using nucleic acids as ligands. *Sensors and Actuators B: Chemical*, 101(3):308–315, jul 2004. ISSN 09254005. doi: 10.1016/j.snb.2004.03.015.

[155] Eric Berkenpas, Shivashanker Bitla, Paul Millard, and Mauricio Pereira Da Cunha. Pure shear horizontal SAW biosensor on langasite. *IEEE Transactions on Ultrasonics, Ferroelectrics, and Frequency Control*, 51(11):1404–1411, nov 2004. ISSN 08853010. doi: 10.1109/TUFFC.2004.1367479. URL http://ieeexplore.ieee.org/document/1367479/.

[156] Deepti D. Deobagkar, Veena Limaye, Sweta Sinha, and R. D S Yadava. Acoustic wave immunosensing of Escherichia coli in water. *Sensors and Actuators, B: Chemical*, 2005. ISSN 09254005. doi: 10.1016/j.snb.2004.04.106.

[157] Effie Howe and Geoffrey Harding. A comparison of protocols for the optimisation of detection of bacteria using a surface acoustic wave (SAW) biosensor. *Biosensors and Bioelectronics*, 15(11):641–649, 2000. ISSN 09565663. doi: 10.1016/S0956-5663(00)00116-0.

[158] D Li, J Wang, R Wang, Y Li, D Bi-Ghanem, et al. A nanobeads amplified QCM immunosensor for the detection of avian influenza virus H5N1. *Biosens.Bioelectron.*, 2011.

[159] Ronghui Wang and Yanbin Li. Hydrogel based QCM aptasensor for detection of avian influenza virus. *Biosensors and Bioelectronics*, 2013. ISSN 09565663. doi: 10.1016/j.bios.2012.10.038.

[160] D F Tai, C Y Lin, T Z Wu, J H Huang, and P Y Shu. Artificial receptors in serologic tests for the early diagnosis of dengue virus infection, 2006.

[161] Fedor N. Dultsev and Andrei V. Tronin. Rapid sensing of hepatitis B virus using QCM in the thickness shear mode. *Sensors and Actuators, B: Chemical*, 2015. ISSN 09254005. doi: 10.1016/j.snb.2015.04.027.

[162] Yunxia Wang, Ming Chen, Liqun Zhang, Yi Ding, Yang Luo, et al. Rapid detection of human papilloma virus using a novel leaky surface acoustic wave peptide nucleic acid biosensor. *Biosensors and Bioelectronics*, 2009. ISSN 09565663. doi: 10.1016/j.bios.2009.04.034.

[163] Hun Joo Lee, Kak Namkoong, Eun Chol Cho, Christopher Ko, Jae Chan Park, et al. Surface acoustic wave immunosensor for real-time detection of hepatitis B surface antibodies in whole blood samples. *Biosensors and Bioelectronics*, 2009. ISSN 09565663. doi: 10.1016/j.bios.2009.04.009.

[164] Konstantinos Mitsakakis and Electra Gizeli. Detection of multiple cardiac markers with an integrated acoustic platform for cardiovascular risk assessment. *Analytica Chimica Acta*, 2011. ISSN 00032670. doi: 10.1016/j.aca.2011.05.016.

[165] S. P. Martin, D. J. Lamb, J. M. Lynch, and S. M. Reddy. Enzyme-based determination of cholesterol using the quartz crystal acoustic wave sensor. *Analytica Chimica Acta*, 2003. ISSN 00032670. doi: 10.1016/S0003-2670(03)00504-X.

[166] Dezhong Liu, Kai Ge, Kang Chen, Lihua Nie, and Shouzhuo Yao. Clinical analysis of urea in human blood by coupling a surface acoustic wave sensor with urease extracted from pumpkin seeds. *Analytica Chimica Acta*, 307(1):61–69, may 1995. ISSN 00032670. doi: 10.1016/0003-2670(95)00046-3. URL http://linkinghub.elsevier.com/retrieve/pii/0003267095000463.

[167] Thomas M. A. Gronewold, Antje Baumgartner, , Eckhard Quandt, and Michael Famulok*. Discrimination of Single Mutations in Cancer-Related Gene Fragments with a Surface Acoustic Wave Sensor. 2006. doi: 10.1021/AC060296C. URL http://pubs.acs.org/doi/abs/10.1021/ac060296c.

[168] Xuesong Ye, Lu Fang, Bo Liang, Qiong Wang, Xuejun Wang, et al. Studies of a high-sensitive surface acoustic wave sensor for passive wireless blood pressure measurement. *Sensors and Actuators, A: Physical*, 2011. ISSN 09244247. doi: 10.1016/j.sna.2011.05.022.

[169] Jun Kondoh, Yoshikazu Matsui, Showko Shiokawa, and Wojciech B. Wlodarski. Enzyme-immobilized SH-SAW biosensor. *Sensors and Actuators B: Chemical*, 20 (2):199–203, 1994. ISSN 09254005. doi: 10.1016/0925-4005(94)01182-6.

[170] Mikihiro Goto, Osamu Iijima, Takashi Kogai, and Hiromi Yatsuda. Point-of-care SH-SAW biosensor. In *2010 IEEE International Ultrasonics Symposium*, pages 736–739. IEEE, oct 2010. ISBN 978-1-4577-0382-9. doi: 10.1109/ULTSYM.2010.5935551. URL http://ieeexplore.ieee.org/document/5935551/.

[171] Youngjune Hur, Jinho Han, Jooheon Seon, Yukeun Eugene Pak, and Yongrae Roh. Development of an SH-SAW sensor for the detection of DNA hybridization. *Sensors and Actuators A: Physical*, 120(2):462–467, 2005. ISSN 09244247. doi: 10.1016/j.sna.2005.01.027.

[172] S.J. Martin and A.J. Ricco. Effective utilization of acoustic wave sensor responses: simultaneous measurement of velocity and attenuation. In *Proceedings., IEEE Ultrasonics Symposium*, pages 621–625. IEEE, 1989. doi: 10.1109/ULTSYM.1989.67058. URL http://ieeexplore.ieee.org/document/67058/.

[173] Jun Kondoh and Showko Shiokawa. A liquid sensor based on a shear horizontal saw device. *Electronics and Communications in Japan (Part II: Electronics)*, 76(2):69–82, 1993. ISSN 8756663X. doi: 10.1002/ecjb.4420760208. URL http://doi.wiley.com/10.1002/ecjb.4420760208.

[174] Jun Kondoh, Showko Shiokawa, Michael Rapp, and Stefan Stier. Simulation of Viscoelastic Effects of Polymer Coatings on Surface Acoustic Wave Gas Sensor under Consideration of Film Thickness. *Japanese Journal of Applied Physics*, 37(Part 1, No. 5B):2842–2848, may 1998. ISSN 0021-4922. doi: 10.1143/JJAP.37.2842. URL http://stacks.iop.org/1347-4065/37/2842.

[175] Takashi Kogai, Naoyuki Yoshimura, Toshimasa Mori, and Hiromi Yatsuda. Liquid-Phase Shear Horizontal Surface Acoustic Wave Immunosensor. *Japanese Journal of Applied Physics*, 49(7):07HD15, jul 2010. ISSN 0021-4922. doi: 10.1143/JJAP.49.07HD15. URL http://jjap.jsap.jp/link?JJAP/49/07HD15/.

[176] Surface acoustic wave element and equipment for measuring characteristics of liquid material. http://www.google.com/patents/WO2009066640A1?cl=en, May 2009.

[177] B Chesebro, K Wehrly, J Nishio, and S Perryman. Macrophage-tropic human immunodeficiency virus isolates from different patients exhibit unusual V3 envelope sequence homogeneity in comparison with T-cell-tropic isolates: definition of critical amino acids involved in cell tropism. *Journal of virology*, 66(11):6547–54, nov 1992. ISSN 0022-538X.

[178] ForteBio Interactions :: Spring 2012, 2012. URL http://www.fortebio.com/interactions/Spring{_}2012/page5.html.

[179] Electron spectroscopy - Tampere University of Technology. URL http://www.tut.fi/en/about-tut/departments/optoelectronics-research-centre/research/surface-science/electron-spectroscopy/index.htm.

[180] Gábor Késmárky, Péter Kenyeres, Miklós Rábai, and Kálmán Tóth. Plasma viscosity: a forgotten variable. *Clinical hemorheology and microcirculation*, 39(1-4):243–6, 2008. ISSN 1386-0291. URL http://www.ncbi.nlm.nih.gov/pubmed/18503132.

[181] DG Altman and JM Bland. Measurement in Medicine: The Analysis of Method Comparison Studies. *The statistician*, 32(3):307–317, 2009. ISSN 00390526. doi: 10.2307/2987937.

[182] Davide Giavarina. Understanding Bland Altman analysis. *Biochemia medica*, 25(2):141–51, 2015. ISSN 1330-0962. doi: 10.11613/BM.2015.015. URL http://www.ncbi.nlm.nih.gov/pubmed/26110027.

[183] J. W. Bartlett and C. Frost. Reliability, repeatability and reproducibility: Analysis of measurement errors in continuous variables. *Ultrasound in Obstetrics and Gynecology*, 31(4):466–475, apr 2008. ISSN 09607692. doi: 10.1002/uog.5256. URL http://doi.wiley.com/10.1002/uog.5256.

[184] Jamie Ghuman, Patricia A. Zunszain, Isabelle Petitpas, Ananyo A. Bhattacharya, Masaki Otagiri, et al. Structural Basis of the Drug-binding Specificity of Human Serum Albumin. *Journal of Molecular Biology*, 353(1):38–52, 2005. ISSN 00222836. doi: 10.1016/j.jmb.2005.07.075.

[185] D C Carter, X M He, S H Munson, P D Twigg, K M Gernert, et al. Three-dimensional structure of human serum albumin. *Science (New York, N.Y.)*, 244(4909):1195–8, jun 1989. ISSN 0036-8075. URL http://www.ncbi.nlm.nih.gov/pubmed/2727704.

[186] A J Lomant and G Fairbanks. Chemical probes of extended biological structures: synthesis and properties of the cleavable protein cross-linking reagent [35S]dithiobis(succinimidyl propionate). *Journal of molecular biology*, 104(1):243–61, jun 1976. ISSN 0022-2836. URL http://www.ncbi.nlm.nih.gov/pubmed/957432.

[187] H. D. Abruña. Dithiobissuccinimidyl propionate as an anchor for assembling peroxidases at electrodes surfaces and its application in a H2O2 biosensor. *Analytical Chemistry*, 71(24):5530–5537, dec 1999. ISSN 00032700. doi: 10.1021/ac990759x. URL http://www.ncbi.nlm.nih.gov/pubmed/10624158.

[188] Richard I. Masel. *Principles of adsorption and reaction on solid surfaces*. Wiley, 1996. ISBN 9780471303923.

[189] Reichert Life Sciences Technologies. Human Serum Albumin (HSA) Binding to Biotinylated Anti-HSA lgG Captured on Planar Neutravidin Surface. Technical report, 1999.

[190] J Böni, M Opravil, Z Tomasik, M Rothen, L Bisset, et al. Simple monitoring of antiretroviral therapy with a signal-amplification-boosted HIV-1 p24 antigen assay with heat-denatured plasma. *AIDS (London, England)*, 11(31):F47–F52, may 1997. ISSN 0269-9370. doi: 10.1097/00002030-199706000-00001. URL http://www.ncbi.nlm.nih.gov/pubmed/9143600.

[191] Christian Erikstrup, Per Kallestrup, Rutendo B L Zinyama-Gutsire, Exnevia Gomo, Margrethe Lüneborg-Nielsen, et al. p24 as a predictor of mortality in a cohort of HIV-1-infected adults in rural Africa. *Journal of acquired immune deficiency syndromes (1999)*, 48(3):345–349, jul 2008. ISSN 1525-4135. doi: 10.1097/QAI.0b013e31817dc3d1. URL http://www.ncbi.nlm.nih.gov/pubmed/18545150.

[192] L A Spacek, F Lutwama, H M Shihab, J Summerton, M R Kamya, et al. Diagnostic accuracy of ultrasensitive heat-denatured HIV-1 p24 antigen in non-B subtypes in Kampala, Uganda. *International journal of STD & AIDS*, 22(6):310–4, jun 2011. ISSN 1758-1052. doi: 10.1258/ijsa.2009.009363.

[193] C Hamers-Casterman, T Atarhouch, S Muyldermans, G Robinson, C Hamers, et al. Naturally occurring antibodies devoid of light chains. *Nature*, 363(6428):446–8, jun 1993. ISSN 0028-0836. doi: 10.1038/363446a0. URL http://www.ncbi.nlm.nih.gov/pubmed/8502296.

[194] Andrea Gorlani, Joachim Brouwers, Christopher McConville, Pieter van der Bijl, Karl Malcolm, et al. Llama antibody fragments have good potential for application as HIV type 1 topical microbicides. *AIDS research and human retroviruses*, 28(2):198–205, feb 2012. ISSN 1931-8405. doi: 10.1089/aid.2011.0133. URL http://www.ncbi.nlm.nih.gov/pubmed/21864083.

[195] E.R. Gray, J.C. Brookes, V. Turbé, B.L.J. Webb, L.A. Granger, et al. To be determined - manuscript in preparation. 2016.

[196] Alfredo De La Escosura-Muñiz, Claudio Parolo, and Arben Merkoi. Immunosensing using nanoparticles. *Materials Today*, 13(7-8):24–34, 2010. ISSN 13697021. doi: 10.1016/S1369-7021(10)70125-5.

[197] Alfredo de la Escosura-Muñiz, Claudio Parolo, Flavio Maran, and Arben Mekoçi. Size-dependent direct electrochemical detection of gold nanoparticles: application in magnetoimmunoassays. *Nanoscale*, 3(8):3350–6, aug 2011. ISSN 2040-3372. doi: 10.1039/c1nr10377f. URL http://www.ncbi.nlm.nih.gov/pubmed/21761067.

[198] Claudio Parolo and Arben Merkoçi. Paper - based nanobiosensors for diagnostics. *Chem . Soc . Rev . Chem . Soc . Rev*, 42(42):450–457, 2013. doi: 10.1039/c2cs35255a.

[199] Claudio Parolo, Alfredo de la Escosura-Muñiz, and Arben Merkoçi. Enhanced lateral flow immunoassay using gold nanoparticles loaded with enzymes. *Biosensors and Bioelectronics*, 40(1):412–416, 2013. ISSN 09565663. doi: 10.1016/j.bios.2012.06.049.

[200] G-Biosciences. A Non-Animal Protein Blocking Buffer for Immunoblots and ELISA — NAP-BLOCKER — G-Biosciences [Accessed on 14/04/2016], 2016. URL http://www.gbiosciences.com/ResearchProducts/NAP-(Non-Animal-Protein)-BLOCKER.aspx.

[201] A. Cabie, F. Bissuel, P. Huc, L. Paturel, and S. Abel. Impact of rapid HIV testing on the return rate for routine test results in sexually transmitted infection testing centres. *International Journal of STD & AIDS*, 22(12):757–758, dec 2011. ISSN 0956-4624. doi: 10.1258/ijsa.2009.009267.

[202] Juliette Pavie, Anne Rachline, Bénédicte Loze, Laurence Niedbalski, Constance Delaugerre, et al. Sensitivity of five rapid HIV tests on oral fluid or finger-stick whole blood: a real-time comparison in a healthcare setting. *PloS one*, 5(7):

e11581, 2010. ISSN 1932-6203. doi: 10.1371/journal.pone.0011581. URL http://www.ncbi.nlm.nih.gov/pubmed/20657834.

[203] Massimiliano Lanzafame, Antonella Zorzi, Fabio Rigo, Irene Adami, Paola Del Bravo, et al. Performance of Alere Determine HIV-1/2 Ag/Ab Combo rapid test for acute HIV infection: a case report. *Le infezioni in medicina : rivista periodica di eziologia, epidemiologia, diagnostica, clinica e terapia delle patologie infettive*, 23(1):48–50, mar 2015. ISSN 1124-9390. URL http://www.ncbi.nlm.nih.gov/pubmed/25819051.

[204] Beatrice N Vetter, Vanessa Orlowski, Katrien Fransen, Christoph Niederhauser, Vincent Aubert, et al. Generation of a recombinant Gag virus-like-particle panel for the evaluation of p24 antigen detection by diagnostic HIV tests. *PloS one*, 9(10):e111552, jan 2014. ISSN 1932-6203. doi: 10.1371/journal.pone.0111552.

[205] A. Einstein. Eine neue Bestimmung der Molek??ldimensionen. *Annalen der Physik*, 324(2):289–306, feb 1906. ISSN 15213889. doi: 10.1002/andp.19063240204. URL http://doi.wiley.com/10.1002/andp.200590008.

[206] W Haynes. CRC Handbook of Chemistry and Physics, 94th Edition - CRC Press Book, 2013. URL https://www.crcpress.com/CRC-Handbook-of-Chemistry-and-Physics-94th-Edition/Haynes/p/book/9781466571143.

[207] M Weiss, W Welsch, M von Schickfus, and S Hunklinger. Viscoelastic behavior of antibody films on a shear horizontal acoustic surface wave sensor. *Analytical chemistry*, 70(14):2881–7, jul 1998. ISSN 0003-2700. URL http://www.ncbi.nlm.nih.gov/pubmed/9684545.

[208] W Humphrey, A Dalke, and K Schulten. VMD: visual molecular dynamics. *Journal of molecular graphics*, 14(1):33–8, 27–8, feb 1996. ISSN 0263-7855. URL http://www.ncbi.nlm.nih.gov/pubmed/8744570.

[209] Jens Feder. Random sequential adsorption. *Journal of Theoretical Biology*, 87(2): 237–254, nov 1980. ISSN 00225193. doi: 10.1016/0022-5193(80)90358-6. URL http://linkinghub.elsevier.com/retrieve/pii/0022519380903586.

[210] G. B. Jeffery. The Motion of Ellipsoidal Particles Immersed in a Viscous Fluid. *Proceedings of the Royal Society A: Mathematical, Physical and Engineering Sciences*,

102(715):161–179, nov 1922. ISSN 1364-5021. doi: 10.1098/rspa.1922.0078. URL http://rspa.royalsocietypublishing.org/cgi/doi/10.1098/rspa.1922.0078.

[211] Jos Buijs, James W.Th. Lichtenbelt, Willem Norde, and Johannes Lyklema. Adsorption of monoclonal IgGs and their F(ab)2 fragments onto polymeric surfaces. *Colloids and Surfaces B: Biointerfaces*, 5(1-2):11–23, sep 1995. ISSN 09277765. doi: 10.1016/0927-7765(95)98205-2. URL http://www.sciencedirect.com/science/article/pii/0927776595982052.

[212] Rami N. Foster, Elisa T. Harrison, and David G. Castner. ToF-SIMS and XPS Characterization of Protein Films Adsorbed onto Bare and Sodium Styrenesulfonate-Grafted Gold Substrates. *Langmuir*, 32(13):3207–3216, apr 2016. ISSN 15205827. doi: 10.1021/acs.langmuir.5b04743.

[213] WHO. HIV/AIDS Programme. Guidance on Pre-exposure prophylaxis (PrEP) for serodiscordant couples, men and tansgender women who have sex with men at high risk of HIV: Recommendations for use in the context of demonstration projects. Technical report, WHO, 2012. URL http://apps.who.int/iris/bitstream/10665/75188/1/9789241503884{_}eng.pdf.

[214] Sumedha D. Jayasena. Aptamers: An Emerging Class of Molecules That Rival Antibodies in Diagnostics. *Clinical Chemistry*, 45(9), 1999.

[215] Kun Han, Zhiqiang Liang, and Nandi Zhou. Design strategies for aptamer-based biosensors. *Sensors (Basel, Switzerland)*, 10(5):4541–57, 2010. ISSN 1424-8220. doi: 10.3390/s100504541. URL http://www.ncbi.nlm.nih.gov/pubmed/22399891.

[216] Kyung-Mi Song, Seonghwan Lee, and Changill Ban. Aptamers and Their Biological Applications. *Sensors*, 12(12):612–631, jan 2012. ISSN 1424-8220. doi: 10.3390/s120100612.

[217] Jeong-Gun Lee, Kwang Ho Cheong, Nam Huh, Suhyeon Kim, Jeong-Woo Choi, et al. Microchip-based one step DNA extraction and real-time PCR in one chamber for rapid pathogen identification. *Lab on a Chip*, 6(7):886, 2006. ISSN 1473-0197. doi: 10.1039/b515876a. URL http://xlink.rsc.org/?DOI=b515876a.

[218] Ken-ichi Ohno, Kaoru Tachikawa, and Andreas Manz. Microfluidics: Applications for analytical purposes in chemistry and biochemistry. *ELECTROPHORESIS*, 29

(22):4443–4453, nov 2008. ISSN 01730835. doi: 10.1002/elps.200800121. URL http://doi.wiley.com/10.1002/elps.200800121.

[219] N. Reginald Beer, Benjamin J. Hindson, Elizabeth K. Wheeler, Sara B. Hall, Klint A. Rose, et al. On-chip, real-time, single-copy polymerase chain reaction in picoliter droplets. *Analytical Chemistry*, 79(22):8471–8475, nov 2007. ISSN 00032700. doi: 10.1021/ac701809w. URL http://www.ncbi.nlm.nih.gov/pubmed/17929880.

[220] Yves Benhamou, Marie Bochet, Vincent Thibault, Vincent Di Martino, Eric Caumes, et al. Long-term incidence of hepatitis B virus resistance to lamivudine in human immunodeficiency virus-infected patients. *Hepatology*, 30(5):1302–1306, nov 1999. ISSN 02709139. doi: 10.1002/hep.510300525. URL http://doi.wiley.com/10.1002/hep.510300525.

[221] Stéphanie Pasche, Susan M. De Paul, Janos Vörös, Nicholas D. Spencer, and Marcus Textor. Poly(l-lysine)-graft-poly(ethylene glycol) Assembled Monolayers on Niobium Oxide Surfaces: A Quantitative Study of the Influence of Polymer Interfacial Architecture on Resistance to Protein Adsorption by ToF-SIMS and in Situ OWLS. *Langmuir*, 19(22):9216–9225, 2003. ISSN 07437463. doi: 10.1021/la034111y.

[222] Gregory L. Kenausis, Janos Vörös, Donald L. Elbert, Ningping Huang, Rolf Hofer, et al. Poly(l -lysine)- g -Poly(ethylene glycol) Layers on Metal Oxide Surfaces: Attachment Mechanism and Effects of Polymer Architecture on Resistance to Protein Adsorption . *The Journal of Physical Chemistry B*, 104(14):3298–3309, 2000. ISSN 1520-6106. doi: 10.1021/jp993359m. URL http://dx.doi.org/10.1021/jp993359m.

[223] Stephanie VandeVondele, Janos Vörös, and Jeffrey A. Hubbell. RGD-grafted poly-l-lysine-graft-(polyethylene glycol) copolymers block non-specific protein adsorption while promoting cell adhesion. *Biotechnology and Bioengineering*, 82(7):784–790, jun 2003. ISSN 00063592. doi: 10.1002/bit.10625. URL http://doi.wiley.com/10.1002/bit.10625.

[224] Ning Ping Huang, Janos Vörös, Susan M. De Paul, Marcus Textor, and Nicholas D. Spencer. Biotin-derivatized poly(L-lysine)-g-poly(ethylene glycol): A novel polymeric interface for bioaffinity sensing. *Langmuir*, 18(1):220–230, 2002. ISSN 07437463. doi: 10.1021/la010913m.

[225] Constance Oliver. Use of immunogold with silver enhancement. In *Methods in molecular biology (Clifton, N.J.)*, volume 588, pages 311–316. 2010. ISBN 978-1-58829-463-0. doi: 10.1007/978-1-59745-324-0_30. URL http://www.ncbi.nlm.nih.gov/pubmed/20012841.

[226] Anna Forsman, Els Beirnaert, Marlén M I Aasa-Chapman, Bart Hoorelbeke, Karolin Hijazi, et al. Llama antibody fragments with cross-subtype human immunodeficiency virus type 1 (HIV-1)-neutralizing properties and high affinity for HIV-1 gp120. *Journal of virology*, 82(24):12069–81, dec 2008. ISSN 1098-5514. doi: 10.1128/JVI.01379-08.

[227] Laura E McCoy, Anna Forsman Quigley, Nika M Strokappe, Bianca Bulmer-Thomas, Michael S Seaman, et al. Potent and broad neutralization of HIV-1 by a llama antibody elicited by immunization. *The Journal of experimental medicine*, 209(6): 1091–103, jun 2012. ISSN 1540-9538. doi: 10.1084/jem.20112655.